Simultaneous Determination of Three Phenolic Compounds in Water Samples by Pre-column Derivatization Coupled with Reversed-Phase High Performance Liquid Chromatography

Üç Fenolik Bileşiğin Kolon Öncesi Türevlendirme ile Ters-Faz Sıvı Kromatografisi Yöntemi Kullanılarak Su Örneklerinde Eşzamanlı Tayini

Research Article

Adem Asan[1]*, M. Umut Konanc[2], Bediha Akmese[3]

[1]Ondokuz Mayis University, Faculty of Science, Department of Chemistry, Kurupelit-Samsun, Turkey.

[2]Artvin Coruh University, Research laboratory, Artvin, Turkey.

[3]Hitit University, Faculty of Science, Department of Chemistry, Corum, Turkey.

ABSTRACT

In this study, a sensitive and accurate method for simultaneous separation and determination of three phenolic compounds (phenol, m-cresol and resorcinol) in water by revesed-phase high performance liquid chromatography using uv-visible detection has been described. Pre-column derivatization with 4-aminoantipyrine is used for the seperation and determination phenol, m-cresol and resorcinol in water. The derivatives formed within 5 min were extracted with chloroform and then analyzed by liquid chromatography with UV-visible detection at 440 nm. Chromatographic separation was performed using a reversed-phase column and acetonitrile-water (45:55%, v/v) as the mobile phase. The three derivatives were elueted in 13 min. The detection limits of phenol, m-cresol and resorcinol in a standard water sample were between 0.07 and 0.09 $\mu g.L^{-1}$ for 100 mL respectively. The recoveries of the derivatives from pure water were betweeen 97.1-102.3% within relative standard deviations of 2.3-4.7%. The method was applied to the analysis of phenols in different water samples.

Key Words

Phenols, derivatization, reversed-phase liquid chromatography, 4-aminoantipyrine.

ÖZ

Bu çalışmada; suda üç fenolik bileşiğin (fenol, m-kresol ve resorsinol), UV-görünür detektör kullanılarak ters-faz yüksek performanslı sıvı kromatografisi ile ayrılması ve eş zamanlı tayini için hassas ve doğru bir yöntem geliştirildi. Fenol, m-krezol ve resorsinolün sudaki tayini ve ayrılması için kolon öncesi 4-aminoantipirin ile türevlendirilmiştir. 5 dakika içinde oluşan türevler kloroform ile ODS kolondan geri alınmıştır ve daha sonra 440 nm'de UV-görünür detektörde sıvı kromatografisi ile analiz edilmiştir. Kromatografik ayırım, ters-faz kolonda ve mobil faz olarak asetonitril-su (%45:55, v/v) karışımı kullanılarak gerçekleştirilmiştir. Üç fenol türevi 13 dakikada içerisinde başarıyla ayrılmıştır. Standart bir su numunesinde fenol, m-kresol ve resorsinolün tayin sınırı sırasıyla 100 mL için 0.07 ve 0.09 $\mu g.L^{-1}$ arasındadır. Türevlerin saf sudan geri kazanımı, %2.3-4.7'lik bağıl standart sapma ile %97.1-102.3 düzeylerinde bulundu. Yöntem, farklı su numunelerindeki fenollerin analizi için başarıyla uygulandı.

Anahtar Kelimeler

Fenoller; türevlendirme, ters faz sıvı kromatografisi; 4-aminoantipirin.

Article History: Received: Jan 16, 2018; Revised: Jan 30, 2018; Accepted: Feb 23, 2018; Available Online: Mar 26, 2018.

DOI: 10.15671/HJBC.2018.224

Correspondence to: A. Asan, Ondokuz Mayis University, Faculty of Science, Department of Chemistry, Kurupelit-Samsun, Turkey.

Tel: +90 362 312 1919 Fax: +90 362 457 6081 E-Mail: aasan@omu.edu.tr

INTRODUCTION

Phenolic compounds are toxic substances that occur naturally in the environment, in plants and food [1]. Therefore, these compounds are typically found in domestic and industrial products, natural waters and potable water supplies. Owing to their toxicity, persistence and unpleasant organoleptic properties [2,3], both the US Environmental Protection Agency (EPA) and the European Union (EU) have classified several phenols as priority pollutant [4].

They have also been employed as raw materials for drugs, pesticides, synthetics fibers, resins, and dyes. Thus, they are discharged from a variety of industrial plants to environmental water. Their input into the ecosystems results directly from human activity or indirectly from the transformation of natural or synthetic chemicals and they are found in waters from various sources [5-8]. Several methods have been reported for the determination of phenolic compounds in different samples including spectrophotometric methods [9], high-performance liquid chromatography (HPLC) [10-17] gas chromatography (GC) [18-23] and capillary electrophoresis [24,25]. Owing to the complex nature of samples (biological, water, etc) and low concentration of phenolic compounds in such samples, their isolation and preconcentration are commonly necessary prior to their quantitative determination. Liquid-liquid extraction [26] and solid-phase extraction [27] are the most usual techniques for this purpose.

In this study, a sensitive and accurate method for simultaneous separation and determination of three phenolic compounds (phenol, m-cresol and resorcinol) in water by reversed-phase high performance liquid chromatography using UV-visible detection has been established. The main objective of this study is to develop and validate a selective and sensitive method for the simultaneous determination of phenolic compounds in water. A reversed-phase liquid chromatographic and UV-visible detection was accomplished based on pre-column the reaction between phenols and 4-aminoantipyrine (4-AA). 4-AA is a common reagent and that has been previously studied [28]. Although in the present study, the derivatization reaction between 4-AA and phenolic compounds were modified in the presence of potassium peroxydisulfate as oxidizer. Then obtained derivatives (quinoneimines) exhibited intense absorption at 440 nm were separated in RP-HPLC system and determined using visible spectrophotometric detector. Consequently, a simple pre-column derivatization plus reversed-phase liquid chromatographic procedure for the determination of phenolic compounds in water at ppb levels was obtained.

MATERIALS and METHODS

Reagents and Chemicals

The phenolic compounds (phenol, m-cresol and resorcinol) and the derivatization agent (4-aminoantipyrine) (4-AA) were obtained from Sigma-Aldrich. The tested extraction solvents were purchased from Merck. All other reagents were of analytical reagent grade and were used without further purification. Individual standard phenol stock solutions (500 $mg.L^{-1}$) were prepared by dissolving 50 mg of phenol in 100 mL of deionized water. Working standard solutions of various concentrations were prepared daily by diluting the stock solution with deionized water. Ultrapure Milli-Q water (Millipore) was used for the preparation of solutions. The stock solutions were stable for up to 2 week when stored in the dark at room temperature. The 4-aminoantipyrine stock solution (88 $mmol.L^{-1}$) was prepared by dissolving 1.8 g of 4-aminoantipyrine in 100 mL of deionized water.

The ammonia buffer solution was prepared by dissolving 6.75 g of ammonium chloride in 57 mL of ammonia and diluted to 100 mL with deionized water. An ammonium peroxodisulfate stock solution (88 $mmol.L^{-1}$) of pH 10 was prepared by dissolving 2.0 g of ammonium peroxodisulfate in 80 mL of water, while adjusting to pH 10 by the addition of a potassium hydroxide solution (2 $mol.L^{-1}$) and diluting to 100 ml of water.

The water samples (Borcka dam lake and Murgul stream) were collected (in 1-1 dark colored glass bottles) from the Artvin in Turkey. The area where the samples are taken was the place where

the garbage is laid and near to the mine site. The bottles were previously washed with 0.1 mol.L^{-1} HCl and repeatedly rinsed with deionized water. During sampling, the bottles were rinsed twice with the sample water, then filled and tightly capped. Samples were filtered through Millipore membrane filters (0.45-μm pore size, Millipore, Bedford, USA) and analyzed immediately.

Apparatus

Chromatographic analysis was performed using a Shimadzu liquid chromatograph LC-20AD (Kyoto, Japan), equipped with binary solvent delivery units (LC-20AD), UV-vis detector (SPD- M20A), LC solution Version 1.25 and an auto sampler (SIL-20 MT). The LC solution workstation software was used to control the gradient setting and data acquisition.

Absorbance measurements for phenol derivatives were performed using a UV-visible spectrophotometer (Shimatzu UV-1800, Tokyo, Japan). For pH measerements, the pH meter (WTW ino lab pH level 1) with a pH-electrode Sentix-41 was used.

A GL Sciences Inertsil ODS-2 C18 reversed-phase column (250 mm x 4.6 mm, 5 μm particle size) was used for the separation of the target analysts. Mobile phase composition that providing the best separation was a mixture acetonitrile and water (45:55%, v/v), which was filtered and degassed prior to use. The flow-rate was 1.0 mL/min, the sample injection volume was 20 μL, and the detection wavelength was 440 nm.

Derivatization and Extraction Procedure

The 4-aminoantipyrine (4-AA) derivatives of the phenols were prepared according to the procedure described by Morita and Nakamura [28], after a major modification. To a 100 mL 1x10^{-4} mol.L^{-1} each phenolic compound solution, 5x10^{-4} mol.L^{-1} of 4-AA and 5x10^{-4} mol.L^{-1} of potassium peroxydisulfate ($K_2S_2O_8$) were added.

The mixture was alkalinized to pH 9 using 0.1 M ammonia/ammonium buffer solution which was added dropwise under vigorous shaking for 5 min. The reaction is as shown in Figure 1. The thus-prepared solution was left standing for 5 min at room temperature, and then both solid-liquid and liquid-liquid extraction procedures were applied to collect the quinoneimine derivatives obtained as a result of the reaction. The derivatization reaction is shown in Figure 1.

For the solid-phase extraction, the solution was passed through the ODS-functionalized silica cartridge (60x8 mm constructed in the laboratory), which was washed with 5 mL of methanol and 10 mL of deionized water subsequently before use. The adsorbed quinoneimine derivatives were eluted with 2 mL of different extraction solvents (chloroform, hexane, dichloromethane and diethyl ether). For the liquid-liquid extraction, extraction efficiencies were compared by adding different extraction solvents onto the phenol derivatives solution. The highest extraction yield was obtained using chloroform. The samples were extracted with 1x10 mL and 1x5 mL of chloroform. The water layer was saved and potassium chloride

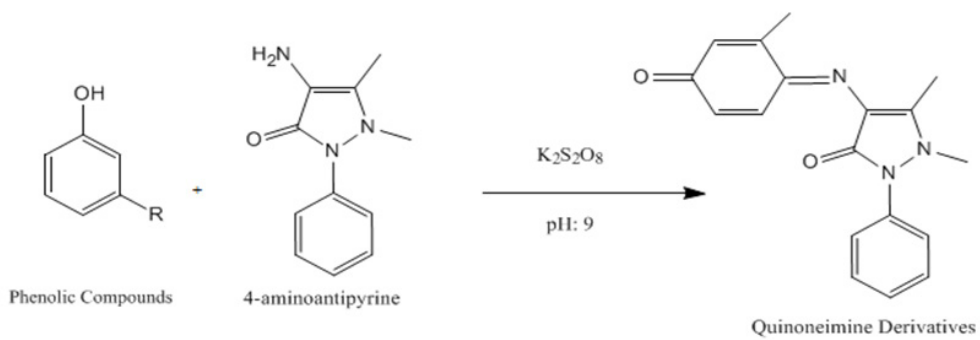

Figure 1. Derivatization reaction between phenol compounds and 4-aminoantipyrine.

(1.2 g) added to increase the ionic strength and promote the transfer of quinoneimine derivatives into the organic extract. For all extractions, separating funnels were shaken for 1 min and the phases were allowed to separate for 3 min. The extracts were evaporated to dryness at 40°C in a water bath. The precipitates were redissolved in 1 mL of mobil phase (acetonitrile and water, 45:55, v/v) and 20 μL of each sample was injected onto the RP-HPLC system. In applications of the method, a sample volume of a 100 mL was used for the extraction, since a reasonable linearity was obtained for all phenols studied. The phenols were identified from their retention times and quantitatively determined their peak areas.

RESULTS and DISCUSSION

Optimization of the derivatization reaction

As the derivatization reaction of phenolic compounds with 4-aminoantipyrine proceeded in a basic medium, the effect of the pH in the presence of ammonia/ammonium buffer solution was examined using a standard solution of the phenols at a concentration of $1x10^{-4}$ mol.L^{-1}. The peak heights of all compounds reached maxima at pH 8-10. The highest peak height was obtained at pH 9. For this reason, the pH value was 9 throughout the study. The effect of peak height with pH change is shown in Figure 2.

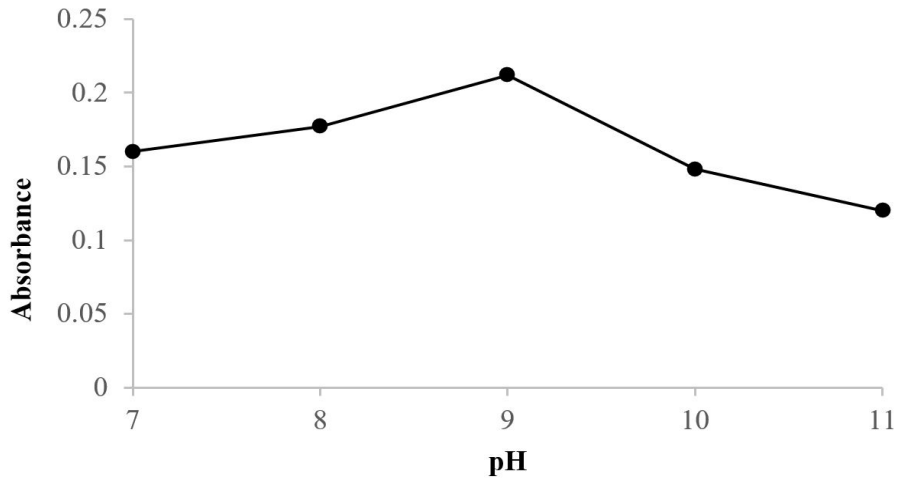

Figure 2. Effect of pH on the derivatization reaction between phenol compounds and 4-aminoantipyrine (phenol: $1x10^{-4}$ M; peroxydisulfate: $5x10^{-4}$ M; 4-aminoantipyrine: $5x10^{-4}$ M).

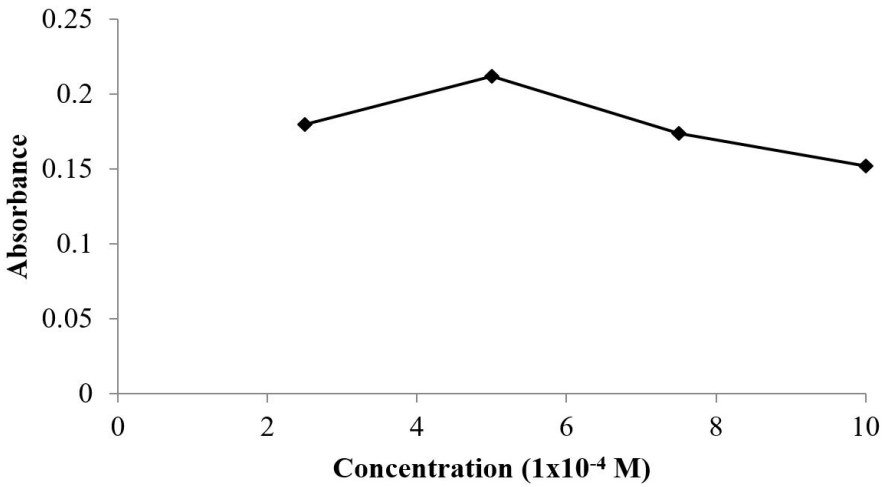

Figure 3. Effect of 4-aminoantipyrine concentration on the derivatization reaction (phenol: $1x10^{-4}$ M; peroxydisulfate: $5x10^{-4}$ M).

The effect of 4-aminoantipyrine concentrations on the reaction was tested. The highest absorption value was obtained when 4-aminoantipyrine was used at a concentration of $5x10^{-4}$ mol.L^{-1}. The effect of absorption with 4-aminoantipyrine concentration change is shown in Figure 3.

The amount of peroxydisulfate ($K_2S_2O_8$) used as oxidant in the reaction was tested. It was determined that the optimum amount of peroxydisulfate for the derivatization reaction was $5x10^{-4}$ mol.L^{-1}. The effect of absorption with peroxydisulfate concentration change is shown in Figure 4.

Temperatures of 30, 40 and 50°C were tested. All peak heights reached a maximum after a reaction time 10 min at all temperatures. For this reason, the work was done at room temperature. Figure 5 shows the effect of temperature on peak height. As a result, all the parameters in the reaction are optimized.

Calibration, Detection Limits and Repeatability

Calibration graphs were performed using the external standard technique following.Linear regression analysis by plotting concentration (μg.L^{-1}) against peak area. Table 1 shows the

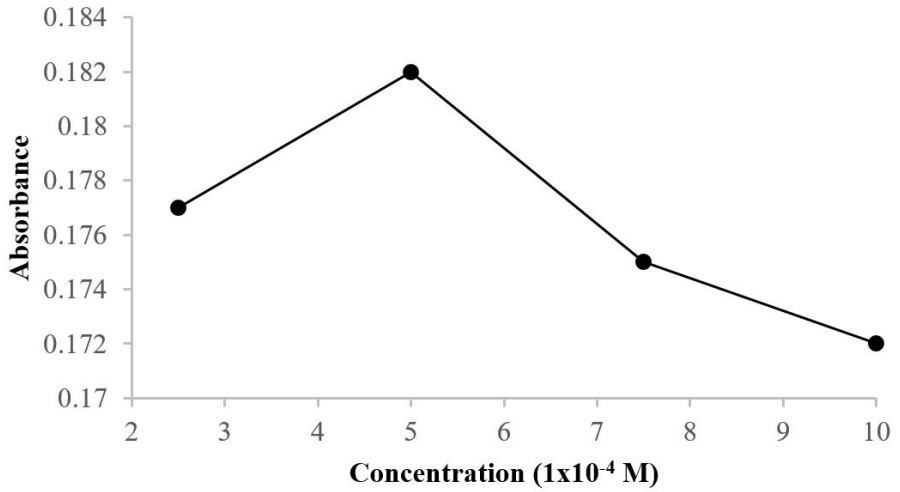

Figure 4. Effect of peroxydisulfate concentration on derivatization reaction (phenol: $1x10^{-4}$ M; 4-aminoantipyrine: $5x10^{-4}$ M).

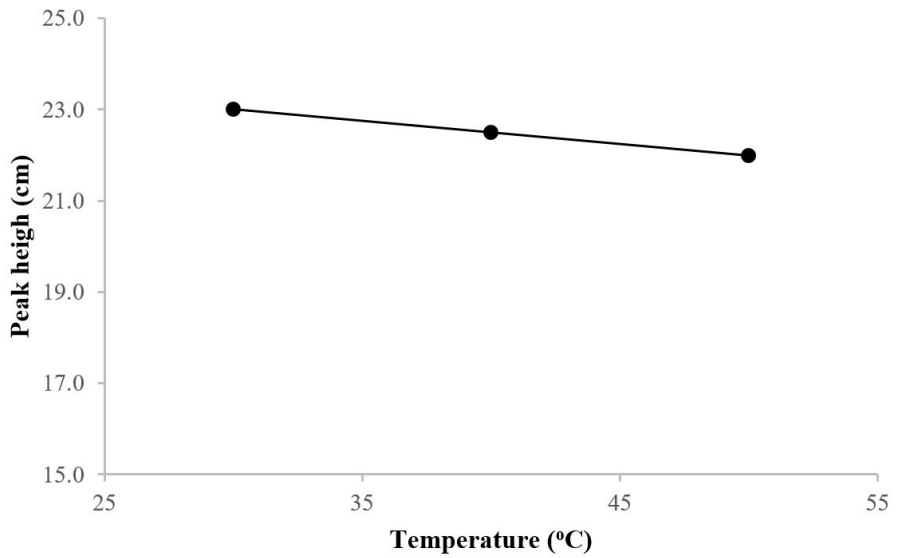

Figure 5. Effect of temperature on peak height.

equations obtained fort the calibration graphs and the regression coefficients. The repeatability of the method was calculated using the average relative standard deviation (RSD) for 10 replicate injections of the same sample at 10 μg.L^{-1}. The reproducibility was calculated using the RSD. For 10 injections of the same sample (10 μg.L^{-1}) on different days. The LOD and LOQ were calculated using the standard deviation (s) of response and the slope (m) of the calibration curve as LOD= 3.3 s/m; LOQ= 10 s/m [29-31]. All values obtained are given in Table 1. precision and accuracy for intra-day and inter-day assays of these derivatives are shown in Table 2. In the intra-day assay, the range of standard deviation for retention time was within 0.23 to 0.39% and standard deviation for peak area was within 2.17 to 3.73. In the inter-day assay, the range of standard deviation for retention time was within 0.26 to 0.41% and standard deviation for peak area was within 2.66 to 3.68%. Figure 6 shows the standard chromatogram of derivatives of phenol compounds.

Recovery

Both liquid-solid and liquid-liquid extraction were carried out for the extraction of quinoneimine derivatives. It was determined that the best extraction method for these derivatives was liquid-liquid extraction. For this reason, liquid-liquid extraction method was used for isolating the derivatives. Different solvents (chloroform, hexane, dichloromethane and diethyl ether) were used for extraction. Chloroform was chosen as the best among them. Extraction of quinoneimine derivatives with chloroform resulted a substantial improvement enabling a high recovery for the phenolic compounds from Murgul stream water and Borcka Dam Lake.

The efficiency of the extraction procedure and the recovery of phenols from 100 mL of Murgul stream water and Borcka Dam Lake are shown in Table 3 and Table 4. At the same time, Tables also show repeatability and reproducibility. For the Murgul stream water, the quantities of phenols were spiked to different concentrations and over 97.1-102.3% of the phenols was recovered from water with relative standard deviations 2.3-4.7% and also Borcka Dam Lake, the quantities of phenols were spiked to different concentration and over 97.4-103.1% of the phenols was recovered from water with relative standard deviations 2.3-4.1%.

Applications

The described method was used to determine phenol, m-cresol and resorcinol in tap water and water samples. As shown in Table 5, the level of phenol, m-cresol and resorcinol in tap water was below the lower limit of quantification. In Table 5,

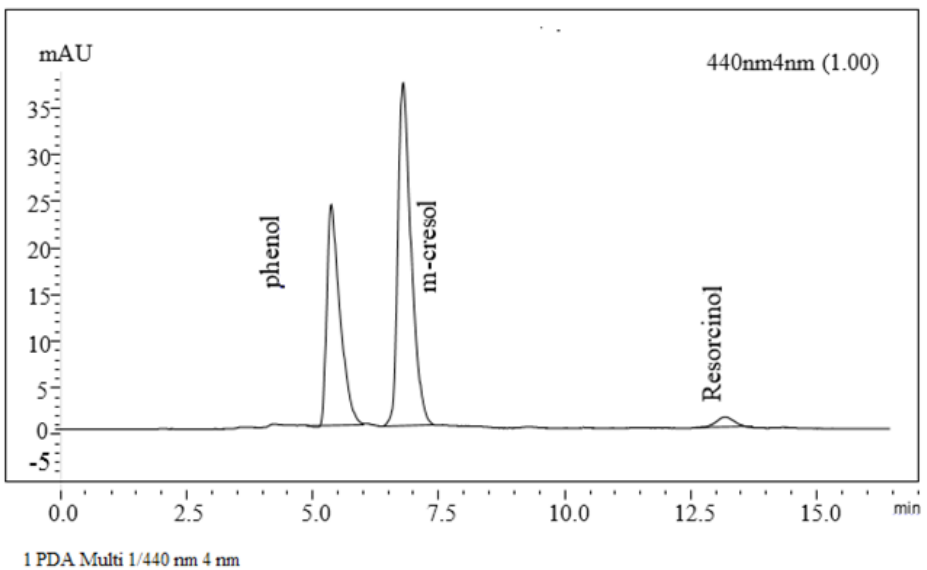

Figure 6. Reversed-phase HPLC-UV-vis. chromatograms of quinoneimine derivatives of phenols. Phenol, 6.0 ng; m-cresol, 7.4 ng; resorcinol, 2.0 ng. Column: GL Science Inertsil C_{18} RP (5μm, 250mm x 4.6 mm ID). Mobil phase: aceto-nitrile-water (45:55%, v/v); Flow-rate: 1.0 mL min^{-1}.

Table 1. Retention time (t_R) and linear regression parameters, LOD and LOQ, of the determined phenolic compounds.

Analyte	t_R (min)	Calibration curve	r^2	Linearity range ($\mu g.L^{-1}$)	LOD ($\mu g.L^{-1}$)	LOQ ($\mu g.L^{-1}$)
phenol	6.1	y= 62.821x+7067	0.9968	5.0-250	0.07	0.31
m-cresol	7.2	y= 58.374x+5535	0.9995	10-300	0.08	0.35
resorcinol	12.6	y= 73.811x-3052	0.9988	2.0-100	0.09	0.38

Table 2. Precision of three phenolics for retention time (t_R) and peak area (pa) (n= 5).

Analyte	Intra-day variations		Inter-day variations	
	RSD for t_R (%)	RSD for pa (%)	RSD for t_R (%)	RSD for pa (%)
phenol	0.23	2.17	0.26	3.56
m-cresol	0.33	2.67	0.38	2.66
resorcinol	0.39	3.73	0.41	3.68

Table 3. Summary of results from analysis of phenols in spiked 100 mL of Murgul stream water (n= 5).

Analyte	Amount added (ng)	Recovery (%)	RSD (%)	Repeatability RSD (%)	Reproducibility RSD (%)
phenol	10	98.7	2.4	1.7	2.3
	100	97.1	3.7		
	200	102.3	2.3		
m-cresol	20	99.3	3.5	1.9	2.5
	150	98.1	2.9		
	250	101.2	3.2		
resorcinol	5	98.3	3.1	2.5	2.9
	50	97.3	4.7		
	75	102.1	3.8		

the results for the water samples are given. The concentration of phenolic compounds in different water samples were successfully determined. In Figure 7 and 8 typical chromatograms of phenols in 100 mL of Murgul stream and Borcka Dam Lake water samples are shown. Obviously, low $ng.mL^{-1}$ levels of phenols can be successfully determined in environmental samples. As Table 5 shows, phenolic compounds could not be assigned to tap water. The maximum amount of m-cresol was found in the Borcka Dam Lake water. On the other hand, the amount of resorcinol is the most in the Murgul stream water.

The comparison of the new method and reported methods (published over the period 2001-2016) is presented in Table 6. The proposed method without complex pre-treatment offered the linear range is 2-300 $\mu g.L^{-1}$ and LOD is 0.07 $\mu g.L^{-1}$ for phenolic compounds, which were significantly lower than the reported methods in Table 6.

Table 4. Summary of results from analysis of phenols in spiked 100 mL of Borcka dam lake water (n= 5).

Analyte	Amount added (ng)	Recovery (%)	RSD (%)	Repeatability RSD (%)	Reproducibility RSD (%)
phenol	10	97.7	2.3	1.9	2.1
	100	98.6	2.7		
	200	102.9	2.6		
m-cresol	20	97.8	3.1	1.4	2.3
	150	99.1	2.8		
	250	102.5	3.4		
resorcinol	5	97.4	2.9	2.1	2.8
	50	99.2	4.1		
	75	103.1	3.6		

Table 5. Analytical results of water samples from different locations*.

Analyte	Tap water	Borcka dam water**		Murgul stream water**	
		$\bar{X}$	ts	$\bar{X}$	ts
phenol	ND	7.6	2.3	9.8	2.9
m-cresol	ND	11.2	3.8	12.9	4.1
resorcinol	ND	8.5	2.9	17.3	3.2

*Samples were collected at Artvin, Turkey.

**Values represent the average (= μg.L^{-1}), standard deviation (ts= %), for n = 5 with a confidence of 95%.

ND: Not detected

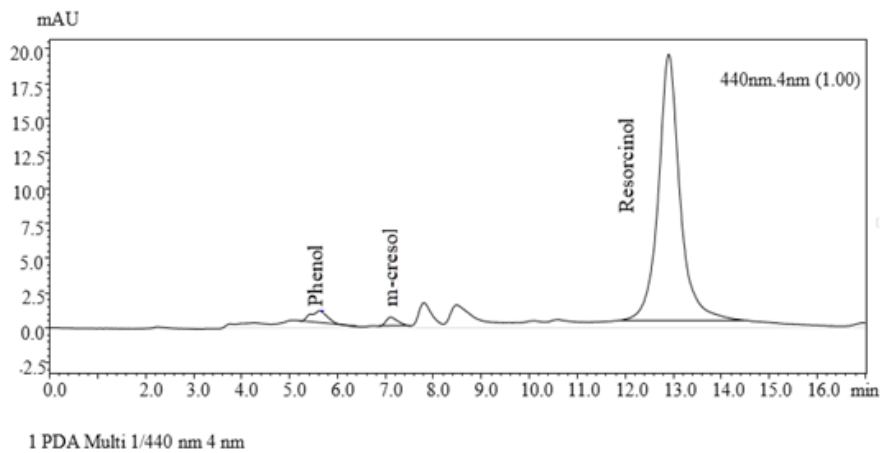

Figure 7. Reversed-phase HPLC-UV-vis. chromatograms of quinoneimine derivatives of phenols obtained from 100 mL of Murgul stream water. For conditions and peak assignment, see Figure 2.

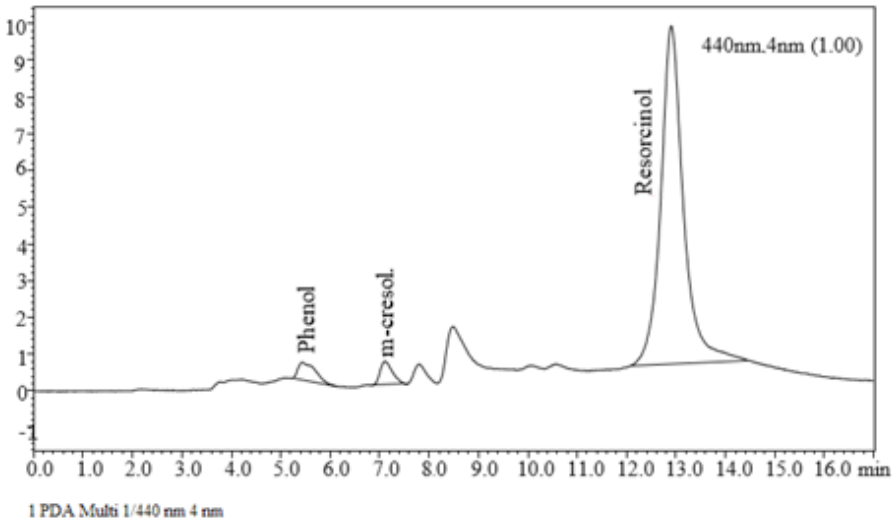

Figure 8. Reversed-phase HPLC-UV-vis. chromatograms of quinoneimine derivatives of phenols obtained from 100 mL of Borcka dam lake water. For conditions and peak assignment, see Figure 2.

Table 6. Comparison of literature HPLC methods (published over the period 2001-2016) for proposed method and some reported procedures for phenolic compound determination.

Method	Sample	Linear renge	Limit of detection	Reference
HPLC-UV	Aqueous sample	0.5-2.5 $\mu g.L^{-1}$	0.05 $\mu g.L^{-1}$	Zhao and Lee, 2001. [11]
HPLC-UV	Tap water, River water	0.2-5 $\mu g.L^{-1}$	0.06 $\mu g.L^{-1}$	H. Bagheri et al., 2004. [12]
HPLC-FD	Human urine	0.5-50 $mg.L^{-1}$	0.05 $mg.L^{-1}$	G. Marrubini et al., 2005. [13]
HPLC-UV	Bambo pulp	0.01-10 $mg.L^{-1}$	1.5 $\mu g.L^{-1}$	N. Sharma et al., 2011. [14]
HPLC-UV	River water, Tap water	100-500 $ng.L^{-1}$	82.1 $ng.L^{-1}$	M. C. Alcudia et al., 2011. [15]
HPLC-UV	Rice wines	0.5-50 $\mu g.L^{-1}$	0.02 $\mu g.L^{-1}$	Y. Huang et al., 2015. [16]
HPLC-UV	Soil extract, Sea water, River water, Tap water, Ground water	1.2-11.6 $\mu g.L^{-1}$	0.5 $\mu g.L^{-1}$	R. G. Dolatto et al., 2016. [17]
HPLC-UV	Tap water, Stream water, Dam lake water	2-300 $\mu g.L^{-1}$	0.07 $\mu g.L^{-1}$	This work

CONCLUSION

We have developed a pre-column RP-HPLC UV-visible method for simultaneous determination of phenol, m-cresol and resorcinol in water by using 4-aminoantipyrine as a labeling reagent, without complicated sample cleanup. The results showed that this new method was simple, rapid, practicable and feasible with high precision, sensitivity and repeatability, and could also provide a good resolution of the phenolic compounds in water samples. Thus, this procedure can be used to determine the basic phenolic compounds in various type of environmental samples.

ACKNOWLEDGEMENT

The authors are grateful for the financial support of the scientific Research projects of Ondokuz Mayis University (project no. PYO.FEN.1904.11.021).

References

1. M.L. Soto, A. Moure, H. Domínguez, J.C. Parajó, Recovery, concentration and purification of phenolic compounds by adsorption: a review, J. Food Eng., 105 (2011) 1-27.
2. A. Penalver, E. Pocurrull, F. Borrull, R.M. Marce, Solid-phase microextraction coupled to high-performance liguid chromatography to determine phenolic compounds in water samples, J. Chromatogr. A, 953 (2002) 79-87.
3. H. Xu, Y. Liao, J. Yao, Development of a novel ultrasound-assisted head-space liquid-phase microextraction and its application to the analysis of chlorophenols in real aqueous samples, J. Chromatogr. A, 1167 (2007) 1-8.
4. EPA. Methad 604, Phenols, Part VIII, 40 CFR part 136. US Environmental Protection Agecy, 26 july 2014.
5. M. L. Barrico, C. Nabais, M.J. Martins, H. Freitas, Sources of phenolic compounds in two catchments of southern Potugal-effect of season, land use and soil type, Chemosphere, 65 (2006) 482-488.
6. A.R. Sousa, M.A. Trancoso, Validation of an environmental friendly segmented flow method for the determination of phenol index in waters as alternative to the conventional one, Talanta, 79 (2009) 769-803.
7. S. Lacorte, A. Latorre, D. Barcelo, A. Rigol, A. Malmiqvist, T. Welander, Organic compounds in papwer-mill process waters and effluents, Trends Anal. Chem., 22 (2003) 725-737.
8. J. Michalowich, W. Duda, Phenols-sources and toxicity, Pol. J. Environ. Stud., 16 (2007) 347-362.
9. K.O. Lupetti, F.R.P. Rocha, O. Fatibello-Filho, An immproved flow system for phenols determination explieting multicommutation and long pathlength spectrophotometry, Talanta, 62 (2004) 463-469.
10. A. Asan, I. Isildak, Determination of major phenolic compounds in water by reversed-phase liquid chromatography after pre-column derivatization with benzoyl chloride. J. Chromatogr. A, 988 (2003) 145-149.
11. L. Zhao, K.H. Lee, Determination of phenols in water using.Liquid phase microextraction with back extraction combined with high-prformance liquid chromatography, J. Chromatogr. A, 931 (2001) 95-105.
12. H. Bagheri, A. Mohammadi, A. Salemi, On-line trace enrichment of phenolic compounds from water using a pyrrole-based polymer as the solid-phase extraction sorbent coupled with high-performance liquid chromatography, Anal. Chim. Acta, 513 (2004) 445-449.
13. G. Marrubini, E. Calleri, T. Coccini, A.F. Castoldi, L. Manzo, Direct analysis of phenol, catechol and hydroquinone in human urine by coupled-column HPLC with fluorimetric detection, Chromatographia, 62 (2005) 25-31.
14. N. Sharma, A. Jain, V. Kumari Singh, K.K. Verma, Solid-phase extraction combined with headspace single-drop microextraction of chlorophenols as their methyl ethers and analysis by high-performance liquid chromatography-diode array detection, Talanta, 83 (2011) 994-999.
15. M.C. Alcudia-León, R. Lucena, S. Cárdenas, M. Valcárcel. Determination of phenols in waters by stir membrane liquid-liquid-liquid micro extraction coupled to liquid chromatography with ultraviolet detection, J. Chromatogr. A, 1218 (2011) 2176-2181.
16. Y. Huang, W.W. Lu, B. Chen, M. Wu, S.G. Li, Determination of 13 phenolic compounds in rice wine by high-performance liquid chromatography, Food Anal. Methods, 8 (2015) 825-832.
17. R.G. Dolatto, I. Messerschmidt, B.F. Pereira, R. Martinazzo, G. Abate, Preconcentration of polar phenolic compounds from water samples and soil extract by liquid-phase micro extraction and determination via liquid chromatography with ultraviolet detection, Talanta, 148 (2016) 292-300.
18. L. Montero, S. Conradi, H. Weiss, P. Popp, Determination of phenols in lake and ground water samples by stir bar sorptive extraction-thermal desorption-gas chromatography-mass spectrometry, J. Chromatogr. A, 1071 (2005) 163-169.
19. H. Faraji, M.S.Tehrani, S.W. Husain, Pre-concentration of phenolic compounds in water samples by novel liquid-liquid microextraction and determination by gas chromatography-mass spectrometry, J. Chromatogr. A, 1216 (2009) 8569-8574.
20. J.A. Padilla-Sánces, P. Plaza-Bolaños, R. Romero-González, N. Barco-Bonilla, J.L. Martínez-Vidal, A. Garrido-Frenich, Simultaneous analysis of chlorophenols, alkylphenols, nitrophenols and cresols in wastewater effluents, using solid phase extraction and further determination by gas chromatography-tandem mass spectrometry, Talanta, 85 (2011) 2397-2404.
21. H. Ghorbanpour, A. Yadeghari, L. Khoshmaram, M.A. Farajzadeh, Air-assisted liquid-liquid microextraction for simultaneous derivatization, extraction, and preconcentration of some phenolic compounds. Anal. Methods, 6 (2014) 7733-7743.
22. Y.C. Fiamegos, A-P. Kefala, C.D. Stalikas, Ion-pair single-drop microextraction versus phase-transfer catalytic extraction for the gas chromatographic determination of phenols as tosylated derivatives, J. Chromatogr. A, 1190 (2009) 44-51.
23. E.L.B. Lourenço, A. Ferreira, E. Pinto, M. Yonamine, S.H.P. Farsky, On-fiber derivatization of SPME extracts of phenol, hydroquinone and catechol with GC-MS detection, Chromatographia, 62 (2006) 175-179.
24. W. Wei, X. Yin, X. He, pH-mediated dual-cloud point extraction as a preconcentration and clean-up technique for capillary electrophoresis determination of phenol and m-nitrophenol, J. Chromatogr. A, 1202 (2008) 212-215.
25. T. Li, Q. Jia, L. Song, R. Su, Y. Lei, W. Zhou, H. Li, Coupling poly-(methacrylic acid-co-ethylene glycol dimethacrylate) monolith micro extraction to capillary electrophoresis for the determination of phenols in water samples. Talanta, 78 (2009) 1497-1502.
26. L. Zhu, H.K. Ee., L. Zhao, H.K. Lee, Analysis of phenoxy herbicides in bovine milk by means of liquid-liquid micro extraction with a hollow-fiber membrane. J. Chromatogr. A, 963 (2002) 335-343.

27. W.L. Chen, G.S. Wang, J.C. Gwo, C.Y. Chen, Ultra-high performance liquid chromatography/tandem mass spectrometry determination of feminizing chemicals in river water, sediment and tissue pretreated using disk-type solid-phase extraction and matrix solid-phase dispersion, Talanta, 89 (2012) 237-245.
28. E. Morita, E. Nakamura, Solid-phase extraction of antipyrine dye for spectrophotometric determination of phenolic compounds in water, Anal. Sci., 27 (2011) 489-492.
29. S.R. Tambe, R.H. Shinde, L.R. Gupta, V. Pareek, S.B. Bhalerao, Development of lle and spe procedures and its applications for determination of olmesartan in human plasma using RP-HPLC and HPTLC. J. Liq. Chromatogr. Relat. Technol., 33 (2010) 423-430.
30. Topic Q2A, Validation of analytical Procedures, Methodology, International Conference on Harmonization, Brussels, Belgium, 1995.
31. C.M. Riley, T.W. Rosanske, Development and validation analytical methods, Amsterdam: Elsevier, 1996.

Multilayer Graphene Oxide-Silver Nanoparticle Nanostructure as Efficient Peroxidase Mimic

Etkili Peroksidaz Taklitçi Olarak Çok Tabakalı Grafen Oksit-Gümüş Nanopartikül Nanoyapısı

Research Article

Burak Derkus[1*], Pinar Acar Bozkurt[2]

[1]Department of Biomedical Engineering, Engineering Faculty, Eskisehir Osmangazi University, Eskisehir, Turkey.

[2]Science Faculty, Department of Chemistry, Ankara University, Ankara, Turkey.

ABSTRACT

In this work, platinum (Pt), titanium (Ti) and silver (Ag) doped graphene oxide (GO) nanostructures were synthesized by using sonochemical technique, a relatively new technique in nanomaterial synthesis, and characterized in detail. The synthesized nanomaterials were characterized utilizing transmission electron microscopy (TEM) and X-ray photoelectron spectroscopy (XPS). TEM images and XPS spectras showed that the dopping process was successful. In addition, a multilayer graphene oxide-silver nanoparticles (M-GO-AgNPs) nano-structure was synthesized in this study for the first time, and it's electrochemical performance was compared with GO-AgNPs. As a result of electrochemical study, the rate constants of the GO-AgNPs and M-GO-AgNPs modified electrodes were found as ks_{anodic}= 6.62 s^{-1} and ks_{anodic}= 6.78 s^{-1}, respectively. Finally, the M-GO-AgNPs nano-structure obtained by sonochemical technique, a green chemistry synthesis technique, has been found to be suitable for use as an electrochemical sensor matrix.

Key Words

Graphene oxide, silver, platinum, titanium, nanoparticle, sonochemistry, green chemistry.

ÖZ

Bu çalışmada, nanomalzeme sentezinde nispeten yeni bir teknik olan sonokimyasal tekniğin kullanılmasıyla platin (Pt), titanyum (Ti) ve gümüş (Ag) doplanmış grafen oksit (GO) nano-yapılar sentezlenmiş ve detaylı bir şekilde karakterize edilmiştir. Sentezlenen nano-malzemeler transmisyon elektron mikroskobu (TEM) ve X-ışınları fotoelektron spektroskopisi (XPS) ile karakterize edilmiştir. TEM görüntüleri ve XPS spektrumları doplama işleminin başarılı bir şekilde gerçekleştiğini göstermiştir. Ayrıca bu çalışmada ilk kez çok tabakalı grafen oksit-gümüş nanopartikül nano-yapısı (M-GO-AgNPs) sentezlenmiş ve elektrokimyasal performansı GO-AgNPs ile karşılaştırılmıştır. Elektrokimyasal çalışmalar sonucunda GO-AgNPs ve M-GO-AgNPs hız sabitleri sırası ile ks_{anodik}= 6.62 s^{-1} ve ks_{anodik}= 6.78 s^{-1} olarak bulunmuştur. Sonuç olarak bir yeşil kimya sentez tekniği olan sonokimyasal teknik ile elde edilen M-GO-AgNPs nano-yapının elektrokimyasal sensör matriksi olarak kullanım için uygun olduğu görülmüştür.

Anahtar Kelimeler

Grafen oksit, gümüş, platin, titanyum, nanopartikül, sonokimya, yeşil kimya.

Article History: Received: Jan 06, 2018; Revised: Jan 23, 2018; Accepted: Jan 29, 2018; Available Online: Mar 26, 2018.

DOI: 10.15671/HJBC.2018.225

Correspondence to: B. Derkus, Dept. Biomed. Eng., Engineering Faculty, Eskisehir Osmangazi University, Eskisehir, Turkey.

Tel: +90 0312212 6040 Fax: +90 0312212 6040 E-Mail: burakderkus@gmail.com

INTRODUCTION

Recently, direct fuel cells which use liquid fuels attract much more attention than the hydrogen based ones mainly because of the high cost of Graphene oxide (GO), a one-atom-thick material consisting of sp^2-bonded carbons, have been widely evaluated as electrocatalyst for electrochemical reactions, and as highly conductive matrix for loading catalysts of metals, and/or biological catalyzing materials such as enzymes. This conductive and electroactive material is a suitable candidate for biocatalytic reactions in which enzymes take part, thus they enable to design electrochemical biosensors having lower detection limits [1,2].

Previous works show that chemisorption or contact of metallic or insulating structures affect the electronic properties of graphene or GO significantly [3,4]. While chemisorption phenomenon alters the electronic structure, it's preserved by a weak adsorption on various surfaces such as silver (Ag) or platinum (Pt) [3]. This is a result of deviation of Fermi level from the conical points in graphene when the graphene contacts with conductive metals weakly, which is in turn doped with electrons.

Various techniques have been introduced to the literature by researchers describing the preparation of nanoparticle (NP) decorated or doped graphen oxide. To prepare graphene/metal nanoparticle composites, GO and metal salt are generally prefered as the precursors. A reduction process takes up a critical place in this method. For instance, palladium (Pd)/rGO (reduced GO) nanocomposite structure could be succesfully prepared by reducing palladium acetate to Pd on rGO [5]. Pt composite of GO is another widely encountered structure in this field [6]. Another commonly used technique, electrochemical deposition, enables to researchers controllable preparation of graphene/metal nanoparticle nanostructures. Maiyalagan et al. (2012) could uniformly electrodeposited Pt nanoparticles on GO coated indium tin oxide (ITO) substrate using chloroplatinic acid salt (H_2PtCl_6) [7]. Besides conventional methods, a considerably new technique, sonochemical method, takes attentions for graphene dopping in recent years. The superior property of ultrasound arises from acoustic cavitation, that is, the formation, growth, and implosive collapse of bubbles in liquid medium, which generates extreme reaction conditions such as ~5000 K temperature and ~1800 atm pressure [8]. The point is that the number of study, in which nanoparticle doped GO was synthesized sonochemically, is limited. Researchers have shown the synthesis of GO doped with some nanoparticles such as TiO_2 (titanium dioxide), Pt, iron(II, III) oxide (Fe_3O_4), and lead selenide (PbSe), so far [9-12]. However, shapes and dimensions of those nanostructures were not as desired.

In the current study, we prepared various doped GO nanostructures namely GO-PtNPs, GO-TiNPs, GO-AgNPs, and multilayer GO-AgNPs (M-GO-AgNPs) using sonochemical technique. While GO-PtNPs, GO-TiNPs, and GO-AgNPs synthesis and their electrocatalytic applications exist in the literature, a multilayer nanoparticle-GO sandwich (M-GO-AgNPs in this study) was synthesized for the first time and characterized in order to enhance the peroxidase reaction. The obtained nanostructures were characterized utilizing transmission electron microscopy (TEM) and X-ray photoelectron spectroscopy (XPS), followed by preparation of modified electrodes towards to use in electrochemical hydrogen peroxide (H_2O_2) catalysing.

MATERIALS and METHODS

Materials and Apparatus

Horse radish peroxidase (HRP), graphene oxide, chloroplatinic acid, titanium(IV) butoxide, silver nitrate ($NaNO_3$), sodium citrate ($Na_3C_6H_5O_7$), hydrazine (24-26%), hydrogen peroxide (H_2O_2, 27% w/w), potassium chloride (KCl), potassium ferrocyanide ($K_4[Fe(CN)_6]$), potassiumferricyanide ($K_3[Fe(CN)_6]$), sodium dihydrogen orthophosphate (NaH_2PO_4), and disodium hydrogen orthophosphate (Na_2HPO_4) were purchased from Sigma (St Louis, MO, USA). De-ionized water was purified using a Millipore Simplicity unit to a resistivity ≥18.2 MΩ. Electrochemical measurements were carried out with a Gamry Instrument using Framework Version 5.50 software. OriginPro 8 was utilized for obtaining the graphs.

Synthesis of Graphene Oxide Based Nanostructures

Four different graphene oxide based nanostructures were synthesized using sonochemical technique which gives us simple, rapid and controllable synthesis opportunity. The method presented by Giovanni et al. (2012) was modified for sonochemical synthesis of PtNPs doped GO [13]. Graphene oxide (200 mg) was redispersed in water (20 mL) for 15 min, than ultrasonicated for 30 min in the presence of chloroplatinic acid (5 mg) under 750 W power and 20 kHz frequency conditions. Lastly, the obtained PtNPs doped GO (GO-PtNPs) was dried under vacuum (60°C) for 12 h. Similarly, the method presented by Shang et al. (2014) was modified for the synthesis of GO-TiNPs. 5 mL of GO was added into 95 mL distilled water under ultrasonic conditions for 30 min, folloed by dropwise addition of $Ti(OC_4H_9)_4$ (1 mL) slowly. 5 mL nitric acid (1M) was added in order to restrain $Ti(OC_4H_9)_4$ hydrolysis. Finally, the product was calcified at 400°C for 4 h, following solvent evaporation at 200°C (2 h). GO-AgNPs nanostructures were prepared in one step reaction. For this purpose, 200 mg GO was dispersed in 100 mL of water by ultrasonication for 0.5 h, followed by addition of 50 mg $AgNO_3$. Subsequent to 1 g sodium citrate addition, GO-AgNPs nanostructures were formed via 1 h of ultrasonication. Finally, the mixture was washed with ethanol and deionized water by centrifugation, and the resulting GO-AgNPs were dried in a vacuum oven at 60°C for 12 h. Differently, 2 mL hydrazine (24-26%) was added dropwise during AgNPs formation step in order to obtain GO-AgNPs multilayer structure (M-GO-AgNPs), that has been presented for the first time in this study. The mechanism is based on amid formation between carboxyl groups of GO and double-sided amine groups of hydrazine. Schematic presentation of GO-AgNPs and M-GO-AgNPs can be seen in Figure 1. All the methods mentioned above also carry the feature of being green synthesis.

Preperation of Modified Electrods

Two different approaches were followed for the fabrication of screen-printed carbon electrods (SPCE), one of which was dropdown modification providing easy and one-step modification of materials. For this purpose, 10 mL of doped graphene nanostructures (GO-PtNPs, GO-TiNPs,

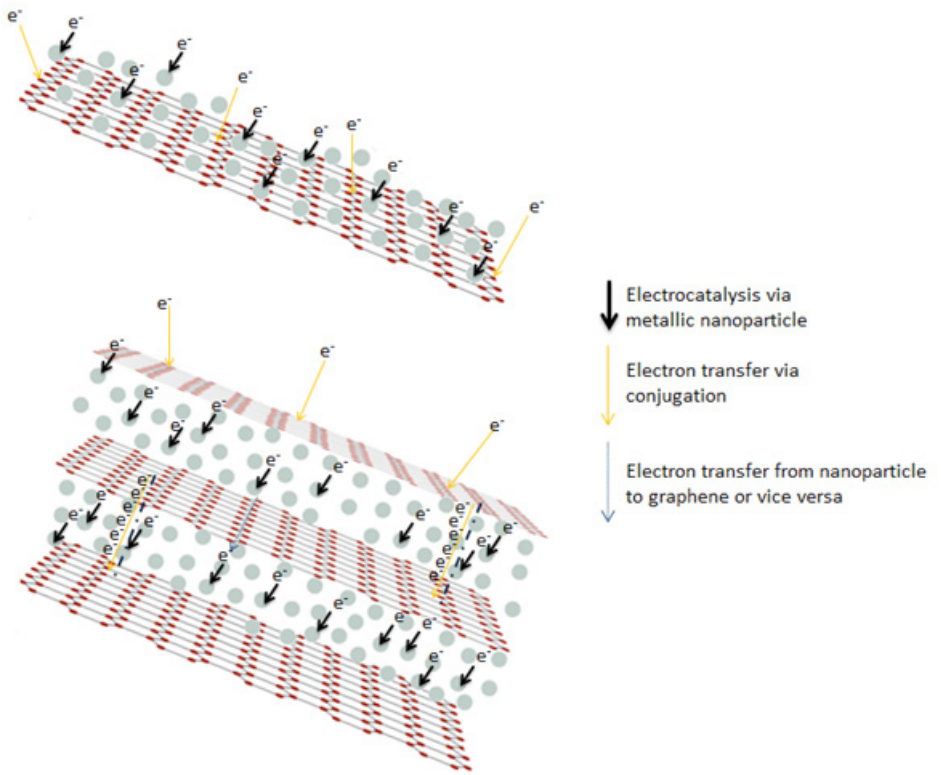

Figure 1. Schematical representation of electron transfer process in GO-AgNPs and M-GO-AgNPs.

GO-AgNPs, and M-GO-AgNPs) was droped onto seperate SPCEs. The modified electrodes were left at room temperature for 2h to ensure a stable dry surface, followed by enzyme immobilization using 10 mL hydrogen peroxidase (1 mg.mL^{-1}). Crosslinker was not necessary owing to adhesion property of enzymes onto graphene. Enzyme-free (peroxidase mimicking) electrodes were prepared using the same protocol without enzyme immobilization step. Second method includes electrodeposition of graphene based materials at 3V potential. To this end, SPCEs were dipped into 1 mL electrochemical cell including phosphate buffer, KCl, and nanoparticle doped graphene material, than 3V potential was applied for 5 min. Next, the electrods were washed with deionized water and dried in air. Two different approaches were carried out for enzyme immobilization. First, 10 mL hydrogen peroxidase (1 mg.mL^{-1}) was droped onto nanostructure electrodeposited electrodes likewise in the first method. To examine the effect of immobilization protocol on peroxide sensing, in the second method, electrodeposition was also used for entrapment of peroxidase enzyme into graphene based nanostructures. Electrochemical entrapment method has been firstly used for this kind of system in this study.

Electrochemical Study

Electrochemical measurements were carried out in a 1 mL electrochemical cell. In order to trigger the converison reaction, the desired concentration of hydrogen peroxide in 100 μL of buffer was injected into the cell containing 0.9 mL total volume of buffer and 0.1 M KCl. Then amperometric measurement was obtained.

CV and EIS were performed in PB buffer containing 0.1 M KCl and 0.5 mM $Fe(CN)_6^{3-/4-}$. Cyclic voltamograms were obtained by cycling the potential between -0.4 to 0.6 V with a scan rate of 100 mVs^{+1}. EIS measurements were recorded within the frequency range of 0.01 Hz to 100 kHz at open circuit potential.

$$Epc = E^{\prime\prime 0} + \frac{RT}{\alpha snF} - \frac{RT}{\alpha snF}\ln v \quad (1)$$

$$Epa = E^{\prime 0} + \frac{RT}{(1-\alpha s)nF} - \frac{RT}{(1-\alpha s)nF}\ln v \quad (2)$$

The electron-transfer coefficient and electron-transfer rate constant could be determined based on the Laviron theory (Equations 1 and 2) applying the scan rates of 10, 50, 100, 200, 500, and 1000 mVs^{-1} to the electrode system [14]:

$$ks = \frac{\alpha nFv}{RT} \quad (3)$$

where n is the electron transfer number, R is the gas constant (R= 8.314 Jmol^{-1}K^{-1}), T is the temperature in Kelvin (T= 298 K) and F is the Faraday constant (F=96493 C mol^{-1}). When nΔEp>200 mV, the electron transfer rate ks could be estimated with the Laviron's equation (Equation 3) [14]:

RESULTS and DISCUSSION

Characterization of Doped Graphene Oxide Nanostructures

TEM and XPS analysis were performed for the detailed characterization of the nanostructures. Figure 2A shows TEM image of the synthesized GO-PtNPs nanocomposite. A large number of Pt nanoparticles with a dimension of about 4-5 nm were well-distributed and deposited on GO nanosheets due to hydroxyl, epoxide, and carboxylic groups existing on GO [15]. In this sonochemical assisted synthesis, Pt nanoparticles were formed by reduction of H_2PtCl_6 without adding any reducing agent, which was attributed to redox reaction between GO and $PtCl_6^{2-}$ and enabled a spontaneous deposition. Pt nanoparticles with 4-5 nm size are pretty good to be used as electrocatalyst. XPS results proved the reduction of platinic acid salt to Pt^0 (Pt $4f_{5/2}$ peak was observed at 74.7 eV) and indicated that the deposited nanoparticles were platinum indeed (Figure 3A and S1). Since the Pt peak was weak, we also performed an EDAX analysis to show the presence of PtNPs using another technique. EDAX spectrum supported the XPS results and the intensive Pt signals suggested that the existing material was made of Pt (Figure S2). Figure 2B shows the TEM image of GO-TiO_2 nanocomposite and helps us to understand that TiO_2 nanoparticles with size of about 5-6 nm were successfully binded onto GO. This well-dispersed nanostructure looks like an ideal candidate for electrocatalysis application. The further

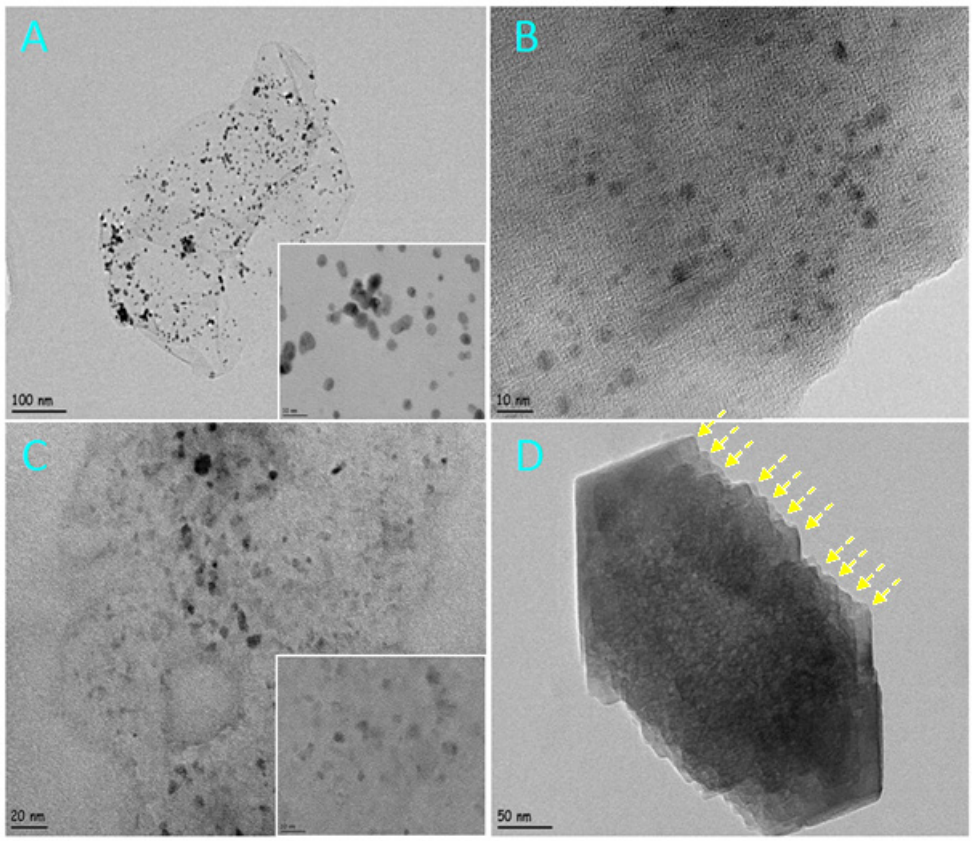

Figure 2. TEM images of (A) GO-PtNPs, (B) GO-TiNPs, (C) GO-AgNPs, and (D) M-GO-AgNPs nanostructures. The yellow arraws indicate individual GO nanolayers.

interaction between TiO_2 and GO was determined by XPS as shown in Figure 3B. Two peaks located at 462.5 and 456.7 eV took attention, which were related to Ti $2p_{1/2}$ and Ti $2p_{3/2}$ spin-orbitals, had a splitting of 5.8 that indicates the presence of anatase TiO_2 (Figure 3B inset and S3 Ti2p graph) [16]. Furthermore, there were two peaks at 465.8 and 460.2 eV that demonstrate the formation of Ti-O-C bond between TiO_2 and GO in addition to peak centered at 282 eV (Figure S3, C1s graph) [17]. Figure 2C shows the TEM image of GO-AgNPs. TEM image of AgNPs/GO nanocomposite reveals that the formed silver nanoparticles with size of 4-5 nm are homogeneously deposied on the GO surface (Figure 2C). When the XPS survey specta of Ag-GO nanostructure is investigated, C=C or sp^2 component related to GO is seen at 284.5 eV, just as in the previous ones. Figure 3C and S4 also shows Ag 3d5/2 and 3d3/2 core levels at around 366 and 372 eV, respectively, corresponding to the binding energies of silver ions (Ag^+) originated from Ag_2O [18]. It is clear that the silver nanoparticle itself was oxidized with the reduction of GO simultaneously. The split between the 3d doublet of Ag is around 6.0 eV, suggesting the formation of metallic silver nanoparticles [19]. Similar results could be found in the literature [20]. Figure 2D shows the TEM image of multilayer GO-AgNPs nanostructure. As indicated with yellow arrows, seperate GO nanosheets were binded each other via hydrazine chemistry while keeping the silver nanoparticle at the interface. Formation of a 3D structure like seen in Figure 2D is a proof of this concept. Although the individual AgNPs cannot be recognised in this thick structure, it can be easily observed in a less layered structure (Figure S5) that the size of the nanoparticles are nearly same with the previous one. The layers and the nanoparticles on different layers can also be recognised considering the contrast difference in this top view image. For instance, the Ag nanoparticle marked with red arrow is darker than the one marked with green. Besides, the layer indicated with yellow arrow is brighter than that indicated with blue, that also demonstrate the multilayer structure. An XPS pattern similar to GO-AgNPs is also seen in XPS diagram of M-GO-AgNPs, that shows the success

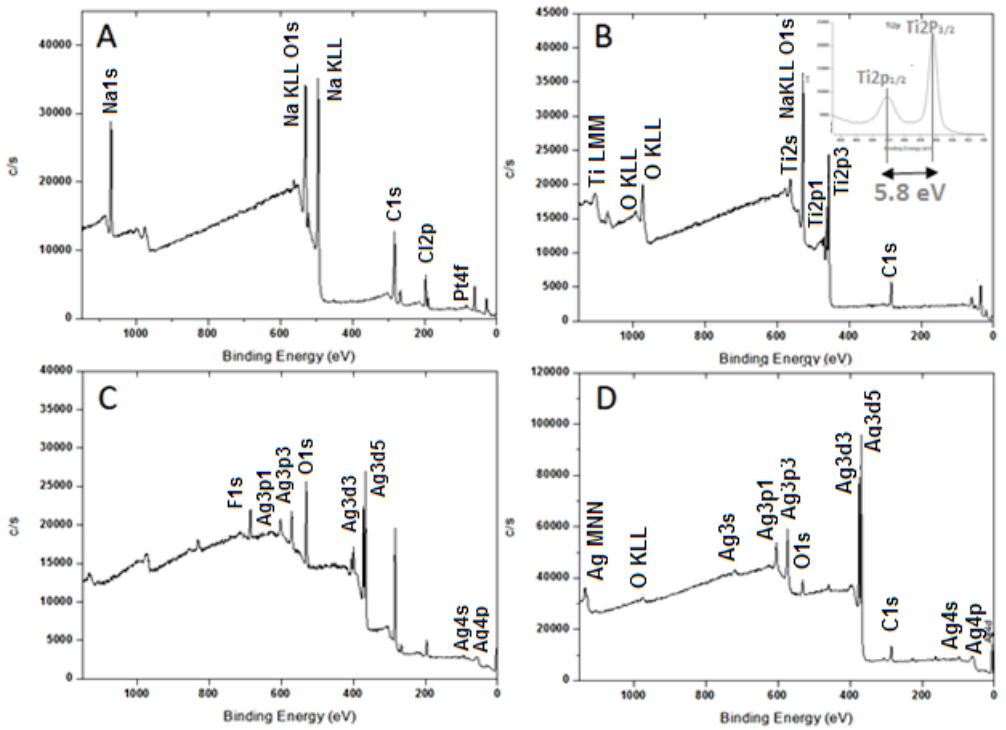

Figure 3. XPS spectra of (A) GO-PtNPs, (B) GO-TiNPs, (C) GO-AgNPs, and (D) M-GO-AgNPs nanostructures.

of formation of the nanostructure (Figure 3D and S6). The big difference in peak intensity of silver ions between GO-AgNPs (for instance, the peak intensities of Ag3d are c.a. 25-30.000 c/s) and M-GO-AgNPs (the peak intensities of Ag3d are c.a. 70-80.000 c/s) supports the formation of multilayer structure, at which silver nanoparticles are entrapped between GO layers and thus improved the peak intensity of silver ions. Last of all, it can be said that all nanostructures were successfully prepared considering the XPS results.

Peroxidase-Like Activity of Doped GO Nanostructures

Obtained nanostructures were dropwise modified on SPCE in order to investigate their peroxidase-like activity. For a comperative study, nanostructure modified electrodes including HRP enzyme were aslo prepared. The amperometric responses of the electrodes against 10 mM H_2O_2 is seen in Figure 4.

Examining Figure 4, three main conclusions can be drawn. First, considering the metal nanoparticles doped GO, the amperometric response of Pt and Ag doped GO are higher than that of TiO_2 doped GO. This is not an unexpected result. Silver is more conductive, as commonly known, than platinum and titanium. TiO_2 nanoparticle, on the other hand, is less conductive than platinum due to its semiconducture nature. GO-PtNPs modified electrode exhibits a more efficient electrochemical response than GO-AgNPs as shown in Figure 4, which is tought to be a result of dopping efficiency diversity. Yet, this difference is too small. Secondly, a slight decrease in the amperometric response of the modified electrodes, except GO-TiNPs, was observed following the enzyme immobilization. This result is interesting and shows that the electrochemical activity of the doped GOs obtained for a 10 mM H_2O_2 concentration is better than that uses HRP as electrocatalyst. Since enzyme immobilization also produces a resistance at the electrode surface, the enzyme-immobilized electrodes show a somewhat lower response. However, this is only true for low peroxide concentrations like 50 mM H_2O_2.

Investigation of the Effect of Modification Techniques

In this study, two different approaches were employed to achieve the most effective modification technique. The first technique includes dropwise addition of the prepared nanostructures onto SPCE, while the second

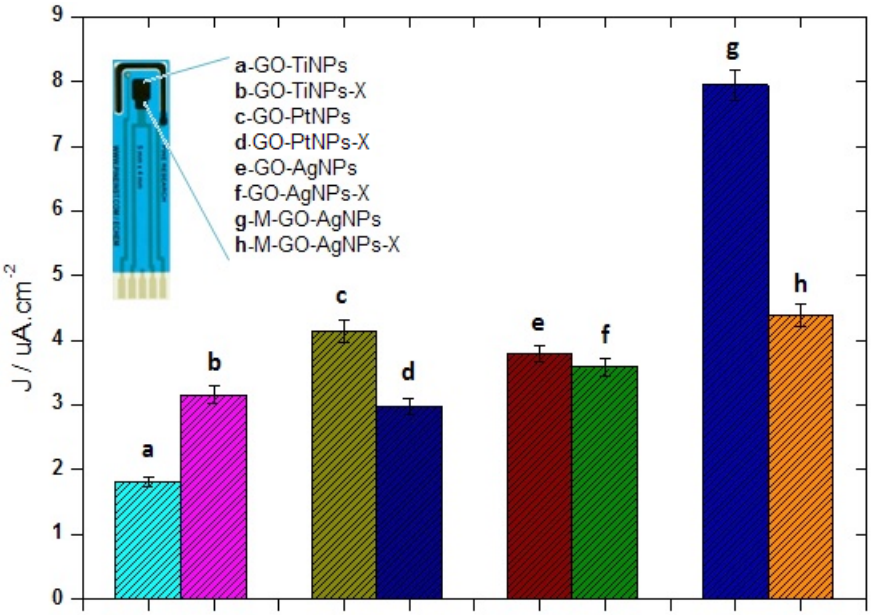

Figure 4. Amperometric responses of (a) GO-TiNPs, (b) GO-TiNPs-X, (c) GO-PtNPs, (d) GO-PtNPs-X, (e) GO-AgNPs, (f) GO-AgNPs-X, (g) M-GO-AgNPs, and (h) M-GO-AgNPs-X to 10 **m**M H_2O_2.

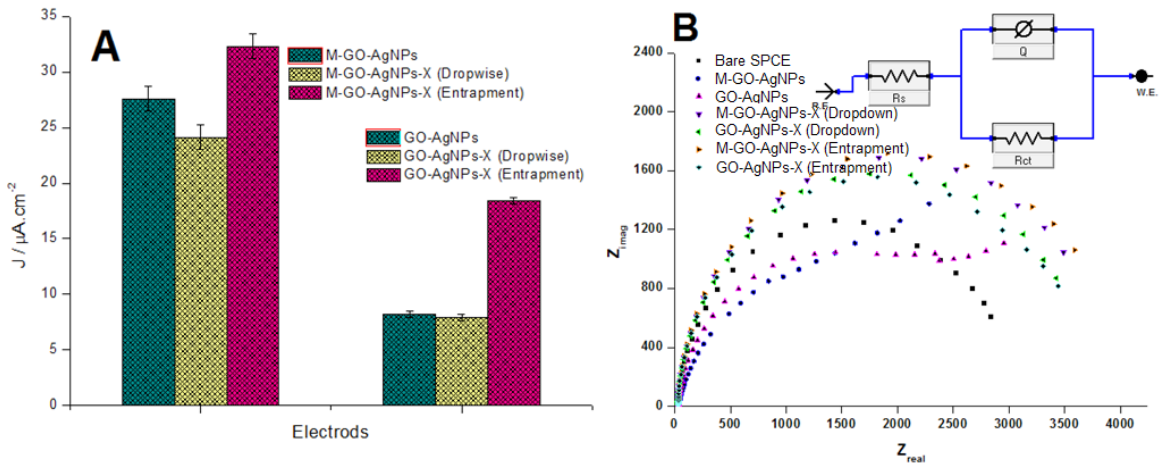

Figure 5. (A) Column graph showing amperometric responses of different enzyme immobilization methods against 50 µM H_2O_2 addition: Dropwise or entrapment. **(B)** Impedimetric diagram showing different modification steps.

technique was based on the electrochemical entrapment of the doped GO nanostructures together with enzymes. Amperometric peak intensity of the electrodes developed using dropwise addition of GO-AgNPs-X and M-GO-AgNPs-X were around 6 and 23.5 mA, respectively, wherease the peak intensity of the GO-AgNPs-X and M-GO-AgNPs-X electrodes prepared with electrochemical entrapment were 18 and 32 mA, respectively (Figure 5A). Amperometric study showed that the entrapment technique enabled a more efficient enzyme immobilization compared to dropwise addition. In addition, the difference of electrochemical performance between GO-AgNPs-X and M- GO-AgNPs-X can be clearly seen in this graph. Differently, the current intensity of the enzyme electrode was seen to increased when the entrapment technique was used. Nyquiste plote that is seen in Figure 5B supported the amperometric study.

Electrokinetic Study

The plots of the peak potential (Ep_a, Ep_c) vs the natural logarithm of scan rate (lnυ) for GO-

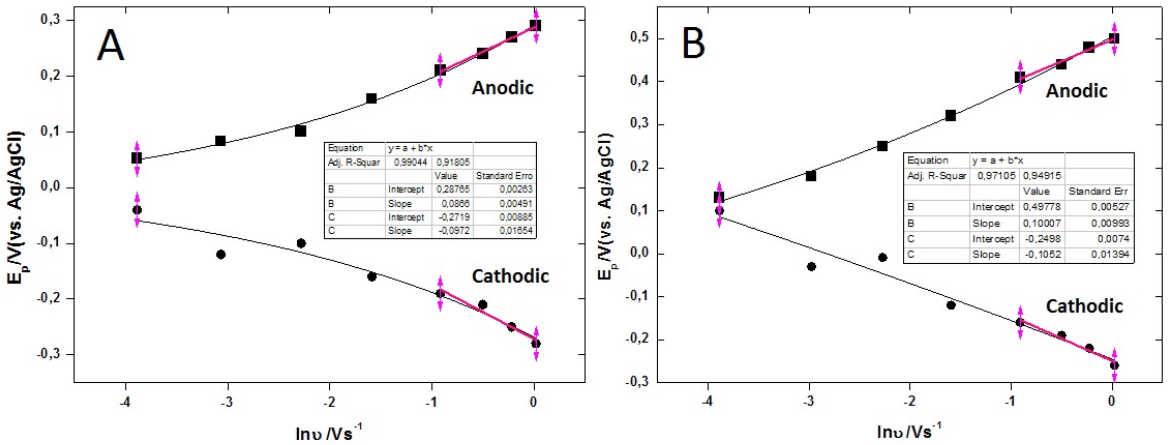

Figure 6. Inυ/Ep graph related to GO-AgNPs **(A)** and M-GO-AgNPs **(B)** nanostructure modified electrode to be used for the calculation of kinetic parameters.

AgNPs (Figure 6A) and M-GO-AgNPs (Figure 6B) electrodes were obtained by CV in 0.5 mM $Fe(CN)_6^{3-/4-}$/0.1 M KCl solution in the potential range of -400 to +600 mV. Utilizing the equations above, the a values that are corresponded to electron transfer coefficients were calculated for GO-AgNPs and M-GO-AgNPs electrodes as $a_{cathodic,}$ = 0.13, a_{anodic} = 0.85, $a_{cathodic}$ = 0.12, a_{anodic} = 0.87, respectively. Using Laviron's equations, the electron transfer rate constant (ks) values were calculated as ks_{anodic}= 6.62 s^{-1} and ks_{anodic}= 6.78 s^{-1} for GO-AgNPs and M-GO-AgNPs, respectively. The results showed that the electron transfer rate constant of the electrode including M-GO-AgNPs to be higher than that of the other electrode. However the difference was abut 2.5%.

CONCLUSION

Various GO based nanostructures such as GO-TiNPs, GO-PtNPs, GO-AgNPs and multilayer GO-AgNPs that aims to improve the electrochemical performace of enzymatic biosensors or to mimick them could be successfully synthesized using sonochemical technique and characterized in detail. The prefered amperometric method results showed that the GO-AgNPs enabled a more effective catalysis of H_2O_2. What is more, the multilayer GO-AgNPs, that is M-GO-AgNPs, was superior and showed nearly 2 times more intense amperometric response compared to other nanostructures. This electrochemical result was supported by TEM and XRD. An apparent and well ordered layer-by-layer structure was observed from TEM micrograph. In addition, having a more intensive XPS signal in multilayer structure is a proof of nanoparticle trapping. To optimize and get a better amperometric result, two different electrode modification strategy was studied. Entrapment technique was seen to more efficient in terms of catalyzing the reaction compared to dropwise modification. Finally, the M-GO-AgNPs nanostructure is tought to be used as electrochemical biosensor matrix and it's a suitable candidate for enzyme-free electrochemical sensors.

References

1. J. Liu, X. Bo, Z. Zhao, L. Guo, Highly exposed Pt nanoparticles supported on porous graphene for electrochemical detection of hydrogen peroxide in living cells, Biosens. Bioelectron., 74 (2015) 71-77.
2. Z. Liu, Y. Guo, C. Dong, A high performance nonenzymatic electrochemical glucose sensor based on polyvinylpyrrolidone–graphene nanosheets–nickel nanoparticles–chitosan nanocomposite, Talanta, 137 (2015) 87-93.
3. G. Giovannetti, P.A. Khomyakov, G. Brocks, V.M. Karpan, J. van den Brink, and P.J. Kelly, Doping Graphene With Metal Contacts, Phys. Rev. Let., 101 (2008) 268031-268034.
4. B. Uchoa, C.Y. Lin, and A.H. Castro Neto, Tailoring graphene with metals on top, Phys. Rev. B, 77 (2008) 035421-035425.
5. G.M. Scheuermann, L. Rumi, P. Steurer, W. Bannwarth, R. Mulhaupt, Palladium nanoparticles on graphite oxide and its functionalized graphene derivatives as highly active catalysts for the Suzuki–Miyaura coupling reaction, J. Am. Chem. Soc., 131, 2009, 8262-8270.
6. Y. Li, L. Tang, J. Li, Preparation and electrochemical performance for methanol oxidation of pt/graphene nanocomposites, Electrochem. Commun., 11 (2009) 846-849.

7. T. Maiyalagan, X. Dong, P. Chen, X. Wang, Electrodeposited Pt on three-dimensional interconnected graphene as a free-standing electrode for fuel cell application, J. Mater. Chem., 22 (2012) 5286-5290.
8. K.S. Suslick, Ultrasound: Its chemical, physical and biological effects, VCH Verlagsgesellschaft, Weinheim, Germany, 1988.
9. B. Neppolian, C. Wang, Muthupandian Ashokkumar. Sonochemically synthesized mono and bimetallic Au-Ag reduced graphene oxide based nanocomposites with enhanced catalytic activity, Ultrason. Sonochem., 21 (2014) 1948-1953.
10. B. Neppolian, A. Bruno, C.L. Bianchi, M. Ashokkumar, Graphene oxide based Pt-TiO_2 photocatalyst: Ultrasound assisted synthesis, characterization and catalytic efficiency, Ultrason. Sonochem., 19 (2012) 9-15.
11. S. Zhu, J. Guo, J. Dong, Zn Cui, T. Lu, C. Zhu, D. Zhang, J. Ma, Sonochemical fabrication of Fe_3O_4 nanoparticles on reduced graphene oxide for biosensors, Ultrason. Sonochem., 20 (2013) 872-880.
12. L. Zhu, J.D. Chung, W.C. Oh, Rapid sonochemical synthesis of novel PbSe-graphene-TiO_2 composite sonocatalysts with enhanced on decolorization performance and generation of ROS, Ultrason. Sonochem., 27 (2015) 252-261.
13. M. Giovanni, H.L. Poh, A. Ambrosi, G. Zhao, Z. Sofer, F. Sanek, B. Khezri, R.D. Webster and M. Pumera, Noble metal (Pd, Ru, Rh, Pt, Au, Ag) doped graphene hybrids for electrocatalysis, Nanoscale, 4 (2012) 5002.
14. E. Laviron, General expression of the linear potential sweep voltammogram in the case of diffusionless electrochemical systems, J. Electroanal. Chem. 101 (1979) 19-28.
15. H.L. Wang, L.F. Cui, Y.A. Yang, H.S. Casalongue, J.T. Robinson, Y.Y. Liang, Y. Cui, H.J. Dai, J. Am. Chem. Soc., 132 (2010) 13978-13980.
16. G. Jiang, Z. Lin, C. Chen, L. Zhu, Q. Chang, N. Wang, W. Wei, H. Tang, TiO_2 nanoparticles assembled on graphene oxide nanosheets with high photocatalytic activity for removal of pollutants, Carbon, 49 (2011) 2693-2701.
17. J. Guo, S. Zhu, Z. Chen, Y. Li, Z. Yu, Q. Liu, J. Li, C. Feng, D. Zhang, Sonochemical synthesis of TiO_2 nanoparticles on graphene for use as photocatalyst, Ultrason. Sonochem., 18 (2011) 1082-1090.
18. E. Sumesh, M.S. Bootharaju, A.T. Pradeep, A practical silver nanoparticle-based adsorbent for the removal of Hg^{2+} from water, J. Hazard. Mater. 189 (2011) 450.
19. C. Gunawan, W.Y. Teoh, C.P. Marquis, J. Lifia and R. Amal, Reversible antimicrobial photoswitching in nanosilver, Small, 5 (2009) 341-344.
20. P. Prieto, V. Nistor, K. Nouneh, M. Oyama, M.A. Lefdil, R. Díaz, XPS study of silver, nickel and bimetallic silver-nickel nanoparticles prepared by seed-mediated growth, Appl. Surf. Sci., 258 (2012) 8807.

Arylidene Carbazole Carbohydrazides: Synthesis and Characterization

Ariliden Karbazol Hidrazitler: Sentezi ve Karakterizasyonu

Research Article

Cevher Gündoğdu Hızlıateş
Department of Chemistry, Faculty of Sciences, Dokuz Eylul University, Buca, Izmir, Turkey.

ABSTRACT

Because of the wide range of pharmacological activities and their distinctive structural features hydrazones and carbazole alkaloids have attracted considerable attention in medicinal chemistry. In this study, new carbazole acyl hydrozones (3a-k) which may have high biological activity potential, were synthesized with condensation reaction between carbazole hydrazide and benzaldehyde derivatives. After determination of the melting points of all synthesized derivatives, their structures were identified by FT-IR and ^{1}H-NMR spectroscopic methods.

Key Words
Carbazole, carbohydrazide, hydrazide-hydrazone, biological activity.

ÖZ

Geniş farmakolojik etkinlikleri ve kendine özgü yapısal özellikleri nedeniyle, hidrazonlar ve karbazol alkaloitleri tıbbi kimyada büyük ilgi görmektedir. Bu çalışmada, karbazol hidrazit bileşiği ile benzaldehit türevleri arasındaki kondenzasyon reaksiyonu ile yüksek biyolojik aktiflik potansiyeline sahip olabilecek yeni karbazol açil hidrazon türevleri (3a-k) sentezlenmiştir. Sentezlenen türevlerin erime noktaları belirlendikten sonra, yapıları FT-IR ve 1H-NMR spektroskopik yöntemleri ile aydınlatılmıştır.

Anahtar Kelimeler
Karbazol, karbohidrazit, hidrazit-hidrazon, biyolojik aktiflik.

Article History: Dec 13, 2017; Revised: Feb 27, 2018; Accepted: Feb 28, 2018; Available Online: Mar 26, 2018.

DOI: 10.15671/HJBC.2018.226

Correspondence to: C. Gündoğdu Hızlıateş, Department of Chemistry, Faculty of Sciences, Dokuz Eylul University, Izmir, Turkey.
Tel: +90 232 301 79 09 Fax: +90 0232 453 41 88 E-Mail: cevher.gundogdu@deu.edu.tr

INTRODUCTION

Studies on the diagnosis and treatment of cancer, which is one of the most common diseases of our age, are increasing day by day. The discovery of new medicines and agents in cancer treatment is very important because the number of drugs used in the treatment of cancer disease is insufficient and the side effects are too high.

Hydrazide-hydrazone derivatives are important compounds for pharmaceutical chemistry. The biological activity associated with these compounds was attributed to the presence of the (–CONHN=CH–) moiety. Because of their broad spectrum of biological activities such as anticonvulsant [1,2], antidepressant [3], analgesic and antiinflammatory [4], antiplatelet [5], antimalarial [6], antimicrobial [4,7,8], anti tuberculosis [9-14], antitumoral [15,16] activities, there are lots of study about hydrazides. Especially antitumor activity researches about hydrazide derivatives are important for breast [17,18], ovarian [19], renal [20], prostate [16] cancer.

Carbazole alkaloids have been had significant pharmacological activities such as anti-microbial [21], anti-tumor [22,23], anti-HIV [24], anti-oxidant [25] activity since their discovery and the attention on carbazole alkaloids has increased rapidly. The studies until today show that carbazole alkaloids and it's synthetic derivatives have cytotoxic, apoptosis inducing and antiproliferating activities on pancreatic [26], leukemia [27,28], prostate [29] and lung [30] cancer.

In this study, by combining these two biologically active groups, carbazole bearing new arylidene carbohydrazide derivatives were synthesized. After determination of the melting points of all synthesized derivatives, their structures were identified by FT-IR and ^{1}H-NMR spectroscopic methods.

MATERIALS and METHODS

Chemicals and Instrument

All solvents and chemicals were used as purchased without further purification. Thin-layer chromatography (TLC) was conducted on aluminium sheets coated with silica gel 60 F_{254}, obtained from Merck (Darmstadt, Germany)., with visualisation by UV lamp (254 or 360 nm). Column chromatography was carried out with silica gel 60 (particle size 0.040-0.063 mm, 230-400 mesh; (Merck, Darmstadt, Germany) and commercially available solvents. All melting points were measured on a Gallenkamp melting-point apparatus in open capillaries and are uncorrected. For characterization of synthesized molecules, Fourier transform infrared spectroscopy (FTIR) analysis was studied with PerkinElmer Spectrum BX-II Model FTIR spectrophotometer. The samples within KBr pellets were measured in the range of 4000 and 400 cm^{-1}. Proton (^{1}H) NMR spectra was obtained on a Varian AS-400 NMR spectrometer with tetramethylsilane as an internal standard.

Synthesis of 4-Methyl-9H-carbazole-3-carbohydrazide (2)

Ethyl 4-methyl-9H-carbazole-3-carboxylate, (10 g, 39.5 mmol) was refluxed with hydrazine hydrate (25 mL, 80%) in ethanol (50 mL) for 6 h (Scheme 1). After cooling the separated solid was filtered. The compound was obtained as white needles (8.5 g, 90%), mp: 290-292ºC. IR (KBr, ν_{max}, cm^{-1}): 3159 (NH), 3280 (NH), 2974 (CH), 1684 (C=O). ^{1}H NMR (DMSO-d_6): 2.85 (s, 3H, CH_3), 4.47 (s, 2H, NH_2), 7.20 (t, 1H, J= 8.0 Hz, ArH), 7.31-7.37 (m, 2H, ArH), 7.41 (t, 1H, J= 8.0 Hz, ArH), 7.53 (d, 1H, J= 8.0 Hz, ArH), 8.18 (d, 1H, J= 7.6 Hz, ArH), 9.32 (s, 1H, CONH), 11.42 (s, 1H, NH).

General Procedure for the Synthesis of Carbazole Acyl Hydrazone Derivatives (3a-k)

Carbazole hydrazide 2 (5 mmol) was refluxed with benzaldehyde derivatives (5 mmol) in the presence of one drop of glacial acetic acid in ethanol (25 mL) for 4 h (Scheme 1). Then the reaction mixture was cooled and precipitate was filtered. The crude product was recrystallized from ethanol yielded carbazole acyl hydrazone derivatives.

N'-Benzylidene-4-methyl-9H-carbazole-3-carbohydrazide (3a)

Yield: 70%; mp: 312-314ºC. IR (KBr, ν_{max}, cm^{-1}): 3246 (NH), 3214 (NH), 3054 (CH), 1631 (C=O), 1540 (C=N). ^{1}H NMR (400 MHz, DMSO-d_6): δ 2.92 (s, 3H, CH_3), 7.23 (t, 2H, J= 7.2 Hz, ArH), 7.41-7.57 (m, 6H, ArH), 7.74 (d, 2H, J= 7.2 Hz, ArH), 8.22 (d, 1H, J= 7.2 Hz, ArH), 8.37 (s, 1H, N=CH), 11.52 (s, 1H, CONH), 11.73 (s, 1H, NH).

N′-(4-Fluorobenzylidene)-4-methyl-9H-carbazole-3-carbohydrazide (3b)

Yield: 67%; mp: 299-302ºC. IR (KBr, ν_{max}, cm^{-1}): 3222 (NH), 3068 (CH), 1636 (C=O), 1547 (C=N). ^{1}H NMR (400 MHz, DMSO-d_6): δ 2.90 (s, 3H, CH_3), 7.23 (t, 1H, J= 7.2 Hz, ArH), 7.30 (t, 2H, J= 8.4 Hz, ArH), 7.40-7.46 (m, 2H, ArH), 7.51 (d, 1H, J= 8.4 Hz, ArH), 7.55 (d, 1H, J= 8.0 Hz, ArH), 7.79 (t, 2H, J= 7.6 Hz, ArH), 8.21 (d, 1H, J= 8.0 Hz, ArH), 8.34 (s, 1H, N=CH), 11.52 (s, 1H, CONH), 11.73 (s, 1H, NH).

N′-(4-Chlorobenzylidene)-4-methyl-9H-carbazole-3-carbohydrazide (3c)

Yield: 62%; mp: 271-273ºC. IR (KBr, ν_{max}, cm^{-1}): 3285 (NH), 3203 (NH), 3049 (CH), 1618 (C=O), 1535 (C=N). ^{1}H NMR (400 MHz, DMSO-d_6): 2.88 (s, 3H, CH_3), 7.21 (d, 1H, J= 8.0 Hz, ArH), 7.34-7.55 (m, 6H, ArH), 7.74 (d, 2H, J= 8.4 Hz, ArH), 8.20 (d, 1H, J= 7.6 Hz, ArH), 8.31 (s, 1H, N=CH), 11.50 (s, 1H, CONH), 11.76 (s, 1H, NH).

N′-(4-Bromobenzylidene)-4-methyl-9H-carbazole-3-carbohydrazide (3d)

Yield: 72%; mp: 281-283ºC. IR (KBr, ν_{max}, cm^{-1}): 3289 (NH), 3199 (NH), 3047 (CH), 1622 (C=O), 1537 (C=N). ^{1}H NMR (400 MHz, DMSO-d_6): δ 2.90 (s, 3H, CH_3), 7.22 (t, 1H, J= 7.6 Hz, ArH), 7.40-7.52 (m, 4H, ArH), 7.55 (d, 1H, J= 8.0 Hz, ArH), 7.65-7.74 (m, 3H, ArH), 8.21 (d, 1H, J= 8.0 Hz, ArH), 8.31 (s, 1H, N=CH), 11.52 (s, 1H, CONH), 11.78 (s, 1H, NH).

4-Methyl-N′-(4-methylbenzylidene)-9H-carbazole-3-carbohydrazide (3e)

Yield: 70%; mp: 339-340ºC. IR (KBr, ν_{max}, cm^{-1}): 3226 (NH), 3048 (CH), 1625 (C=O), 1542 (C=N). ^{1}H NMR (400 MHz, DMSO-d_6): 2.35 (s, 3H, CH_3), 2.90 (s, 3H, CH_3), 7.22 (t, 1H, J= 7.2 Hz, ArH), 7.27 (d, 2H, J= 8.0 Hz, ArH), 7.38-7.46 (m, 2H, ArH), 7.50 (d, 1H, J= 8.4 Hz, ArH), 7.55 (d, 1H, J= 8.0 Hz, ArH), 7.62 (d, 2H, J= 8.4 Hz, ArH), 8.21 (d, 1H, J= 8.4 Hz, ArH), 8.30 (s, 1H, N=CH), 11.52 (s, 1H, CONH), 11.65 (s, 1H, NH).

N′-(4-tert-Butylbenzylidene)-4-methyl-9H-carbazole-3-carbohydrazide (3f).

Yield: 65%; mp: 268-270ºC. IR (KBr, ν_{max}, cm^{-1}): 3402 (NH), 3212 (NH), 2960 (CH), 1632 (C=O), 1538 (C=N). ^{1}H NMR (400 MHz, DMSO-d_6): 1.29 (s, 3H, $C(CH_3)_3$), 2.90 (s, 3H, CH_3), 7.20 (t, 1H, J= 8.4 Hz, ArH), 7.37-7.48 (m, 4H, ArH), 7.50 (d, 1H, J= 8.4 Hz, ArH), 7.54 (d, 1H, J= 8.4 Hz, ArH), 7.65 (d, 2H, J= 8.4 Hz, ArH), 8.19 (d, 1H, J= 8.0 Hz, ArH), 8.31 (s, 1H, N=CH), 11.53 (s, 1H, CONH), 11.69 (s, 1H, NH).

N′-(4-Hydroxybenzylidene)-4-methyl-9H-carbazole-3-carbohydrazide (3g)

Yield: 64%; mp: 293-294ºC. IR (KBr, ν_{max}, cm^{-1}): 3582 (NH), 3260 (NH), 3200 (OH), 3070 (CH), 1635 (C=O), 1581 (C=N). ^{1}H NMR (400 MHz, DMSO-d_6): δ 2.48 (s, 3H, CH_3), 6.79 (d, 2H, J= 8.0 Hz, ArH), 7.19 (t, 1H, J= 7.6 Hz, ArH), 7.32-7.56 (m, 6H, ArH), 8.14-8.20 (m, 2H, ArH, N=CH), 11.49 (s, 1H, CONH), 11.67 (s, 1H, NH).

N′-(4-Methoxybenzylidene)-4-methyl-9H-carbazole-3-carbohydrazide (3h)

Yield: 73%; mp: 319-321ºC. IR (KBr, ν_{max}, cm^{-1}): 3254 (NH), 3075 (CH), 1616 (C=O), 1547 (C=N). ^{1}H NMR (400 MHz, DMSO-d_6): 2.89 (s, 3H, CH_3), 3.80 (s, 3H, OCH_3), 7.01 (d, 2H, J= 7.6 Hz, CH_3O-ArH), 7.21 (t, 1H, J= 8.0 Hz, ArH), 7.35-7.44 (m, 2H, ArH), 7.48 (d, 1H, J= 8.0 Hz, ArH), 7.52 (d, 1H, J= 8.0 Hz, ArH), 7.67 (d, 2H, J= 7.6 Hz, ArH), 8.20 (d, 1H, J= 8.0 Hz, ArH), 8.26 (s, 1H, N=CH), 11.50 (s, 1H, CONH), 11.59 (s, 1H, NH).

N′-(4-(Dimethylamino)benzylidene)-4-methyl-9H-carbazole-3-carbohydrazide (3i)

Yield: 68%; mp: 313-315ºC. IR (KBr, ν_{max}, cm^{-1}): 3269 (NH), 2909 (CH), 1643 (C=O), 1552 (C=N). ^{1}H NMR (400 MHz, DMSO-d_6): 2.88 (s, 3H, CH_3), 2.95 (s, 6H, $N(CH_3)_2$), 6.55 (d, 2H, J= 8.0 Hz, $(CH_3)_2$N-ArH), 7.18 (t, 1H, J= 7.6 Hz, ArH), 7.35-7.55 (m, 6H, ArH), 8.18-8.21 (m, 2H, ArH and N=CH), 11.42 (s, 1H, CONH), 11.50 (s, 1H, NH).

4-Methyl-N′-(4-nitrobenzylidene)-9H-carbazole-3-carbohydrazide (3j)

Yield: 73%; mp: 288-289ºC. IR (KBr, ν_{max}, cm^{-1}): 3267 (NH), 1654 (C=O), 1529 (C=N). ^{1}H NMR (400 MHz, DMSO-d_6): 2.94 (s, 3H, CH_3), 7.23 (t, 1H, J= 7.6 Hz, ArH), 7.42-7.60 (m, 4H, ArH), 7.92-8.30 (m, 5H, ArH), 8.46 (s, 1H, N=CH), 11.55 (s, 1H, CONH), 12.05 (s, 1H, NH).

N′-(4-Cyanobenzylidene)-4-methyl-9H-carbazole-3-carbohydrazide (3k)

Yield: 67%; mp: 268-269ºC. IR (KBr, ν_{max}, cm^{-1}): 3374 (NH), 3207 (NH), 3053 (CH), 2232 (CN), 1647 (C=O), 1537 (C=N). ^{1}H NMR (400 MHz, DMSO-d_6): δ 2.90 (s, 3H, CH_3), 7.21 (d, 1H, J= 7.6 Hz, ArH), 7.39-

7.57 (m, 5H, ArH), 7.82-7.94 (m, 3H, ArH), 8.19 (d, 1H, J= 7.2 Hz, ArH), 8.38 (s, 1H, N=CH), 11.54 (s, 1H, CONH), 11.98 (s, 1H, NH).

RESULTS and DISCUSSION

In this work, firstly carbazole carbohydrazide compound was synthesized. And then via condensation reaction with various benzaldehyde derivatives and carbazole carbohydrazide compound, arylidene carbazole carbohydrazide derivatives were obtained (Scheme 1). After determination of the melting points of all synthesized derivatives, their structures were identified by FT-IR and ^{1}H-NMR spectroscopic methods.

From the spectroscopic studies, IR spectra of the target hydrazones showed NH (indol) stretching bands in the range 3222-3582; NH stretching bands in the range 3199-3269; C=O stretching bands in the range 1616–1654 and C=N stretching bands in the range 1529-1581 cm^{-1}, respectively. In the ^{1}H NMR spectra of the Arylidene Carbazole Carbohydrazide derivatives , the azomethine –N=CH- proton appeared at 8.20-8.46 ppm as a sharp singlet, and whereas characteristic of the –CONH- group at 11.42-11.55 ppm was a broad singlet. The singlet peaks which appeared at 11.50-12.05 ppm were indole NH protons. The other protons appeared at the expected chemical shifts and integral values.

N-acylhydrazones can exist in four possible forms (Scheme 2). In respect to C=N two of them are geometrical isomers (E/Z) and the other two rotamers (antiperiplanar (*Ap*) and synperiplanar (Sp)) about amide N-CO (Figure 1). According to the literature, because of the steric hindrance $Z_{C=N}$ conformer is not reliazed [31,32]. Similarly, the existence of non-plannar form of C=N-NH moiety can be ruled out as it would disturb the n-π conjugation thereby the energy of stabilization [32]. So that N-acylhydrazones which are derived from aromatic aldehydes are expected in $E_{C=N}$ form according to the X-ray data of the Syakaev's study and the ratio of rotamers present in solution can be calculated from the ^{1}H NMR spectra of each compound [33]. In another previous study some tetrahydrocarbazole derivatives were synthesized and their conformer properties were studied by energetically calculations. And they had found that in solution two $E_{C=N}$ isomers are more stable than $Z_{C=N}$ and the most stable conformer is $E_{C=N}Ap_{C(O)-N}$ [34].

In former works it was suggested that when an aromatic structure was connected to the amide bond (ArCO-NH-), because of the sp^2 hybridizied C atoms a rotation around C(O)-N was not observed. So that this type of compounds can be in only one conformational structure that is $E_{C=N}$ which is the most stable conformer [35-38].

According to this results when we analyzed ^{1}H NMR spectras of the Arylidene Carbazole Carbohydrazide derivatives (for example Figure 2), only one set of signal was observed for all spesific groups such as –CO-NH- and –N=CH-.

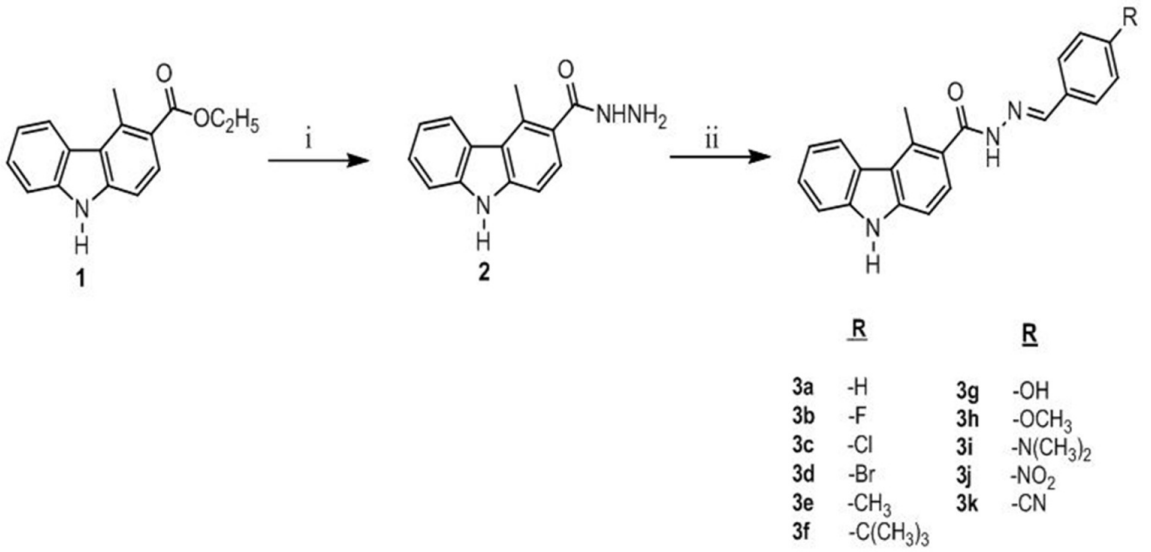

Scheme 1. Synthesis route of Some Arylidene Carbazole Carbohydrazides. Reagent and Conditions: i) $NH_2NH_2.H_2O$, ethanol, reflux, 4h; ii) ArCHO, ethanol, AcOH, reflux, 6h.

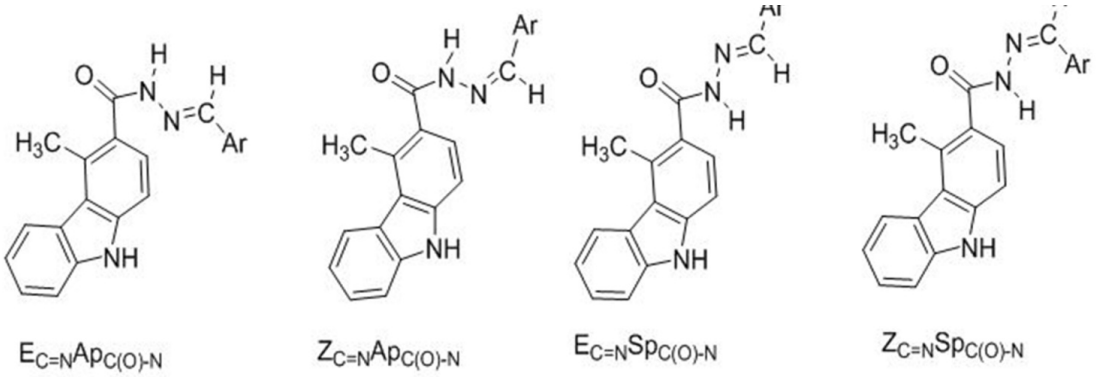

Scheme 2. Possible structures for E and Z conformers of 3a-k.

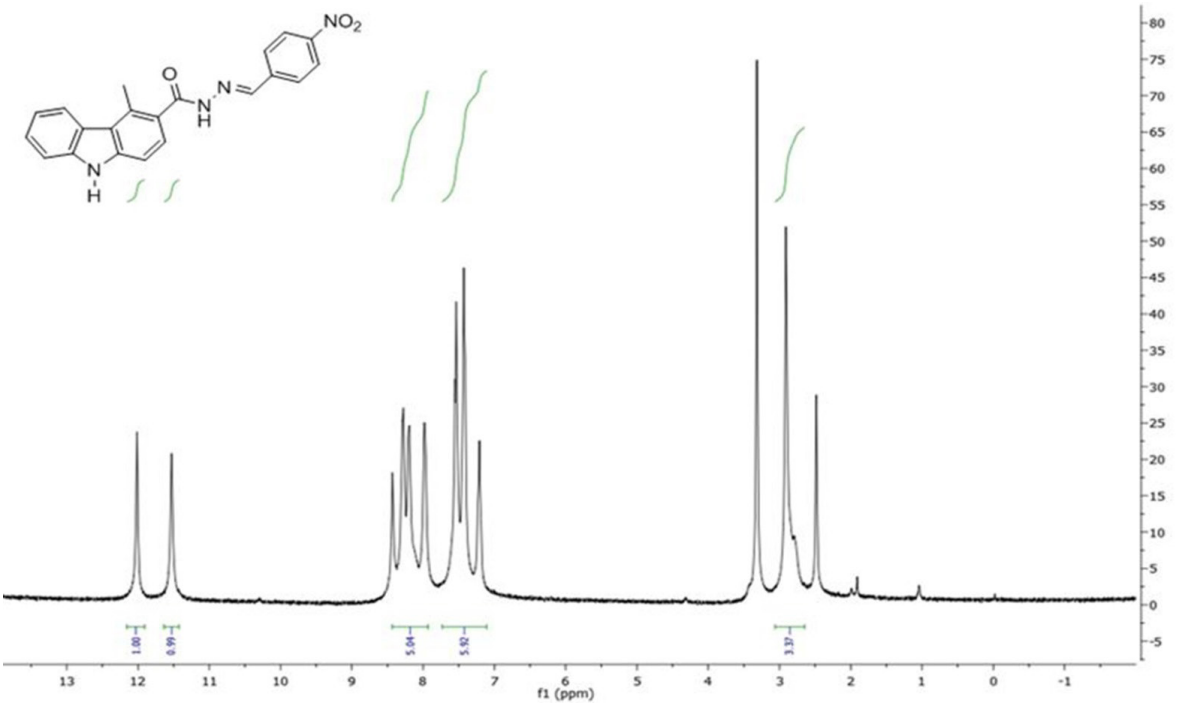

Figure 1. ^{1}H NMR spectrum of 4-Methyl-N'-(4-nitrobenzylidene)-9H-carbazole-3-carbohydrazide (3j) in DMSO-d_6.

Because of the aromatic carbazole moiety there is not a rotation around the C(O)-N bond and so there is only $E_{C=N}$ conformational structure in our solutions.

Because of the wide pharmacological activities of the hydrazide derivaties and carbazole alkaloids, the new synthesized Arylidene Carbazole Carbohydrazide derivatives whose yields are in the range 62-73%, may have high biological activity potential.

References

1. J.R. Dimmock, S.C. Vashishtha, J.P. Stables, Anticonvulsant properties of various acetylhydrazones, oxamoylhydrazones and semicarbazones derived from aromatic and unsaturated carbonyl compounds, Eur. J. Med. Chem., 35 (2000) 241-248.
2. J. Ragavendran, D. Sriram, S. Patel, I. Reddy, N. Bharathwajan, J. Stables, Design and synthesis of anticonvulsants from a combined phthalimide-GABA-anilide and hydrazone pharmacophore, Eur. J. Med. Chem., 42 (2007) 146-151.
3. N. Ergenç, N.S. Günay, Synthesis and antidepressant evaluation of new 3-phenyl-5-sulfonamid indole derivatives, Eur. J. Med. Chem., 33 (1998) 143-148.
4. A.R. Todeschini, A.L. Miranda, C.M. Silva, S.C. Parrini, E.J. Barreiro, Synthesis and evaluation of analgesic, antiinflammatory and antiplatelet properties of new 2-pyridylarylhydrazone derivatives, Eur. J. Med. Chem., 33 (1998) 189-199.

5. A.G.M. Fraga, C.R. Rodrigues, A.L.P. Miranda, E.J. Barreiro, C.A.M. Fraga, Synthesis and pharmacological evaluation of novel heterocyclic acylhydrazone derivatives, designed as PAF antagonists, Eur. J. Pharm. Sci., 11 (2000) 285-290.
6. Walcourt, M. Loyevsky, D.B. Lovejoy, V.R. Gordeuk, D.R. Richardson, Novel aroylhydrazone and thiosemicarbazone iron chelators with anti-malarial activity against chloroquine-resistant and -sensitive parasites, Int. J. Biochem. Cell Biol., 36 (2004) 401-407.
7. P. Vicini, F. Zani, P. Cozzini, I. Doytchinova, Hydrazones of 1,2-benzisothiazole hydrazides: synthesis, antimicrobial activity and QSAR investigations, Eur. J. Med. Chem., 37 (2002) 553-564.
8. J. Jayabharathi, A. Thangamani, M. Padmavathy, B. Krishnakumar, Synthesis and microbial evaluation of novel N(1)-Arilidene-N(2)-t(3)-methyl-r(2), c(6)-diaryl-piperidin-4-one azine derivatives, Med. Chem. Res., 15 (2007) 431-442.
9. MT. Cocco, C. Congiu, V. Onnis, MC. Pusceddu, ML. Schivo, A. Logu, Synthesis and antimycobacterial activity of some isonicotinoylhydrazones, Eur. J. Med. Chem., 34 (1999) 1071-1076.
10. S.G. Küçükgüzel, S. Rollas, I. Küçükgüzel, M. Kiraz, Synthesis and antimycobacterial activity of some coupling products from 4-aminobenzoic acid hydrazones, Eur. J. Med. Chem., 34 (1999) 1093-1100.
11. B.K. Kaymakçıoğlu, S. Rollas, Synthesis, characterization and evaluation of antituberculosis activity of some hydrazones, Farmaco, 57 (2002) 595-599.
12. D.G. Rando, D.N. Sato, L. Siqueira, A. Malvezzi, C.Q. F. Leite, A.T. Amaral, Potential tuberculostatic agents. Topliss application on benzoic acid [(5-nitro-thiophen-2-yl)-methylene]-hydrazide series, Bioorg. Med. Chem., 10 (2002) 557-560.
13. S.G. Küçükgüzel, A. Mazi, F. Sahin, S. Oztürk, J. Stables, Synthesis and biological activities of diflunisal hydrazide-hydrazones, Eur. J. Med. Chem., 38 (2003) 1005-1013.
14. B.N. Swamy, T.K. Suma, G.V. Rao, G.C. Reddy, Synthesis of isonicotinoylhydrazones from anacardic acid and their in vitro activity against Mycobacterium smegmatis, Eur. J. Med. Chem., 42 (2007) 420-424.
15. H. Zhang, J. Drewe, B. Tseng, S. Kasibhatla, S.X. Cai, Discovery and SAR of indole-2-carboxylic acid benzylidenehydrazides as a new series of potent apoptosis inducers using a cellbased HTS assay, Bioorg. Med. Chem., 12 (2004) 3649-3655.
16. S.A.M. El-Hawash, A.E. Abdel Wahab, M.A. El-Dewellawy, Cyanoacetic acid hydrazones of 3- (and 4-) acetylpyridine and some derived ring systems as potential antitumor and anti-HCV agents, Arch. Pharm. Chem. Life Sci., 339 (2006) 14-23.
17. J. Pandey, R. Pal, A. Dwivedi, K. Hajela, Synthesis of some new diaryl and triaryl hydrazone derivatives as possible estrogen receptor modulators, Arzneimittelforschung., 52 (2002) 39-44.
18. N. Demirbas, S. Karaoglu, A. Demirbas, K. Sancak, Synthesis and antimicrobial activities of some new 1-(5-phenylamino-[1,3,4]thiadiazol-2-yl)methyl-5-oxo-[1,2,4]triazole and 1-(4-phenyl-5- thioxo-[1,2,4] triazol-3-yl)methyl-5-oxo-[1,2,4]triazole derivatives, Eur. J. Med. Chem., 39 (2004) 793-804.
19. N. Terzioğlu, A. Gürsoy, Synthesis and anticancer evaluation of some new hydrazone derivatives of 2,6-dimethylimidazo[2,1-b]-[1,3,4]thiadiazole-5-carbohydrazide, Eur. J. Med. Chem., 38 (2003) 781-786.
20. Gürsoy, N. Karali, Synthesis and primary cytotoxicity evaluation of 3-[[(3-phenyl-4(3H)-quinazolinone-2-yl) mercaptoacetyl]hydrazono]-1H-2-indolinones, Eur. J. Med. Chem., 38 (2003) 633-643.
21. M.T.H. Nutan, A.Hasnat, M.A. Rashid, Antibacterial and cytotoxic activities of *Murraya koenigii*, Fitoterapia, 69 (1998) 173-175.
22. M. Fiebig, J.M. Pezzuto, D.D. Soejarto, A.D. Kinghorn, Koenoline, a further cytotoxic carbazole alkaloid from *Murraya koenigii*, Phytochemistry, 24 (1985) 3041-3043.
23. M. Chakrabarty, A.C. Nath, S. Khasnobis, M. Chakrabarty, Y. Konda, Y. Harigaya, K. Komiyama, Carbazole alkaloids from *Murraya koenigii*, Phytochemistry, 46 (1997) 751-755.
24. K. Hirata, C. Ito, H. Furukawa, M. Itoigawa, L.M. Cosentino, K.H. Lee, Substituted 7H-pyrido[4,3-c] carbazoles with potent anti-HIV activity, Bioorg. Med. Chem. Lett., 9 (1999) 119-122.
25. B.A. Khan, A. Abraham, S. Leelamma, Antioxidant effects of Curry leaf, *Murraya koenigii* and mustard seeds, *Brassica juncea* in rats fed with high fat diet, Indian J. Exp. Biol., 35 (1997) 148-150.
26. S. Sarkar, D. Dutta, S.K. Samanta, K. Bhattacharya, B.C. Pal, J. Li, K. Datta, C. Mandal, Oxidative inhibition of Hsp90 disrupts the super-chaperone complex and attenuates pancreatic adenocarcinoma in vitro and in vivo, Int. J. Cancer, 132 (2013) 695-706.
27. C. Ito, M. Itoigawa, K. Nakao, T. Murata, N. Kaneda, H. Furukawa, Apoptosis of HL-60 leukemia cells induced by carbazole alkaloids isolated from *Murraya euchrestifolia*, J. Nat. Med., 66 (2012) 357-361.
28. M.K. Roy, V. N. Thalang, G. Trakoontivakorn, K. Nakahara, Mechanism of mahanine-induced apoptosis in human leukemia cells (HL-60), Biochem. Pharm., 67 (2004) 41-51.
29. S. Sinha, B.C. Pal, S. Jagadeesh, P.P. Banerhee, A. Bandyopadhaya, S. Bhattacharya, Mahanine inhibits growth and induces apoptosis in prostate cancer cells through the deactivation of akt and activation of caspases, The Prostate, 66 (2006) 1257-1265.
30. T. Thongthoom, P. Promsuwan, C. Yenjai, Synthesis and cytotoxic activity of the heptaphylline and 7-methoxyheptaphylline series, Eur. J. Med. Chem, 46 (2011) 3755-3761.
31. G. Palla, G. Predieri, P. Domiano, Conformational behaviour and E/Z isomerization of N-acyl and N-aroylhydrazones, Tetrahedron, 42 (1986) 3649-3654.
32. O. Unsal Tan, K. Ozden, A. Rauk, A. Balkan, Synthesis and cyclooxygenase inhibitory activities of some N-acylhydrazone derivatives of isoxazolo[4,5-d] pyridazin-4(5H)-ones, Eur. J. Med. Chem., 45 (2010) 2345-2352.
33. V.V. Syakaev, S.N. Podyachev, B.I. Buzykin, S. K. Latypov, W.D. Habicher, A.I. Konovalov, NMR study of conformation and isomerization of aryl- and heteroarylaldehyde 4-tert-butylphenoxyacetylhydrazones, J. Mol. Struct. 788 (2006) 55-62.

34. D. Sarıgöl, D. Yüksel, G. Okay, A. Uzgören-Baran, Synthesis and structural studies of acyl hydrazone derivatives having tetrahydrocarbazole moiety, J. Mol. Struct., 1086 (2015) 146–152.
35. B.S. Holla, M. Mahalinga, M.S. Karthikeyan, B. Poojary, P.M. Akberali, N.S. Kumari, Synthesis, characterization and antimicrobial activity of some substituted 1,2,3-triazoles, Eur. J. Med. Chem., 40 (2005) 1173-1178.
36. K.A. Metwally, L.M. Abdel-Aziz, E.M. Lashine, M.I. Husseiny, R.H. Badawy, Hydrazones of 2-aryl-quinoline-4-carboxylic acid hydrazides: synthesis and preliminary evaluation as antimicrobial agents, Bioorg. Med. Chem., 14 (2006) 8675-8682.
37. V. Judge, B. Nrasimhan, M. Ahuja, D. Sriram, P. Yogeeswari, E.D. Clercq, C. Pannecouque, J. Balzarini, Isonicotinic acid hydrazide derivatives: Synthesis, antimicrobial activity, and QSAR studies, Med. Chem. Res., 21 (2011) 1-20.
38. B. Koçyiğit Kaymakçıoğlu, E.E. Oruç Emre, S. Unsalan, S. Rollas, Antituberculosis activity of hydrazones derived from 4-fluorobenzoic acid hydrazide, Med. Chem. Res., 18 (2009) 277-286.

A New Approach for Quorum Sensing System in Several Halophilic Bacteria Isolated from Salt Lake in Central Anatolia

İç Anadolu'daki Tuz Gölü'nden İzole Edilen Çeşitli Halofilik Bakterilerdeki Quorum Sensing Sistemine Yeni Bir Yaklaşım

Research Article

Demet Erdönmez[1]*, Kübra Erkan Türkmen[2] and Nilüfer Aksöz[2]
[1]Department of Biology, Aksaray University, Aksaray, Turkey.
[2]Department of Biology, Division of Biotechnology, Hacettepe University, Ankara, Turkey.

ABSTRACT

Quorum sensing (qs) is the system that microorganisms use to improve common behavior with another population member in their environment. Salt Lake in Turkey that is considered as an extreme environment due to its salt concentration, teems in plankton and bacteria. Especially, it is an important field for halophilic bacteria because it provides suitable growth conditions. In this study, it was determined that 20 halophilic bacteria strain isolated from Salt Lake could produce qs signal molecules which are N-acyl homoserine lactone (HSL) derivatives. For detection of these bacterial signal molecules, thin layer chromatography was utilized by using *Chromobacterium violaceum* cv026 and *Agrobacterium tumefaciens* A136 that are biosensor bacteria strains. Genomic analysis of strains that produce signal molecules was carried out via 16s rRNA. *Halobacterium salinarium*, *Salicola* sp., *Halovibrio,* and *Halomonas* were found to be common in Salt Lake. It was also observed that these strains could produce C6-HSL and C8-HSL signaling molecules and produce biofilms.

Key Words
Homoserine lactone, quorum sensing, halophilic bacteria, Salt Lake.

ÖZ

Quorum sensing (qs), bir mikroorganizmanın yaşadığı ortamdaki diğer popülasyon üyeleri ile ortak davranışları geliştirmek için kullandığı bir sistemdir. İçeriğindeki tuz yoğunluğundan dolayı ekstrem ortamlardan sayılan Tuz Gölü, bünyesinde barındırdığı planktonik canlılar ve bakteriler yönünden zengindir. Özellikle tuz gölü uygun üreme koşullarını sağladığı halofilik bakteriler için çok önemli bir alandır. Tuz Gölü›nden izole edilen Halofilik karakterli 20 bakteri türünün qs sinyal moleküllerinden N-asil homoserin lakton (AHL) türevlerini üretebildikleri saptanmıştır. Bu bakteriyel sinyal moleküllerini tespit etmek için biyosensör bakteriler *Chromobacterium violaceum* cv026 ve *Agrobacterium tumefaciens* A136 kullanılarak ince tabaka kromatografisinden yararlanılmıştır. Sinyal molekülü üretebilen suşların 16sRNA ile genomik analizleri gerçekleştirilmiştir. *Halobacterium salinarium*, *Salicola* türleri, *Halovibrio* ve *Halomonas* türlerinin Tuz Gölü içerisinde yaygın olduğu görüldü. Ayrıca bu suşların C6-AHL ve C8-AHL sinyal moleküllerini üretebildikleri ve biyofilm oluşturabildikleri gözlenmiştir.

Anahtar Kelimeler
Homoserin lakton, quorum sensing, halofilik bakteriler, Tuz Gölü.

Article History: Received: January 16, 2018; Revised: Mar 15, 2018; Accepted: Mar 26, 2018.

DOI: 10.15671/HJBC.2018.227

Correspondence to: D. Erdönmez, Department of Biology, Aksaray University, Aksaray, Turkey.
Tel: +90 382 288 21 69 Fax: +90 382 288 21 00 E-Mail: demet.erdonmez@gmail.com

INTRODUCTION

The technological and economic developments initiated by the industrial revolution have made it possible to reach many points of the world through different trade lines. The most common of these lines is the method of shipping method. By shipping, it became ordinary to carry heavy cargos among different points of the world. It is observed that costs of this common trading way have increased with the increase of fuel consumption caused by biofilm on the ship hull formed by interaction between bacteria in the salty environment and ship hull. There is some info about biofilm layer formed by bacteria living in salty environments like sea salt. It is needed to carry out biotechnological and microbial-based studies to prevent biofilm layer formation. A specific part of these studies is carried out for having enough knowledge about how bacteria orient environment, biofilm formation abilities or if bacteria can communicate with each other and if possible, how they communicate? Studies based on usage of bacteria living in a salty environment in biotechnologically different areas are common. Quorum sensing defined as bacterial communication, arise with gene regulation arranged by bacteria population that reach specific majority depending on population [1-5]. Although quorum sensing system is spotted in Gram-negative bacteria first, it is a microbial communication system used for Gram-positive bacteria and some funguses [6-8]. Reproduction and continuity of metabolic activities of microorganisms in different environments show that both structural and cellular specifications of these organisms should be confirmed.

In this study, biofilm formation abilities and detection of quorum sensing signals of different bacteria species isolated from water and soil samples, which are taken from Salt Lake that is a halophilic and extreme environment, are targeted.

MATERIALS and METHODS

Soil and water samples were taken aseptically from parts of the Salt Lake near Şereflikoçhisar were brought to the laboratory under sterile conditions. 20 of these isolates were used for these study. The isolates which were grown in HS medium were kept Hacettepe University Faculty of Science, Department of Biology, Division of Biotechnology and ASÜBTAM Laboratory of Microbiology at -20°C.

Isolation of Halophilic Bacteria

Soil and water samples were diluted with a sterile saline solution with the ratio of 1:10 (g/ml). 1 ml of each sample were inoculated to the Sea Water medium(Sea Water medium (NaCl 202.5 g, $MgCl_2$ 17.5 g, $MgSO_4$ 24 g, $CaCl_2$ 0.9 g, KCl 5 g, $NaHCO_3$ 0.15 g, NaBr 0.065 g, Yeast extract 5 g/L^{-1} pH 7.2) and HS medium(250 g of NaCl, 20 g of MgSO4 ·$7H_2O$, 3 g of trisodium citrate·$2H_2O$, 2 g of KCl and 10 g of Oxoid bacteriological peptone L-34 , pH 6.5-7.4) and incubated for 7 days at 37-39°C , 150 rpm (Figure 1). 100 µl of each culture were spread on HS agar plaques. After 7-10 days incubation, selected colonies and control microorganism were inoculated to HS medium again. Third days of incubation colorless colonies and after 10-15 days pink-red colonies were observed at plaques (Figure 2). Gram-negative isolates were selected for this research [1-3].

Figure 1. Halophilic bacterial cultures obtained from water and soil samples.

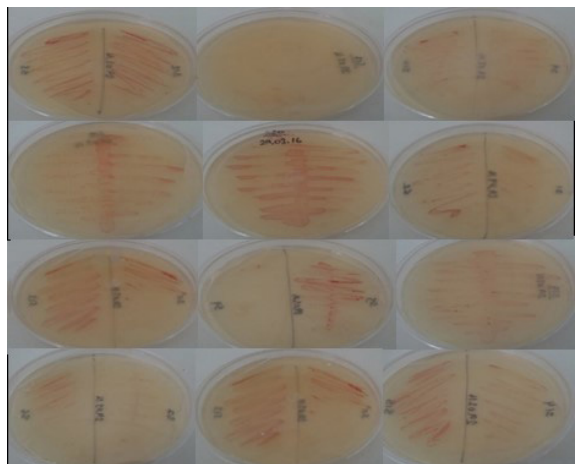

Figure 2. All isolated pure halophilic bacteria.

Bacterial DNA Isolation

Biospeedy Bacterial DNA isolation kit was used for DNA isolation and DNA was obtained according to the procedure. The obtained DNA's were stored at -20°C until running for 16s rRNA analysis.

Real-Time PCR (Q-PCR)

Biospeedy Bacterial Diversity Kit was used for identifying bacterial diversity. Primers in which was used during the procedure, were special to 16s rRNA side of bacterial genomic DNA (forward primer AGA GTT TGA TCC TGG CTC AG and reverse primer AAG GAG GTG ATC CAG CCG CA) [4,5]. BIORAD CFX Connect (Bio-Rad Laboratories, USA) Real-time PCR instrument was used for all reactions. The reaction contained 1.5 mM $MgCl_2$, 0.2 mM dNTP mix, 1x Reaction Buffer, 0.1 U Fast Start Taq DNA Polymerase, 1x Eva Green, 4 ng/µl template cDNA and 0.5 µM of each primer. In the device, the following heat cycle program has been applied with an optimized primer pair (Table 1). During Q-PCR, melting curve analysis was performed at 65°C to 95°C to determine that only the desired product was replicated. Then, it was analyzed by Q-PCR Biorad CFX Connect Software 3.0.

16s RNA Sequencing

Obtained bacterial amplicon sequence, were determined through Sanger Method with ABI Prism Big Dye Terminator Cycle Sequencing Ready Reaction Kit and ABI Prism 377 DNA Sequencer (Applied Biosystems, USA).

Phylogenetic Analysis

Obtained sequences from each bacteria were analyzed by Chromas software package version 1.45 (http://www.technelysium.com/au/chromas.html). Sequences were compared with known bacteria species in NCBI DNA databank (BLAST-(http://blast.ncbi.nlm.nih.gov/Blast.cgi) and were determined most similar species, similarity rates, and accession number.

Table 1. Q-PCR reaction contents.

Detection Format		**Reaction volume**		
SYBR Green		10 µl		
Programmes				
Programme name	**Cycle**	**Analyse mode**		
Pre-incubation	1			
Enhancement	45	Enumeration		
Melting curve	1	Meeting curve		
Cooling	1			
Temperature				
Target(°C)	**Mood**	**Duration (hh:mm:ss)**	**Speed (°C/s)**	**Reading (per °C)**
Pre-incubation				
95		00:10:00	4,8	-
Enhancement				
95		00:00:15	4,8	-
53		00:00:20	2,5	-
72	Single	00:00:40	4,8	-
Melting curve				
95		00:00:02	-	-
65		00:01:00	-	-
98	Continuous	-	0.2	10
Cooling				
35	Single	00:00:10	2,5	-

Extraction and Purification of N-Acyl Homoserine Lactone from Halophilic Bacteria Culture Medium

For signal molecule extraction, halophilic Gram-negative bacteria culture were inoculated loop-full to 10 ml HS liquid medium and incubated at 37ºC until stationary phase [6,7]. Obtained cultures were centrifuged at 4ºC' 4000 rpm 10 minutes. The supernatant was transferred into a new tube and dichloromethane was added equal volume. Organic phase that was transferred new tube was filtered by 0.2 μm pore size sterile syringe filter (non-pyrogenic, Sartorius). Dichloromethane was removed via evaporator [2]. The residue in the tube that included the completely evaporated organic phase was dissolved in 20 μL of methanol and stored at -20ºC until use [8,9].

Signal Molecules Analysis by Thin Layer Chromatography

Signal molecules analysis were conducted by Reverse-phase C18 thin layer chromatography (RP-C18 TLC). N-butanoyl homoserine lactone (C4-HSL), N-hexanoyl homoserine lactone (C6-HSL), N-octanoyl homoserine lactone (C8-HSL) and N-dodecanoyl homoserine lactone (C12-HSL) (Sigma, Germany) molecules were used as standard signal molecules. The signal molecules dissolved in methanol were applied to the reversed phase TLC plates (RP-18 F254; Merck) with a 1.5 cm interval for each sample loading area up to the starting point. Chloroform- Methanol (95:5, v/v) was prepared as the mobile phase. Mobile phase ran up to 2 cm below the top of TLC plate. After the separation process was completed, TLC plates were dried in fume hood during 2 h. *Chromobacterium violaceum cv026* and *Agrobacterium tumefaciens A136 (pCF218)(pCF372)* were used as biosensor strains to detect molecules. The dried TLC plates were spread onto 50ml of AB mineral soft agar medium (50ºC) + 0.9ml agar containing 10% *Agrobacterium tumefaciens* A136 (pCF218) (pCF372) (100 ml for 48 h) and X-gal (60 μg/ml). Besides, other TLC plates were spread onto LB soft agar medium (%0.9 agar contained) + 10ml *Chromobacterium violaceum CV026* (24 h culture) culture. When medium solidified, TLC plates were incubated at 30ºC 24-48 h [10-12]. During the experiment, methanol was used as negative control. The spots where AHL molecules located were determined with violaceus or greenish spot occurrence.

Determination of Biofilm Formation Capabilities of Halophilic Bacteria

Biofilm formation was determined with crystal violet method which is a classical method for biofilm formation [13]. Halophilic isolates were incubated at 37-39ºC during 7 days in HS medium. Then all isolates were diluted with HS medium at 0.05 O.D. value at 600 nm and inoculation of isolates was performed with 50 ml culture to 100 ml HS medium. All medium which was inoculated before were incubated 200 rpm for 7 days. After incubation, 900μl HS medium + 100μl halophilic bacteria were added to 24 well polystyrene plate. Two different experimental setups were designed for 37-39ºC and 7-10 days produced cultures. The medium was discharged from the plate in which incubated cultures. Each well was washed with 1xPBS buffer three times. Washed plate well was dried at 65ºC. Wells were stained with 1% crystal violet for 2 minutes. After, stained wells were washed at three times and were dried at room temperature. Crystal violet in the well was solubilized with 30% Acetic acid solution and was measured by spectrophotometer at 595 nm [14,15].

RESULTS and DISCUSSION

When the test results were examined, it was observed that the bacterial isolates from soil and water samples could not be grown on medium with higher salt content but they could be grown on medium containing 4-5 M NaCl, so preliminary definitions were made in accordance with the characteristics of halophilic bacteria. In addition, as gram features, the selection was made among Gram-negative bacillus or coccobacillus morphology isolates [16]. After DNA isolations of the isolates were carried out in the microbiology laboratory of ASUBTAM, their genomic identification was done by Bioeksen [17,18]. In this context, according to 16S rRNA results for species differentiation, *Halobacterium salinarium, Halovibrio,* and *Halomonaras* species were determined to be widespread in Salt Lake (Table 2).

Table 2. Types of strains isolated by 16sRNA analysis.

Isolate Number	Identity	Similarity Rate	Accession No
HS1	*Halobacterium salinarum*	355/364(98%)	FJ236084.1
HS2	*Salicola sp.*	663/669(99%)	KR611161.1
HS3	*Halovibrio sp.*	470/585(80%)	AM774418.1
HS4	*Salicola sp.*	691/719(96%)	EU931298.1
	Halomonas sp	690/719(96%)	KF321909.1
HS5	*Salicola sp.*	715/763(94%)	KR611161.1
HS6	*Salicola sp.*	328/358(92%)	KF511768.1
HS7	*Salicola sp.*	915/955(96%)	KR611161.1
HS8	*Salicola sp.*	529/549(96%)	KR611161.1
HS9	*Salicola sp.*	468/490(96%)	KR611161.1
	Halomonas sp.	468/490(96%)	KF321909.1
HS10	*Salicola sp*	621/653(95%)	KR611161.1
HS11	*Halomonas sp.*	663/688(96%)	KF321909.1
HS12	*Halophilic bacterium (Halobacterium salinarum)*	959/1016(94%)	FJ236084.1
HS13	*Salicola sp.*	641/656(98%)	KR611161.1
HS14	*Salicola sp.*	558/568(98%)	CP003412.1
HS15	*Salicola sp.*	921/945(97%)	KR611161.1
HS15	*Halophilic bacterium*	921/945(97%)	KC142106.1
HS16	*Salicola sp.*	538/628(86%)	KR611161.1
	Halomonas sp.	538/628(86%)	KF321909.1
HS17	*Salicola sp.*	503/507(99%)	EU931298.1
HS18	*Halophilic bacterium*	721/752(96%)	FJ236084.1
HS19	*Salicola sp.*	537/572(94%)	KF511768.1
	Halomonas sp	537/573(94%)	KF321909.1
HS20	*Salicola sp*	911/953(96%)	KR611161.1

As a reason for the condensation of genotypically and phenotypically identified strains among certain species in our study, it can be suggested that *Dunaliella salina* species algae, which is common in Salt Lake during the sampling period, affects the bacterial population. This is supported by the study of Le Chevanton et al. , in which some metabolites that produce *Dunaliella* algae in the *saline* environment cause inhibition of the population of bacteria in the environment [19]. Liu et al. found that some gram-negative and positive bacteria, in the study conducted, carried out the excessive proliferation of the algae population, which was expressed as algae bloom [20]. In this context, halophilic bacteria are considered to play an active role in hyperproliferation of *Dunaliella* in *Halobacterium*, *Salicola*, *Halovibrio* and *Halomonas* species of bacteria.

Disclosure of the biofilm mechanism regulated by the quorum sensing system, a bacterial communication system, and the detection of signaling molecules that play an active role in the formation of the biofilm mechanism has an important role in explaining the metabolism of bacteria. According to the data obtained from the study; it has been found that HS2, HS5, HS7, HS8, HS9, HS10, HS14, HS15, HS18 and HS19 from halophilic isolates can also produce the C6-AHL signaling molecule in thin layer chromatography in proportion to cross-validation. On the other hand, it has been found with cross-validation with *Agrobacterium* sp species that each strain is able to produce signal molecule in the detection of strains which are able to produce signal molecule but signal molecules have not been detected in thin layer chromatography (C8-AHL). It

has been shown that HS1, HS3, HS5, HS6, HS7, HS8, HS9, HS11, HS13, HS14, HS15, HS16 and HS18 from the isolated strains can produce C8-AHL signaling molecules. The isolates HS5, H7, HS8, HS9, HS14, HS15, and HS18 were able to produce both C6-AHL and C8-AHL signaling molecules (Table 3).

Enzymes to be used in industrial areas are also required to exhibit high activity in extreme conditions. For this reason, it is necessary to know what kind of signal molecules are produced by many bacterial strains in the extreme conditions, which features are expressed with these signal molecules (enzyme production, antibiotic production, biofilm, exopolysaccharide production) [2,21,22]. *Agrobacterium tumefaciens* NTL4 (pZRL4) and *Chromobacterium violaceum* CV026 have been identified in N-acyl homoserine lactones produced by these bacteria in a study showing that a sufficient number of perceptions also play an important role in hyperphosphorous environments [2]. Since the biofilm formation ability was regulated by the quorum sensing system, the biofilm production characteristics of the isolates producing signal molecules were examined and it was found that HS1, HS5, HS17 strains had higher biofilm forming abilities than the other isolates. 16 sRNA analysis showed that these strains are HS1; *Halobacterium salinarium*, HS2, and HS17; *Salicola sp*. It has been found that other isolates have biofilm producing properties even though they are few (Figure 3).

Table 3. The Rf values of the signal molecules of the halophilic isolates in TLC result.

Strain Number	AHL detection with CV026	AHL detection with A136	RF1	RF2	RF3	RF4	C4- AHL	C6-AHL	C8-AHL	C12-AHL
							Average Rf values			
							0,8	0.42	0.36	0.12
HS1	-	++	-	-	0.35	-	-	-	X	-
HS2	+	+	-	0.40	-	-	-	X	-	-
HS3	-	++	-	-	0.34	-	-	-	X	-
HS4	-	+	-	0.42	-	-	-	X	-	-
HS5	+	++	-	0.40	0.34	-	-	X	X	-
HS6	-	++	-	-	0.30	-	-	-	X	-
HS7	+	++	-	0.40	0.31	-	-	X	X	-
HS8	+	+++	-	0.41	0.32	-	-	X	X	-
HS9	+	++	-	0.42	0.28	-	-	X	X	-
HS10	+	+	-	0.40	-	-	-	X	-	-
HS11	-	++	-	-	0.33	-	-	-	X	-
HS12	-	+	-	-	-	-	-	-	-	-
HS13	-	++	-	-	0.34	-	-	-	X	-
HS14	+	++	-	0.41	0.29	-	-	X	X	-
HS15	+	++	-	0.42	0.31	-	-	X	X	-
HS16	-	++	-	-	0.33	-	-	-	X	-
HS17	-	+	-	-	-	-	-	-	-	-
HS18	+	+++	-	0.41	0.30	-	-	X	X	-
HS19	+	+	-	0.39	-	-	-	X	-	-
HS20	-	+	-	-	-	-	-	-	-	-

C4-AHL ; 0,7-0,84 , C6-AHL; 0,39-0,42 , C8-AHL;0,28-0,36 , C12-AHL; 0,18-0,22.

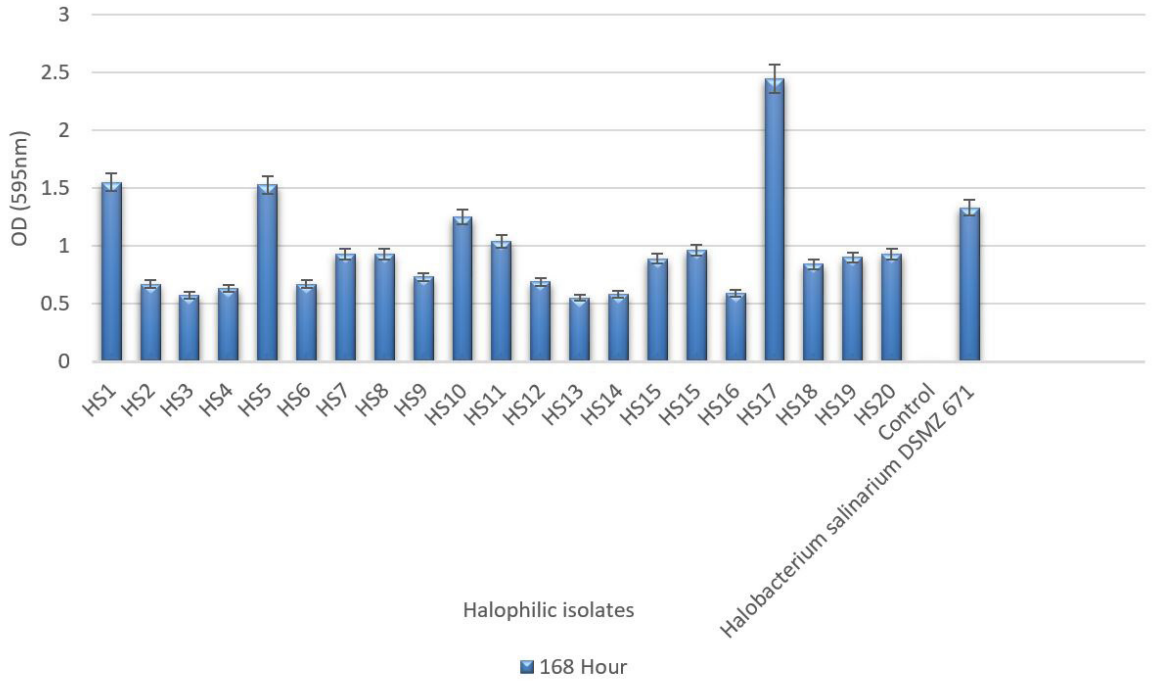

Figure 3. The ability of halophilic isolates to biofilm formation.

The HS12, HS17 and HS20 strains were observed not to produce a quorum sensing signal molecule but were able to generate biofilms. Then these bacteria use different signaling molecules in biofilm formation and it is likely that there is a signal molecule except from the one used as a standard. Figure 3 and Table 3 show that bacteria can produce biofilms regardless of producing quorum sensing signal molecule. In many studies, it is stated that these two systems are coordinated.

In the species of *Halomonas anticariensis*, In the species *Halomonas anticariensis*, the quorum sensing system regulates the ability to form biofilms with hanR (the default transcription regulator) and hanI (the autoinducer synthase gene), which are the luxR/luxI homologs [21]. In extreme conditions, it is emphasized by many scientists that this system works more actively [23,24]. Formations and densities of biofilms are a result of microbial evolution [25]. Halophilic bacteria in Salt Lake-like environment have developed some features that can give them an advantage over time. Some of them are capable of producing biofilms and being protected from other negativities in the environment. For instance, Salt Lake is exposed to the pollution of some factories and domestic wastes even though it is in the natural conservation areas [26]. Therefore, this leads to pollution, heavy metal accumulation, and many other factors leading to the resistance of the immune system to infection. Another effect is that these bacteria protect themselves by producing biofilms. While biofilm formation is advantageous for salty bacteria, it causes disadvantages in sectors where commercial losses are high, such as maritime transport. In maritime transport, retention of various sea creatures to the parts of the ships exposed to seawater increases depending on the biofilm created by bacteria. This causes the economy to slow down over time and increase fuel consumption. At the same time, a serious amount of resource transfer is required in the elimination of biofilm formation. There are studies based on the reduction or elimination of this condition, but it has been observed that chemicals to be used on the surface of the ship have toxic effects on marine life. In this context, it is necessary to develop low-toxicity and high-availability chemicals for ship surface coatings [27]. First, the identification of quorum sensing molecules, which form biofilms on the surface of the ship and are effective in the formation of this biofilm, should be a priority in order to avoid such losses. Our work carries a preliminary qualification in order to achieve these results. Further research is needed to for future studies on the biofilm properties of halophilic bacteria. Considering the long

reproduction time of halophilic bacteria, we believe that the signal molecules in the environment may degrade. In addition, these bacteria are thought to have enzymes that can degrade these signaling molecules due to their improved enzyme systems. It has been shown that signal molecules produced by isolated halophilic bacteria change between C6-C8 AHL molecules.

ACKNOWLEDGEMENTS

This work was supported by Aksaray University Department of Scientific Research Projects Coordination (Projects Number:2015-088).

References

1. J.J. Nieto, R. Fernandez, Castillo, M.C. Marquez, A. Ventosa, E. Quesada, F. Ruiz-Berraquero, Survey of metal tolerance in moderately halophilic eubacteria, Appl. Environ. Microbiol., 55 (1989) 2385-2390.
2. I. Llamas, E. Quesada, M.J. Martinez-Canovas, M. Gronquist, A. Eberhard, J.E. Gonzalez, Quorum sensing in hal-ophilic bacteria: detection of N-acyl-homoserine lactones in the exopolysaccharide-producing species of Halomo-nas, Extremophiles, 9 (2005) 333-341.
3. Ö. Çakıcı, Biochemical and genetic characterization of *Halobacterium Salinarium* strain isolated from Tuz Lake in Central Anatolia,2004, Mıddle East Technıcal Unıversıty.
4. K. Ma, R. Conrad, Y. Lu, Responses of methanogen mcra genes and their transcripts to an alternate dry/wet cycle of paddy field soil, Appl. Environ. Microbiol., 78 (2012) 445-454.
5. J. Penger, R. Conrad, M. Blaser, Stable carbon isotope fractionation by methylotrophic methanogenic archaea, Appl. Environ. Microbiol., 78 (2012) 7596-7602.
6. M.M. Marketon, J.E. Gonzalez, Identification of two quorum-sensing systems in *Sinorhizobium meliloti*, J. Bacteriol., 184 (2002) 3466-3475.
7. M.M. Marketon, M.R. Gronquist, A. Eberhard, J.E. Gonzalez, Characterization of the *Sinorhizobium meliloti* sinR/sinI locus and the production of novel N-acyl homoserine lactones, J. Bacteriol., 184(2002) 5686-5695.
8. V.A. Blana, G.J. Nychas, Presence of quorum sensing signal molecules in minced beef stored under various tem-perature and packaging conditions, Int. J. Food. Microbiol., 173 (2014) 1-8.
9. H. Lade, D. Paul, J.H. Kweon, Isolation and molecular characterization of biofouling bacteria and profiling of quorum sensing signal molecules from membrane bioreactor activated sludge, Int. J. Mol. Sci., 15 (2014) 2255-2273.
10. R.H. González, A. Nusblat, B.C. Nudel, Detection and characterization of quorum sensing signal molecules in Acinetobacter strains, Microbiol. Res., 155 (2001) 271-277.
11. D. Anbazhagan, M. Mansor, G.O. Yan, M.Y. Md Yusof, H. Hassan, S.D. Sekaran, Detection of quorum sensing sig-nal molecules and identification of an autoinducer synthase gene among biofilm forming clinical isolates of *Acinetobacter* spp, PloS one, 7 (2012)
12. S.D. Saroj, P.N. Rather, Streptomycin inhibits quorum sensing in *Acinetobacter baumannii*, Antimicrob. Agents Chemother., 57 (2013) 1926-1929.
13. J.H. Merritt, D.E. Kadouri, G.A. O'Toole, Growing and analyzing static biofilms, Curr. Protoc. Microbiol., Chapter 1 (2005) Unit 1B.1.
14. D. Mack, W. Fischer, A. Krokotsch, K. Leopold, R. Hartmann, H. Egge, R. Laufs, The intercellular adhesin in-volved in biofilm accumulation of *Staphylococcus epidermidis* is a linear beta-1, 6-linked glucosaminoglycan: purification and structural analysis. J. Bacteriol., 178 (1996) 175-183.
15. X. Wang, J.F. Preston, T. Romeo, The pgaABCD locus of Escherichia coli promotes the synthesis of a polysaccha-ride adhesin required for biofilm formation, J. Bacteriol., 186 (2004) 2724-2734.
16. S.B. McGee, C.A. Orengo, M.E. Kunik, V.A. Molinari, R.H. Workman, Delirium in geropsychiatric patients: patient characteristics and treatment outcomes, J. Geriatr. Psychiatry Neurol., 10 (1997) 7-10.
17. R. Rohban, M.A. Amoozegar, A. Ventosa, Screening and isolation of halophilic bacteria producing extracellular hydrolyses from Howz Soltan Lake, Iran, J. Ind. Microbiol. Biotechnol., 36 (2009) 333-340.
18. C. Sánchez- Porro, S. Martin, E. Mellado, A. Ventosa, Diversity of moderately halophilic bacteria producing extra-cellular hydrolytic enzymes, J. Appl. Microbiol., 94 (2003) 295-300.
19. M. Le Chevanton, M. Garnier, G. Bougaran, N. Schreiber, E. Lukomska, J.B. Bérard, E. Fouilland, O. Bernard, J.P. Cadoret, Screening and selection of growth-promoting bacteria for Dunaliella cultures, Algal Res., 2 (2013) 212-222.
20. J. Liu, A.J. Lewitus, P. Brown, S.B. Wilde, Growth-promoting effects of a bacterium on raphidophytes and other phytoplankton, Harmful Algae, 7 (2008) 1-10.
21. A. Tahrioui, E. Quesada, I. Llamas, The hanR/hanI quorum-sensing system of Halomonas anticariensis, a moder-ately halophilic bacterium, Microbiology, 157 (2011) 3378-87.

22. A. Tahrioui, M. Schwab, E. Quesada, I. Llamas, Quorum sensing in some representative species of halomonadaceae, Life (Basel), 3 (2013) 260-75.
23. B.A. Doğaner, L.K. Yan, H. Youk, Autocrine signaling and quorum sensing: Extreme ends of a common spectrum, Trends Cell Biol., 26 (2016) 262-271.
24. K. Montgomery, J.C. Charlesworth, R. Lebard, P.T. Visscher, B.P. Burns, Quorum Sensing in Extreme Environments, Life, 3 (2013) 131-148.
25. H.P. Steenackers, I. Parijs, K.R. Foster, J. Vanderleyden, Experimental evolution in biofilm populations, FEMS Microbiol. Rev., 40 (2016) 373-397.
26. A. Kılıç, E. Uyanık, Tuz Gölü'nde oluşan kirlenmenin göl üzerindeki etkilerinin araştırılması, 4. Endüstriyel Hammaddeler Sempozyumu 18-19 Ekim, (2001) 135-145.
27. M.P. Schultz, J.A. Bendick, E.R. Holm, W.M. Hertel, Economic impact of biofouling on a naval surface ship, Biofouling., 27 (2011) 87-98.

Selective Separation and Preconcentration of Thorium(IV) in Bastnaesite Ore Using Thorium(IV)-Imprinted Cryogel Polymer

Toryum(IV) Baskılı Kriyojel Polimer Kullanılarak Bastnaesit Cevherindeki Toryum(IV)'un Seçici Olarak Ayrılması ve Önderiştirilmesi

Research Article

İbrahim Dolak
Vocational School of Technical Sciences, Dicle University, Diyarbakır, Turkey.

ABSTRACT

In this study, selective separation and preconcentration of Th(IV) in aqueous solutions and bastnaesite ore in the presence various lanthanide ions by using Th(IV)-imprinted polymer was conducted. For this purpose, Th(IV) was complexed with N-methacryloyl antipyrine (MAAP) and the prepared (MAAP)2-Th(IV) complex monomer was polymerized with 2-hydroxyethyl methacrylate (HEMA) cryogel to prepare pHEMA-(MAAP)2-Th(IV) cryogel polymer by free radical polymerization. Th(IV) was desorbed with 5.0 mol.L^{-1} HNO3 and thus Th(IV)-imrinted were created onto p-HEMA-(MAAP)2 cryogel polymer. To determine the optimum conditions, in the process of selective binding of Th(IV) ion to Th(IV)-imprinted p-HEMA-(MAAP)2 cryogel polymer, some parameters such as pH, flow rate, initial Th(IV) concentration were investigated. Under the optimum conditions, the maximum binding capacity was obtained as 48.30 mg.g^{-1}. Selectivity studies were also carried out in the presence of Ce(III), La(III) and Eu(III) ions using Th(IV)-imprinted p-HEMA-(MAAP)2 cryogel polymer. It was found that p-HEMA-(MAAP)2 cryogel polymer displayed high selectivity toward Th(IV) ion.

Key Words
Th(IV)-imprinted polymer, p-HEMA-(MAAP)2, separation, preconcentration.

ÖZ

Bu çalışmada, Th(IV)-baskılı Polimerler kullanılarak çeşitli lantanid iyonlarının varlığında sulu çözeltilerde ve bastnaesit cevherinde Th(IV) iyonunun seçici olarak ayrılması ve önderiştirilmesi gerçekleştirildi. Bu amaçla, Th(IV), N-metakriloil antipirin (MAAP) ile kompleksleştirildi ve hazırlanan (MAAP)2-Th(IV) kompleks monomer, serbest radikal polimerizasyon yöntemiyle 2-hidroksietil metakrilat (HEMA) kriyojel ile etkileştirilerek pHEMA-(MAAP)2-Th(IV) kriyojel polimeri hazırlandı. Th(IV), 5.0 mol.L^{-1} HNO3 ile desorbe edildi ve böylece Th(IV) baskılı p-HEMA-(MAAP)2 kriyojel polimeri oluşturuldu. Th(IV) iyonunun Th(IV)-baskılı p-HEMA-(MAAP)2 kriyojel polimere seçici olarak bağlanması işleminde optimum koşulları belirlemek için pH, akış hızı, başlangıç Th(IV) konsantrasyonu gibi bazı parametreler araştırıldı. Belirlenen bu optimum koşullar altında, maksimum bağlanma kapasitesi 48.30 mg.g^{-1} olarak tespit edildi. Seçicilik çalışmaları da, Th(IV)-baskılı p-HEMA-(MAAP)2 kriyojel polimer kullanılarak Ce(III), La(III) and Eu(III) iyonlarının varlığında gerçekleştirildi. p-HEMA-(MAAP)2 kriyojel polimer, Th(IV) iyonuna karşı yüksek seçicilik gösterdiği bulundu.

Anahtar Kelimeler
Th(IV)-baskılı polimer, p-HEMA-(MAAP)2, ayırma, önderiştirme.

Article History: Received: Nov 17, 2017; Revised: Jan 23, 2018; Accepted: Mar 03, 2018; Available Online: Mar 26, 2018.

DOI: 10.15671/HJBC.2018.228

Correspondence to: İ. Dolak, Vocational School of Technical Sciences, Dicle University, Diyarbakır, Turkey.
Tel: +90 542 531 21 21 Fax: +90 412 248 83 00 E-Mail: idolak@dicle.edu.tr

INTRODUCTION

Thorium is a potential nuclear fuel since ^{232}Th can convert to ^{233}Th by absorbing slow neutrons [1]. Thorium is one of rare earth elements which are widely used for the preparation of advanced materials [2,3]. Thorium can exist in several rare earth ore samples such as bastnaesite and monazite. Therefore, selective extraction of thorium have attracted significant attention to eliminate radioactive pollution [4]. For this purpose, various techniques such as liquid–liquid extraction [5,6] extraction chromatography [7,8], functionalized resins [9,10], different adsorbents [11,12] and ion imprinted polymers [13-17] have been applied for the selective extraction of thorium and other rare earth ions.

Molecular imprinting is a new technique has attracted the attention of researchers for effective recognation of chemical and biological molecules including aminoacids, proteins, enzymes, DNA, drugs and metals [18-22]. This technique allows selective and sensitive recognition of chosen target molecule by leaving artificial imprinted cavities in polymer matrix that provides high affinity to target molecule [23]. To synthesize molecularly imprinted polymer, the template molecule and functional monomers which can arrange around template are complexed interactively before polymerization. Then the rigid polymer matrix is obtained by polymerization of formed pre-complex and cross-linker reagent. After removal of template molecule from the polymer with suitable elution agent, the cavities remaining in the polymer that are complementary in shape, size and chemical functionality to the template. Consequently, the resultant polymer able to recognizes and rebinds selectively the template or other molecules that are chemically related to the template [24,25]. This technique is used in many applications such as selectivity recognation and seperation [26-29], drug delivery systems [30-31], catalysis [32,33] sensor technology [34,35]. In addition, ion imprinted polymers (IIPs) have been used for the selective removal of metal ions from different matrices [36-47].

In this study, the selective separation of Th(IV) in aqueous solutions and bastnaesite ore in the presence of other lanthanide ions such as La(III), Ce(III) and Eu(III) was performed by using Th(IV)-imprinted pHEMA-$(MAAP)_2$-Th(IV) cryogel polymer. For this purpose, Th(IV) was complexed with N-methacryloyl antipyrine (MAAP) and the prepared $(MAAP)_2$-Th(IV) complex monomer was polymerized with 2- hydroxyethyl methacrylate (HEMA) cryogel to prepare pHEMA-$(MAAP)_2$-Th(IV) cryogel polymer by free radical polymerization. Th(IV) was desorbed with 5.0 mol.L^{-1} HNO_3 and thus were created Th(IV) imprinted on to p-HEMA-$(MAAP)_2$ cryogel polymer. In the process of selective binding of Th(IV) ion to Th(IV)-imprinted p-HEMA-$(MAAP)_2$ cryogel polymer, several factors such as medium pH, flow rate, initial Th(IV) concentration were investigated to determine optimum conditions. Selectivity studies were also carried out in the presence of Ce(III), La(III) and Eu(III) ions using Th(IV)-imprinted p-HEMA-$(MAAP)_2$ cryogel polymer. It was found that p-HEMA-$(MAAP)_2$ cryogel polymer displayed high selectivity toward Th(IV) ion.

MATERIALS and METHODS

Chemicals and Reagents

Metacryloylcloride, antipyrine, thorium(IV) nitrate tetrahydrate, Lanthanium(III) nitrate hexahydrate, Cerium(III) nitrate hexahydrate, Europium(III) nitrate hexahydrate, 2-Hydroxyethyl methacrylate (HEMA), Ammonium persulfate (APS) (MW: 27000), N,N,N,N-tetramethylethylenediamine (TEMED), N,N-methylenebisacrylamide (MBAAm), Polyvinyl alcohol (PVA) and all organic solvents were provided from Sigma-Aldrich (Steinheim, Germany).

Instrumentation

A Perkin Elmer model Spectrum 400 FT-IR spectrometer was used for the Fourier transform infrared (FT-IR) measurements. Scanning electron microscopy (SEM) analyses were carried out by using a FEI Quanta FEG 250 SEM system. The analysis of the Th(IV) and the other lanthanide ions was performed using a Agilent 7700 Series inductively coupled plasma-mass spectroscopy (ICP-MS). System with the following parameters: RF Power= 1600 W, sampling depth= 5.5 mm, analyzer pressure= $8,31x10^{-5}$ Pa, helium flow in the collision cell= 5.00 mL.min^{-1} and plasma temperature= 9871 K. the measurements were done with three replicates (95% confidence level).

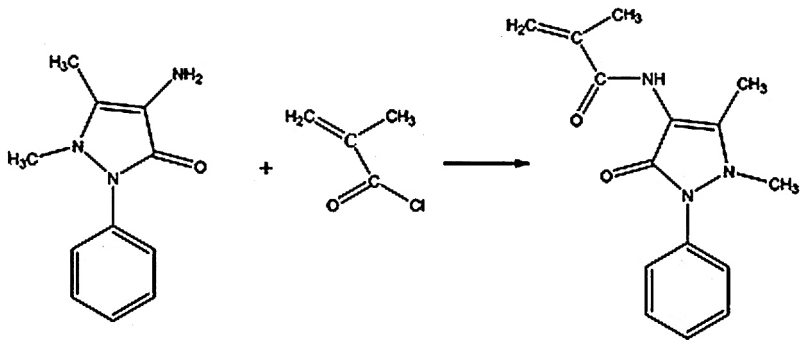

Figure 1. Synthesis of methacryloyl antipyrine (MAAP) monomer.

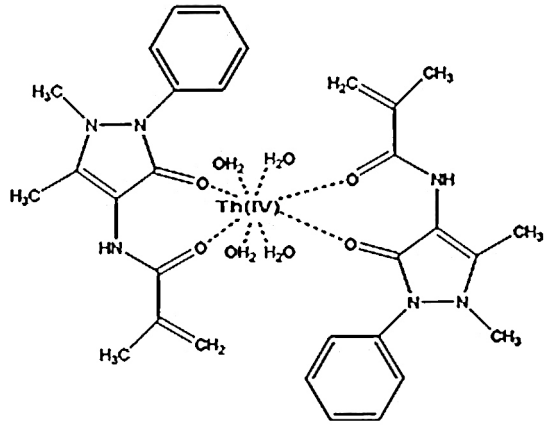

Figure 2. The Prepared $(MAAP)_2$Th(IV) complex monomer.

Preparation of Thorium(IV) Imprinted Cryogel

Polymer Synthesis of Functional Monomer N-Methacryloylamidoantipyrine (MAAP)

The synthesis of the functional monomer MAAP was carried out apply in the previously reported recipe (Figure 1) [48].

Preparation of $(MAAP)_2$-Th(IV) Complex Monomer

For preparation $(MAAP)_2$-Th(IV) functional monomer (Figure 2), MAAP (0.270 mg, 1.0 mmol) was dissolved in ethanol. After slow addition of $Th(NO_3)_4.4H_2O$ (0.240 mg, 0.5 mmol) to this solution, the solution was stirred for 1 day at room temperature. The obtained complex monomer was then filtered and extensive washed with EtOH and deionized H_2O. Then, it was dried at 50°C for 24 h.

Synthesis p-HEMA-$(MAAP)_2$-Th(IV) Cryogel Polymer (IIP)

p-HEMA-$(MAAP)_2$-Th(IV) cryogel polymer was prepared according to a previously reported method(Figure 3) [49]. For this purpose, 0.25 g MBAAm was dissolved in deionized H_2O, and then 1.5 mL HEMA and 1.5 mL $(MAAP)_2$Th(IV) complex monomer were mixed with this solution. Initiator APS (20 mg)/TEMED (20 µl) was added and the final mixture was placed into a syringe closed with parafilm and allowed to polymerize at -18 °C for 24 h. The frozen solution was allowed to thaw at room temperature. Finally, the prepared imprinted cryogel polymer was washed with EtOH and deionized H_2O to remove impurities, which was then stored at +4°C.

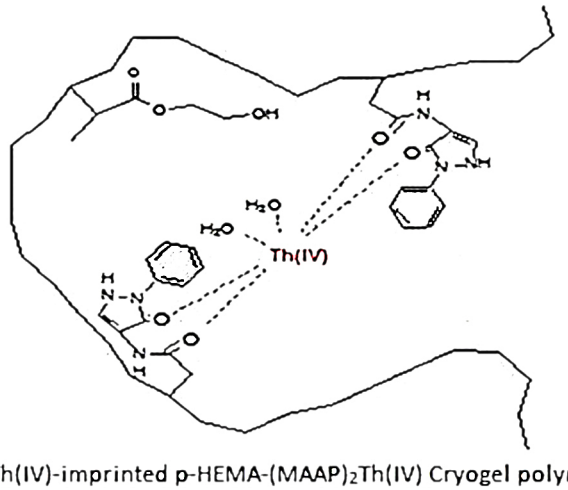

Figure 3. Schematic depiction of the prepared Th(IV)-imprinted p-HEMA-$(MAAP)_2$Th(IV) Cryogel polymer.

Removal of Th(IV) from p-HEMA-$(MAAP)_2$-Th(IV) Cryogel Polymer (IIP)

To obtain the 3-D cavities for re-binding of Th(IV), the template Th(IV) was successfully desorbed from the p-HEMA-$(MAAP)_2$-Th(IV) cryogel polymer. For this purpose, the cryogel polymer was desorbed with 5.0 mol.L^{-1} HNO_3 as the desorbtion solvent for 1 h by using a peristaltic pump. This washing step was repeated until no Th(IV) was determined in the desorption solvent.

Characterization Studies

MAAP monomer and Prepared $(MAAP)_2$-Th(IV) complex monomer were characterized by FT-IR spectroscopy, whereas p-HEMA-$(MAAP)_2$ cryogel polymer were characterized by and SEM technique. To obtain FT-IR spectra p-HEMA-$(MAAP)_2$ cryogel polymer, KBr was mixed with the dried polymer particles and pressed into a pellet form, and the spectra were then recorded.

For the SEM analysis of p-HEMA-$(MAAP)_2$ cryogel polymer were covered on the surface of platinum and coated with gold (thicknes of 20 nm). Then, SEM analyses were carried out.

To calculate the swelling ratio of p-HEMA-$(MAAP)_2$ cryogel polymer, the cryogel was dried and weighed until constant weight (m_{dried}). Then, it was placed in a 30 mL vial containing distilled water and kept at 25°C for 2 h. The cryogel was removed from water, wiped by a filter paper and weighed again (m_{wet}). The swelling ratio was calculated according to;

$S = m_{wet} - m_{dried} / m_{dried}$

For the measurement of macroporosity percentage (M%) of cryogels, the mass of water-saturated cryogels (m_{wet}) was weighed. The cryogel was squeezed to remove free water which is found in the pores (msqueezed), and the mass of cryogel without water was weighted. M% was calculated according to;

$M\% = m_{wet} - m_{squeezed} / m_{wet}$

Binding Studies of Th(IV) Ion to IIP and NIP

Continuous column system was used to bind Th(IV) to Th(IV)-imprinted p-HEMA-$(MAAP)_2$ cryogel polymer (IIP) and non-imprinted p-HEMA-$(MAAP)_2$ cryogel polymer (NIP). For this purpose, firstly, columns containing IIP and NIP was washed with deinozed H_2O and equilibrated with 0.1 mol.L^{-1} phosphate buffer, pH. 7.0. Then, aqueous solution of Th(IV) was passed through the columns containing IIP and NIP at 1 mL.min^{-1} flow rate for 1 h. The amounts of Th(IV) was determined by ICP-MS. Then, 5.0 mol.L^{-1} HNO_3 was used to desorption Th(IV) bound to the IIP and NIP. Sevaral factors such as pH, flow rate and initial Th(IV) concentration were also investigated to obtain the optimum conditions for the binding of Th(IV) to the IIP and NIP. 10 ppm Th(IV) in different pH values (pH 3 to 10) was passed through the columns containing IIP and NIP at 1 mL.min^{-1} flow rate for 1 h in order to test pH influence on Th(IV) binding to the IIP and NIP. Then, the samples came out from the column were analyzed by ICP-MS. The flow rates between 1.0 mL.min^{-1} and 5.0 mL.min^{-1} were applied for the investigation of the effects of these parameters

on the binding of Th(IV) to the IIP and NIP. The initial Th(IV) concentration was varied between 10 pmm and 3000 ppm to determine maximum binding capacity.

Selectivity and Reusability of the Prepared IIP and NIP

The selectivity of the preapred IIP and NIP toward Th(IV) were investigated in the presence of Th(IV)-La(III), Th(IV)-Ce(III) and Th(IV)-Eu(III) ion pairs. For this purpose 25 mL of 10 ppm lanthanide solutions in 10 mM acetate buffer, pH 5.0 were passed from columns containing IIP and NIP at a flow rate of 1 mL.min^{-1} at room temperature. Analysis of the lanthanide ions in the column output samples was performed by ICP-MS.

The distribution coefficient of Th(IV) ion between the columns containing IIP-NIP and aqueous solutions was calculated using the following formula:

$$K_d = (C_i\text{-}C_f/C_i)x(V/m)$$

where K_d is the distribution coefficient, C_i is initial Th(IV) concentration and C_f is final Th(IV) concentration, V represents the solution volume (mL) and m is the polymer mass (g).

The selectivity coefficient (k) and relative selectivity coefficient (k') for Th(IV) in the presence of other competing lanthanide ions can be calculated applying the following equation:

$$k = K(Th(IV))/K(interfering\ ion)$$

$$k' = K(imprinted)/K(nonimprinted)$$

where K(Th(IV)) is the distribution ratio of Th(IV) ion and K(interfering ion) is the distribution ratio of potentially interfering ions.

For the reusability studies, binding and leach studies were repeated 10 times using same IIP. After each step, column containing IIP was washed with 5 mol.L^{-1} HNO_3 and deionized water.

Binding Studies of Th(IV) Ion from Bastnaesite Ore

Bastnaesit ore was selected as the real sample for the selective binding of Th(IV). For this purpose, 1 g powdered bastnaesite ore was leached using concentrated HNO_3 and H_2SO_4 by microwave irradiation. Then, solution pH was adjusted to 5.0 using acetate buffer and volume of the final solution was distilled to 100 mL by deionized water. The prepared bastnaesite solution was passed through the columns containing IIP and NIP the under the optimum conditions. Analysis of the ions in the column output samples was performed by ICP-MS.

RESULTS and DISCUSSION

Characterization of MAAP and $(MAAP)_2$Th(IV) Complex Monomer

Prepared $(MAAP)_2$-Th(IV) complex monomer were characterized by FT-IR spectroscopy, which proved that monomer and complex monomer were synthesized. The obtained FT-IR spectrum of the functional monomer MAAP is given in Figure 4. The spectra shows the characteristic bands of monosubstituted benzene ring at 713.6 cm^{-1} and strong bands at 1412.7 cm^{-1} indicating conjugation at aromatic ring and CH2 vibration band. The absorption bands due to amide carbonyl were observed at 1659.5 cm^{-1}. Aromatic and aliphatic C-H bands were observed at 3032.5 and 2991.0 cm^{-1}, respectively and N-H band at 3209.5 cm^{-1} confirmed the MAAP structure. In the FT-IR spectrum of complex monomer, the absorption band at 1659.5 cm^{-1} due to amide carbonyl was shifted to 1662.3 cm^{-1} due to the interaction between carbonyl bond and Th(IV). The C-N strength band at 1114.7 cm^{-1} was shifted to 1151.4 cm^{-1}, indicating Th(IV) interaction. Thus, this FT-IR spectrum confirmed synthesis of (MAAP)2-Th(IV) complex monomer.

Characterization of Th(IV)-Imprinted p-HEMA-$(MAAP)_2$ Cryogel Polymer (IIP)

p-HEMA and Th(IV)-imprinted p-HEMA-$(MAAP)_2$ cryogel polymer (IIP) were characterized by FT-IR and SEM. Figure 5a shows the FT-IR Spectra p-HEMA and Th(IV)-imprinted p-HEMA-$(MAAP)_2$ cryogel polymer (IIP). As can be seen, p-HEMA and Th(IV)-imprinted p-HEMA-$(MAAP)_2$ cryogel polymer (IIP) exhibited FT-IR patterns with small differences which confirms the similar polymer backbone. The pore structure and pore size of Th(IV)-imprinted p-HEMA-$(MAAP)_2$ cryogel polymer (IIP) were visualized with SEM images as seen in Figure 5b. As shown in the figure

5b, the p-HEMA-$(MAAP)_2$ cryogel polymer has interconnected pores and porous structure. Pore size was found about 50 μm. The equilibrium swelling degree and macroporosity of the p-HEMA-$(MAAP)_2$ cryogel were 6.74 g H_2O/g cryogel and 77.61%, respectively.

Binding Studies of Th(IV) on IIP and NIP

pH effect on Th(IV) Binding

The change in amount of Th(IV) binding to the IIP and NIP as a function of pH was investigated, as seen in Figure 6. The maximum Th(IV) binding to the IIP and NIP pH 5.0. This could be explained by electron transfer based covalent cross-linking between Th(IV) and antypirine of the functional monomer at pH 5.0 [13,50]. Figure 6 clearly shows effect of pH on Th(IV) binding to theIIP and NIP. As seen in the figure, the values higher and lower than pH 5.0 lead to low binding of Th(IV) to the IIP and NIP, which can be explained by the repulsive electrostatic interactions between bound Th(IV) ion and antipyrine monomer. The binding efficiency may decrease because of the size of conformation and the lateral electrostatic interactions between adjacent Th(IV) ion on the IIP and NIP.

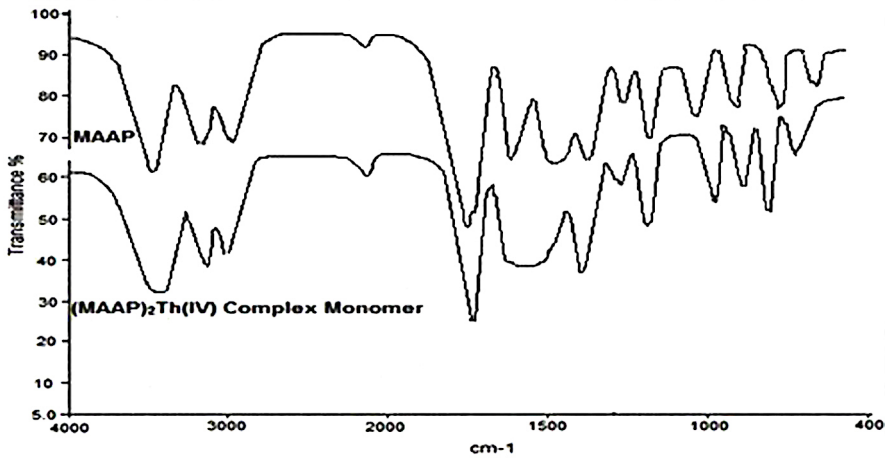

Figure 4. FT-IR spectrum of MAAP and $(MAAP)_2$-Th(IV) complex monomer.

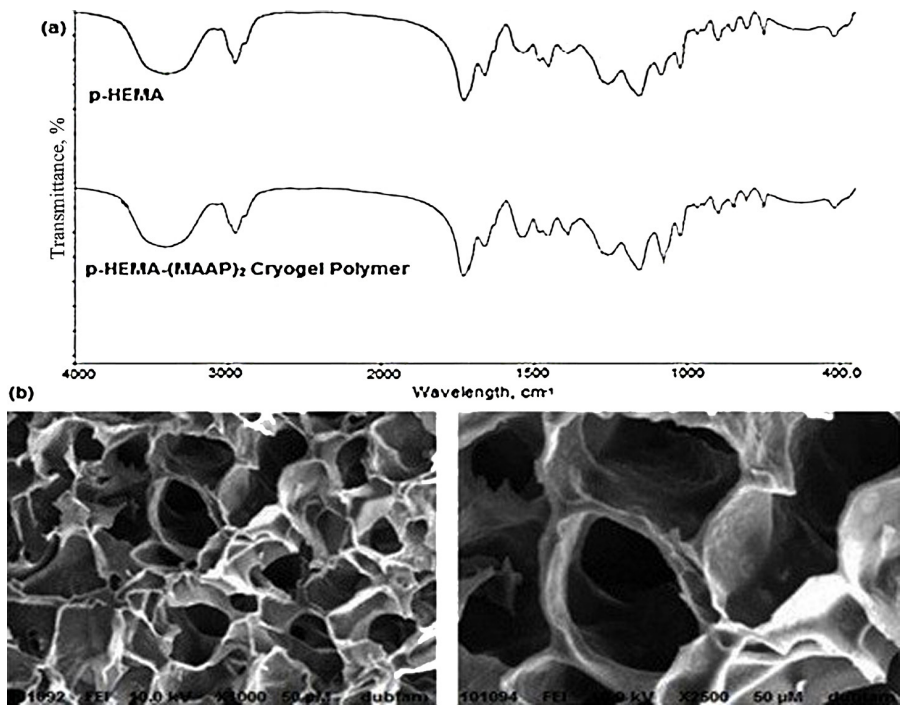

Figure 5. (a) FT-IR Spectra p-HEMA and Th(IV)-imprinted p-HEMA-$(MAAP)_2$ (b) SEM images Th(IV)-imprinted p-HEMA-$(MAAP)_2$ cryogel polymer (IIP).

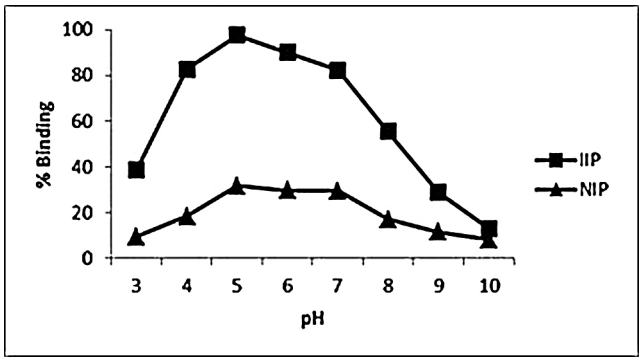

Figure 6. Effect of pH on Th(IV) Binding. Experimental conditions: Initial Th(IV) Concentration: 10 ppm; Temperature: 25°C; Flow rate: 1 mLmin^{-1}; Time: 1 h.

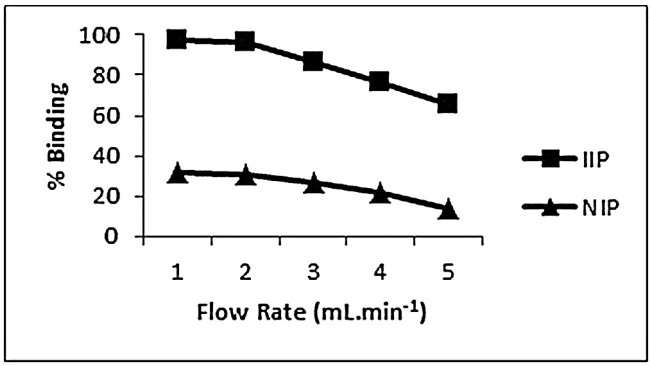

Figure 7. Effect of Flow Rate on Th(IV) Binding. Experimental conditions: pH: 5; Initial Th(IV) Concentration: 10 mg.L^{-1}, Temperature: 25°C; Time: 1 h.

Flow Rate Effect on Th(IV) Binding

The flow rate of the Th(IV) solution pumped through the cryogel is one of the crucial parameter for the control of binding process [51]. The flow rate effect on the binding of Th(IV) was explored by changing the flow rate from 1.0 to 5.0 mL.min^{-1}. 10 mg.L^{-1} Th(IV) solution was used for this purpose. Owing to the back pressure produced by the column, the flow rates higher than 5.0 mL.min^{-1} could not be investigated. As shown in Figure 7, increasing flow rate resulted in a decrease in the binding of Th(IV) from 97.52% to 65.26% binding capacity.

Initial Th(IV) Concentration Effect on Th(IV) Binding

Initial Th(IV) concentration dependence of the bound amount of the Th(IV) on to IIP and NIP is depicted in Figure 8. As can be seen, Th(IV) binding increased when initial Th(IV) concentration is increased, and an equilibrium was obtained at a Th(IV) concentration of 3000 ppm. The maximum binding capacity was obtained as 48.30 mg.g^{-1} for IIP , while that of NIP was 6.72 mg.g^{-1}. it was found that maximum binding yield obtained was fairly good result when compared to other studies [13-51,52].

Regeneration and Reusability of the Th(IV)-Impirinted pHEMA-$(MAAP)_2$ Cryogel Polymer (IIP)

One of the crucial advantage for an affinity material for the recognition and separation processes is its reusability. To test the reusability of the prepared IIP, Th(IV) binding and elution cycle was repeated 10 times using the same cryogel (Figure 9).

The elution of Th(IV) from the IIP was performed by using 5.0 mol.L^{-1} HNO_3 as the desorption solution and complete removal of Th(IV) was achieved after the desorption step. It was found that the binding behavior of the IIP towards Th(IV) did not changed significantly after ten binding and desorption cycles. Thus, one can easily say that the IIP are stable and the IIP can be used many times without significantly loss of their binding capacity.

Selectivity Studies

Competitive binding of Th(IV)-La(III), Th(IV)-Ce(III) and Th(IV)-Eu(III) were also explored in a column system. The obtained results are given in Table 1. Th(IV) imprinted cryogel polymer (IIP) exhibited higher selectivity toward Th(IV) ions over La(III), Ce(III) and Eu(III) ions. Kd values for the IIP were compared with NIP. The obtained

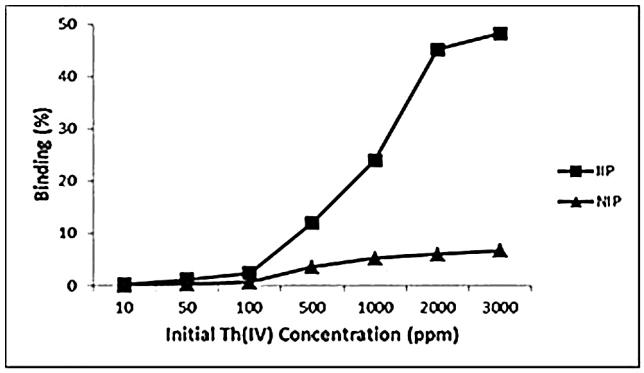

Figure 8. Effect of Initial Th(IV) Concentration on Th(IV) Binding. Experimental conditions: pH: 5; Temperature: 25°C; Flow rate: 1 mL.min^{-1}; Time: 1 h.

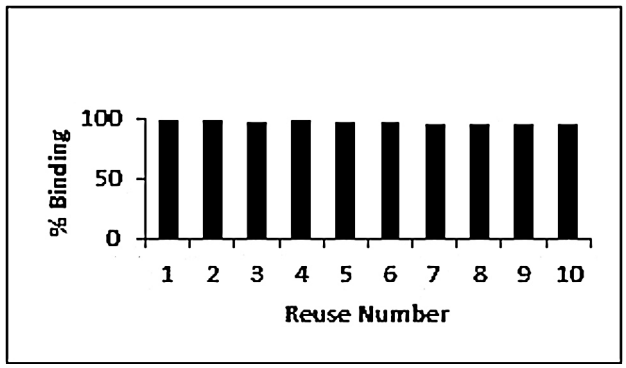

Figure 9. Reusability of IIP. Experimental conditions: pH: 5; Initial Th(IV) Concentration: 10 mg L^{-1}; Temperature: 25°C; Flow rate: 1 mL.min^{-1}; Time: 1 h.

Table 1. K_d, k and k' values of La(III), Ce(III) and Eu(III) with respect to Th(IV). Experimental conditions: pH: 5; Temperature: 25°C; Flow rate: 1 mL.min^{-1}; Time: 1 h.

Cryogel Column	Th(IV) (mg/L)	La(III) (mg/L)	Kd (Th(IV))	Kd (La(III))	k	k'
Non-imprinted	10	10	467.8	2874.4	0.16	-
Th(IV)-imprinted	10	10	11206	863.5	12.3	77
Cryogel Column	Th(IV) (mg/L)	Ce(III) (mg/L)	Kd (Th(IV))	Kd (Ce(III))	k	k'
Non-imprinted	10	10	1095.4	3026.0	0.36	-
Th(IV)-imprinted	10	10	97335	2492.5	39	108
Cryogel Column	Th(IV) (mg/L)	Eu(III) (mg/L)	Kd (Th(IV))	Kd (Eu(III))	k	k'
Non-imprinted	10	10	530.7	1978.5	0.27	-
Th(IV)-imprinted	10	10	66764	2578.6	26	96

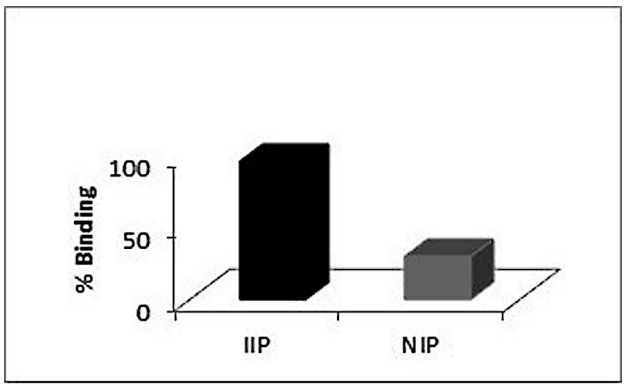

Figure 10. Selective Separation of Th(IV) from Bastnaesite Ore. Experimental Conditions: $C_{Th(IV)}$= 2.65 mg.L^{-1} (in the real sample), pH= 5.0, Flow Rate= 1 mL.min^{-1}, T= 25°C.

results confirmed that the relative selectivity coefficients of the IIP for the Th(IV)/La(III), Th(IV)/Ce(III) and Th(IV)/Eu(III) were 77, 108 and 96 times higher than the corresponding NIP, respectively. As a result, it was found that the prepared Th(IV)-imprinted cryogel polymer exhibited a high selectivity to Th(IV) ion in the presence of other lanthanides [13].

Selective Separation of Th(IV) from Basnaesite Ore

The outcomes of the binding experiments of Th(IV) from bastnaesite ore, which provided from Eskişehir-Sivrihisar region are given in Figure 10. The results showed that the IIP displayed 95.88% binding toward Th(IV) while NIP showed 29.76% binding.

CONCLUSION

In this study, a new IIP (p-HEMA-(MAAP)$_2$) that shows high affinity and selectivity toward Th(IV) was prepared. The obtained results showed that the prepared IIP selectively binds Th(IV) ions in the presence of other lanthanide ions Eu(III), Ce(III) and La(III) from aqueous solutions and bastnaesite ore . Under the optimum conditions, the maximum binding capacity of the prepared IIP was obtained as 48.30 mg.g^{-1}. Consequently, a separation material has been developed which will contribute to the separation and preconcentration of the Th(IV) by the IIP, specially designed for use in nuclear power plants as an alternative to uranium, from other components with high selectivity.

References

1. S.F. Ashley, G.T. Parks, W.J. Nuttall, C. Boxall, R.W. Grimes, Thorium fuel has risks, Nature, 492 (2012) 31–33.
2. Y.P. Du, Y.W.Zhang, Z.G. Yan, L.D. Sun, C.H. Yan, Highly luminescent self-organized sub-2-nm EuOF nanowires, J. Am. Chem. Soc., 131 (2009) 16364–16365.
3. B.G. Shen, J.R. Sun, F.X. Hu, H.W. Zhang, Z.H. Cheng, Recent progress in exploring magnetocaloric materials, Adv. Mater., 21 (2009) 4545–4564.
4. V.K. Jain, A. Handa, S.S. Sait, P. Shrivastav, Y.K. Agrawal, Pre-concentration, separation and trace determination of lanthanum(III), cerium(III), thorium(IV) and uranium(VI) on polymer supported o-vanillinsemicarbazone, Anal. Chim. Acta, 429 (2001) 237–246.
5. I. Dolak, M. Karakaplan, B. Ziyadanoğulları, R. Ziyadanoğulları, Solvent extraction, preconcentration and determination of thorium with monoaza 18-Crown-6 derivative, Bul. Kor. Chem. Soc., 32 (2011) 1564-1568.
6. S.K. Sahu, V. Chakravortty, M.L.P. Reddy, T.R. Ramamohan, The synergistic extraction of thorium(IV) and uranium(VI) with mixtures of 3-phenyl-4-benzoyl-5-isoxazolone and crown ethers, Talanta, 51 (2000) 523–530.
7. Q. He, X. Chang, Q. Wu, X. Huang, Z. Hu, Y. Zhai, Synthesis and applications of surface-grafted Th(IV)-imprinted polymers for selective solid-phase extraction of thorium(IV), Anal. Chim. Acta, 605 (2007) 192-197.
8. C. Lin, H. Wang, Y. Wang, Z. Cheng, Selective solid-phase extraction of trace thorium(IV) using surface-grafted Th(IV)-imprinted polymers with pyrazole derivative, Talanta, 81 (2010) 30-36.
9. Y. Chen, Y. Wei , L. He, F. Tang, Separation of thorium and uranium in nitric acid solution using silica based anion exchange resin, J. Chrom. A, 1466 (2016) 37-41.
10. S. Chandramouleeswaran, J. Ramkumar, n-Benzoyl-n-phenylhydroxylamine impregnated Amberlite XAD-4 beads for selective removal of thorium, J. Haz. Mat., 280 (2014) 514-523.

11. M.A.A. Aslani, F. Celik, S. Yusan, C.R.K. Aslani, Assessment of the adsorption of thorium onto styrene–divinylbenzene-based resin: Optimization using central composite design and thermodynamic parameters, Pro. Saf. Enviro. Pro., 109 (2017) 192-202.
12. F. Khalili, G. Al-Banna, Adsorption of uranium(VI) and thorium(IV) by insolubilized humic acid from Ajloun soil e Jordan, J. Enviro. Radio., 146 (2015) 16-26.
13. S. Buyuktiryaki, R. Say, A. Ersoz, E. Birlik, A. Denizli, Selective preconcentration of thorium in the presence of UO_2^{2+}, Ce^{3+} and La^{3+} using Th(IV)-imprinted polymer, Talanta, 67 (2005) 640-645.
14. N. Bereli, D. Türkmen, K. Köse, A. Denizli, Glutamic acid containing supermacroporous poly(hydroxyethyl methacrylate) cryogel disks for UO_2^{2+} removal, Mat. Sci. Eng. C, 32 (2012) 2052-2059.
15. M.M. Yusoff, N. Rohani, N. Mostapa, M.S. Sarkar, T.K. Biswas, M.L. Rahman, S.E. Arshad, M.S. Sarjadi, A.D. Kulkarni, Synthesis of ion imprinted polymers for selective recognition and separation of rare earth metals, J. Rare Earths, 35 (2017) 177-185.
16. L. Uzun, R. Uzek, S. Şenel, R. Say, A. Denizli, Chiral recognition of proteins having L-histidine residues on the surface with lanthanide ion complex incorporated-molecularly imprinted fluorescent nanoparticles, Mat. Sci. Eng. C, 33 (2013) 3432-3439.
17. İ. Dolak, R. Keçili, D. Hür, A. Ersöz, R. Say, Ion-imprinted polymers for selective recognition of neodymium (III) in environmental samples, Ind. Eng. Chem. Res., 54 (2015) 5328-5335.
18. M. Gedikli, Ş. Ceylan, M. Erzengin, M. Odabaşı, A novel matrix for hydrophobic interaction chromatography and its application in lysozyme adsorption, Acta Biochim. Pol., 61 (2014) 731–737.
19. I. Göktürk, R. Üzek, L. Uzun, A. Denizli, Synthesis of a specific monolithic column with artificial recognition sites for L-glutamic acid via cryo-crosslinking of imprinted nanoparticles, Nanomedicine Biotech., 44 (2016) 1133–1140.
20. M. Odabaşı, G. Baydemir, M. Karatas, A. Derazshamshir, Preparation and characterization of metal-chelated poly(HEMA-MAH) monolithic cryogels and their use for DNA adsorption, J. App. Pol. Sci., 116 (2010) 1306–1312.
21. K. Balamurugan, K. Gokulakrishnan, T. Prakasam, Preparation and evaluation of molecularly imprinted polymer liquid chromatography column for the separation of Cathine enantiomers, Saudi Pharm. J., 20 (2012) 53–61.
22. R. Say, E. Birlik, A. Ersöz, F. Yilmaz, T. Gedikbey, A. Denizli, Preconcentration of copper on ion-selective imprinted polymer microbeads, Anal. Chim. Acta. 480 (2003) 251–258.
23. E. Tamahkar, Adil Denizli, Metal ion coordination interactions for biomolecule recognition: a Review, Hittite J. Sci. and Eng., 2014, 1 21-26.
24. Y. Saylan, F. Yilmaz, E. Özgür, A. Derazshamshir, H. Yavuz, A. Denizli, Molecular imprinting of macromolecules for sensor applications, Sensors, 17 (2017) 1-30.
25. G. Vasapollo, R.D. Sole, L. Mergola, M.R. Lazzoi, A. Scardino, S. Scorrano, G. Mele, Molecularly imprinted polymers: Present and future prospective, Int. J. Mol. Sci. 12 (2011) 5908–5945.
26. H.J. Monodispersed, molecularly imprinted polymers as affinity-based chromatography media, J. Chrom. B, 866 (2008) 3–13.
27. S. Wei, B. Mizaikoff, Recent advances on noncovalent molecular imprints for affinity separations, J. Sep. Sci., 30 (2007) 1794–1805.
28. M. Lasáková, P. Jandera, Molecularly imprinted polymers and their application in solid phase extraction, J. Sep. Sci., 32 (2009) 788–812
29. B. Sellergren, Imprinted chiral stationary phases in high-performance liquid chromatography, J. Chrom. A, 906 (2001) 227–252.
30. F. Puoci, F. Lemma, N. Picci, Stimuli-responsive molecularly imprinted polymers for drug delivery: A review, Curr. Drug Deliv., 5 (2008) 85–96.
31. A. Concheiro, Molecularly imprinted polymers for drug delivery, J Chrom. B, 804 (2004) 231-45.
32. G. Wulff, Enzyme-like catalysis by molecularly imprinted polymers, Chem. Rev., 102 (2002) 1–27.
33. S. Vidyasankar, F.H. Arnold, Molecular imprinting: Selective materials for separations, sensors and catalysis, Curr. Opin. Biotech., 6 (1995) 218–224.
34. G. Selvolini, G. Marrazza, MIP-Based Sensors: Promising New Tools for Cancer Biomarker Determination, Sensors, 17 (2017) 718-736.
35. B.D. Gupta, A.M. Shrivastav, S.P. Usha, Surface plasmon resonance-based fiber optic sensors utilizing molecular imprinting, Sensors, 16 (2016) 1381-1413.
36. S.M. Madhappan, K.T. Pradip, S.P. Sung, M. Aneesh, J.C. Hun, S.H. Chang, On-imprinted mesoporous silica hybrids for selective recognition of target metal ions, Micropor. Mesopor. Mat., 180 (2013) 162-171.
37. M. Monier, D.A. Abdel-Latif, Fabrication of Au(III) ion-imprinted polymer based on thiol-modified chitosan, Int. J. Bio. Macro., 105 (2017) 777-787.
38. R. Msaadi, S. Ammar, M.M. Chehimi, Y. Yagci, Diazonium-based ion-imprinted polymer/clay nanocomposite for the selective extraction of lead(II) ions in aqueous media, Eur. Pol. J., 89 (2017) 367-380.
39. M. Monier, D.A. Abdel-Latif, Y.G. Abou El-Reash, Ion-imprinted modified chitosan resin for selective removal of Pd(II) ions, J. Col. Inter. Sci., 469 (2016) 344-354.
40. M. Roushani, S. Abbasi, H. Khani, R. Sahraei, Synthesis and application of ion-imprinted polymer nanoparticles for the extraction and preconcentration of zinc ions, Food Chem., 173 (2015) 266-273.
41. M. Mitreva, I. Dakova, I. Karadjova, Iron(II) ion imprinted polymer for Fe(II)/Fe(III) speciation in wine, Microchem. J., 132 (2017) 238-244.
42. M. Moussa, V. Pichon, C. Mariet, T. Vercouter, N. Delaunay, Potential of ion imprinted polymers synthesized by trapping approach for selective solid phase extraction of lanthanides, Talanta, 161 (2016) 459-468.

43. M. Fayazi, M. Ghanei-Motlagh, M.A. Taher, R. Ghanei-Motlagh, M.R. Salavati, Synthesis and application of a novel nanostructured ion-imprinted polymer for the preconcentration and determination of thallium(I) ions in water samples, J. Haz. Mat., 309 (2016) 27-36.
44. B. Gao, J. Meng, Y. Xu, Y. Zhang, Preparation of Fe(III) ion surface-imprinted material for removing Fe(III) impurity from lanthanide ion solutions, J. Ind. Eng. Chemi., 24 (2015) 351-358.
45. M. Andaç, R. Say, A. Denizli, Molecular recognition based cadmium removal from human plasma, J. Chrom. B, 811 (2004) 119-126.
46. N. Candan, N. Tüzmen, M. Andaç, C.A. Andaç, R. Say, A. Denizli, Cadmium removal out of human plasma using ion-imprinted beads in a magnetic column, Mat. Sci. and Eng. C, 29 (2009) 144-152.
47. A. Ersöz, R. Say, A. Denizli, Ni(II) ion-imprinted solid-phase extraction and preconcentration in aqueous solutions by packed-bed columns, Anal. Chim. Acta, 502 (2004) 91-97.
48. R. Keçili, R. Say, A. Ersöz, H. Yavuz, A. Denizli, Purification of penicillin acylase through a monolith column containing methacryloyl antipyrine, Sep. Pur. Tech., 55 (2007) 1-7.
49. Z. Baysal, E. Aksoy, İ. Dolak, A. Ersöz, R. Say, Adsorption Behaviours of lysozyme onto poly-hydroxyethyl methacrylate cryogels containing methacryloyl antipyrine-Ce(III), Int. J. Poly. Mat. Poly. Biomat., 67 (2018) 199-204.
50. E. Birlik , S. Büyüktiryaki , A. Ersöz , A. Denizli, R. Say, Selective separation of thorium using ion imprinted chitosan-phthalate particles via solid phase extraction, Sep. Sci. Tech., 41 (2006) 3109-3121.
51. H. Lianga, Qi. Chen, J. Mab, Y. Huang, X. Shen, Synthesis and characterization of a new ion-imprinted polymer for the selective separation of thorium(IV) ions at high acidity, Royal Soc. of Chem., 7 (2017) 35394-35402.
52. I. Yener, E. Varhan Oral, I. Dolak, S. Ozdemir, R Ziyadanogullari, A new method for preconcentration of Th(IV) and Ce(III) by thermophilic Anoxybacillus flavithermus immobilized on Amberlite XAD-16 resin as a novel biosorbent, Eco. Eng., 103 (2017) 43–49.

Petaloid Monocotyledonous Flora of Tunceli Province (Turkey)

Tunceli (Türkiye)'nin Monokotil Petaloidleri

Research Article

Metin Armağan*
Department of Medicinal and Aromatic Plants, Buharkent Vocational School, Adnan Menderes University, Aydın, Turkey.

ABSTRACT

This study was carried out to determine the monocotyl petaloids of Tunceli Province (Turkey). The research area is located in B7 square and a little part in B8 square based on the quadratic system of Davis. In this research, the field studies were carried out in Tunceli during 2014-2015. Totally 150 taxa (142 species, 4 subspecies and 4 varieties) which are 33 endemic were identified belonging to 11 families. Of the taxa found in the area, 26 were newly recorded for the province of Tunceli. This study is part of the ongoing research to determine for Flora of Tunceli.

Key Words
Tunceli, petaloid, monocotyledonous, geophyte, Turkey.

ÖZ

Bu çalışma, Tunceli (Türkiye) ilinin monokotil petaloidlerini tespit etmek amacıyla yapılmıştır. Araştırma alanı Davis'in kareleme sistemine göre çoğunluğu B7, az bir kısmı ise B8 karesindedir. Bu araştırmada, 2014–2015 yılları arasında Tunceli'de arazi çalışmaları yapılmıştır. Tayin edilen bitkilerden 11 familyaya ait toplam 150 takson (142 tür, 4 alttür ve 4 varyete) tespit edilmiş olup, bunlardan 33 tanesi endemiktir. Alanda tespit edilen taksonlardan 26 tanesi Tunceli ili için yeni kayıttır. Bu çalışma devam eden Tunceli Florası'nın belirlenmesi çalışmasının bir bölümüdür.

Anahtar Kelimeler
Tunceli, petaloid, monokotil, geofit, Türkiye.

Article History: Received: Feb 25, 2018; Revised: Mar 03, 2018; Accepted: Mar 05, 2018; Available Online: Mar 26, 2018.

DOI: 10.15671/HJBC.2018.229

Correspondence to: M. Armağan, Dept. of Med. and Aromatic Plants, Buharkent Voc. School, Adnan Menderes Uni., Aydın, Turkey.
Tel: +90 538 609 0819 Fax: +90 256 391 3151 E-Mail: metinarmagan@gmail.com

INTRODUCTION

Turkey appears as a bridge between Europe and Asia. The flora of Turkey has rich and interesting plant diversity due to the interaction between Mediterranean, Irano-Turanian and Europe-Siberian phytogeographic regions [1]. Anatolia's location at the connections of Europe, the Middle East, Central Asia, and Africa and also its high topographic and climatic heterogeneities lead to high biodiversity and rate of endemism [2].

Tunceli is located on Anatolian diagonal in Eastern region of Turkey. Geography of Tunceli composes of significant elevations (Sultanbaba, Munzur, Hel-Yel-Zel, Buyerbaba, and Düzgünbaba etc.), the rivers (Munzur, Pülümür, Mercan, Tahar, and Perisuyu) and the valleys (Munzur, Pülümür, Rabat, Tahar, and Mercan etc.). The least area of agriculturally fit land of Eastern Anatolia is found in Tunceli, being 114.000 ha. Livestock raising is thus very important. Most of the grasslands are mowed for winter fodder [3].

Figure 1. Some geophytes from Tunceli. a. ***Iris sari*** Schott ex Baker (***endemic***), b. ***Iris galatica*** Siehe (***endemic***), c. ***Ornithogalum munzurense*** Speta (***endemic***), d. ***Ophrys oestrifera*** M.Bieb., e. ***Puschkinia scilloides*** Adams, f. ***Fritillaria imperialis*** L. and Munzur mountains, g. ***Colchicum munzurense*** K.Perss. (***endemic***), h. ***Tulipa armena*** Boiss.

The Munzur Mountains is the most famous and biggest mountains in Tunceli. The 1407 vascular plant taxa belonging to 98 families and 479 genera are reported in these mountains, which forming the border of Erzincan and Tunceli [4].

The geophytes –including some endemics– have been gathered unconsciously or consciously as ornamental, food or medicinal plants by the public collectors due to their economic value in the world (Figure 1). Moreover, the deterioration of natural areas due to human influences threat to their generations. Therefore the conservation of plants species and the prepared reports about distributing areas are important for the biodiversity [5].

MATERIALS and METHODS

In this study, about 3400 plant samples were collected within the borders of Tunceli province during the vegetation seasons in 2014 and 2015, and photos, GPS coordinates, and habitat information were taken in their natural habitats. The collected samples were dried based to herbarium methods, and the collector numbers were given. Prepared samples with respect to herbarium techniques were stored in the AYDN and VANF herbaria. In order to compile an up-to-date and inclusive list, the taxa identified in the study and in previous studies were given together in single list.

During the identification of samples, Flora of Turkey and the East Aegean Islands [6,7,8]) were initially used for the nomenclaturel checking of plant names it was mainly utilized from "Bizim Bitkiler [9]" and "The Plant List [10]". For the locality information of plants, the location, altitude, habitat, date of collection, number of collector, and the reference literature code are given respectively. Locality records belonging to the references were given unchanged in their original form. Tunceli name was not repeatedly written at the beginning of each locality because the study was carried out only in the Tunceli province. The phytogeographic region elements and the endemism status of the taxa were specified at the end of the record of localities.

Literatures and abbreviations used in the Floristic List as follow;
MA = This study, R4 = Reference 4, R6 = Reference 6, R8 = Reference 8, R11 = Reference 11, R12 = Reference 12, R13 = Reference 13, R14 = Reference 14, R15 = Reference 15.

End. = Endemic, Ir.-Tur. = Irano – Turanian, Medit. = Mediterranean, Hyr.-Eux. = Hyrcano – Euxine, Eux. = Euxine, Euro.-Sib. = Euro – Siberian, E.Medit. = East Mediterranean.

AYDN = Herbarium of Adnan Menderes University

VANF = Herbarium of Yüzüncü Yıl University

RESULTS

Totally 150 taxa (142 species, 4 subspecies and 4 varieties) which are 33 endemic belonging to 11 families were identified. Of the taxa found in the area, 26 were newly recorded for the province of Tunceli. The list of taxa and the collection data were given below alphabetically order of the family, genus, species, and if it is present infraspecific category.

ALISMATACEAE

Alisma lanceolatum With./**Kurbağakaşığı**

Mazgirt, c. 3.3 km EESE Mazgirt, Yukarıoyumca, 1430 m, boggy area besides lake, 11.vi.2013, V.Y.E. & M. 13-0017 **(R14).**

AMARYLLIDACEAE

Allium akaka S.G.Gmel. ex Schult. & Schult.f./**Yer soğanı**

Pülümür, 500 m N of Balpayam (3 – 4 km S of Kırklar), 2400 m, mountain steppe, 18.vi.2014, Armağan 4844 **(MA)**. Ir.-Tur.

Allium ampeloprasum L./**Pırasa**

Çemişgezek, between Bozağaç and Ulukale, 1 km E of Ulukale, 1080 m, dried river bed, shade area, 28.vi.2014, Armağan 5148 **(MA).** Medit.

Allium armenum Boiss. & Kotschy/**Pembesırım**

Pülümür, 2 km from Turnadere to Közlüce, 1575 m, rocky areas, 18.vi.2014, Armağan 4765 **(MA)**; Ovacık, banks of Munzur Suyu, 1200 m, 18.vi.1979, Yıldırımlı 2034 **(R4);** Ovacık, Akyayık Köyü, 1315 m, 10.iv.2013, E.Yüce 2794 **(R13);** Munzur Vadisi **(R15).** Ir.-Tur., End.

Allium asperiflorum Miscz./**Benekli soğan**

Mazgirt, Akpazar town, S of Yenice (S of Şevki Mezrası), 1270 m, steppe, 02.vi.2014, Armağan 4129 **(MA)**. Ir.-Tur., End.

Allium atroviolaceum Boiss./**Liflikörmen**

Mazgirt, 1 km E of Geçitveren, 1270 m, steppe, 16.vi.2014, Armağan 4588 **(MA)**; Ovacık, Güneykonak Köyü, 1230 m, E.Yüce 2805 **(R13)**; Tunceli-Ovacık arası, Munzur Vadisi Milli Parkı çıkışı, 1215 m, 03.vii.2013, E.Yüce 2825 **(R13)**; Munzur Vadisi **(R15)**.

Allium balansae Boiss./**Çakılsoğanı**

Mazgirt, Tunceli-Mazgirt arası, Düzgün Baba Dağı, 1940 m, kayalık yamaçlar, 15.vi.2013, E.Vitek, E.Yüce, C.Ergin, H.H.Makal 13-0215 **(R13)**. Ir.-Tur., End.

Allium bingoelense Yıld. & Ö.Çelik

Mazgirt, 1 km S of Geçitveren, 1345 m, steppe and oak openings, 16.vi.2014, Armağan 5472 **(MA). Ir.-**Tur., End.

Allium callidictyon C.A.Mey. ex Kunth/**Kaya soğanı**

Pertek, 3 km from Elazığ-Pertek-Çemişgezek junction to Çemişgezek (1 km S of Çorovan), 870 m, steppe, 28.vi.2014, Armağan 5124 **(MA)**; Pertek, Pertek's Tunceli exit, 1100 m, rocky areas, 19.vii.2014, Armağan 5264 **(MA)**; above Pertek, 1500 m, D. 31513 **(R6)**; Munzur Vadisi **(R15)**.

Allium cardiostemon Fisch. & C.A. Mey./**Yamaçkörmeni**

Pülümür, 700 m W of Kırmızı, 1370 m, field border, 05.vi.2014, Armağan 4320 **(MA)**; Ovacık, 12 km from Ovacık to Hozat, 250 m before from Bilgeç village junction, 1850 m, roadside, 17.vi.2014, Armağan 4738 **(MA)**; Tunceli center, Gözen (iksor) village, 1490 m, field border, 19.vi.2014, Armağan 4982 **(MA)**; Ovacık, S slopes of Kırkmerdivenler, 1200-1700 m, calcereous rocks, stony places and screes, 17.vi.1979, Yıldırımlı 1936 **(R4)**; Pülümür, foots of Silbüs Dağı, 1600-2000 m, clearing of Quercus petraea subsp. pinnatiloba forest, Yıldırımlı 3347 **(R4)**; Ovacık, Ovacık'ın 14 km kuzeydoğusu, 1405 m, taşlık çayırlar, 03.vi.2014, E.Vitek & E.Yüce 14-149 **(R13)**; Road Tunceli - Ovacık, c. 5.7 km NW of Tunceli, 940 m, dry meadow, 30.v.2014, V.Y. & C. 14-048-A **(R14)**; Munzur Vadisi **(R15)**. Ir.-Tur.

Allium cassium Boiss./**Keldağaksoğanı**

Pülümür, Karagöl Köyü, Hengirvan Yaylaları, 11.v.2013 E.Yüce 2592 **(R13)**. E.Medit.

Allium chrysantherum Boiss. & Reut./**Sarı kafa**

Pertek to Tunceli, 43 km from Elazığ, 1400 m, D. 29146 **(R6)**.

Allium colchicifolium Boiss./**Gömülgen**

Tunceli center, road of Tunceli - Sütlüce, 14 km after from Tunceli-Sütlüce junction, 1800 m, steppe scree, 23.v.2014, Armağan 3824 **(MA)**; Tunceli center, 26 km from Tunceli to Ovacık (Munzur valley), 1100 m, steppe, 30.iv.2015, Armağan 6688 **(MA)**; Tunceli to Ovacık, 1100 m, T. Baytop **(R6)**; Tunceli-Ovacık arası, 1092 m, 05.vii.2012, E.Yüce 2414 **(R13)**; Tunceli-Ovacık arası, Venk Köprüsü çevresi, 1040 m, 05.vii.2012, E.Yüce 2420 **(R13)**. Ir.-Tur

Allium dictyoprasum C.A.Mey. ex Kunth/**Top soğan**

Tunceli center, road of Tunceli-Sütlüce, 15 km after from Tunceli-Sütlüce junction (to 10 km Çıralı village), 1844 m, roadside, 27.viii.2014, Armağan 6182 **(MA)**. Ir.-Tur.

Allium eginense Freyn/**Eğin soğanı**

Tunceli center, 8 km from Tunceli to Ovacık (Munzur Valley), 945 m, steep steppe slopes, 25.v.2014, Armağan 3959 **(MA)**; Tunceli center, 26 km from Tunceli to Ovacık (Munzur valley), 1060 m, steppe, 26.v.2014, Armağan 4030 & 4032 **(MA)**; Hozat, between Karacaköy and Uzundal, road of Sarısaltuk Türbesi, 1730 m, steppe, 17.vi.2014, Armağan 4640 **(MA)**; Hozat, between Karacaköy and Uzundal, around of Sarısaltuk Türbesi, 2270 m, steppe, 17.vi.2014, Armağan 4685 **(MA)**. Ir.-Tur., End.

Allium flavum L. subsp. ***tauricum*** (Besser ex Rchb.) K.Richt. var. ***tauricum***/**Torossarısı**

Pertek, 12 km from Pertek to Çemişgezek, around

of Singeç bridge, 865 m, steppe, 24.v.2014, Armağan 3903 **(MA)**; Ovacık, 1.5 km from mainroad of Ovacık-Tunceli to Yakatarla village, 1320 m, steppe, 04.vi.2014, Armağan 4214 **(MA)**; Ovacık, Akyayık Köyü, 1315 m, 26.v.2013, E.Yüce 2661 **(R13)**. Medit.

Allium glumaceum Boiss. & Hausskn./**Yırtık soğan**

Ovacık, 3 km N of Işıkvuran (Munzur Mountains), 2146 m, scree slopes, 08.viii.2014, Armağan 5926 **(MA)**. Ir.-Tur., End.

Allium guttatum Stev./**Benli soğan**

Nazımiye, between Ramazanköy and Ayranlı, 1420 m, eroded slopes, 23.vii.2014, Armağan 5594 **(MA)**; N. of Pülümür, 2000 m, Pasche 78/19 **(R6).**

Allium kharputense Freyn & Sint./**Harputsoğanı**

Tunceli center, road of Tunceli - Sütlüce, after 2 km from junction, 1050 m, steppe, 23.v.2014, Armağan 3809 **(MA)**; Pülümür, 2000 m, It. Leyd. 1959:1616 **(R6)**; Pülümür, foots of Kuzdere Tepesi, steppe, 1500-1700 m, 14.vi.1980, Yıldırımlı 3153 **(R4);** Altınyüzük Köyü, tarla içi, 08.v.2013, E.Yüce 2553 **(R13)**; Munzur Vadisi **(R15)**. Ir.-Tur.

Allium kunthianum Vved./**Kuş körmeni**

Pülümür, between Yalmanlar and Kocatepe, NW of Sarıgül village, 2230 m, steppe, 06.viii.2014, Armağan 5786 **(MA)**; Pülümür, Eğimli - Kocatepe köyü arası, 2341 m, steppe, 06.viii.2014, Armağan 5792 **(MA)**. Ir.-Tur.

Allium myrianthum Boiss./**Paksoğan**

Mazgirt, N of Akdüven village, 1110 m, steppe, 16.vi.2014, Armağan 4592 **(MA)**; above Pertek, 1600 m, D. 31056 **(R6)**; Ovacık, Kırkgözeler, towards Ziyaret Tepesi, Munzur Dağları, 1650-1850 m, 27.vii.1979, Yıldırımlı 2209 **(R4)**; Tunceli-Ovacık arası, Venk Köprüsü çevresi, 1040 m, 05.vii.2012, E.Yüce 2427 **(R13)**. Ir.-Tur.

Allium pallens L. subsp. ***pallens***/**Nursoğanı**

Çemişgezek, 2 km from Vişneli to Arpaderen, 1080 m, field border, roadside, 21.vi.2014, Armağan 5097 **(MA)**; Elazığ to Erzincan, 1560 m, Buttler 15865 **(R6)**; Tunceli-Ovacık arası, 1092 m, 10.vi.2013, E.Yüce 2785a **(R13)**; Munzur Vadisi **(R15)**. Medit.

Allium paniculatum L. subsp. ***paniculatum***/**Sürüsalkım**

Ovacık, Kırkgözeler, towards Ziyaret Tepesi, Munzur Dağları, 1650-1850 m, 27.vii.1979, Yıldırımlı 2208 **(R4)**; Ovacık, Akyayık Köyü, 1315 m, 10.vi.2013, E.Yüce 2785 **(R13)**; Munzur Vadisi **(R15)**. Medit.

Allium pseudoflavum Vved./**Küllüsoğan**

Tunceli center, 10 km from Tunceli to Ovacık (Munzur Valley), 960 m, steppe, 25.v.2014, Armağan 3987 **(MA)**; Mazgirt, main road of Elazığ - Tunceli, crossroad of Kızılcık, 1060 m, steppe, 02.vi.2014, Armağan 4134 **(MA)**; Nazımiye, 3 km from Nazımiye to Tunceli, 1510 m, oak openings, 03.vi.2014, Armağan 4183 **(MA)**; Pertek, 1500 m, D. 31514 **(R6)**; Tunceli-Ovacık arası, 1092 m, 26.v.2013, E.Yüce 2661a **(R13)**. Ir.-Tur.

Allium purpureoviride Koyuncu & İ.Genç/**Renkli soğan**

Pertek, 27 miles from Elazığ to Tunceli, step calcareous south slope, 1400 m a.s.l., 06.vi.1957, Davis 29146 and Hedge (K) **(R12)**; Pertek, 7 km from Pertek to Tunceli, dry rocky slopes, 1300 m a.s.l., 08.vi.1990, N. and E. Özhatay (ISTE 61640) **(R12)**. Ir.-Tur., End.

Allium pustulosum Boiss. & Hausskn./**Beysoğanı**

Tunceli center, 10 km from Aktuluk to Demirkapı, 1450 m, steppe, 21.vii.2014, Armağan 5395 (MA); Ovacık, Mercan Vadisi, 29.v.2012, E.Yüce 2194 **(R13)**; Munzur Vadisi **(R15)**. Ir.-Tur.

Allium roseum L./**Gül soğanı**

50 km N.E. of Tunceli, 2000 m, It. Leyd. 1959:1606 **(R6)**.

Allium schoenoprasum L./**Peynir sirmosu**

Munzur Da. above Ovacık, 2650 m, D. 31427 **(R6)**; Mazgirt, c. 30 km ESE of Tunceli, c. 1 km

E of Akdüven, 1430 m, dry meadow with rocks, 13.vi.2013, V.Y.E. & M. 13-0145 **(R14)**; Pülümür, 35.6 km NNE Tunceli, main road Tunceli - Erzincan, 3.5 km SW Mezra, 1200 m, roadside and dry slope, 17.vi.2013, V.Y.E. & M. 13-0332 **(R14)**.

Allium scorodoprasum L. subsp. ***rotundum*** (L.) Stearn/**Delipırasa**

Pertek, main road Pertek - Çemişgezek, 2.5 km before Singeç bridge, 865 m, steppe, 24.v.2014, Armağan 3889 **(MA)**; Tunceli center, 17 km from Tunceli to Ovacık (Munzur Valley), 1015 m, eroded slopes, 25.v.2014, Armağan 4014 **(MA)**; Tunceli center, Pülümür Valley, 650 m NW of Kutudere, 1070 m, steppe and oak openings, 03.vi.2014, Armağan 4186 **(MA)**; Tunceli-Ovacık arası, Anafatma civarı, 940 m, 21.v.2012, E.Yüce 2090 **(R13)**; Road Tunceli - Ovacık, c. 5.7 km NW of Tunceli, 940 m, dry meadow, 30.v.2014, V.Y. & C. 14-048 **(R14)**; Munzur Vadisi **(R15)**.

Allium sintenisii Freyn./**Dikenli körmen**

Pülümür, 11 km NW of Ardıçlı (Gersunut), Munzur Mountains, 2516 m, rocky areas, 27.vi.2015, Armağan 6655 **(MA)**. Ir.-Tur., End.

Allium stamineum Boiss./**Yabansarımsağı**

Ovacık, 47 km from Tunceli to Ovacık (Munzur Valley), 1200 m, steppe, 26.v.2014, Armağan 4055 **(MA)**; Ovacık, 51 km from Tunceli to Ovacık (Munzur Valley), 1210 m, steppe, 26.v.2014, Armağan 4066 **(MA)**; Ovacık, 8 km from main road of Ovacık - Tunceli to Yakatarla, 1680, steppe, 04.vi.2014, Armağan 4227 **(MA)**; Hozat, between Karacaköy and Uzundal, road of Sarısaltuk Türbesi, 1730 m, steppe, 17.vi.2014, Armağan 4639 **(MA)**; Tunceli-Ovacık arası, 1173 m, 27.v.2013, E.Yüce 2674 **(R13)**. E.Medit.

Allium tauricola Boiss./**Toros soğanı**

Ovacık, 3 km N of Işıkvuran, Munzur Mountains, 2184 m, scree, 08.viii.2014, Armağan 5927 **(MA)**. Ir.-Tur., End.

Allium tchihatschewii Boiss./**Saklı soğan**

Tunceli center, road of Tunceli - Sütlüce, after 500 m from the junction, 940 m, steppe slopes, 23.v.2014, Armağan 3777 **(MA)**. Ir.-Tur., End.

Allium trachycoleum Wendelbo/**Boz sarımsak**

Ovacık, 1.5 km from main road of Ovacık - Tunceli to Yakatarla, 1320 m, steppe, 04.vi.2014, Armağan 4208 **(MA)**. Ir.-Tur.

Allium tripedale Trautv./**Şahsarımsağı**

Ovacık, Munzur Gözeleri çevresi, 08.v.2012, E.Yüce 2998 **(R13)**.

Allium tuncelianum (Kollmann) Özhatay, B.Mathew & Siraneci/**Tuncelisarımsağı**

Ovacık, W of Ziyaret (Munzur Gözeleri), 1340 m, rocky areas, 20.vi.2014, Armağan 4983 **(MA)**; Munzur Da., in Aksu Dere above Ovacık, 1800 m, 21.vii.1957, Davis 31498 **(R6)**; Tunceli to Ovacık, 1100 m, T. Baytop ISTE 23198 **(R6)**; Munzur Dag, Aksu Dere above Ovacık, 1800 m, 21.vii.1957, Davis 31498 **(R8)**; Tunceli-Ovacık arası, Anafatma civarı, 910 m, 05.vii.2012, E.Yüce 2401 **(R13)**; Tunceli-Ovacık arası, Anafatma'ya varmadan, 914 m, 05.vii.2012, E.Yüce 2411 **(R13)**; Tunceli-Ovacık arası, 1173 m, 05.vii.2012, E.Yüce 2431 **(R13)**; Munzur Vadisi **(R15)**. Ir.-Tur., End.

Allium vineale L./**Sirmo**

Ovacık, 1200 m, 25.vii.1979, Yıldırımlı 2077 **(R4)**; Tunceli-Ovacık arası, Ovacık'a 20 km kala, roadside, 03.vii.2013, E.Yüce 2820 **(R13)**; Munzur Vadisi **(R15)**.

Sternbergia clusiana (Ker Gawl.) Ker Gawl. ex Spreng./**Vargetgülü**

Ovacık, W of Ovacık, side of Munzur river, 1240 m, meadow, 21.ix.2014, Armağan 6342 **(MA)**; Ovacık, 1200 m, 27.x.1980, Yıldırımlı 4106 **(R4)**; Tunceli-Ovacık arası, Geyiksuyu Köyü yol ayırımından 2–3 km, roadside, 27.v.2013, E.Yüce & İ.Eker 2701 **(R13)**; Munzur Vadisi **(R15)**. Ir.-Tur.

ARACEAE

Arum orientale M.Bieb./**Yaldıran**

Pülümür, between köprü and Yeşilköy, clearing of Quercus petraea subsp. pinnatiloba forest, 1500-1600 m, 15.vi.1980, Yıldırımlı 3289 **(R4)**; Tunceli-

Ovacık arası, Halbori Gözeleri, 08.v.2013, E.Yüce 2561 **(R13)**; Munzur Vadisi **(R15)**. Euro.-Sib. (Eux.)**.**

Arum rupicola Boiss. var. ***rupicola*** (= Arum conophalloides Kotschy ex Schott)/**Dağsorsalı**

Ovacık, 1.5 km E of Işıkvuran, 1960 m, steppe, 04.vi.2014, Armağan 4315 **(MA)**; Pülümür, Kocatepe Köyü, 1625 m, 02.vi.2014, E.Vitek, E.Yüce, U.Çakılcıoğlu 14-128 **(R13)**. Ir.-Tur., End.

Arum rupicola Boiss. var. ***virescens*** (Stapf) P.C.Boyce/**Dağsorsalı**

Ovacık, 44 km from Tunceli to Ovacık (Munzur Valley), 1190 m, humid places, 26.v.2014, Armağan 4043 **(MA)**; Ovacık, S slopes of Kırkmerdivenler, calcereous rocks, stony places and screes, 1200-1700 m, 17.vi.1979, Yıldırımlı 1928 **(R4)**. Ir.-Tur.

Biarum carduchorum (Schott) Engl./**Kardi**

Tunceli, Sakaltutan Da., 10 km N.E. of Pertek, Watson et al. 2404 **(R6)**; Ovacık, above Paşadüzü Köyü, Korti Deresi, Tepesi and Yaylası, 1250-2100 m, 28.x.1980, Yıldırımlı 4107 **(R4)**; Ovacık, Güneykonak Köyü, 1230 m, 27.ix.2013, E.Yüce 2879 **(R13)**; Munzur Vadisi **(R15).**

Eminium rauwolffii (Blume) Schott var. ***rauwolffii*** /**Yılanbacağı**

Tunceli-Ovacık arası, Anafatma civarı, 940 m, 03.v.2013, E.Yüce 2531 **(R13)**. Ir.-Tur.

ASPARAGACEAE

Bellevalia anatolica B.Mathew & Özhatay/**Yamaç Sümbülü**

N. of Elazığ near Pertek, on road to Tunceli, rocky hillside, 04.vi.1987, fl. cult. Kew, 10.iv.1990, B. Mathew 11033 **(R8)**. Ir.-Tur., End.

Bellevalia fominii Woronow/**Benlisümbül**

Ovacık, 3 km N of Işıkvuran, Munzur Mountains, 2080 m, alpine steppe, 04.vi.2014, Armağan 4256 **(MA)**; Ovacık, Akyayık Köyü, 1315 m, 21.v.2013, E.Yüce 2737 **(R13)**. Ir.-Tur.

Bellevalia gracilis Feinbrun/**Aktepeli**

Tunceli center, 15 km from Tunceli to Ovacık (Munzur Valley), steppe slopes, 11.iv.2015, Armağan 6408 **(MA)**; Ovacık, nr Munzur river, 1200 m, 05.v.1979, Yıldırımlı 1313 **(R6)**; Tunceli-Ovacık arası, 45. km, 08.v.2012, E.Yüce 2042a **(R13)**; Tunceli-Ovacık arası, Munzur Vadisi Milli Parkı çıkışı, 1215 m, 20.iv.2012, E.Yüce 2053 **(R13)**; Munzur Vadisi **(R15)**. Ir.-Tur., End.

Bellevalia kurdistanica Feinbrun/**Alacasümbül**

Tunceli-Ovacık arası, Siliç Köprüsü çevresi, 09.iv.2013, E.Yüce 2484 **(R13)**. Ir.-Tur.

Bellevalia longipes Post/**Saçaksümbül**

Mazgirt, on road Elazığ - Tunceli, 2 km after from Beylermezrası, 855 m, steppe scree, 02.vi.2014, Armağan 4155 **(MA)**; Tunceli center, on road Tunceli - Sütlüce, 2 km after crossroad, 1050 m, steppe, 23.v.2014, Armağan 3810 **(MA)**; Tunceli-Ovacık arası, 45. km, 08.v.2012, E.Yüce 2042 **(R13)**; Atlantı (Pah köprüsü), 935 m, 31.v.2012, E.Yüce 2285 **(R13)**; Tunceli-Ovacık arası, Anafatma civarı, 940 m, 22.iv.2013, E.Yüce 2532 **(R13)**; Tunceli-Ovacık arası, 40. km, 03.v.2013, E.Yüce 2537 **(R13)**; Tunceli-Ovacık arası, Dedeağaç Köyü, 1370 m, 14.v.2013, E.Yüce 2606 **(R13)**. Ir.-Tur.

Bellevalia paradoxa (Fisch. & C.A.Mey.) Boiss. (= Bellevalia pycnantha (K.Koch) Losinsk.)/ **Aşpenceri**

Ovacık, around Beşevler, at the junction of Munzur Suyu and Mercan Çayı, 1100 m, 07.v.1979, Yıldırımlı 1396 **(R4)**; Tunceli-Ovacık arası, Munzur Vadisi Milli Parkı çıkışı, 1215 m, 03.v.2013, E.Yüce 2518 **(R13)**; Munzur Vadisi **(R15)**. Ir.-Tur.

Bellevalia speciosa Woronow ex Grossh. (= Bellevalia sarmatica (Pall. ex Miscz.) Woronow)/ **Saplısümbül**

Tunceli to Pülümür, 9.6 km from Pülümür, D. 29206 **(R6)**; Tunceli-Ovacık arası, Anafatma civarı, 910 m, 08.v.2012, E.Yüce 2061 **(R13)**.

Hyacinthella acutiloba K. Perss. & Wendelbo/ **Sivri sümbül**

Ovacık, Karagöl vadisi, Munzur dağları, 1400 m,

05.v.1979, Yıldırımlı 1327 **(R4)**. Ir.-Tur., End.

Hyacinthus orientalis L. subsp. ***chionophilus*** Wendelbo/**Kopça**

Ovacık, 3 km N of Işıkvuran, Munzur Mountains, 2020 m, rocky areas, 04.vi.2014, Armağan 4254 **(MA)**; Tunceli center, 14 km from Tunceli to Ovacık (Munzur Valley), 1000 m, steppe slopes, 11.iv.2015, Armağan 6384 **(MA)**; Munzur Da. above Ovacık, 2500 m, T. Baytop ISTE 24243 **(R6)**; Ovacık, Karagöl vadisi, Munzur dağları, 1400 m, 05.v.1979, Yıldırımlı 1327 **(R4)**; Tunceli-Ovacık arası, Munzur Vadisi Milli Parkı çıkışı, 1215 m, 20.iv.2012, E.Yüce 2035 **(R13)**; Tunceli-Ovacık arası, Venk Köprüsü'ne varmadan roadside, 20.iv.2012, E.Yüce 2027 **(R13)**; Ovacık, Akyayık Köyü, 1315 m, 31.iii.2013, E.Yüce 2478 **(R13)**; Tunceli-Ovacık arası, Munzur Vadisi Milli Parkı çıkışı, 1215 m, 09.iv.2013, E.Yüce 2486 **(R13)**; Ovacık, Güneykonak Köyü, 1230 m, 08.iv.2013, E.Yüce 2500 **(R13)**; Munzur Vadisi **(R15)**. Ir.-Tur., End.

Muscari armeniacum Leichtlin ex Baker/**Gâvurbaşı**

Pülümür, 12 km NW of Ardıçlı (Gersunut), on Munzur Mountains, 2490 m, steppe scree, 27.vi.2015, Armağan 6670 **(MA)**; Tunceli center, Örenönü Nature Park (Pülümür Valley), 920 m, meadows, 12.iv.2015, Armağan 6410 **(MA)**; Pülümür, 9 km from Pülümür to Tunceli (Pülümür Vallay), S of Kangallı, 1324 m, steppe, 05.vi.2014, Armağan 4429 **(MA)**; Ovacık, 3km N of Işıkvuran, Munzur Mountains, 2100 m, alpine steppe, 04.vi.2014, Armağan 4269 **(MA)**; Ovacık, banks of Munzur Suyu, 1200 m, 05.v.1979, Yıldırımlı 1321 **(R4)**; Tunceli-Ovacık arası, Anafatma civarı, 940 m, 08.v.2012, E.Yüce 2060 **(R13)**; Tunceli-Ovacık arası, Venk Köprüsü çevresi, 1040 m, 08.v.2012, E.Yüce 2081 **(R13)**; Tunceli-Ovacık arası, Anafatma ziyareti üst tarafı, 03.v.2013, E.Yüce 2523 **(R13)**; Tunceli-Ovacık arası, Anafatma Ziyareti çevresi, 916 m, 03.v.2013, E.Yüce 2528 **(R13)**; Munzur Vadisi **(R15)**.

Muscari aucheri (Boiss.) Baker/**Gök müşkürüm**

Ovacık, banks of Munzur Suyu, 1200 m, 05.v.1979, Yıldırımlı 1320 **(R4)**; Munzur Vadisi **(R15)**. End.

Muscari comosum (L.) Mill./**Morbaş**

Tunceli center, on road of Tunceli - Pertek, 1 km after from Kopuzlar, 1114 m, steppe, 22.v.2014, Armağan 3755 **(MA)**; Pülümür, foots of Kuzdere Tepesi, steppe, 1500-1700 m, 14.vi.1980, Yıldırımlı 3153 **(R4)**; Tunceli-Ovacık arası, Avsugar Köprüsü çevresi, 995 m, 29.v.2012, E.Yüce 2148 **(R13)**; Tunceli-Ovacık arası, Munzur Vadisi Milli Parkı çıkışı, 1215 m, 29.v.2012, E.Yüce 2168 **(R13)**; Tunceli-Ovacık arası, Dedeağaç Köyü, 1370 m, 14.v.2013, E.Yüce 2605 **(R13)**; Ovacık, Güneykonak Köyü, 1230 m, 10.v.2013, E.Yüce 2616 **(R13)**; Tunceli-Ovacık arası, Halbori Gözeleri, 26.v.2013, E.Yüce 2664 **(R13)**; Mazgirt, c. 30 km ESE of Tunceli, c. 1 km E of Akdüven, 1430 m, dry meadow with rocks, 01.vi.2013, V.Y.E. & M. 13-0147 **(R14)**; Pülümür, c. 38 km NNE Tunceli, road to Kocatepe, 0.9 km SE Kovuklu, 1625 m, Astragalus spiny shrub steppe, 02.vi.2014, V.Y. & U. 14-133b **(R14)**; Nazımiye, c. 27 km NE of Tunceli, above village Büyükyurt, 1775 m, dry slope, 16.vi.2013, V.Y. & E. 13-0238 **(R14)**. Medit.

Muscari longipes Boiss./**Buğulu sümbül**

Pertek, between Pertek and Mercimek, 1280 m, eroded slopes, 26.v.2017, Armağan 7458 **(MA)**; Pertek to Tunceli, 42 km from Elazığ, 1400 m, D. 29112 **(R6)**.

Muscari massayanum C.Grunert/**Şah müşkürüm**

N. of Pülümür, 2000 m, Pasche 78/18 (cult.E) **(R6)**.

Muscari neglectum Guss. ex Ten./**Arapüzümü**

Pülümür, 500 m N of Balpayam (3-4 km S of Kırklar), 2400 m, 18.vi.2014, Armağan 4843 **(MA)**; Merkez, Atatürk Mahallesi, 920 m, 20.iv.2012, E.Yüce 2015 **(R13)**; Ovacık, Güneykonak Köyü, 1230 m, 21.iv.2013, E.Yüce 2639 **(R13)**.

Ornithogalum alpigenum Stapf/**Akyıldız**

Nazımiye, Dereova township, 5 km SE of Aşağımarkosör, 2144 m, near of melted snow, pastures, 01.vi.2015, Armağan 6525 **(MA)**; Tunceli-Ovacık arası, Venk Köprüsü çevresi, 1040 m, 21.iv.2012, E.Yüce 2093 **(R13)**; Tunceli-Ovacık arası, 40. km, 21.iv.2012, E.Yüce 2095 **(R13)**; Tunceli-Ovacık arası, Munzur Vadisi Milli Parkı çıkışı, 1215 m, 29.v.2012, E.Yüce 2167 **(R13)**; Tunceli-Ovacık arası, Anafatma civarı, 940 m,

05.vii.2012, E.Yüce 2441 **(R13)**. E.Medit., End.

Ornithogalum arcuatum Steven/**Kurtkirişi**

Ovacık, 10 km from Ovacık to Hozat, junction of Kuşluca village, 1710 m, pastures, 17.vi.2014, Armağan 4745 **(MA)**; Hozat, 700 m N of Uzundal, 1700 m, steppe, 17.vi.2014, Armağan 4690 **(MA);** Mazgirt, main road of Elazığ - Tunceli, 2 km after from Beylermezrası, 855 m, steppe, eroded hill, 02.vi.2014, Armağan 4154 **(MA)**; Munzur Da. above Ovacık, 2400 m, D. 31377 **(R6)**; Ovacık, around Munzur Suyu, 1200 m, 06.vii.1980, Yıldırımlı 3439 **(R4)**; Tunceli-Ovacık arası, Işıkvuran Köyü çıkışı, 26.v.2013, E.Yüce & İ.Eker 2675 **(R13)**; Munzur Vadisi **(R15)**. Ir.-Tur.

Ornithogalum cuspidatum Bertol./**Bitik sasal**

Tunceli center, 16 km from Tunceli to Ovacık (Munzur Valley), 980 m, pastures in stream side, 25.v.2014, Armağan 4008 **(MA)**; Ovacık, 48 km from Tunceli to Ovacık (Munzur Valley), 1190 m, pastures in stream side, 26.v.2014, Armağan 4056 **(MA)**.

Ornithogalum hajastanum Agapova/**Çarpık sasal**

Ovacık, 3 km N of Işıkvuran, Munzur Mountains, 1980 m, steppe, 19.vi.2014, Armağan 4946 **(MA)**; Ovacık, 8 km from Eskigedik to Işıkvuran, 2120 m, steppe, 19.vi.2014, Armağan 4926 **(MA)**; Ovacık, 17 km from Ovacık to Hozat, E of Halitpınar, 1895 m, steppe, 17.vi.2014, Armağan 4718 **(MA)**; Hozat, between Karacaköy and Uzundal, around of Sarısaltuk Türbesi, 2270 m, rocky areas, 17.vi.2014, Armağan 4684 **(MA)**; Ovacık, 5 km main road of Ovacık - Tunceli to Yakatarla, 1620 m, steppe, 04.vi.2014, Armağan 4217 **(MA)**; Tunceli center, 26 km from Tunceli to Ovacık (Munzur Valley), 1060 m, steppe, 26.v.2014, Armağan 4031 **(MA)**; Ovacık, 44 km from Tunceli to Ovacık arası (Munzur Valley), 1190 m, in the gardens, 26.v.2014, Armağan 4047 **(MA)**.

Ornithogalum luschanii Stapf./**Çayır sasalı**

Tunceli center, 18 km from Tunceli to Ovacık (Munzur Valley), 915 m, steppe, 17.iv.2015, Armağan 6698 **(MA)**; Pülümür, 12 km NW of Ardıçlı (Gersunut), Munzur Mountains, 2490 m, near to melted snow, 27.vi.2015, Armağan 6672 **(MA)**; Pülümür, 11 km NW of Ardıçlı (Gersunut), Munzur Mountains, 2510 m, rocky steppe, 18.vi.2014, Armağan 4888 **(MA)**. End.

Ornithogalum macrum Speta/**Yer sasalı**

Tunceli center, 700 m from Demirkapı to Çılga, 1410 m, in the gardens, 06.vi.2014, Armağan 4437 **(MA)**. E.Medit., End.

Ornithogalum montanum Cirillo/**Dağ yıldızı**

Ovacık, 27.5 km NNW Tunceli, road Aşağıtorunoba-Agdat, 1825 m, semihumid meadow, 18.vi.2013, V.Y.E. & M. 13-0374 **(R14)**; Ovacık, 27.5 km NNW Tunceli, road Aşağıtorunoba - Agdat, 1825 m, semihumid meadow, 18.vi.2013, V.Y.E. & M. 13-0375a **(R14)**. E.Medit.

Ornithogalum munzurense Speta/**Munzur yıldızı**

Tunceli center, on road Tunceli - Çıralı, 17 km from crossroad of Tunceli - Sütlüce (to 8 km Çıralı), 1810 m, steppe, 01.vi.2015, Armağan 6520 **(MA)**; 19 km from Tunceli along Munzur-River towards Ovacık, steep scree-slopes and cliff-ledges, calcareous rock, 950 m, 11.iv.1990, E.Pasche KPPZ 90205, cult. LI: 21.v.1993, 18.v.1992 **(R11)**. End.

Ornithogalum narbonense L./**Akbaldır**

Ovacık, 1.5 km from main road of Ovacık-Tunceli to Yakatarla, 1320 m, steppe, 04.vi.2014, Armağan 4215 **(MA)**; Tunceli-Ovacık arası, Işıkvuran Köyü yol ayrımından 6-7. km, 26.v.2013, E.Yüce & İ.Eker 2673 **(R13)**; Ovacık, Munzur Vadisi Milli Parkı çıkışı, 1215 m, 27.v.2013, E.Yüce & İ.Eker 2705 **(R13)**. Medit.

Ornithogalum oligophyllum E.D.Clarke/**Kurtsoğanı**

Ovacık, banks of Munzur Suyu, 1200 m, 05.v.1979, Yıldırımlı 1319 **(R4)**; Ovacık (Merkez), Yeşilyazı, 1275 m, 08.v.2012, E.Yüce 2072 **(R13)**; Tunceli-Ovacık arası, Halbori gözeleri, 08.v.2013, E.Yüce 2554 **(R13)**; Munzur Vadisi **(R15)**.

Ornithogalum orthophyllum Ten. subsp. ***kochii*** (Parl.) Zahar/**Bayıryıldızı**

Tunceli-Ovacık arası, Halbori gözeleri, 08.v.2013,

E.Yüce 2554 **(R13)**; Ovacık, Akyayık Köyü, 1315 m, 17.v.2013, E.Yüce 2599 **(R13)**; Tunceli-Ovacık arası, Halbori gözeleri, 26.v.2013, E.Yüce & İ Eker 2662 **(R13)**; Tunceli-Ovacık arası, Geyiksuyu Köyü yol ayrımından 2. km, dağ yamacı, 27.v.2013, E.Yüce & İ Eker 2700 **(R13)**.

Ornithogalum persicum Hausskn. ex Bornm./ **Karayıldız**

Pertek, 4 km from Pertek to Tunceli, 1260 m, steppe, 03.vi.2014, Armağan 7523 **(MA)**; Pülümür, 2 km from Turnadere to Közlüce, 1560 m, steppe, 18.vi.2014, Armağan 4773 **(MA)**; Hozat, between Çığırlı and Dervişcemal, the crossroad of Buzlupınar, 1740 m, steppe, 17.vi.2014, Armağan 4634 **(MA)**; Ovacık, 8 km from Aşağıtorunoba to Ağaçpınar, 1800 m, steppe, 04.vi.2014, Armağan 4308 **(MA)**; Tunceli center, between Tunceli and Pülümür (Pülümür Valley), 650 m NW of Kutudere, 1070 m, steppe, 03.vi.2014, Armağan 4185 **(MA)**; Pertek to Tunceli, 1350 m, D. 29156 **(R6)**; Ovacık-Köseler Köyü arası, 17.vi.2013, E.Yüce 2882 **(R13)**; Munzur Vadisi **(R15)**. Ir.-Tur.

Ornithogalum pyrenaicum L./**Eşeksusamı**

Pertek to Tunceli, 40 km from Elazığ, 1400 m, D. 29106 **(R6)**; Tunceli-Ovacık arası, Işıkvuran Köyü, 19.v.2013, E.Yüce 2763 **(R13)**; Ovacık-Munzur gözeleri arası, Ada Köyü civarı, 1285 m, 03.vii.2013, E.Yüce 2829 **(R13)**; Ovacık, c. 18.3 km NE of Ovacık, c. 0.5 km NNE of small river dam, near locality called Şahverdi, 1500 m, stony meadow, 03.vi.2014, V.Y. 14-155 **(R14)**; Ovacık, road Tunceli-Ovacık, c. 6.2 km EESE Ovacık, 0.2 km W of bridge at mouth of side river, 1215 m, meadow, 03.vi.2014, V.Y. 14-146 **(R14)**.

Ornithogalum sphaerocarpum A.Kern./ **Salkımsakarca**

Ovacık, 47 km from Tunceli to Ovacık (Munzur Valley), 1200 m, steppe, 26.v.2014, Armağan 4054 **(MA)**; Tunceli-Ovacık arası, Anafatma civarı, 940 m, 29.v.2012, E.Yüce 2212 **(R13)**; Ovacık, Akyayık Köyü, 1315 m, 25.v.2013, E.Yüce 2731 **(R13)**; Tunceli-Ovacık arası, Munzur Vadisi Milli Parkı çıkışı, 1215 m, 03.vii.2013, E.Yüce 2827 **(R13)**; Pülümür, 39 km NE Tunceli, road to Kocatepe, southern part of Kovuklu, 1550 m, meadow, 17.vi.2013, V.Y.E. & M. 13-0297 **(R14)**; Ovacık, 27.5 km NNW Tunceli, road Aşağıtorunoba - Agdat, 1825 m, semihumid meadow, 18.vi.2013, V.Y.E. & M. 13-0379 **(R14)**; Ovacık, road Tunceli - Ovacık, c. 6.6 km EESE Ovacık, 0.35 km SE of bridge at mouth of side river, 1230 m, humid meadow, 12.vi.2013, V.Y. E. & M. 13-0023 **(R14)**.

Ornithogalum umbellatum L. **/ Sunbula**

Tunceli-Ovacık arası, Munzur Vadisi Milli Parkı çıkışı, 1215 m, 08.v.2012, E.Yüce 2085 **(R13)**; Tunceli-Ovacık arası, Anafatma civarı, 940 m, 03.v.2013, E.Yüce 2529 **(R13)**; Tunceli-Ovacık arası, Anafatma ziyareti, Munzur çayı kenarı, yolun alt kısmı, 03.v.2013, E.Yüce 2550 **(R13)**.

Puschkinia scilloides Adams/**Serhişing**

Pülümür, 20 km from Pülümür to Tunceli (Pülümür Valley), 1215 m, pastures near to melted snow, 12.iv.2015, Armağan 6392 **(MA)**; Ovacık, around Beşevler, at the junction of Munzur Suyu and Mercan Çayı, 1100 m, 07.v.1979, Yıldırımlı 1397 **(R4)**; Ovacık, Akyayık Köyü, 1315 m, 22.iv.2013, E.Yüce 2574 **(R13)**; Ovacık, Güneykonak Köyü, 1230 m, 01.v.2013, E.Yüce 2621 **(R13)**; Ovacık, Güneykonak Köyü, 1230 m, 14.iv.2013, E.Yüce 2651 **(R13)**; Munzur Vadisi **(R15)**. Ir.-Tur.

Scilla bifolia L./**Ormansümbülü**

Ovacık, 8 km from Ovacık to Tunceli, 500 m N of Yaylagünü, 1212 m, pastures in stream side, 11.iv.2015, Armağan 6406 **(MA)**; Tunceli-Ovacık arası, Munzur Vadisi Milli Parkı çıkışı, 1215 m, 20.iv.2012, E.Yüce 2033 **(R13)**; Ovacık, Akyayık Köyü, 1315 m, 22.iv.2013, E.Yüce 2569-2574 **(R13)**; Ovacık, Güneykonak Köyü, 1230 m, 11.iv.2013, E.Yüce 2649 **(R13)**; Tunceli-Ovacık arası, Munzur Vadisi Milli Parkı çıkışı, 1215 m, 27.v.2013, E.Yüce & İ.Eker 2706 **(R13)**. Medit.

Scilla siberica Haw. subsp. ***armena*** (Gross.) Mordak/**Camışkıran**

Pülümür, 46 km from Tunceli to Pülümür (Pülümür Valley), 1215 m, pastures near to melted snow, 12.iv.2015, Armağan 6389 **(MA)**; Ovacık, 3 km N of Işıkvuran, Munzur Mountains, 2020 m, rocky crevices, 04.vi.2014, Armağan 4244 **(MA)**; Ovacık, Munzur Dağları, Mercan Boğazı, in front of

Şahverdi Köyü, 1500-1800 m, 08.v.1979, Yıldırımlı 1438 **(R4)**; Tunceli-Ovacık arası, Dilek Köyü girişi, roadside, 1110 m, 12.iv.2012, E.Yüce 2010 **(R13)**; Tunceli-Ovacık arası, Anafatma ziyaretinin üst tarafı, 12.iv.2012, E.Yüce 2011 **(R13)**; Tunceli-Ovacık arası, Geyiksuyu karakolu çevresi, 20.iv.2012, E.Yüce 2016 **(R13)**; Tunceli-Ovacık arası, Venk Köprüsüne varmadan, 20.iv.2012, E.Yüce 2029 **(R13)**; Ovacık, Akyayık Köyü, 1315m, 22.iv.2013, E.Yüce 2564 **(R13)**. Ir.-Tur.

BUTOMACEAE

Butomus umbellatus L./**Bataklıkgülü**

Mazgirt, Yukarıoyumca village, 1430 m, sulak alanlar, 15.viii.2014, Armağan 6055**(MA)**; Mazgirt, Yukarıoyumca, 1430 m, 11.vi.2013, E.Vitek, E.Yüce, C.Ergin, H.H.Makal 13-0018 **(R13)**. Euro.-Sib.

COLCHICACEAE

Colchicum kotschyi Boiss./**Acı çiğdem**

Tunceli center, 4 km from Gürbüzler to Günlüce (N of Kıl village), steppe, 01.ix.2014, Armağan 6218 **(MA)**. Ir.-Tur.

Colchicum munzurense K.Perss./**Munzurçiğdemi**

Ovacık, 52 km from Tunceli to Ovacık (Munzur Valley), N of Yaylagünü, 1212 m, steppe, 11.iv.2015, Armağan 6387 **(MA)**; 19 km from Tunceli to Ovacık along Munzur river, steep scree slopes and cliff ledges, calcareous rock, 950 m, 11.iv.1990, Kammerl., Pasche, Perss. & Zetterl. 90-193 **(R8)**; 27 km from Tunceli to Ovacık along Munzur river, 1000 m, Kammerl. & al. 90-208 **(R8)**; Tunceli-Ovacık arası, Anafatma ziyareti üst kısmı, Taht Köyü, 26.iii.2012, E.Yüce 2000 **(R13)**; Tunceli-Ovacık arası, Munzur Vadisi Milli Parkı çıkışı, 1215 m, 20.iv.2012, E.Yüce 2037, 2038 **(R13)**. Ir.-Tur., End.

Colchicum speciosum Steven/**Şepart**

Munzur Vadisi **(R15)**. Euro.-Sib.

Colchicum szovitsii Fisch & C.A.Mey. subsp. ***szovitsii*** (= Colchicum nivale (Boiss. & A.Huet) Boiss. & A.Huet ex Stef.)/**Katırçiğdemi**

Ovacık, 52 km from Tunceli to Ovacık (Munzur Valley), N of Yaylagünü, 1212 m, steppe, 11.iv.2015, Armağan 6386 **(MA)**; Ovacık, around Beşevler, at the junction of Munzur Suyu and Mercan Çayı, 1100 m, 07.v.1979, Yıldırımlı 1398 **(R4)**; Tunceli-Ovacık arası, Venk Köprüsü çevresi, 1040 m, 20.iv.2012, E.Yüce 2024 **(R13)**; Munzur Vadisi **(R15)**. Ir.-Tur.

Colchicum triphyllum Kunze/**Öksüzali**

Munzur Da. above Ovacık, Karagöl vadisi, 1400 m, 05.v.1979, Yıldırımlı 1326 **(R6)**; Ovacık, Munzur Dağları, around Kankala, above Karataş Köyü, 1800-2000 m, 08.v.1979, Yıldırımlı 1489 (R4); Munzur Vadisi (R15). Medit.

IRIDACEAE

Crocus biflorus Mill. subsp. tauri (Maw) B.Mathew/**Berfan**

Ovacık, 52 km from Tunceli to Ovacık (Munzur Valley), N of Yaylagünü, 1212 m, steppe, 11.iv.2015, Armağan 6388 **(MA)**; Ovacık, Karagöl vadisi, Munzur dağları, 1400 m, 05.v.1979, Yıldırımlı 1334 **(R4)**; Tunceli-Ovacık arası, Dilek Köyü girişi, 12.iv.2012, E.Yüce 2009 **(R13)**; Tunceli-Ovacık arası, Munzur Vadisi Milli Parkı çıkışı, 1215 m, 20.iv.2012, E.Yüce 2014, 2039 **(R13)**; Munzur Vadisi **(R15)**. Ir.-Tur.

Crocus kotschyanus K.Koch subsp. *cappadocicus* B.Mathew/**Periçiğdemi**

Hozat, between Karacaköy and Uzundal, road of Sarısaltuk Türbesi, 1800 m, steppe, 22.ix.2014, Armağan 6353 **(MA)**; Ovacık, 8 km from Işıkvuran to Ağaçpınar, 2150 m, steppe, 21.ix.2014, Armağan 6340 **(MA)**; Pülümür, 4 km N of Kırklar, 2300 m, steppe, 20.ix.2014, Armağan 6312 **(MA)**; Pülümür, 11 km NW of Ardıçlı (Gersunut), Munzur Mountains, 2240 m, steppe, 20.ix.2014, Armağan 6287 **(MA)**; Seteri to Pülümür 2000 m, Watson et al. 2401 **(R6)**; Ovacık, above Paşadüzü Köyü, Korti Deresi, Tepesi and Yaylası, 1250-2100 m, 28.x.1980, Yıldırımlı 4108 **(R4)**; Ovacık, Güneykonak Köyü, 1230 m, 16.ix.2013 E.Yüce 2880 **(R13)**. Ir.-Tur., End.

Crocus kotschyanus K.Koch subsp. *kotschyanus* / **Gezgin çiğdem**

Munzur Vadisi **(R15)**.

Gladiolus atroviolaceus Boiss./**Kıraçsüseni**

Tunceli center, between Tunceli and Hozat, 3.5 km from Demirkapı to Hozat, 1760 m, 23.v.2014, Armağan 3855 **(MA)**; Ovacık, Karagöl Vadisi, 1300-1550 m, rocky and screes, 07.vii.1980, Yıldırımlı 3515 **(R4)**; Tunceli-Ovacık arası, Yukarı Torunoba civarı, 1190 m, 29.v.2012, E.Yüce 2197 **(R13)**; Tunceli-Ovacık arası, Venk Köprüsü çevresi, 1040 m, 05.viii.2012, E.Yüce 2426 **(R13)**; Tunceli-Ovacık arası, Işıkvuran Köyü, 18.v.2013, E.Yüce 2812 **(R13)**; Tunceli-Ovacık arası, Halbori gözeleri, 11.vii.2013, E.Yüce 2840 **(R13)**; Tunceli center, c. 14.1 km NE of Tunceli, road D882 to Gökçek, 2.2 km SSW Gökçek, locality called Kutudere, 1000 m, dry meadows and oak forest, 18.v.2011, V.E. 11-0096 **(R14)**; Munzur Vadisi **(R15)**. Ir.-Tur.

Gladiolus illyricus W.D.J.Koch/**Osman çiçeği**

Nazımiye, 700-900 m from Aşağırabat village to Büyükyurt (Hakis), 1070 m, steppe, 30.vi.2014, Armağan 5228 **(MA)**; 10 km NW Tunceli, valley of river Munzur, 1.4 km WSW Dilek, 1005 m, stony slope, 18.vi.2013, V.Y.E. & M. 13-0409 **(R14)**.

Gladiolus italicus Mill./**Kılıçotu**

Tunceli center, road of Tunceli - Elazığ, 700 m after from Aktuluk, 930 m, oak openings, 22.v.2014, Armağan 3687 **(MA)**; Ovacık, S slopes of Kırkmerdivenler, calcereous rocks, stony places and screes, 1200-1700 m, 17.vi.1979, Yıldırımlı 1929 **(R4)**; Ovacık, Güneykonak Köyü, 1210 m, 10.v.2013, E.Yüce 2615 **(R13)**; Tunceli-Ovacık yolu, Işıkvuran Köyü çıkışı, 26.v.2013, E.Yüce & İ.Eker 2676 **(R13)**; Tunceli-Ovacık yolu, Geyiksuyu Köyü yol ayrımı, dağ yamacı, 27.v.2013, E.Yüce & İ.Eker 2699 (R13); Tunceli center, c. 13.6 km ESE of Tunceli, road Çukur - Güleç, 3 km S of Çukur, 1435 m, roadside in oak forest, 13.vi.2013, V.Y.E. & M. 13-0141 **(R14)**; Munzur Vadisi **(R15)**.

Gladiolus kotschyanus Boiss./**Çayır kılıçotu**

Tunceli center, around of Kocalar, 1083 m, steppe scree, 12.v.2015, Armağan 6680 **(MA)**; Nazımiye, c. 32 km NE of Tunceli, NE of Büyükyurt, road to former village Hormek, small side valley above ruines of village, 1820 m, meadow besides rivulet, 01.vi.2014, V.Y. & U. 14-090 **(R14)**. Ir.-Tur.

Iris aucheri (Baker) Sealy/**Kayanavruzu**

Nazımiye, 40 km from Tunceli to Pülümür (Pülümür Valley), 1150 m, steppe slopes, 12.iv.2015, Armağan 6391 **(MA)**; Ovacık, banks of Munzur Suyu, 1200 m, 05.v.1979, Yıldırımlı 1309 **(R4)**; Tunceli-Ovacık arası, Anafatma civarı, 940 m, 20.iv.2012, E.Yüce 2018 **(R13)**; Ovacık (Merkez), Yeşilyazı, 1275 m, 08.v.2012, E.Yüce 2049, 2050, 2051 **(R13)**; Munzur Vadisi **(R15)**. Ir.-Tur.

Iris caucasica Hoffm. subsp. ***turcica*** B. Mathew/**Türknavruzu**

Ovacık, Mollaaliler village (Mercan Valley), 1420 m, steppe, 09.v.2015, Armağan 6679 **(MA)**; Pülümür, 3 km from Sarıgül to Yalmanlar, 2250 m, steppe, 05.vi.2014, Armağan 4367 **(MA)**; Ovacık, Akyayık Köyü, 1315 m, 31.iii.2013, E.Yüce 2572 **(R13)**; Munzur Vadisi **(R15)**. Ir.-Tur.

Iris galatica Siehe/**Kaba navruz**

Ovacık, 48 km from Tunceli to Ovacık (Munzur Valley), 1200 m, steppe, 11.iv.2015, Armağan 6385 **(MA)**. Ir.-Tur., End.

Iris persica L./**Buzala**

Tunceli-Ovacık arası, Dilek Köyü girişi, 12.iv.2012, E.Yüce 2007, 2008 **(R13)**; Tunceli-Ovacık arası, 15. km, 12.iv.2012, E.Yüce 2012 **(R13)**; Tunceli-Ovacık arası, Munzur Vadisi Milli Parkı çıkışı, 1215 m, 20.iv.2012, E.Yüce 2040 **(R13)**; Tunceli-Ovacık arası, Anafatma civarı, 940 m, 06.iii.2013, E.Yüce 2454 **(R13)**; Tunceli-Ovacık arası, Munzur Vadisi Milli Parkı çıkışı, 1215 m, 09.iv.2013, E.Yüce 2488, 2489 **(R13)**; Munzur Vadisi **(R15)**. Ir.-Tur.

Iris reticulata M.Bieb. var. ***reticulata***/**Karakörpeze**

Ovacık, 48 km from Tunceli to Ovacık (Munzur Valley), 1200 m, steppe, 11.iv.2015, Armağan 6383 **(MA)**; Tunceli-Ovacık arası, Munzur Vadisi Milli Parkı çıkışı, 1215 m, 20.iv.2012, E.Yüce 2032 **(R13)**; Tunceli-Ovacık arası, Munzur Vadisi Milli Parkı çıkışı, 1215 m, 09.iv.2013, E.Yüce 2490 **(R13)**; Ovacık, Akyayık Köyü, 1315 m, 22.iv.2013, E.Yüce 2579 **(R13)**; Ovacık, Güneykonak Köyü, 1230 m, 14.iv.2013, E.Yüce 2642, 2650 **(R13)**; Munzur Vadisi **(R15)**. Ir.-Tur.

Iris sari Schott ex Baker/**Anakurtkulağı**

Ovacık, 3 km N of Işıkvuran, Munzur Mountains, 2050 m, mountain steppe, 04.vi.2014, Armağan 4240 **(MA)**; Pülümür, foots of Silbüs Dağı, clearing of Quercus petraea subsp. pinnatiloba forest, 1600-2000 m, Yıldırımlı 3367 **(R4)**; Ovacık (Merkez), Yeşilyazı, 1550 m, 21.v.2012, E.Yüce 2091 **(R13)**; Ovacık, Akyayık Köyü, 1315 m, 12.v.2013, E.Yüce 2601 **(R13)**; Tunceli-Ovacık arası, Munzur Vadisi Milli Parkı çıkışı, 1215 m, 14.v.2013, E.Yüce 2609 **(R13)**; Tunceli-Ovacık arası, Munzur Vadisi Milli Parkı çıkışı, 1215 m, 24.v.2013, E.Yüce 2810 **(R13)**; Munzur Vadisi **(R15)**. Ir.-Tur., End.

IXIOLIRIACEAE

Ixiolirion tataricum (Pall.) Schult. & Schult.f. var. ***tataricum*** **(=** *Ixiolirion tataricum* (Pall.) Schult. & Schult.f. subsp. *montanum* (Labill.) Takht.) **/ Köpekotu**

Tunceli center, 16 km from Tunceli to Pülümür (Pülümür Valley), oak openings, 1060 m, 01.v.2015, Armağan 6683 **(MA)**; Pülümür, 2.5 km from Kocatepe to Sarıgül, near to Sarıgül crossroad, 1970 m, steppe, 05.vi.2014, Armağan 4343 **(MA)**; Pülümür, from Kırmızıköprü to Mezra Köyü, 1400 m, 21.v.1981, Yıldırımlı 4373 **(R4)**; Tunceli-Ovacık arası, Anafatma civarı, 940 m, 08.v.2012, E.Yüce 2063 **(R13)**; Tunceli-Ovacık arası, Avsugar Köprüsü çevresi, 995 m, 29.v.2012, E.Yüce 2144 **(R13);** Tunceli-Ovacık arası, Anafatma civarı, 940 m, 27.iv.2013, E.Yüce 2541 **(R13)**; Tunceli-Ovacık arası, Dedeağaç Köyü, 1380 m, 14.v.2013, E.Yüce 2603 **(R13)**; Tunceli-Ovacık arası, Işıkvuran Köyü çıkışı, 26.v.2013, E.Yüce & İ.Eker 2677 **(R13)**; Tunceli center, c. 14.1 km NE of Tunceli, road D882 to Gökçek, 2.2 km SSW Gökçek, locality called Kutudere, 1000 m, dry meadows and oak forest, 18.v.2011, V.E. 11-0095 **(R14)**; Tunceli center, c. 7.4 km ENE of Tunceli, road D882 to Gökçek, locality called Marçik 940 m, former field and surrounding meadows and shrubland, 18.v.2011, V.E. 11-0077 **(R14)**; Tunceli center c. 14.1 km NE of Tunceli, road D882 to Gökçek, 2.2 km SSW Gökçek, locality called Kutudere, 1000 m, dry meadows and oak forest, 18.v.2011, V. & E. 11-0099 **(R14)**; Munzur Vadisi **(R15)**. Ir.-Tur.

LILIACEAE

Fritillaria alburyana Rix/**Pembelâle**

Ovacık, 3 km N of Işıkvuran, Munzur Mountains, 2480 m, rocky areas, 05.vi.2015, Armağan 6557 **(MA)**; Ovacık, Karagöl vadisi, Munzur dağları, 1300-1500 m, 06.v.1979, Yıldırımlı 1373 **(R4)**; Ovacık, Munzur Dağları, around Kankala, above Karataş Köyü, 1800-2000 m, 08.v.1979, Yıldırımlı 1490 **(R4)**; Ovacık, Mercan Vadisi, 19.v.2013, E.Yüce 2760 **(R13)**; Munzur Vadisi **(R15)**. Ir.-Tur., End.

Fritillaria crassifolia Boiss. & A.Huet subsp. ***crassifolia***/**Boynubükük**

Tunceli center, 19 km from Tunceli to Çıralı, 1870 m, steppe scree, 01.v.2015, Armağan 6686 **(MA)**; Ovacık, Karagöl vadisi, Munzur dağları, 1300-1500 m, 06.v.1979, Yıldırımlı 1393 **(R4)**; Ovacık, Güneykonak Köyü, 1227 m, 08.iv.2013, E.Yüce 2501 **(R13)**; Ovacık, Güneykonak Köyü, 1227 m, 13.iv.2013, E.Yüce 2648 **(R13)**; Munzur Vadisi **(R15)**. Ir.-Tur., End.

Fritillaria imperialis L./**Ağlayangelin**

Ovacık, 7 km from Yoncalı to Ağaçpınar, 2015 m, rocky hillside, 01.vi.2015, Armağan 6538 **(MA)**; Ovacık, 3 km N of Işıkvuran, Munzur Mountains, 2020 m, rocky areas, 04.vi.2014, Armağan 4251 **(MA)**; Tunceli-Ovacık arası, Işıkvuran Köyü çıkışı, 26.v.2013, E.Yüce & İ.Eker 2678 **(R13)**; Munzur Vadisi **(R15)**. Ir.-Tur.

Fritillaria pinardii Boiss. (=Fritillaria armena Boiss.)/**Mahçuplâle**

Ovacık, 7 km from Yoncalı to Ağaçpınar, 2015 m, pastures, 01.vi.2015, Armağan 6542 **(MA)**; Ovacık, Munzur Dağları, around Kankala, above Karataş Köyü, 1800-2000 m, 08.v.1979, Yıldırımlı 1483 **(R4)**; Tunceli-Ovacık arası, 45. km, 08.v.2012, E.Yüce 2044 **(R13)**; Ovacık, Havaçor Vadisi girişi, dağ yamacı, 08.v.2012, E.Yüce 2069 **(R13)**; Tunceli-Ovacık arası, Venk Köprüsü çevresi, 1040 m, 14.v.2013, E.Yüce 2608 **(R13)**; Tunceli-Ovacık arası, Güneykonak Köyü, 1230 m, 11.iv.2013, E.Yüce 2643 **(R13)**; Ovacık, Köseler Köyü, 27.iv.2013, E.Yüce 2626 **(R13)**; Munzur Vadisi **(R15)**. Ir.-Tur.

Fritillaria whittallii Baker/**Çam lalesi**

Ovacık, Karagöl vadisi, Munzur dağları, 1400 m, 05.v.1979, Yıldırımlı 1333 **(R4)**; Munzur Vadisi **(R15)**. E.Medit., End.

Gagea bulbifera (Pall.) Salisb./**Düğmeli yıldız**

Tunceli center, 15 km from Tunceli to Ovacık (Munzur Valley), 995 m, steppe, 11.iv.2015, Armağan 6401 **(MA)**. Euro.-Sib.

Gagea bohemica (Zauschn.) Schult. & Schult.f./**Sarıyıldız**

Nazımiye, 31 km from Tunceli to Pülümür (Pülümür Valley), 1050 m, steppe, 10.ii.2015, Armağan 6368 **(MA)**; Tunceli-Ovacık arası, Anafatma civarı, 940 m, 30.iii.2013, E.Yüce 2474 **(R13)**.

Gagea chanae Grossh./**Çan yıldızı**

Tunceli center, 15 km from Tunceli to Ovacık (Munzur Valley), 995 m, steppe, 11.iv.2015, Armağan 6401 **(MA)**; Ovacık, Karagöl vadisi, Munzur dağları, 1400 m, 05.v.1979, Yıldırımlı 1328 **(R4)**; Tunceli-Ovacık arası, 30. km, 08.v.2012, E.Yüce 2065 **(R13)**; Munzur Vadisi **(R15)**. Ir.-Tur.

Gagea gageoides (Zucc.) Vved./**Tokalıyıldız**

Nazımiye, 12 km NE of Büyükyurt, (Dereova town, 5 km SE of Aşağımarkosör), 1926 m, 01.vi.2015, Armağan 6527 **(MA)**; Pülümür, 11 km NW of Ardıçlı (Gersunut), Munzur Mountains, 2510 m, rocky areas, 18.vi.2014, Armağan 4873 **(MA)**; Ovacık, 3 km N of Işıkvuran, Munzur Mountains, 2080 m, rocky crevices, 04.vi.2014, Armağan 4257 **(MA)**; Nazımiye, Tunceli–Erzincan yolu, Büyükyurt Köyü, 1745 m, 21.v.2011, E.Vitek, C.Ergin 11-0174 **(R13)**; Nazımiye, side valley of road D882 Tunceli - Erzincan, upper part of village Büyükyurt 1745 m, at fence, 21.v.2011, V.E. 11-0174 **(R14)**. Ir.-Tur.

Gagea glacialis K. Koch/**Buzyıldızı**

Nazımiye, Dereova town, 5 km SE of Aşağımarkosör, 2144 m, near to melted snow in slopes, 01.vi.2015, Armağan 6524 **(MA)**; Munzur Da. above Ovacık, turf by melting snow, c. 2800 m, 17.vii.1957, Davis 31286 & Hedge **(R6)**; Tunceli-Ovacık arası, Munzur Vadisi Milli Parkı çıkışı, 1215 m, 09.iv.2013, E.Yüce 2493 **(R13)**; Ovacık, Güneykonak Köyü, 1230 m, 08.iv.2013, E.Yüce 2497 **(R13)**. Ir.-Tur.

Gagea liotardii (Sternb.) Schult. & Schult.f. **(=*Gagea fragifera*** (Vill.) E.Bayer & G.López, = ***Gagea fistulosa*** (Ramond ex DC) Ker-Gawl.)/**Yayla yıldızı**

Tunceli center, 7 km from Tunceli to Pülümür (Pülümür Valley), 934 m, steppe, 12.iv.2015, Armağan 6425 **(MA)**.

Gagea luteoides Stapf/**Altınyıldız**

Ovacık, 8 km from Ovacık to Tunceli, 500 m N of Yaylagünü, 1212 m, pastures in stream side, 11.iv.2015, Armağan 6407 **(MA)**; Munzur Da. above Ovacık, around Kankala, above Karataş Köyü, 1800-2000 m, 08.v.1979, Yıldırımlı 1494 **(R6)**; Tunceli-Ovacık arası, Anafatma civarı, 940 m, 20.iv.2012, E.Yüce 2019 **(R13)**.

Gagea minima (L.) Ker Gawl./**Minik yıldız**

Munzur vadisi **(R15)**. Ir.-Tur.

Tulipa armena Boiss. var. *armena*/**Dağlâlesi**

Ovacık, 7 km from Yoncalı to Ağaçpınar, 2015 m, steppe, 01.vi.2015, Armağan 6543 **(MA)**; Ovacık, Munzur Dağları, around Kankala, above Karataş Köyü, 1800-2000 m, 08.v.1979, Yıldırımlı 1495 **(R4)**; Tunceli-Ovacık arası, 45. km, 08.v.2012, E.Yüce 2046 **(R13)**; Ovacık, Munzur gözeleri, 1300 m, 08.v.2012, E.Yüce 2075 **(R13)**; Tunceli-Ovacık arası, Venk Köprüsü çevresi, 1040 m, 08.v.2012, E.Yüce 2079 **(R13)**; Ovacık (Merkez), Yeşilyazı, 1275 m, 21.v.2012, E.Yüce 2089 **(R13)**; Ovacık, Akyayık Köyü, 1315 m, 22.iv.2013, E.Yüce 2565a **(R13)**; Ovacık, Güneykonak Köyü, 1230 m, 08.v.2013, E.Yüce 2653 **(R13)**; Ovacık, c. 18 km NE of Ovacik, NE of small river dam, locality called Şahverdi, 1505 m, 17.v.2011, V.E. 11-0040 **(R14)**; Munzur Vadisi **(R15)**. Ir.-Tur.

Tulipa armena Boiss. var. *galatica* (Freyn) Eker/**Dağlâlesi**

Ovacık, 7 km from Yoncalı to Ağaçpınar, 2015 m, steppe, 01.vi.2015, Armağan 6695 **(MA)**; Ovacık, Akyayık Köyü, 1315 m, 22.iv.2013, E.Yüce 2565b **(R13)**; Munzur Vadisi **(R15)**. Ir.-Tur.

Tulipa julia K.Koch/**Yabanlâlesi**

Tunceli center, 26 km from Tunceli to Ovacık (Munzur Valley), 1060 m, steppe, 26.v.2014,

Armağan 4029 **(MA)**; Munzur Da. above Ovacık, 1800 m, D. 31882 **(R6)**; Ovacık, Akyayık Köyü, 1315 m, 22.iv.2013, E.Yüce 2582; Ovacık, Güneykonak Köyü, 1230 m, 24.iv.2013, E.Yüce 2638 **(R13)**. Ir.-Tur.

ORCHIDACEAE

Anacamptis pyramidalis (L.) Rich./**Sivrisalep**

Ovacık, N of Eskigedik, Munzur Mountains, 2160 m, oak openings, 19.vi.2014, Armağan 4950 **(MA)**; Mazgirt, road of Elazığ - Tunceli, between Güneşdere and Kızılcık, 1090 m, oak openings, 02.vi.2014, Armağan 4113 **(MA)**; Tunceli center, road of Tunceli - Elazığ, 700 m after from Aktuluk, 930 m, oak openings, 22.v.2015, Armağan 3690 **(MA)**; Elazığ to Tunceli, 900 m, Taub. 78.277 **(R6)**; Tunceli-Ovacık arası, Aşağıtorunoba, 09.vi.2013, E.Yüce 2994 **(R13)**; Ovacık, 27.5 km NNW Tunceli, road Aşağıtorunoba-Agdat, 1825 m, semihumid meadow, 18.vi.2013, V.Y.E. & M. 13-0373 **(R14)**.

Cephalanthera damasonium (Mill.) Druce/ **Ormankuşçuğu**

Ovacık, Güneykonak Köyü, 1230 m, 08.v.2013, E.Yüce 2652 **(R13)**. Euro.-Sib.

Cephalanthera epipactoides Fisch. & C.A.Mey./ **Ana çamçiçeği**

Tunceli center, c. 8.1 km ESE of Tunceli, road to Ambar, 970 m, roadside in oak forest, 19.v.2011, V.E. 11-0105 **(R14)**. E.Medit.

Cephalanthera kotschyana Renz & Taubenheim/ **Koç salebi**

c. 3 km N. of Pülümür pass, 1600 m, Baumann 5550 **(R6)**. End.

Cephalanthera kurdica Bornm. ex Kraezl./ **Kurtkuşçuğu**

Tunceli center, 17 km from Tunceli to Pülümür (Pülümür Valley), 986 m, moist shaded places, 29.v.2015, Armağan 6460 **(MA)**; Tunceli center, road of Tunceli - Sütlüce, 2 km after from junction, 1050 m, oak openings, 23.v.2015, Armağan 3806 **(MA)**; Ovacık, Akyayık Köyü, 1315 m, 10.vi.2013, E.Yüce 2791 **(R13)**. Ir.-Tur.

Cephalanthera longifolia (L.) Fritsch / **Kuğusalebi**

Tunceli center, 12 km from Geyiksuyu to Eğriyamaç, 1575 m, under the forest, 23.v.2015, Armağan 6682 **(MA)**; Tunceli, Kalan river valley, 1 km from Sarıtaş to Gözen (iksor), 1160 m, under the forest, 30.v.2015, Armağan 6504 **(MA)**; Ovacık, Akyayık Köyü, 1315 m, 13.v.2013, E.Yüce 2602 **(R13)**. Euro.-Sib.

Cephalanthera x taubenheimii H.Baumann/ **Melez ormankuşçuğu**

Inter Tunceli et Erzincan, 8 km N. Pülümür Geçidi, 1600 m, 30.v.1981, H. Baumann **(R6)**. End.

Dactylorhiza iberica (M.Bieb. ex Willd.) Soó/ **Kırım salebi**

Pülümür, road of Pülümür - Yedisu, 6 km after from Derindere, 1960 m, moist meadows, 22.vii.2014, Armağan 5551 **(MA)**; Pülümür, between Bardakçı and Derindere, 1980 m, moist meadows, 22.vii.2014, Armağan 5512 **(MA)**; above Pülümür, 1900 m, D. 31594 **(R6)**; Ovacık, banks of Munzur Suyu, 1200 m, 18.vi.1979, Yıldırımlı 2037 **(R4)**; Ovacık, Akyayık Köyü, 1315 m, 10.vi.2013, E.Yüce 2792 **(R13)**; Ovacık, Güneykonak Köyü, 1230 m, 05.vi.2013, E.Yüce 2804 **(R13)**; Tunceli center, c. 14.1 km NE of Tunceli, road D882 to Gökçek, 2.2 km SSW Gökçek, locality called Kutudere, 1000 m, dry meadows and oak forest, 18.v.2011, V.E. 11-0097 **(R14)**; Munzur Vadisi **(R15)**. E.Medit.

Dactylorhiza osmanica (Klinge) P.F.Hunt & Summerh. var. *anatolica* (Nelson) Renz & Taubenheim/**Osmanlısalebi**

Pülümür pass, 1900 m, Renz & Taub. 78.452 **(R6)**. End.

Dactylorhiza osmanica (Klinge) P.F.Hunt & Summerh. var. *osmanica*/**Osmanlısalebi**

Ovacık, 8 km from Eskigedik to Işıkvuran, 2120 m, 19.vi.2014, Armağan 4925 **(MA)**; Ovacık, 6 km from Işıkvuran to Eskigedik, 2250 m, meadows, 19.vi.2014, Armağan 4921 **(MA)**; Ovacık, 48 km from Tunceli to Ovacık (Munzur Valley), 1190, meadows, 26.v.2014, Armağan 4059 **(MA)**; Ovacık, Karagöl vadisi, Munzur dağları, 1400 m, 05.v.1979, Yıldırımlı 1331 **(R4)**; Pülümür, by stream,

1500 m, 15.vi.1980, Yıldırımlı 3253 **(R4)**; Ovacık, Mercan Vadisi, 29.v.2012, E.Yüce 2119 **(R13)**; Ovacık, Güneykonak Köyü, 1230 m, 08.v.2013, E.Yüce 2635 **(R13)**; Tunceli-Ovacık yolu, Örenönü-Yakatarla Köyü arası, 26.v.2013, E.Yüce & İ.Eker 2668 **(R13)**; Ovacık, road Ovacık - Hozat, c. 6.4 km SSSW Ovacık, 1665 m, humid place in oak forest, 12.vi.2013, V.Y.E. & M. 13-0046 **(R14)**; Ovacık, 27.5 km N Tunceli, road Aşağıtorunoba - Agdat, 1860 m, stony slope, limestone, 18.vi.2013, V.Y.E. & M. 13-0399b **(R14)**; Ovacık, c. 14 km WWSW Ovacık, 0.35 km W Ziyaret, near the fountains of river Munzur, 1320 m, near river, 12.vi.2013, V.Y.E. & M. 13-0038 **(R14)**. Ir.-Tur., End.

Dactylorhiza romana (Seb.) Soo subsp. *georgica* (Klinge) Soó ex Renz & Taubenheim/**Çamkökü**

Ovacık, 7 km from Yoncalı to Ağaçpınar, 2165 m, meadows, 01.vi.2015, Armağan 6536 **(MA)**.

Dactylorhiza romana (Sebast.) Soó subsp. *romana*/**Elçik**

Tunceli center, road of Tunceli - Çıralı, 12 km after from Tunceli - Sütlüce crossroad (13 km to Çıralı), 1760 m, meadows, 01.vi.2015, Armağan 6515 **(MA)**; Ovacık, along Mercan Çayı, 1100-1200 m, 07.v.1979, Yıldırımlı 1429 **(R6)**; Ovacık, Güneykonak Köyü, 1230 m, 08.v.2013, E.Yüce 2656a **(R13)**. Medit.

Dactylorhiza umbrosa (Karelin & Kirilow) Nevski var. *umbrosa*/**Gövdeli salep**

Pülümür, 14 km from Pülümür to Tunceli (Pülümür Valley), 1232 m, moist meadows, 29.v.2015, Armağan 6485 **(MA)**; Ovacık, Işıkvuran village, 1710 m, meadows, 04.vi.2014, Armağan 4291 **(MA)**. Ir.-Tur.

Epipactis palustris (L.) Crantz/**Danakıranotu**

Above Pülümür, 1900 m, D. 31595 **(R6)**.

Limodorum abortivum (L.) Sw. var. *abortivum*/**Saçuzatan**

10 km W. of Geyiksu, 1450 m, Taub. 81.148 **(R6)**.

Ophrys apifera Huds./**Arısalebi**

Tunceli-Hozat arası, Büyükçeşme, 01.vi.2012, E.Yüce 2317 **(R13)**; Tunceli-Pülümür yolu, Kutik Şelalesi, 04.vi.2012, E.Yüce 2374 **(R13)**.

Ophrys oestrifera M.Bieb. subsp. *oestrifera*/**Sineksalebi**

Tunceli center, 17 km from Tunceli to Pülümür (Pülümür Valley), 986 m, meadows, 29.v.2015, Armağan 6459 **(MA)**; Pülümür, 700 m W of Kırmızı bridge, 1370 m, meadows, 05.vi.2014, Armağan 4318 **(MA)**; 3 km E. of Ovacık, 1150 m, Taub. 81.139 **(R6)**; Tunceli-Ovacık arası, Halbori Gözeleri, 26.v.2013, E.Yüce 2665 **(R13)**.

Ophrys phrygia H.Fleischm. & Bornm./**Yunus salebi**

Nazımiye, 6.5 km from Nazımiye to Tunceli, 400 m after from crossroad of Geriş, 1340 m, meadows, 03.vi.2014, Armağan 4161 **(MA)**; c. 8 km S. of Tunceli, 850 m, Taub. & Mangold 81.78 **(R6)**.

Ophrys reinholdii Spruner ex Fleischm. subsp. *straussii* (H.Fleischm.) E.Nelson / **Sidikli salep**

Nazımiye, 4 km NE of Büyükyurt, 1710 m, under the forest, 01.vi.2015, Armağan 6521 **(MA)**; Tunceli to Pülümür 1150 m, Taub. 78.280 **(R6)**.

Orchis coriophora L. subsp. *coriophora*/**Pirinççiçeği**

Pülümür, 6 km from Kocatepe to Çakırkaya, 1510 m, humid places, 05.vi.2014, Armağan 4330 **(MA)**; Ovacık, 4 km from Aşağıtorunoba to Ağaçpınar, 1800 m, moist meadows, 04.vi.2014, Armağan 4311 **(MA)**; Ovacık, 15 km from road of Ovacık - Tunceli to Işıkvuran, 1670 m, moist meadows, 04.vi.2014, Armağan 4236 **(MA)**; Ovacık, 48 km from Tunceli to Ovacık (Munzur Valley), 1190 m, moist meadows, 26.v.2014, Armağan 4060 **(MA);** Tunceli center, 5 km from Tunceli to Ovacık (Munzur Valley), 940 m, meadows in stream side, 25.v.2014, Armağan 3950 **(MA)**; Ovacık, banks of Munzur Suyu, 1200 m, 18.vi.1979, Yıldırımlı 2035 **(R4)**; Tunceli-Ovacık arası, Halbori Gözeleri, 26.v.2013, E.Yüce & İ.Eker 2663 **(R13)**; Tunceli-Hozat arası, 20. km, 27.v.2013, E.Yüce & İ.Eker 2694 **(R13)**; Munzur Vadisi **(R15)**.

Orchis laxiflora Lam. subsp. *dielsiana* Soó/**Horanta salebi**

Pülümür, 14 km from Pülümür to Tunceli (Pülümür Valley), 1232 m, humid places, 29.v.2015, Armağan 6484 **(MA)**.

Orchis laxiflora Lam. subsp. *laxiflora*/**Salepsümbülü**

Ovacık, 48 km from Tunceli to Ovacık (Munzur Valley), 1190 m, moist meadows, 26.v.2014, Armağan 4062 **(MA)**; Tunceli-Hozat arası, 20. km, 27.v.2013, E.Yüce & İ.Eker 2692 **(R13)**.

Orchis mascula (L.) L. subsp. *mascula*/**Ersalebi**

Tunceli-Ovacık arası, Işıkvuran Köyü, 18.v.2013, E.Yüce 2812a **(R13)**.

Orchis mascula (L.) L. subsp. *pinetorum* (Boiss. & Kotschy) G.Camus/**Çam salebi**

Pülümür, 2.5 km from Kocatepe to Sarıgül, near to Sarıgül's crossroad, 1970 m, oak openings, 05.vi.2014, Armağan 4357 **(MA)**; c. 10 km S. of Tunceli, 1050 m, Taub. 78.278 **(R6)**.

Orchis militaris L. subsp. *stevenii* (Rchb.f.) B.Baumann, R.Lorenz & Ruedi Peter/**Gürbüzsalep**

3 km E. of Ovacık, 1150 m, Taub. 81.135 **(R6)**; Pülümür, Kırmızıköprü, Salördek Köyü, 19.v.2013, E.Yüce 2712 **(R13)**. Hyr.-Eux.

Orchis pallens L./**Solgunsalep**

Ovacık, Akyayık Köyü, 1315 m, 04.v.2013, E.Yüce 2578 **(R13)**. Euro.-Sib.

Orchis palustris Jacq. subsp. *palustris*/**Çayırsalebi**

Tunceli center, 5 km from Tunceli to Sütlüce, 1085 m, steppe, 12.v.2015, Armağan 6680 **(MA)**; c. 48 km from Tunceli to Pülümür, 1300 m, D. 29246 **(R6)**; Ovacık, banks of Munzur Suyu, 1200 m, 18.6.1979, Yıldırımlı 2036 **(R4)**; Pülümür, foots of Kuzdere Tepesi, steppe, 1500-1700 m, 14.6.1980, Yıldırımlı 3077 **(R4)**; Ovacık, Akyayık Köyü, 1315 m, 23.iv.2013, E.Yüce 2580 **(R13)**; Munzur Vadisi **(R15)**.

Orchis punctulata Steven ex Lindl./**Selef**

Tunceli center, 3 km from Tunceli to Ovacık (Munzur Valley), 920 m, steppe, 01.v.2015, Armağan 6685 **(MA)**; Pülümür, N of Turnadere, 1424 m, dried steppe hills, 29.v.2015, Armağan 6492 **(MA)**; Erdige to Çemişgezek, Attila ISTF 16629 **(R6)**; Pülümür, Kırmızıköprü, Salördek Köyü, 19.v.2013, E.Yüce 2707 **(R13)**. E.Medit.

Orchis sancta L./**Püren salebi**

Ovacık, 27.5 km NNW Tunceli, road Aşağıtorunoba - Agdat, 1825 m, semihumid meadow, 18.vi.2013, V.Y.E. & M. 13-0372 **(R14)**.

Orchis simia Lam./**Salep püskülü**

Tunceli center, 3 km from Tunceli to Ovacık (Munzur Valley), 920 m, steppe, 01.v.2015, Armağan 6689 **(MA)**. Medit.

Orchis spitzelii Sauter ex W.D.J.Koch/**Dağ salebi**

Tunceli center, road of Tunceli - Çıralı, 12 km from Tunceli - Sütlüce crossroad (13 km to Çıralı), 1760 m, steppe, 30.v.2015, Armağan 6514 **(MA)**; Tunceli center, road of Tunceli - Çıralı, 15 km from crossroad of Tunceli - Sütlüce (10 km to Çıralı), 1850 m, steppe, 23.v.2014, Armağan 3829 **(MA)**. Medit.

Orchis tridentata Scop./**Katranalacası**

Tunceli center, 16 km from Tunceli to Pülümür (Pülümür Valley), 1060 m, oak openings, 02.v.2015, Armağan 6684 **(MA)**; Tunceli center, road of Tunceli - Çıralı, 12 km from Tunceli - Sütlüce crossroad (13 km to Çıralı), 1760 m, meadows, 30.v.2015, Armağan 6513 **(MA)**; Tunceli-Ovacık arası, Anafatma Ziyareti, 940 m, 03.v.2013, E.Yüce 2548 **(R13)**. Medit.

Platanthera chlorantha (Cruster) Rchb./**Çarpıksalep**

Ovacık, Akyayık Köyü, 1315m, 10.vi.2013, E.Yüce 2799 (R13); Ovacık, Güneykonak Köyü, 1230 m, 05.vi.2013, E.Yüce 2806 **(R13)**.

XANTHORRHOEACEAE

Asphodeline damascena (Boiss.) Baker subsp. *damascena*/**Çekiçlik**

Ovacık, Ovacık'ın 9.2 km kuzeydoğusu, 1400 m, 17.v.2011, E.Vitek, C.Ergin 11-0051 **(R13)**. Ir.-Tur.

Asphodeline tenuior (Fisch. ex M.Bieb.) Ledeb. subsp. *tenuiflora* (K.Koch) Tuzlaci var. *puberulenta*

Tuzlaci/**Tesbihçik**

Pülümür, 3 km from Çakırkaya to Dereboyu, 1830 m, steppe, 05.vi.2014, Armağan 4390 **(MA)**; d. Ovacık, nr Köseköyü, 1200 m, Yıldırımlı 1370 **(R6)**; Pülümür, E.S. Brown 2434 **(R6)**; 11 km from Tunceli to Pülümür, 1350 m, Tuzlacı **(R6)**; Ovacık, below Köse köyü, Karagöl Vadisi, 1200 m, 05.v.1979, Yıldırımlı 1370 **(R4)**; Ovacık, Akyayık Köyü, 1315 m, 22.iv.2013, E.Yüce 2571 **(R13)**; Ovacık, Akyayık Köyü girişi, tarla içi, 27.v.2013, E.Yüce & İ.Eker 2703 **(R13)**. Ir.-Tur., End.

Asphodeline tenuior (Fisch. ex M.Bieb.) Ledeb. subsp. *tenuiflora* (K.Koch) Tuzlacı var. ***tenuiflora***/**Tesbihçik**

Mazgirt, Akpazar town, S of Yenice (N of Şevki mezrası), 1250 m, steppe, 02.vi.2014, Armağan 4122 **(MA)**; Nazımiye, road Nazımiye - Dereova, 3.9 km SE Dereova 1415 m, dry gravel, 15.vi.2013, V.Y.E. & M. 13-0222 **(R14)**. Ir.-Tur.

Eremurus cappadocicus J.Gay ex Baker/**Mor çiriş**

Mazgirt, road of Elazığ - Tunceli, between Güneşdere and Kızılcık, 1090 m, steppe, 02.vi.2014, Armağan 4118 **(MA)**. Ir.-Tur.

Eremurus spectabilis M.Bieb./**Çiriş**

Tunceli center, 18 km from Tunceli to Ovacık (Munzur Valley), 990 m, steppe, 30.v.2015, Armağan 6511 **(MA)**; Ovacık, 3 km N of Işıkvuran, Munzur Mountains, 2050 m, mounatin steppe, 04.vi.2014, Armağan 4241 **(MA)**; Tunceli center, road of Tunceli - Çıralı, 16 km from crossroad of Tunceli - Sütlüce (9 km to Çıralı), 1850 m, steppe, 23.v.2014, Armağan 3832 **(MA)**; Pülümür, foots of Silbüs Dağı, clearing of Quercus petraea subsp. pinnatiloba forest, 1600-2000 m, Yıldırımlı 3351 **(R4)**; Ovacık, Karagöl Vadisi, from Dılap Yaylası to Koyungölü Köyü by path, 1250-2250 m, 08.vii.1980, Yıldırımlı 3608 **(R4)**; Tunceli-Ovacık arası, 40. km, 21.v.2012, E.Yüce 2087 **(R13)**; Munzur Vadisi **(R15)**. Ir.-Tur.

DISCUSSION

Accounting for taxa according to floristic regions were as follows; 50% (74 taxa) Irano – Turanian, 22% (15 taxa) Mediterranean, 6% (9 taxa) Euro – Siberian, and 29% (44 taxa) wide spread and/or unknown regions (Figure 2).

The families with the most taxa in the research area were Amaryllidaceae (37 taxa), Orchidaceae (33 taxa), Asparagaceae (18 taxa), and Liliaceae (16

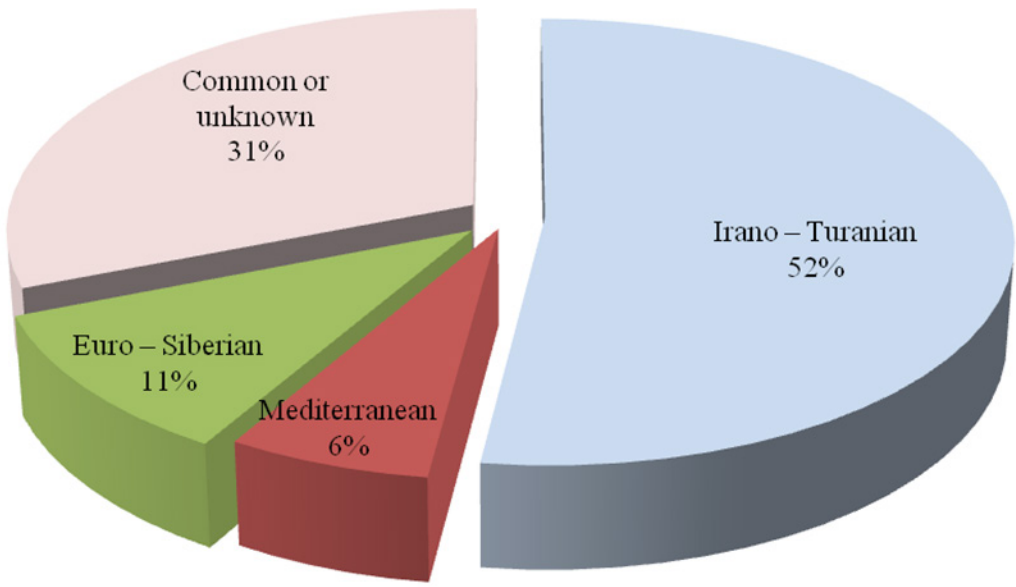

Figure 2. The distribution of taxa depending on phytogeographical regions.

taxa) (Figure 3, Table 1). The major genera in this study with relation to the number of taxa were ***Allium*** L. (36 taxa), ***Ornithogalum*** L. (15 taxa), ***Orchis*** L. (13 taxa), ***Gagea*** Salisb. (8 taxa), ***Bellevalia*** Lapeyr. (7 taxa), Iris L. (6 taxa), ***Muscari*** Mill. (6 taxa), ***Dactylorhiza*** Necker ex Nevski (6 taxa), and ***Cephalanthera*** Rich. (6 taxa). Five of 32 genera contain 53% of all taxa in the research area (Figure 4, Table 2).

In comparison the results of the current study and the previous floristic studies in Tunceli province; 105 taxa in this study, 44 taxa in Reference 4, 41 taxa in Reference 6, 3 taxa in Reference 8, one taxon in Reference 11, one taxon in Reference 12, 91 taxa in Reference 13, 21 taxa in Reference 14, and 49 taxa in Reference 15 were found. As a result, 26 taxa were newly recorded for the province of Tunceli.

Table 1. A comparison of studies in Tunceli in terms of major families.

The studies	The number of taxa belonging to families					
	Amaryllidaceae	*Orchidaceae*	*Asparagaceae*	*Liliaceae*	*Iridaceae*	Total
This study	28	20	21	14	11	94
Reference 6	11	15	8	3	1	38
Reference 4	7	5	11	7	6	36
Reference 8	1	0	1	0	0	2
Reference 11	0	0	1	0	0	1
Reference 12	1	0	0	0	0	1
Reference 13	19	18	22	12	9	80
Reference 14	3	5	4	2	4	18
Reference 15	12	3	9	9	9	42

Table 2. A comparison of studies in Tunceli in terms of first five genera.

The studies	The number of taxa belonging to families					
	Allium	*Ornithogalum*	*Orchis*	*Gagea*	*Bellevalia*	Total
This study	27	10	9	7	3	56
Reference 4	6	2	2	2	2	14
Reference 6	11	3	4	2	2	22
Reference 8	1	0	0	0	1	2
Reference 11	0	1	0	0	0	1
Reference 12	1	0	0	0	0	1
Reference 13	18	9	8	5	6	46
Reference 14	3	3	1	1	0	8
Reference 15	11	3	2	2	2	20

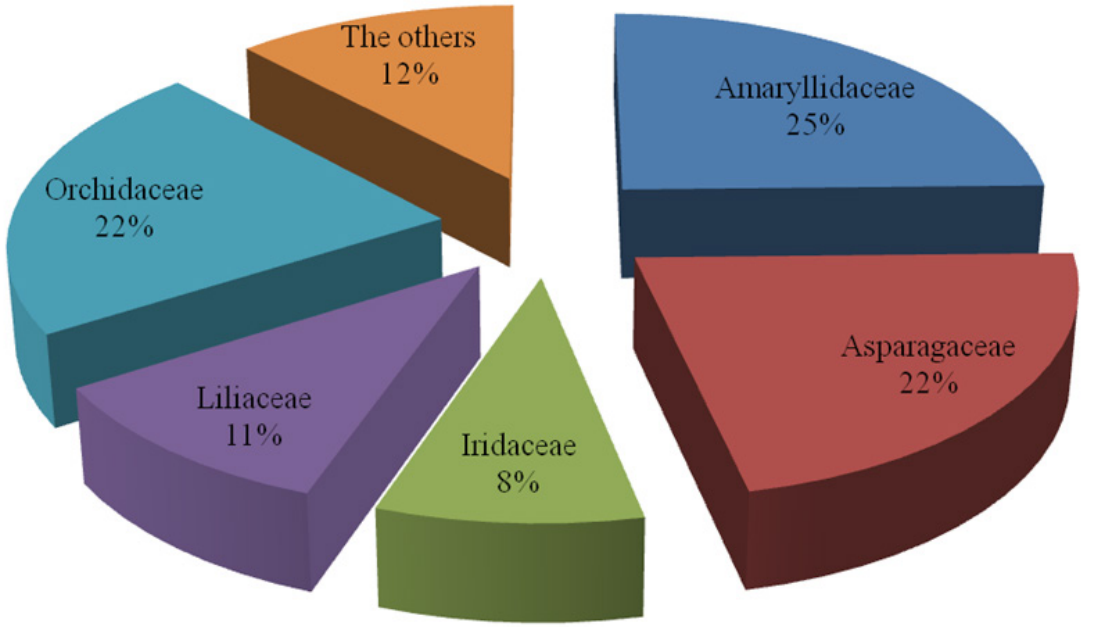

Figure 3. The distribution of families according to number of taxa.

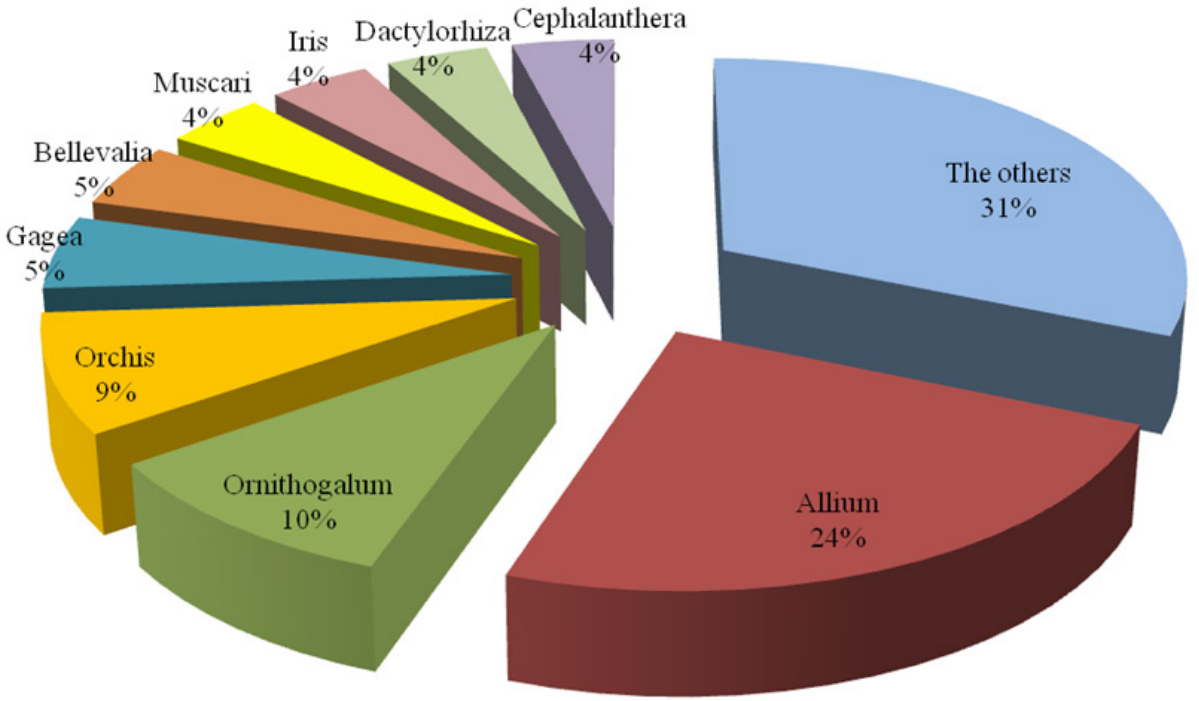

Figure 4. The distribution of genera according to number of taxa.

Allium cardiostemon Fisch. & C.A.Mey., ***Muscari comosum*** (L.) Mill., ***Gladiolus atroviolaceus*** Boiss., ***Gladiolus italicus*** Mill., ***Ixiolirion tataricum*** (Pall.) Schult. & Schult.f. var. ***tataricum***, ***Tulipa armena*** Boiss. var. ***armena***, ***Dactylorhiza iberica*** (M.Bieb. ex Willd.) Soó, and ***Dactylorhiza osmanica*** (Klinge) P.F.Hunt & Summerh. var. ***osmanica*** were the most common taxa in floristic studies carried out in Tunceli.

There are some contradictions between previous research findings, for example ***Gagea minima*** (L.) Ker Gawl., given as a new record for the Flora of Turkey from Van in 2015 [16], were determined from the Munzur Valley (Tunceli) by Koyuncu and Aslan in 2009 [15]. ***Gagea chanae*** Grossh., given as an interesting finding in previous studies, was already found in Munzur Valley in the researches of Yıldırımlı and Koyuncu & Aslan [4,15].

The endemism ratio of monocotyledonous petaloids in Tunceli province is 22% (33 taxa). The ratio of endemism is high because Tunceli has a lot of the microclimatic areas. The climate is so suitable to living of the geophytic plants [13].

The in-situ and ex-situ studies for the preservation of future genetic resources, especielly the endemic species, and also the applied researches such as cultivation of the geophytes for the ornamental plants will be more effective in Tunceli because it has the more suitable and various habitats.

The nature tourism and the transhumance are preferred so much in public of Tunceli. Therefore, the awareness of the public about the recognition and conservation of natural vegetation will contribute to the conservation of nature and the sustainable tourism.

ACKNOWLEDGEMENTS

This study is based on field studies as part of "Biodiversity Inventory and Monitoring Works on Terrestrial and Inland Water Ecosystems of Tunceli Province" carried out by the Tunceli Office of Turkish Republic of Forestry and Water Affairs, General Directorate of Nature Conservation and National Parks. I would like to thank the aforementioned institution, A.H. Gürsönmez, M. Özel, and Z. Duman.

References

1. P.H. Davis, Distribution patterns in Anatolia with particular reference to endemism, in: P.H. Davis, P.C. Harper, I.C. Hedge (Eds.), Plant Life of South-West Asia, The Botanical Society of Edinburgh, Edinburgh, UK, 1971.
2. H. Gür, The Anatolian diagonal revisited: Testing the ecological basis of a biogeographic boundary, Zoology in the Middle East, 62 (2016), 189-199.
3. M. Öztürk, A. Tatlı, H. Özçelik, L. Behçet, General Characteristics of Flora and Vegetation Formations of Eastern Anatolia Region and Its Environs (Türkiye), SDU J. Sci., 10 (2015) 23-48.
4. Ş. Yıldırımlı, Flora of Munzur Dağları (Erzincan-Tunceli), Ot Sis Bot Dergisi 2 (1995) 1–78.
5. S.C. Demir, İ. Eker, Petaloid Monocotyledous Flora of Bolu Province, Including Annotations on Critical Petaloid Geophytes of Turkey, PEGEM Akademi, Ankara, Turkey, 2015.
6. P.H. Davis, R.R. Mill, K. Tan, Flora of Turkeyandthe East AegeanIslands, vol. 8, Edinburgh Univ. Press, Edinburgh, UK, 1984.
7. P.H. Davis, R.R. Miller, K. Tan, Flora of Turkeyandthe East AegeanIslands, vol. 10, Edinburgh Univ. Press, Edinburgh, UK, 1988.
8. Güner, N. Özhatay, T. Ekim, K.H.C. Başer, Flora of Turkey and the East Aegean Islands, vol. 11 (supp. 2), Edinburgh Univ. Press, Edinburgh, UK, 2000.
9. Bizim Bitkiler (2018). Version 3.1. Published on the Internet; http://www.bizimbitkiler.org.tr/v3/demo/details.php?id=402&t=1 (accessed: 21st February).
10. The Plant List, http://www.theplantlist.org, 2013 (accessed: February 2018).
11. N. Özhatay, Ş. Kültür, Check-List of Additional Taxa to the Supplement Flora of Turkey III, Turk J Bot, 30 (2006) 281-316.
12. N. Özhatay, Ş. Kültür, B. Gürdal, Check-List of Additional Taxa to the Supplement Flora of Turkey VI, Istanbul Ecz. Fak. Derg., 43 (2013) 33-82.
13. E. Babacan Yüce, İ. Eker, Munzur Vadisi (Tunceli) ve yakın çevresinin geofit florası, Bağ Bahçe Bil. Derg., 4 (2017) 31-49.
14. E. Babacan Yüce, E. Vitek, U. Çakılcıoğlu, Contributions to the Flora of Tunceli (Turkey), International J. Natur. Life Sci., 1 (2017) 39-66.
15. M. Koyuncu, N. Arslan, Munzur Vadisi'nin Biyolojik Çeşitliliğinin Korunması, Ulaşılabilir Yaşam Derneği, Ankara, Turkey, 2009.
16. M. Tekşen, İ. Eker, S. Aslan, ***Gagea minima*** (L.) Ker Gawl. (Liliaceae): Türkiye için yeni kayıt, Bağbahçe Bil. Derg., 2 (2015) 9-18.

Economically Productive Features of Turkeys Breed in Azerbaijan

Azerbaycan'da Üretilen Hindilerin Ekonomik Açıdan Üretim Özellikleri

Research Article

Minura Kazimova
Azerbaijan State Agricultural University, Department of Veterinary, Ganja, Azerbaijan.

ABSTRACT

Turkey breeding is an important source of increased production of high-quality bird meat. Many years of experience shows the effectiveness of industrial turkey breeding. Among the meat species of poultry, the turkey occupies a special place. By its biological and economic characteristics, it is one of the most promising species of meat poultry. Turkeys have a high fertility and high yield of edible parts per unit of live weight. The aim of the research was creating new highly productive breeds, lines and to study the dynamics of the economic-useful qualities of turkeys of various lines, breeds and productive, interior features, quality of meat of turkeys breed in the conditions of Azerbaijan.

Key Words
Poultry farming, turkey, turkey meat, red meat, quality, meat production, white meat.

ÖZ

Hindi yetiştiriciliği yüksek kaliteli kuş eti üretiminin önemli bir kaynağıdır. Uzun yıllara dayanan tecrübeler, endüstriyel hindi ıslahının etkinliğini göstermektedir. Kanatlı hayvan eti türleri arasında hindiler özel bir yere sahiptir. Hindiler yüksek doğurganlık ve canlı ağırlığın birimi başına yenilebilir kısımlarının fazla olması nedenile önemli et kaynaklarından biridir. Araştırmanın amacı yeni, yüksek üretken hatlar oluşturmakla beraber Azerbaycan koşullarında yetişdirilen hindilerin çeşitli hatlarının üretkenliyini, iç mekan özelliklerini, kalitesini, ekonomik yararlı niteliklerinin dinamikliyini incelemekten ibarettir.

Anahtar Kelimeler
Kümes hayvanları yetiştiriciliği, hindi, hindi eti, kırmızı et, kalite, et üretimi, beyaz et.

Article History: Received: Nov 11, 2017; Revised: Dec 06, 2017; Accepted: Feb 15, 2018; Available Online: Mar 26, 2018.

DOI: 10.15671/HJBC.2018.230

Correspondence to: M. Kazimova, Azerbaijan State Agricultural University, Department of Veterinary, Ganja, Azerbaijan.
Tel: (+994) 55 5918099 Fax: (+994) 55 5918099 E-Mail: minura-cahan@hotmail.com

INTRODUCTION

Young domestic turkeys readily fly short distances, perch and roost. These behaviors become less frequent as the birds mature, but adults will readily climb on objects such as bales of straw. [1,2]Young birds perform spontaneous, frivolous running ('frolicking') which has all the appearance of play. Commercial turkeys show a wide diversity of behaviors including 'comfort' behaviors such as wing-flapping, feather ruffling, leg stretching and dust-bathing [3].

Turkeys are highly social and become very distressed when isolated [4,5]. Many of their behaviors are socially facilitated i.e. expression of a behavior by one animal increases the tendency for this behavior to be performed by others [6-8]. Adults can recognise 'strangers' and placing any alien turkey into an established group will almost certainly result in that individual being attacked, sometimes fatally [9]. Turkeys are highly vocal, and 'social tension' within the group can be monitored by the birds' vocalisations [10]. A high-pitched trill indicates the birds are becoming aggressive which can develop into intense sparring where opponents leap at each other with the large, sharp talons, and try to peck or grasp the head of each other [5,11]. Aggression increases in frequency and severity as the birds mature [12].

Male domestic turkey sexually displaying by showing the snood hanging over the beak, the caruncles hanging from the throat, and the 'beard' of small, black, stiff feathers on the chest [13,14].

Maturing males spend a considerable proportion of their time sexually displaying. [15]. This is very similar to that of the wild turkey and involves fanning the tail feathers, drooping the wings and erecting all body feathers, including the 'beard' (a tuft of black, modified hair-like feathers on the centre of the breast) [16]. The skin of the head, neck and caruncles (fleshy nodules) becomes bright blue and red, and the snood (an erectile appendage on the forehead) elongates, the birds ‹sneeze› at regular intervals, followed by a rapid vibration of their tail feathers [13,17]. Throught, the birds strut slowly about, with the neck arched backward, their breasts thrust forward and emitting their characteristic 'gobbling' call [18-20].

Experimental studies were conducted in private farms. The productive and pedigree qualities of turkeys of all breeds of lines were estimated on the basis of studying such indicators as: live weight, egg production over 20 weeks, egg mass, fertilization and hatchery, turkey output, young animals safety, feed costs, body article measurements, breast musculature and others.

MATERIALS and METHODS

Turkeys of all sex and age groups were fed with feed-mixtures prepared by the firm «Sheker Yem» in the republic. From the diurnal to 4 week old age, all turkeys, without separation by sex, were kept on the floor and grown to 16 weeks of age. At 16 weeks of age, they were separated by sex and subsequently grown separately.

From the 18th week of age, the females are transferred to a limited light day (under our conditions for 7 hours), the males were grown at 14-15 hours light, the illumination is 15 lux. Density of growing of young turkey at the age of 1-16 weeks 4 heads/m^2, 17-30 weeks 3 heads/m^2. Density of growing of adult birds females 2 head / m^2, males 1 goal / m^2. The feeding front at the age of 1-16 weeks 4 cm per head, at the age of 17-30 weeks 8 cm per head. The front of drinking at the age of 1-16 weeks 2 cm per head, at 17-30 weeks 3 cm. During the growing of daily young animals the temperature in the room is maintained at 28-30°C: under the brooder 35-37°C, then it is reduced by 3-6°C, bringing to 18°C by the end of the 6th week of growing. The temperature in the room from 7 to 16 weeks of age is maintained at least 17-18°C, over 16 weeks of age, not below 16°C. The relative humidity in the turkey room is maintained at 60-70%.

Growth, development and preservation of turkeys. An important indicator that characterizes the level of productivity of turkeys is their live weight and energy of its growth. The results of our studies showed that with the same feeding and maintenance technology, the live weight of the experimental turkeys varied in different ages (Table 1). At the diurnal age, the live weight of the turkeys of the North Caucasian breed group was 55.92 g, which is 5.92 g or 11.84% more than in the turkeys of the Local populations (B > 0.999). Further studies

Table 1. Dynamics of live weight of turkeys of different crosses.

Age, days		Breed and populations	
		Local populations	«North-Caucasus»
1		50.00±0.11	55.92±0.13
56		1807±103.15	2800±106.74
91	Males	3523±115.69	4951±118.25
	Females	4645±116.18	6955±119.43
	On average	4084	5953
112	Males	4748±152.67	6584±147.86
	Females	6452±141.95	9156±139.56
	On average	5600	7870
140	Males	5860±123.43	8111±120.75
	Females	8240±119.96	11713±116.67
	On average	7050	9912

have shown that the genotype shows a significant effect on the growth and development of turkeys. At 56 days of age (8 weeks) the turkeys of the North Caucasian breed exceeded the peers of the local population by 993 g, or 54.95% (B> 0.999). At the age of 91 days, females and males of the North Caucasian breed exceeded the peers of the local population by 1428g, respectively, or 40.53% and 2310g, or 49.73% (B > 0.999).

A similar pattern has been preserved in the following age periods. At 112 days old, the live weight of females and males of the North Caucasian breed was more than that of the peers of the Local Populations, by 1836 g respectively, or 38.67% and 2704 g, or 41.91% (B > 0.999).

At the age of 140 days the live weight of females and males of the North Caucasian breed was more than in the peers of the Local populations by 2251 g, respectively, or by 38.41% and 3473 g, or by 42.15% (B > 0.999).

On average, females and males of the North Caucasian breed exceeded the analogues of the Local populations in the live weight at the age of 91 days for 1869 g (45.76%); at the age of 112 days-2270g (40.53%); at the age of 140 day 2862

Table 2. Indicators of growth intensity of experimental turkeys.

Age, days		Breed and populations	
		Local populations	«North-Caucasus»
1		50.00±0.11	55.92±0.13
56		1807±103.15	2800±106.74
91	Males	3523±115.69	4951±118.25
	Females	4645±116.18	6955±119.43
	On average	4084	5953
112	Males	4748±152.67	6584±147.86
	Females	6452±141.95	9156±139.56
	On average	5600	7870
140	Males	5860±123.43	8111±120.75
	Females	8240±119.96	11713±116.67
	On average	7050	9912

g (40.59%). The study of the growth intensity of experimental turkeys also showed significant differences. More intensively grew and developed turkeys of the North Caucasian breed (Table 2). Absolute growth of live weight for the entire period of their growing was higher than for peers of Local populations by 2856.08 g or 40.80%, respectively.

An important indicator of the growth of young animals is the average daily increase in live weight. The results of our studies indicate that the turkeys of the North Caucasian breed exceeded the peers of the Local populations by the average daily weight gain for the period from 1 to 56 days at 17.04 g (51.87%); for the period from 57 to 91 days at 25.03 g 38.47%; for the period from 92 g to 112 day at 19.10 g (26.46%); for the period from 113 to 140 days at 21.14 g (40.82%); for the entire period of growing (20 weeks) at 20.55 g or 40.81%.

The growth energy of turkeys is determined by the relative increase in live weight. The highest relative increase was in the turkeys of the North Caucasian breed. For the entire period of growing turkeys of the North Caucasian breed highly significantly exceeded the peers of the Local populations in this indicator, respectively, by 3625.32 absolute percent. It should be noted that the highest growth energy in turkeys of all experimental groups is observed for the first time 8 weeks after birth. In the future, the energy of growth is reduced. Thus, the relative increase in live weight in the turkeys of the Local populations decreased by 3488.11 by the 20 week age, and by the North Caucasian breed by 4881.20 absolute percent.
An important zoo-technical economic indicator is the preservation of young animals during the growing period. The profitability of turkey farming is largely depended from this indicator. The results of our studies showed a slight difference in the safety of the turkeys of the experimental groups (Table 3).

Preservation of turkeys for the entire period of growing was 93-95% in the experimental groups. The reason for the withdrawal of turkeys in all groups was mainly mechanical injuries. It should be noted good viability of turkeys of all experimental groups, which confirms the possibility of growing both the local populations and the North Caucasian breed under industrial production conditions.

Feed conversion in turkeys. The most important zoo-technical and economic indicator of the intensity of growth and the productive action of feed are the costs of feed and nutrients of the ration per unit of output.

A study of the dynamics of feed costs per unit of growth in live weight showed that the turkeys of the experimental groups consumed a different number of feeds and unequally paid for food with products. During the eight weeks of growing on one head of turkeys of the North Caucasian breed was spent for 846 g more mixed feed, than in turkeys of local populations. Despite the greater intake of feed, turkeys of the North Caucasian breed had better feed payment by a gain of live weight. They spent 1 kg of increase in live weight less on 0.78 kg of mixed feed and 9.33 MJ of exchange energy than their peers from local populations. During the growing period from 57 to 91 days, turkeys of the North Caucasian breed spent 1 kg increase of live weight 0.56 kg less than feed and 6.89 MJ of exchange energy compared with turkeys of local populations.

A similar picture was observed in subsequent periods of growing and fattening. So, during the breeding periods from 92 to 112 days and from 113

Table 3. Preservation of experimental turkeys.

Age, days	Local population		North-Caucasus	
	head	%	head	%
1	100	100	100	100
56	96	96	97	97
91	94	94	96	96
112	93	93	95	95
140	93	93	95	95

to 140 days the turkeys of the North Caucasian breed exceeded the peers of the cross "Universal" for the payment of feed increase in live weight by 0.5 and 0.95 kg and 1 kg increase in the live weight, respectively, spent correspondingly less at 6.03 and of 11.02 MJ of exchange energy, respectively. It should be noted that in all experimental groups, the increase in feed costs per unit of growth in live weight occurred with age. The highest feed costs were during the growing period from 113 to 140 days in the crossbreeds of the cross «Local Population» 6.24 kg, and in the North Caucasian breed 5.29 kg.

Over the entire period of growing (from 1 to 140 days), the North Caucasian breed turkeys outperformed peers from local populations paying for feed increase in live weight by 0.71 kg and 8.61 MJ of exchange energy. On the basis of the conducted studies, it can be concluded that turkeys of the North Caucasian breed in all age periods outperform peers from local populations in terms of live weight, absolute average daily, relative growth, preservation and conversion of feed. To intensify the production of turkey meat, we recommend growing turkeys of the North Caucasian breed, which have high quality and low feed costs per unit of production.

RESULTS and DISCUSSION

A more complete understanding of meat qualities can be obtained only after the slaughter of turkeys, as the quantitative and qualitative characteristics of the produce become available. Turkey is one of the largest agricultural birds. According to V. Guschina, V.A. Kanivets. (2012), the fattening period of turkeys is determined by sex, breed and the purpose of their use. In this connection, the production of turkeys is subdivided into a light class (broilers) when fattening for 12-14 weeks, the middle class (turkeys) when fattening 20-24 weeks and the heavy class (turkeys) more than 20-24 weeks, at processing of which 3 weight groups of gutted carcasses are obtained: broilers up to 4.5 kg, female turkeys 4.5-7.2 kg and male turkeys more than 7.2 kg.

The results of sorting the carcasses of females and males by category are shown in Table 4.

It is established that the females of the North Caucasian breed exceeded the cross peers "Local Population" by the quality of carcasses. Most carcasses of females of the North Caucasus

Table 4. The results of the evaluation of turkey carcasses by category.

Indicator	Breeds			
	Local population		North-Caucasus	
	head	%	head	%
Females				
Total	47	100	47	100
Including: 1st category	37	78.72	42	89.36
2nd category	10	21.28	5	10.64
Non-standards	–	–	–	–
Males				
Total	46	100	48	100
Including: 1st category	33	71.74	41	85.42
2nd category	13	28.26	7	14.58
Non-standards	–	–	–	–

(89.36%) were classified in the first category, which is 13.51% more than in females of local populations. The second category included 21.28% of the carcasses of females of local populations, which was larger than the cross of non-standard carcasses when females were slaughtered. During assessing the quality of male carcasses, it is established that 85.42% of carcasses belong to the first category in the North Caucasian breed, this is 13.68 % more than that of local populations. The smallest number of carcasses of males of the second category (14.58%) was in the North Caucasian breed. Non-standard carcasses were absent in males. Thus, it can be concluded that more qualitative carcasses are obtained from females and males of the North Caucasian breed than from peers of local populations.

T

Studying the slaughter and meat qualities of turkeys showed that females of the North Caucasian breed have high slaughter characteristics (Table 5). They outperform their peers of local populations on before slaughter weight at 2.24 kg, or 38.62% (B> 0.999), by weight of the eviscerate carcass 2.09 kg, or 42.14% (B> 0.999), by weight of gutted carcass at 1.82 kg, or 41.18% (B> 0.999), slaughter output by 1.40 absolute percent.

The control slaughter of males also showed significant differences in the meat qualities between the experimental groups. The turkeys of the North Caucasian breed were significantly more reliable than peers in the local population on before slaughter weight at 3.43 kg, or 42.03% (B>0.999), by weight of eviscerate carcass at 3.19 kg, or 44.24% (B>0.999), by weight of gutted carcass at 2.78 kg, or 43.99% (B>0.999), slaughter output by 1.07 absolute percent, respectively.

Thus, we can conclude that the turkeys of the North Caucasian breed have the best slaughter and meat qualities and are highly superior to the peers of the local populations.

Table 5. Meat quality of experimental turkeys.

Indicator	Cross	
	«Local population»	«North-Caucasus»
Females		
The number of dead females, heads	47	47
Pre - slaughter weight of female, kg	5.80±0.12	8.04±0.14
Weight of eviscerate carcass, kg	4.96±0.08	7.05±0.09
From pre-slaughter weight,%	85.52	87.69
Weight of gutted carcass, kg	4.42±0.07	6.24±0.08
Slaughter output ,%	76.21	77.61
Males		
The number of dead males, heads	46	48
Pre - slaughter weight of female, kg	8.16±0.13	11.59±0.12
Weight of eviscerate carcass, kg	7.21±0.10	10.40±0.09
From pre-slaughter weight,%	88.35	89.73
Weight of gutted carcass, kg	6.32±0.09	9.10±0.11
Slaughter output ,%	77.45	78.52

CONCLUSIONS

Turkeys of the North Caucasian breed in all age periods excel peers of local populations in terms of live weight, absolute average daily, relative growth, and preservation. On average, females and males of the North Caucasian breed exceeded the analogues of local populations by live weight at the age of 91 days in 1869 g (45.76%); at the age of 112 days on 2270g (40.53%); in the 140 day old on 2862g (40.59%). Turkeys of the North Caucasian breed have a high feed conversion.

References

1. F. Alekseyev, O. Vorokova, Turkeys from the Moscow region. Poultry farming 9 (2012) 5-6.
2. B. Belenkiy, Features of industrial production of turkey meat. Poultry farming 6 (2007) 22.
3. GOST 230042-86, Meat and meat products. Methods for determining fat. Standard Inform, (2010).
4. H.M. Hajiyev, Feeding technology of young birds. Azer Publishing, Baku (1987) 32-42.
5. E.E. Epimakhova, The scientific and practical justification for increasing the yield of hatching eggs and conditioned young animals of agricultural birds in the early postnatal period: author's abstract. dis. of the dr. of the agricultural sciences, Stavropol, (2013) 43.
6. V.V. Gushin, V.N. Makhonina, V.A. Kanivets, L.A. Shinkarenko, Quality indices of meat of gutted turkey carcasses, Meat industry, 3 (2011) 12-15.
7. M.F. Zonov, Technological methods for increasing the productivity of turkeys and eggs: auto ref. Dr. of agric. Sciences (2011) 45.
8. G.M. Erastov, Nutritional value of poultry meat Poultry farming 3 (2014) 28-30.
9. V.A. Kanivets, O.N. Petrukhin, L.A. Shinkarenko, Molecular genetic analysis of two linear crosses Local Population, Innovative developments and their familiarization in industrial poultry farming: XVII International Conference of the Russian Branch of the World Scientific Association for Poultry Farming. (2012) 68-70.
10. V.A. Pogodaev, O.N. Petrukhin, L.A. Shinkarenko, Development and productivity of turkeys of white broad-chested breed in the breeding poultry plant "North-Caucasian Zone Experimental Station for Poultry Farming, Zootechnics. 1 (2015) 28-29.
11. V.A. Pogodaev,V.A. Kanivets, L.A. Shinkarenko, Genetic parameters of breeds of turkeys bred in North Caucasian Zone Experimental Station for Poultry, Bird and poultry products. 3 (2013) 19-22.
12. V.I. Fisinin, The rate for development, Poultry farming. 2 (2015) 2-6.
13. A.I. Shevchenko, Systems of turkey breeding. Bird and poultry products. 6 (2010) 23-25.
14. F.F. Alekseyev, A.V. Aralov, L.S. Belyakova, Under the generaledit. Meat poultry farming. St. Petersburg.: Lan, (2007) 416.
15. L.A. Shinkarenko, V.A. Pogodaev, The development of new genotypes of domestic turkeys and their use for the production of environmentally friendly products. Monograph-Cherkessk: BIC, North Caucasus. GGTA, (2014) 156.
16. Flock, Diet mar K. Poultry breeding-the next 25 years, Poultry Processing, 1 (2009) 22-23.
17. Battery cages in EU declining but still dominant. World Poultry.net, 2010, 16 June.
18. Clements, Mark. Poultry export to Europe could face new hurdles, Poultry Int., 8 (2010) 4.
19. Morrison' scon firm free-range for all own label eggs, World Poultry.net, (2010) 13 April.
20. Pet and Gerrys introduces heirloom-breed blue eggs, World Poultry. net, (2010) 16 March.

Detection of Lipase Production from Newly Isolated *Trichoderma Citrinoviride*

Yeni İzole Ediilmiş *Trichoderma Citrinoviride*'den Lipaz Üretiminin Saptanması

Research Article

Muhammed Hasan Akyıl* **and Nilüfer Cihangir**
Hacettepe University Department of Biology, Faculty of Science, Beytepe, Ankara, Turkey.

ABSTRACT

The production of lipase is aimed from a new fungal source in this study. Fungus was isolated from soil locality Kocaeli. It was determined as *Trichoderma citrinoviride* by the analysis of 18S rRNA sequence. Various parameters and media components were investigated for production of lipase. Glucose and peptone were found to be most suitable carbon and nitrogen source, respectively. To determine the suitable oil as carbon source, various oils were added to the production medium. Olive oil was found to be the optimal oil for lipase production from *Trichoderma citrinoviride*. pH 5.5, temperature 30°C and incubation time for 4 days were found to be optimal incubation conditions for lipase production. We also determined lipase yield from *Trichoderma citrinoviride* which is produced in molasses medium as an alternative carbon source.

Key Words
Lipase, *Trichoderma citrinoviride*, microbial lipase production.

ÖZ

Bu çalışmada yeni izole edilmiş bir fungustan lipaz üretimi amaçlanmıştır. Fungus Kocaeli bölgesinden topraktan izole edilmiştir. 18S rRNA analizi sonucu *Trichoderma citrinoviride* olarak saptanmıştır. Lipaz üretimi için çeşitli parametreler ve besiyeri bileşenleri araştırılmıştır. Sırasıyla, glikoz ve pepton en uygun karbon ve azot kaynağı olarak bulunmuştur. Karbon kaynağı olarak uygun yağı tespit edilmesi için, üretim ortamına çeşitli yağlar eklenmiştir. Zeytinyağının *Trichoderma citrinoviride*'den lipaz üretimi için en uygun yağ olduğu bulunmuştur. pH 5.5, sıcaklık 30°C ve 4 günlük inkübasyon süresi lipaz üretimi için en uygun inkübasyon koşulları olarak bulunmuştur. Alternative karbon kaynağı olarak melas ortamında üretilen *Trichoderma citrinoviride*'den lipaz verimi de tespit edilmiştir.

Anahtar Kelimeler
Lipaz, *Trichoderma citrinoviride*, mikrobiyal lipaz üretimi.

Article History: Received: Jan 16, 2018; Revised: Feb 09, 2018; Accepted: Feb 22, 2018; Available Online: Mar 26, 2018.

DOI: 10.15671/HJBC.2018.231

Correspondence to: M.H. Akyıl, Hacettepe University Department of Biology, Faculty of Science, Beytepe, Ankara, Turkey.
Tel: +90 312 297 80 24 Fax: +90 312 299 20 28 E-Mail: m.hasanakyil@gmail.com

INTRODUCTION

Enzymes are defined as biological catalysts that accelerate chemical reactions and allow the maintenance of biological activity, also can be used repeatedly [1]. More before enzymes described they were used in food and textile production [2]. The commercially most widely used enzymes are carbohydrases, proteases and lipases [3]. Lipases (triacylglycerol acylhydrolases, EC. 3.1.1.3) catalyze hydrolysis of triacylglycerol to free fatty acids and glycerol [4]. The use of lipases is becoming more popular in food industry pharmaceutical industry and in cleaning products [5]. Also biodiesel can be synthesized via lipase-catalyzed transesterification [6,7].

It is possible to produce lipase enzyme from fungi that isolated from; oil contaminated soils, waste oils from plants, dairy industry, seeds and perishable food [5]. Lipase production from different fungal sources is possible; Aspergillus, Rhizopus, Mucor, Penicillium, Geotrichumand and Trichoderma [7-9].

Trichoderma is a fungus that has a filament structure, grows very rapidly and can found in any kind of soil, manure or rotting plants. Because of its competitive structure, Trichoderma is predominantly concentrated in the soil. Trichoderma frequently isolated from forest and agricultural soil. Also such as many plant pathogens fungi lives on decaying organic material [8,10-12].

In recent years assessment of waste from the sugar factory, have an important place in lipase production studies. Molasses occurs during the processing of sugar beet to obtain a dark brown colloidal effluent. It is a dark brown colloidal waste. 4 kg molasses occurs in every 100 kg of processed sugar beet [13].

Various studies show that Ülker and colleagues produced extracellular lipase from Trichoderma harzianum, Kashmiri et.al. isolated lipase from Trichoderma viride and Krastanov et.al. isolated laccase from Trichoderma longibrachiatum [8,14,15].

In this paper describes for the first time, the characterization of a novel extracellular lipase from *Trichoderma citrinoviride* that isolated from soil in İlimtepe/Kocaeli, Turkey.

MATERIALS and METHODS

In this study *Trichoderma citrinoviride* that isolated from soil (ilimtepe/ Kocaeli/Turkey) was used for lipase source. After isolation Bioeks Medical and Biotechnology Research Systems isolated DNA accordance with the protocol by Bioseepdy DNA isolation kit® and 18S rRNA sequence analysis has determined the fungi as *Trichoderma citrinoviride*. The microorganism matched with *Trichoderma citrinoviride*(accession number: EU280098.1, 99%).

To determination lipolytic activity, inoculated on tributyrin agar(1% agar, 0.5% peptone, 3% yeast extract) Many researchers have used tributyrin agar for determination microorganisms lipolytic activity. The microorganisms that having lipase enzyme, create a zone while during reproduction [16-18].

Lipase Production Medium

After the determination of the lipase enzyme the organism was cultured in 100 mL of basal mineral medium that Hatzinikolau et.al. described [19]: ((g/L): 12 NaH_2PO_4, 2 KH_2PO_4, 0.330 $CaCl_2.2H_2O$, 0.030 $ZnSO_4.7H_2O$, 0.030 $MgSO_4.7H_2O$, 0.005 $FeSO_4.7H_2O$), and 1 ml olive oil added as a carbon source, in a 250 mL conical flask shaken at 150 rpm at 30°C and pH setted to 5.5.

Determination of Growth Curve

To determinate *Trichoderma citrinoviride* growth curve we inoculated it in lipase production medium for ten days. Each day lipase production medium media was filtered through pre-weighted filter paper (Whatman No. 1) to extract the biomass. Thus measuring the dry weight the growth curve occurred.

Lipase Activity Assay

The filtrate of the lipase production medium used for enzyme source. Titrimetric assay performed for measuring the lipolytic activity as Sugihara described [20].

1 ml olive oil, 4.5 ml 50 mM acetate buffer 0.1 ml 0,5 M $CaCl_2$ and 1 ml filtrate has added for incubation area. Distilled water was added instead of filtrate to prepare blind tube. After 30 minutes incubation time, 20 ml of ethanol added for reaction stop. After this step both 50 mM KOH tube was added until the

pH rises to 10.5. After titration, amount of expended KOH formulated to calculate lipase activity,

(50xexpended KOH)/(30 (incubation time))=U/ml

Special activity was calculated by dividing the lipase activity to dry weight.

Determination of the Optimal Incubation Time, pH and Temperature

Trichoderma citrinoviride inoculated in lipase production medium and incubated it for ten days. Each day lipase activity measured to find optimal incubation time. To find out optimal pH and temperature, lipase production medium was setted between pH 3-9 and incubation temperature was setted between 10-40°C.

Effect of Carbon and Nitrogen Source

Sunflower oil, soybean oil, corn oil and hazelnut oil were used as carbon source instead of olive oil. In addition, it added various carbon sources were added to lipase production medium; glucose, galactose, fructose, lactose, maltose and sucrose. After this step, added optimal oil and sugar source to detect together effects.

To determinate optimal nitrogen source in addition to peptone, we added ammonium sulfate, urea, yeast extract, casein, ammonium oxalate, ammonium nitrate, ammonium carbonate and proteose peptone, described by Sugihara and colleagues [20].

Lipase Production in Molasses Medium

The cost of production media for lipase production and to evaluate this food industrial waste, *Trichoderma citrinoviride* was inoculated in media that include only molasses. To examine the effect of molasses to lipase production, we diluted molasses in different proportions. Accordingly, the total molasses rate is prepared to 1%, 2%, 3%, 4% and 5%. 1 ml of our culture inoculated in production media. Lipase activity and optimal molassesration were determined after incubation.

RESULTS and DISCUSSION

After ten days incubation, and each day measuring the dry weight, growth curve occurred. (Figure1). In first five days *Trichoderma citrinoviride* grown increasingly, after then grow has been decreased.

Optimal Incubation Time, pH and Temperature

After ten days incubation and measuring lipase activity we determined highest activity on 4th day, after then lipase activity started to decrease. Thence in this study optimal incubation time was regarded as 4th day (Figure 2). And remaining study incubated for 4 days.

The effect of hydrogen ion concentration of production medium for lipase activity of *Trichoderma citrinoviride* was studied. At pH 5 lipase activity measured 9.29 U/ml, and at pH 6 it measured 8.13 U/ml. These values is the highest rates in different pH levels. When we compare the

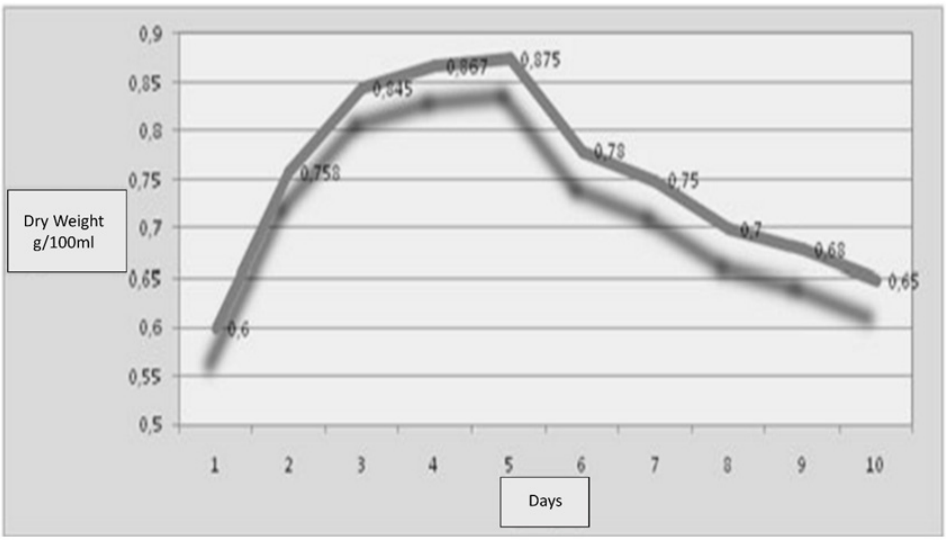

Figure 1. Trichoderma citrinoviride growth curve.

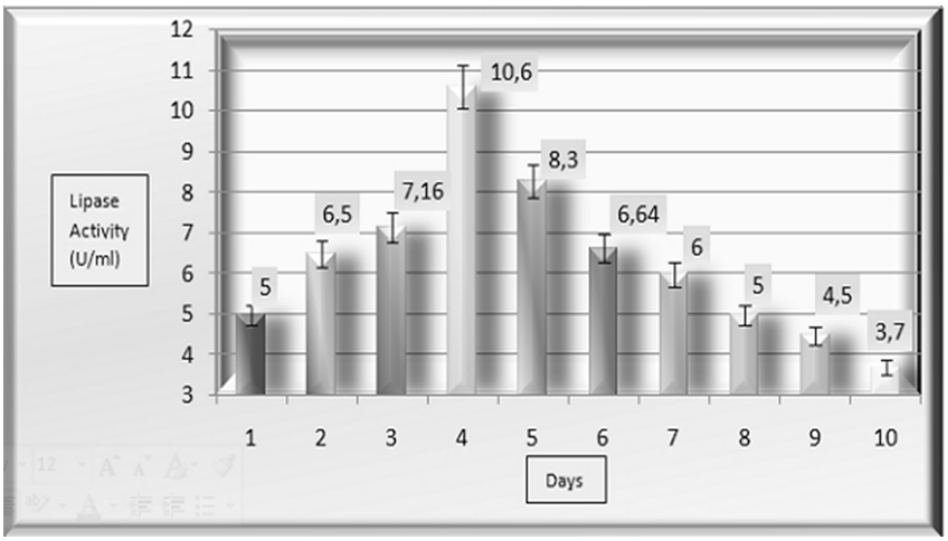

Figure 2. Effect of incubation time on lipase activity.

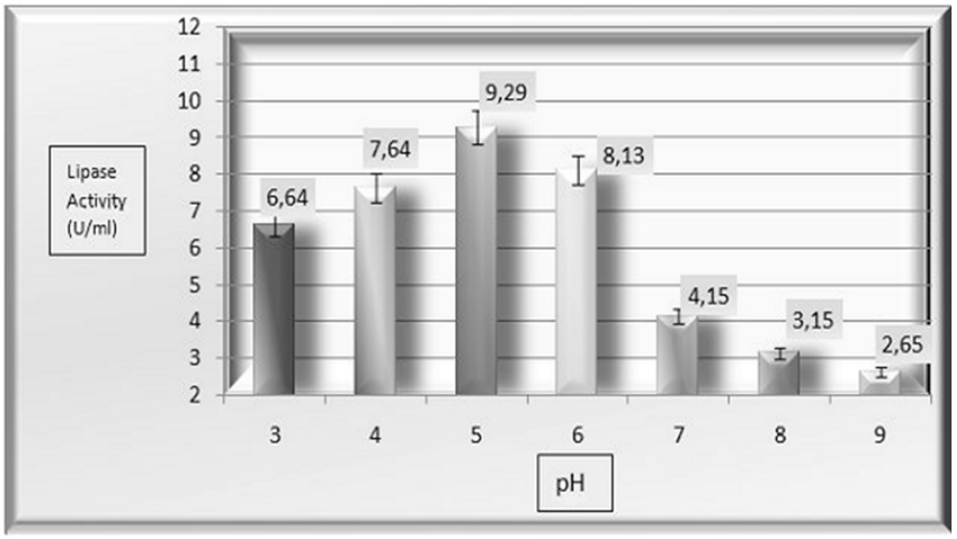

Figure 3. Effect of pH on lipase activity.

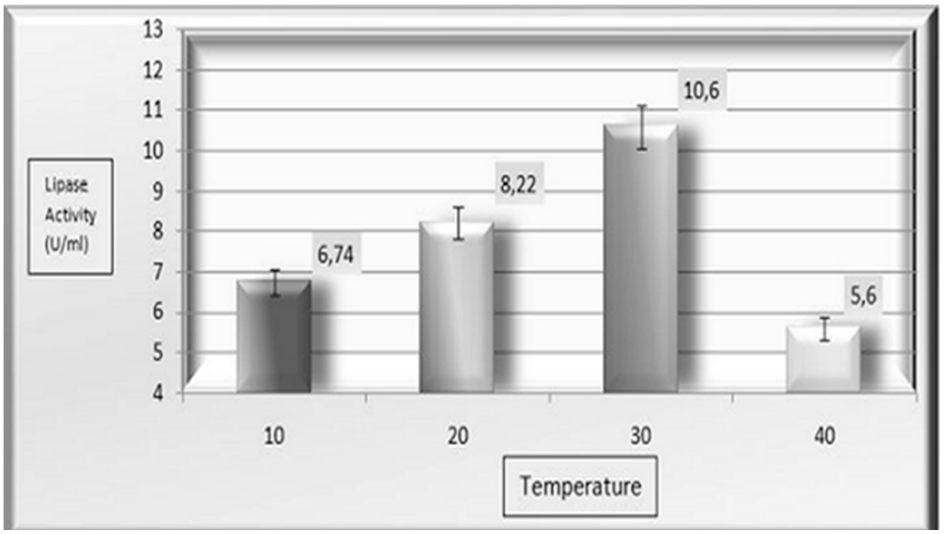

Figure 4. Effect of temperature on lipase activity.

results with the beginning conditions we saw that pH 5.5 (10.6U/ml) is the optimum pH for lipase production from *Trichoderma citrinoviride* (Figure 3). And optimum temperature for lipase production was founded as 30°C (Figure 4).

Highest activity was observed in the medium that includes olive oil, and we found out that lowest lipase activity is in the medium that includes corn oil (Fig. 5). We also detected that glucose is most suitable carbon source(Figure 6) and peptone is most suitable nitrogen source for lipase activity from *Trichoderma citrinoviride* (Figure 7).

Finally we detected lipase activity under the optimum conditions we determined for lipase activity (Carbone source glucose, and olive oil, nitrogen source: peptone, pH: 5.5, temperature: 30°C). The activity was detected 13.68 U/ml. (Figure 8).

We determined the highest lipase activity at 4th day of the incubation. We compare our results with other studies; Kashmiri et.al. detected that 50 hours is optimum incubation time for *Trichoderma viride* in their study [14]. Açıkel et al. find out optimum incubation time is 5 day for Rhizopus

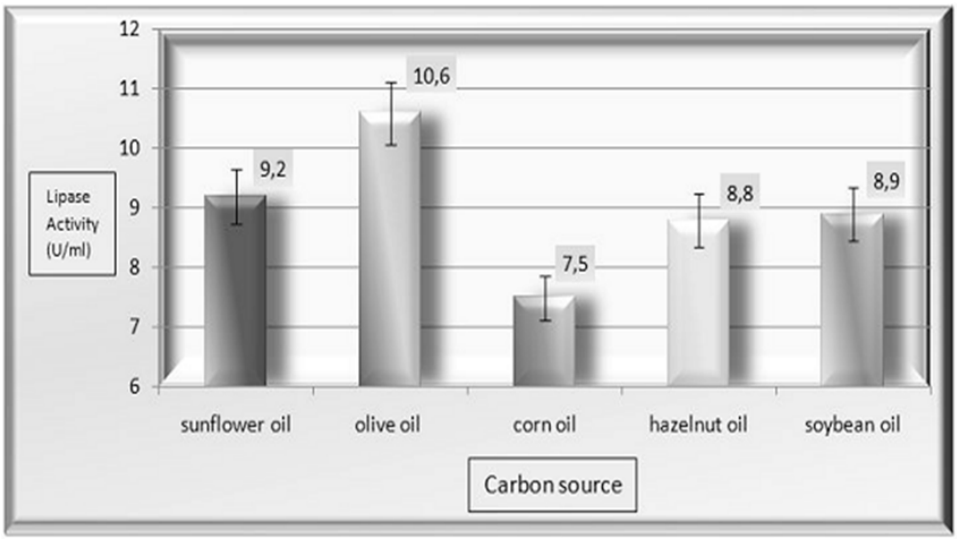

Figure 5. Effect of carbon source (oil varieties) on lipase activity.

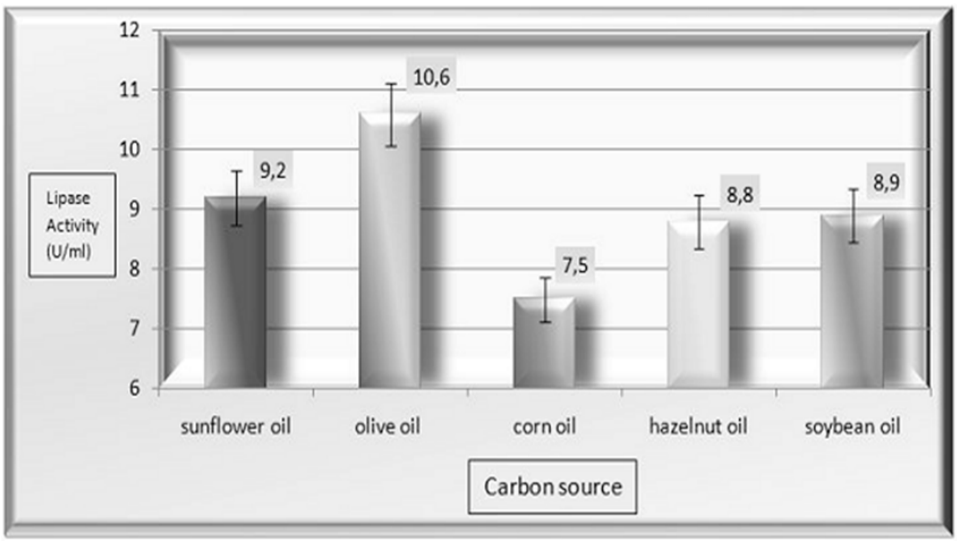

Figure 6. Effect of carbon source (sugar varieties) on lipase activity.

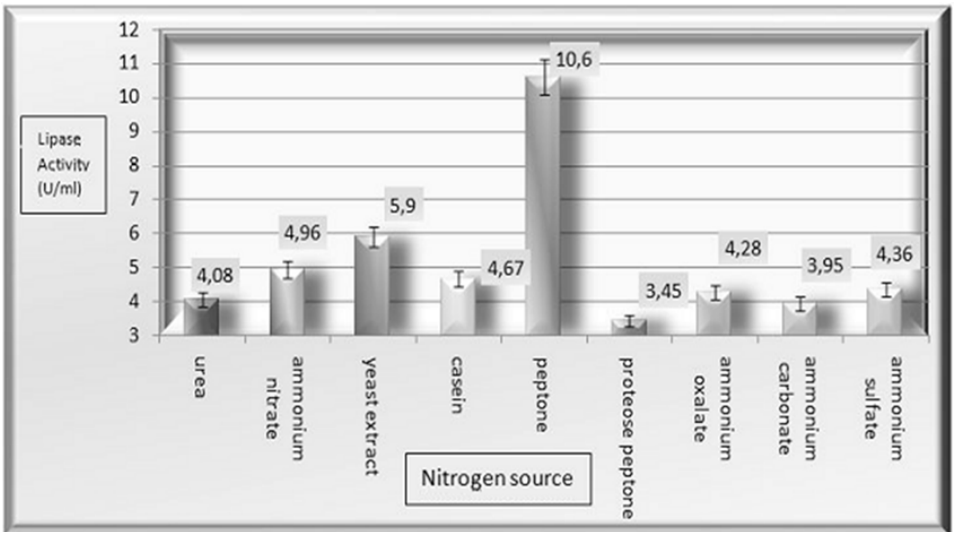

Figure 7. Effect of nitrogen source on lipase activity.

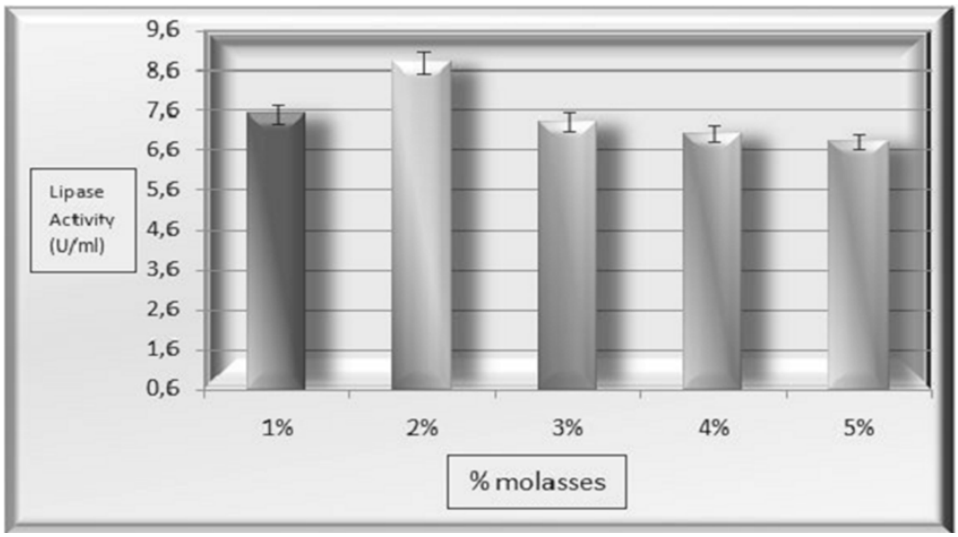

Figure 8. Lipase activity in molasses medium.

delemar [21], Ulker et al. detected the 7th day is optimum incubation time for lipase activity from Trichoderma harziamum [8].Optimum lipase activity was determined at pH 5. Decrease was observed at lipase activity in alkaline pH, acidic pH is more suitable for *Trichoderma citrinoviride* lipase activity. Kumar et.al. find out the optimum pH 8.5, for al alkaliphilic Bacillus coagulans [22].

Optimum incubation temperature was founded 30°C. Considering the cleaning industry; optimum 30°C for lipase activity is very useful especially in terms of energy saving. In lower temperature (10-20°C) despite the reduction, the activity was observed substantially. Especially in detergent formulation cold active lipase is used for cold washing also reduces the wear and tear of textile fibers. Toscano et.al. determined that Trichoderma harzianum lipase activity had started to decrease after 50°C [23].

The oils that added to the growth medium have not any direct effect on *Trichoderma citrinoviride* reproduction. But it is observed that there is a significant effect on lipase activity.The growth medium that added olive oil as carbon source

showed the highest lipase activity. Sunflower oil hazelnut oil and soybean oil has showed close activity. The medium with corn oil as carbon source was showed the lowest activity. We also found out that glucose is most suitable carbon source for lipase activity from *Trichoderma citrinoviride*. And galactose is not convenient for lipase production. Peptone was found to have a remarkable effect on lipase activity. Various nitrogen sources except peptone, caused a decrease in lipase activity.

There has been shown slightly decline of lipase activity after using molasses for production *Trichoderma citrinoviride*. But when considering the costs, it was concluded that molasses can be used for Trichoderma production.

References

1. P.K. Robinson, Enzymes: principles and biotechnological applications, Essays Biochem., 59 (2015) 1–41.
2. E.R. Riegel J.A. Kent, Kent and Riegel's Handbook of Industrial Chemistry and Biotechnology, Ebook, (2007) 1–1833.
3. Ö.E. Kiran, U. Çömlekçioğlu, N. Dostbil, Bazı Mikrobiyal Enzimler ve Endüstrideki Kullanım Alanları, Fen ve Mühendislik Derg., 9 (2006) 12–19.
4. F. Ferrato, F. Carriere, L. Sarda, R. Verger, A critical reevaluation of the phenomenon of interfacial activation, Methods Enzymol., 286 (1997) 327–347.
5. A. K. Singh, M. Mukhopadhyay, Overview of fungal lipase: a review., Appl. Biochem. Biotechnol., 166 (2012) 486–520.
6. P.S. Bisen, B.S. Sanodiya, G.S. Thakur, R.K. Baghel, G.B.K.S. Prasad, Biodiesel production with special emphasis on lipase-catalyzed transesterification, Biotechnol. Lett., 32 (2010) 1019–1030.
7. X. Zhao, F. Qi, C. Yuan, W. Du, and D. Liu, Lipase-catalyzed process for biodiesel production: Enzyme immobilization, process simulation and optimization, Renew. Sustain. Energy Rev., 44 (2015)182–197.
8. S. Ülker, A. Özel, A. Çolak, Ş.A. Karaoğlu, Isolation, production, and characterization of an extracellular lipase from *Trichoderma harzianum* isolated from soil, Turk. J. Biol., 35 (2011) 543–550.
9. H. Musa, P.C. Han, F.H. Kasim, S.C.B. Gopinath, M.A. Ahmad, Turning oil palm empty fruit bunch waste into substrate for optimal lipase secretion on solid state fermentation by *Trichoderma* strains, Process Biochem., 63 (2017) 35–41.
10. T. Andrade Marques, C. Baldo, D. Borsato, J. Batista Buzato, M. Antonia Pedrine Colabone Celligoi, Production And Partial Characterization Of a Thermostable, Alkaline And Organic Solvent Tolerant Lipase From *Trichoderma atroviride* 676, Int. J. Sci. Technol. Res., (2014) 5
11. K. Kuhls, E. Lieckfeldt, T. Borner, E. Gueho, Molecular reidentification of human pathogenic *Trichoderma* isolates as *Trichoderma longibrachiatum* and *Trichoderma citrinoviride*., Med. Mycol., 37 (1999) 25–33.
12. G. J. Samuels, *Trichoderma*: a review of biology and systematics of the genus, Mycol. Res., 100 (1996) 923–935.
13. M. Kahyao, Ğ. Lu, V. Konar, Şeker Fabrikası Atık Maddeleri Kullanılarak *Pseudomonas aeruginosa*'dan Ramnolipit Biyosürfektan Elde Edilmesi, 18 (2006) 493–498.
14. M.A. Kashmiri, A. Adnan, B. W. Butt, Production, purification and partial characterization of lipase from *Trichoderma viride*, African J. Biotechnol., 5 (2006) 878–882.
15. A.I. Krastanov, V.K. Gochev, T.D. Girova, Nutritive medium dependent biosynthesis of extracellular laccase from *Trichoderma* spp., Bulg. J. Agric. Sci., 13 (2007) 349–355.
16. D. Kumar, L. Kumar, S. Nagar, C. Raina, R. Parshad, V.K. Gupta, Screening, isolation and production of lipase/esterase producing *Bacillus* sp. strain DVL2 and its potential evaluation in esterification and resolution reactions, Arch. Appl. Sci. Res., 4 (2012) 1763–1770.
17. E. Sirisha, N. Rajasekar, M.L. Narasu, Isolation and optimization of lipase producing bacteria from oil contaminated soils, Adv. sin Biol. Res., 4 (2010) 249–252.
18. M.Y. a. Samad, C.N. a. Razak, A.B. Salleh, W.M. Zin Wan Yunus, K. Ampon, and M. Basri, A plate assay for primary screening of lipase activity, J. Microbiol. Meth., 9 (1989) 51–56.
19. D.G. Hatzinikolaou, J.B. Macris, P. Christakopoulos, D. Kekos, F.N. Kolisis, G. Fountoukidis, Production and partial characterisation of extracellular lipase from *Aspergillus niger*, Biotechnol. Lett. 18 (1996) 547–552.
20. A. Sugihara, T. Tani, Y. Tominaga, Purification and characterization of a novel thermostable lipase from *Bacillus* sp., J. Biochem., 109 (1991) 211–216.
21. U. Açıkel and M. Erşan, Acid phosphatase production by *Rhizopus delemar*: a role played in the Ni(II) bioaccumulation process, J. Hazardous Materials, 184 (2010) 1-3.
22. S. Kumar, K. Kikon, A. Upadhyay, S.S. Kanwar, R. Gupta, Production, purification, and characterization of lipase from thermophilic and alkaliphilic *Bacillus coagulans* BTS-3, Protein Expr. Purif., 41 (2005) 38–44.
23. L. Toscano, G. Montero, L. Cervantes, M. Stoytcheva, V. Gochev, and M. Beltrán, Production and partial characterization of extracellular lipase from *Trichoderma harzianum* by solid-state fermentation, Biotechnol. Biotechnol. Equip., 27 (2013)3776–3781

Cytotoxic Effects of Thiazolo[3,2-C]Pyrimidines Against Mcf-7 And Hepg2/C3a Carcinoma Cell Lines

Tiyazolo[3,2-C]Pirimidinlerin Mcf-7 ve Hepg2/C3a Kanser Hücre Hatlarına Karşı Sitotoksik Etkileri

Research Article

Arzu Birinci Yıldırım[1], Esra Mutlu[2], Muhammet Yıldırım[3]*

[1]Department of Field Crops, Faculty of Agriculture and Natural Sciences, Abant İzzet Baysal University, Bolu, Turkey.
[2]Scientific Industrial and Technological Application and Research Center, Abant İzzet Baysal University, Bolu, Turkey.
[3]Department of Chemistry, Faculty of Sciences and Arts, Abant İzzet Baysal University, Bolu, Turkey.

ABSTRACT

In the present study, a series of thiazolo[3,2-c]pyrimidines (4,5) have been produced via simple and efficient synthetic method and their in vitro cytotoxicities have been performed on human breast (MCF-7) and hepatocellular (HEPG2/C3A) adenocarcinoma cell lines. The results of these in vitro tests revealed that at least five of thiazolo[3,2-c]pyrimidines exhibited strong cytotoxic effects at very low concentrations, which were very similar or lower than that of reference anticancer agent, 5-FU, against MCF-7 and HEPG2/C3A cancer cell lines.

Key Words
Anticancer, breast cancer, Mannich cyclisation, thiazolopyrimidines.

ÖZ

Çalışmamızda, yeni tiyazolo[3,2-c]pirimidinlerin (4,5) bir serisi, basit ve etkili bir yöntemle hazırlandı ve bu bileşiklerin in vitro sitotoksisiteleri insan meme (MCF-7) ve karaciğer (HEPG2/C3A) kanser hücre hatları üzerinde çalışıldı. In vitro çalışma sonuçları, tiyazolo[3,2-c]pirimidinlerin en az 5 tanesinin düşük derişimlerde MCF-7 ve HEPG2/C3A kanser hücre hatlarına karşı kuvvetli sitotoksik etki gösterdiğini ortaya koymaktadır ki bu etki kullanılan referans antitümör ajanın, 5-FU, etkisiyle aynı veya daha düşüktür.

Anahtar Kelimeler
Antikanser, meme kanseri, Mannich halkalaşması, tiyazolopirimidinler.

Article History: Received: Nov 21, 2017; Revised: Dec 08, 2017; Accepted: Feb 16, 2018; Available Online: Mar 26, 2018.

DOI: 10.15671/HJBC.2018.232

Correspondence to: M. Yıldırım, Dept. of Chemistry, Faculty of Sciences and Arts, Abant İzzet Baysal University, Bolu, Turkey .
Tel: +90 374 254 1000-1260 Fax: +90 374 253 46 42 E-Mail: muhammetyildirim@ibu.edu.tr

INTRODUCTION

The active agents used for cancer therapy have not been diversified too much overtime. Although in last decades, great efforts have been performed for the preparation of more precise and smart synthetic ones, which may bring a new hope for cancer patients during chemotherapy and diagnosis phases [1]. The popular active agents such as doxorubicin (DOX), camptothecin, paclitaxel (or docetaxel), 5-fluorouracil (5-FU) have been widely used with broad spectrum of antitumor effects since 1960s [1-3]. They exhibit anticancer effects by various mechanisms such as breaking the strands of DNA double helix, interfering with the religation of DNA and interrupting the feeding and proliferation of cancer cells by division [2,4-7].

Over many years, aforementioned anticancer agents (paclitaxel, docetaxel, camptothecin, doxorubicin) have been used for cancer treatments, but their higher dose toxicities, side effects, and also, the difficulties originated from their multistep preparations sometimes diminished their use as cancer therapeutics [8-10]. Thereof, the development of new molecules, which are able to do much stronger apoptosis and have less toxic effects with much simpler synthetic methodologies, have gain much more importance recently.

Among the well-known anticancer drugs, 5-fluorouracil (5-FU) is a cancer antimetabolite and structurally similar to thiazolopyrimidines which consisted of a thiazole and a pyrimidine ring. Thiazolopyrimidines are known to display many important biological properties such as antimicrobial, antipsychotic, anti-inflammatory, antiparkinson, antidepressant and anti-HIV, especially anticancer activities [11-13].

Today, three main classes of thiazolopyrimidines are known to exist in chemical literature [14] and two of the main structural classes; thiazolo[4,5-d]pyrimidines and thiazolo[3,2-a]pyrimidines, have been extensively utilized in many types of cytotoxic activity studies. Besides, a diverse range of anticancer or antitumor thiazolopyrimidines in these two main classes have been identified due to their strong cytotoxic effects against various carcinoma cell lines such as HepG-2 (liver), PC-3 (prostate), HCT-116 (colon), A549 (lung), A431 (epidermal), T98G (glioblastoma), HL-60 (leukemia), SF-268 (CNS) and MCF-7(breast) [15-20]. For instance, some new thiazolo[3,2-a]pyrimidines have been developed as CDC25 phosphatase inhibitors and have displayed very strong cytotoxicity against HeLa cells at very low concentrations [21]. In another antitumor study of newly developed pyrrolothiazolo- and triazolopyrrolo-[3,2-a]pyrimidinones, good cyctotoxic effects have been obtained against ascite tumor cells in mice [22]. In 2015, Yahya et al. found that the arylidenethiazolo[3,2-a]pyrimidinones exhibited strong cytotoxic effects at very low concentrations against breast tumor cell lines [18]. In a more recent study, new pyridothiazolo[3,2-a] pyrimidines have been evaluated in vitro against HepG-2, PC-3 and HCT-116 cancer cell lines and some halogenated thiazolo[3,2-a]pyrimidines have been found to exhibit cytotoxic effects on HCT-116 cancer cell lines [19].

In similar fashion, many different cytotoxicity studies of thiazolo[4,5-d]pyrimidines have been carried out against a variety of cancer cell lines. For instance, in the study of Lin and co-workers (2009), some 2,7-diaminothiazolo[4,5-d] pyrimidines have been evaluated to determine their potency, selectivity and bioavailability as EGFR kinase inhibitors [16]. Three of the derivatives exhibited antiproliferative activity on human ovarian adenocarcinoma (SK-OV-3) cells at very low micromolar concentrations. Also, in the recent work of Singh et al. (2013), new 2-amino-7-chlorothiazolo[4,5-d]pyrimidines have been screened against lung (NCI-H322 and A549), epidermal (A431), glioblastoma (T98G), pancreatic (MIAPaCa-2), prostate (PC-3), human leukemia (HL-60) and breast (T47D) cell lines[17]. One molecule exhibited antiproliferative activity against lung (NCI-H322 and A549), epidermal (A431), glioblastoma (T98G) cells at relatively low concentrations and two molecules were very cytotoxic against lung (A549) and human leukemia (HL-60) cell lines.

Thiazolo[3,2-c]pyrimidines, being the last main class of thiazolopyrimidines, are very

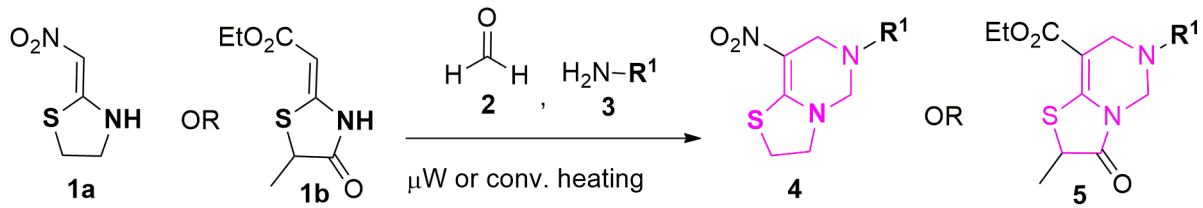

Figure 1. General method for preparation of thiazolo[3,2-c]pyrimidines (4a-d,5a-k).

new derivatives and unstudied in the sense that no cytotoxicity study is present in the literature. With this in mind, very recently, a series of nitrothiazolo[3,2-c]pyrimidines (4) and oxothiazolo[3,2-c]pyrimidine carboxylates (5) have been produced via simple and efficient methods resulting in excellent yields by our group for the first time[14,23]. Whereupon, in the present work, successive in vitro cytotoxic activity studies of thiazolo[3,2-c]pyrimidines (4, 5) at varying concentrations have been performed against human breast (MCF-7) and hepatocellular (HEPG2/C3A) adenocarcinoma cell lines. The results of in vitro tests revealed that mostly the oxothiazolo[3,2-c]pyrimidine carboxylates (5) exhibited better cytotoxic effects than nitrothiazolo[3,2-c]pyrimidines (4) against both MCF-7 and HEPG2/C3A carcinoma cell lines.

MATERIALS and METHODS

Chemicals and Equipments

All the necessary reagents, chemicals and the solvents were purchased in analytical and reagent grades (Merck, Sigma-Aldrich). Reactions were monitored with precoated TLC plates (Merck 5735) and column chromatography were performed for purifications of title compounds by using silica gel 60 (Merck 109385). Starting materials, 2-(nitromethylene)thiazolidine (1a) and (Z)-ethyl 2-(5-methyl-4-oxothiazolidin-2-ylidene) acetate (1b), were prepared and characterized according to reported methods [14,24].

Preparation of Thiazolo[3,2-c]pyrimidines (4a-d, 5a-k). [14,25,23]

General method: One equivalent amount of 2-(nitromethylene)thiazolidine, (1a) or (Z)-ethyl 2-(5-methyl-4-oxothiazolidin-2-ylidene)acetate (1b) and primary amine (3) were dissolved in acetonitrile (or water), then, two equivalents of formaldehyde (2) was added dropwise and resulting mixture was refluxed (or irradiated in a microwave reactor) under inert atmosphere until reaction completion in 3-4 h (or 3-4 min) (Figure 1). After work-up, final products (4 or 5) were purified by flash column chromatography on silica gel or recrystallization from suitable solvents and obtained in excellent yields. ^{1}H-NMR and ^{13}C-NMR spectral data confirmed the structures of title compounds, 4a-d and 5a-k [14,23,25].

In Vitro Cytotoxic Activity Studies of Thiazolo[3,2-c]pyrimidines

Cell Preparation and Culturing

Human breast (MCF-7) and hepatocellular (HEPG2/C3A) adenocarcinoma cell lines were obtained from Abant İzzet Baysal University, Faculty of Medicine, Department of Pharmacology. The cells were maintained in Dulbecco's modified eagle's medium (DMEM, Invitrogen) containing 10% fetal bovine serum (FBS) and 100 ng/ml of penicillin and streptomycin (Sigma). Cells were allowed to grow in tissue culture flasks and were kept in a CO_2 incubator at 37°C in a humidified atmosphere of 5% CO_2 and 95% air.

Cell Viability with MTT Assay [26]

The MTT assay is based on the reduction of yellow 3-(4,5-dimethylthiazol-2-yl)-2,5-diphenyl tetrazolium bromide (MTT) to purple formazan in living cells which corresponds to the activity of mitochondria and this color change is subsequently measured at 570 nm. For the assay, about 1x10^4 viable cells in 100 μl of culture medium (DMEM) were added to each well in of a 96-well cell culture plate. The plates were allowed to incubate for 16 hours at 37°C under 5% CO_2 in a humidified incubator allowing the cells to attach the 96-well cell culture plates. After the cell attachment was checked, the cells were treated with serial concentrations of thiazolo[3,2-c] pyrimidine compounds (4,5) and then incubated for 24-72 h [26].

Thiazolo[3,2-c]pyrimidines were initially dissolved in 0.5% DMSO by adjusting the concentration of the compounds to 500, 300, 200, 100, 10, 1 μM. Likewise, 5-fluorouracil (5-FU) concentrations were adjusted to 500, 300, 200, 100, 10, 1 μM in 0.5% DMSO. The plates were incubated for 24, 48 and 72 h. After incubation periods, the culture medium was removed and replaced with 90 μL of fresh culture medium (DMEM). Then, 10 μL of MTT solution (5 mg/ml) in phosphate buffered saline (PBS, pH 7.4) was added to each well and the final concentration of MTT of 0.5 mg/L which was allowed to incubate at 37°C, in a 5% CO_2 humidified incubator for 4 h. After 4 h incubation, 100 μL/well of DMSO were added to all samples for dissolving the formazan that is the final product of MTT reaction and were allowed to incubate at 37°C, in a 5% CO_2 humidified incubator for overnight. After incubation, absorbance of formazan was measured spectrophotometrically in a Multiskan FC microplate photometer reader at 570 nm. Each experiment was carried out in triplicate. 0.5% DMSO and PBS was used as negative control groups. The percent cytotoxicities of thiazolo[3,2-c]pyrimidines (% cell viability) were calculated according to their control groups as;

% cell viability = 100 × A570 nm (sample) / A570 nm (control)

All data were analyzed by ANOVA with the last factor as a within subject or repeated design using SPSS version 15 (SPSS Inc., Chicago, IL, USA). Values were considered statistically significant at $p \leq 0.05$. The data were presented as mean ± standard error (SE) after back transforming from ANOVA results. IC_{50} of the compounds were determined by plotting triplicate data points over a concentration range and calculating values using regression analysis of SPSS program.

RESULTS and DISCUSSION

Preparation of Thiazolo[3,2-c]pyrimidines (4, 5)

Synthesis of thiazolo[3,2-c]pyrimidines (4 or 5) were performed via three-component reaction of enamines 1a, 1b with corresponding primary aryl or alkyl amines (3) and formaldehyde (2) as described in material and method part. The structures of purified compounds 4 and 5 given in Figure 2 were characterized by ^{1}H- and ^{13}C-nuclear magnetic reasonance (NMR) and high-resolution mass (HR-MS) analyses. Spectroscopic data of title compounds 4 and 5 were consistent with the literature data.[14,23].

MTT Assay with Thiazolo[3,2-c]pyrimidines against MCF-7 and HEPG2/C3A Cell lines

As reported in literature, thiazolopyrimidine-based compounds exhibited good cytotoxic effects against various human carcinoma cell lines [16,17,18,19,22](Abdel-Latif, Sabry et al. 2007). In the present study, we were interested to find out whether thiazolo[3,2-c]pyrimidines (4,5) would exhibit similar and stronger cytotoxic effects against human breast and hepatocellular adenocarcinoma cell lines as much as the

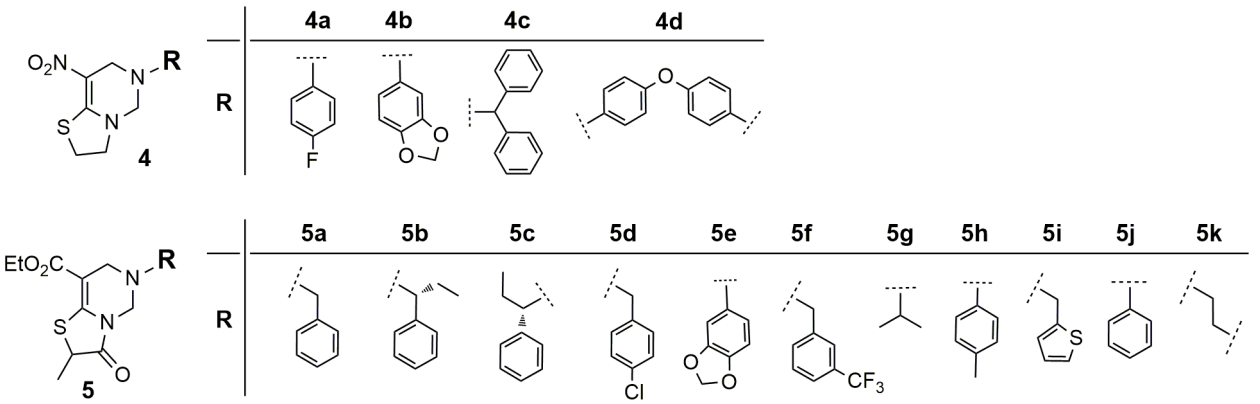

Figure 2. Prepared thiazolo[3,2-c]pyrimidines (4a-d, 5a-k) for cytotoxicity studies.

derivatives which belong to two other main classes of thiazolopyrimidines. Thus, fifteen thiazolo[3,2-c]pyrimidines (4a-d, 5a-k) along with 5-FU (reference anticancer agent) were investigated through different concentrations (1, 10, 100 μM) for their cytotoxic effects against MCF-7 cancer cell line in a 72 h cell viability test. Three different concentrations of thiazolo[3,2-c] pyrimidines were adjusted in 0.5% DMSO to a final concentration of 1,10,100 μM prior to determine their cytotoxic effects. Cytotoxicities of the compounds were calculated according to percentage viability of MCF-7 cells in 0.5% DMSO after 72 h. 0.5% DMSO was also used as the negative control and 5-FU was used as positive control due to its structural similarity to thiazolo[3,2-c]pyrimidines. According to the results of 72 h cell viability test, at 100 μM concentration, five of thiazolo[3,2-c]pyrimidines (4d, 5d, 5f, 5h, 5j) containing meta-, para-subtituted phenyl and benzyl groups was found to exhibit the strong to moderate cytotoxic effects against MCF-7 cells when compared to reference antitumor agent (5-FU) (Table 1, Figure 3). At 10 μM concentration level, compound 4d (p-oxyphenyl substituted) exhibited the best but the moderate cytotoxic effect and compound 4b (3,4-methylenedioxyphenyl substituted) exhibited similar cytotoxicity as that of reference anticancer agent (5-FU) against MCF-7 cell lines. Hovewer, at 1 μM concentration level, there were no significant difference between cell viability test results of the compounds and antitumor agent, 5-FU. The results of 72 h cell viability test showed that three derivatives, 5j (phenyl substituted), 5f (3-CF_3-benzyl substituted), 5d (p-Cl-benzyl substituted) exhibited the strongest and two derivatives 4d (p-oxyphenyl substituted), 5h (p-methylphenyl substituted) exhibited less strong cytotoxic effects against MCF-7 cell lines (Table 1).

Table 1. Cytotoxic effects of thiazolo[3,2-c]pyrimidines against MCF-7 Cell Lines for 72 h.

Treatments	% Cell Viability[a]		
	1 μM	10 μM	100 μM
4a	103.14±2.31	93.79±2.31	77.02±4.99
4b	91.98±4.87	85.77±4.36	65.16±4.06
4c	110.86±0.28	97.96±0.40	95.30±4.52
4d	100.99±3.30	66.71±3.53	52.97±3.99
5a	110.95±8.20	107.95±4.63	72.47±2.73
5b	111.67±4.07	108.50±1.89	84.95±2.63
5c	114.63±1.41	113.66±4.93	70.95±4.36
5d	116.30±2.89	110.61±3.46	49.77±2.10
5e	113.57±1.91	108.71±7.20	61.48±3.39
5f	116.83±6.43	99.79±6.12	46.98±2.48
5g	97.73±2.44	91.66±7.86	87.24±2.12
5h	92.33±5.33	91.48±8.80	57.45±5.33
5i	102.33±4.33	97.77±4.64	67.20±1.11
5j	102.94±8.44	103.45±4.41	45.75±0.80
5k	114.71±3.94	109.23±9.98	65.18±2.26
5-FU	108.16±8.24	85.48±5.31	47.65±5.46

[a] Mean values (±standard deviation) for triplicate assays.

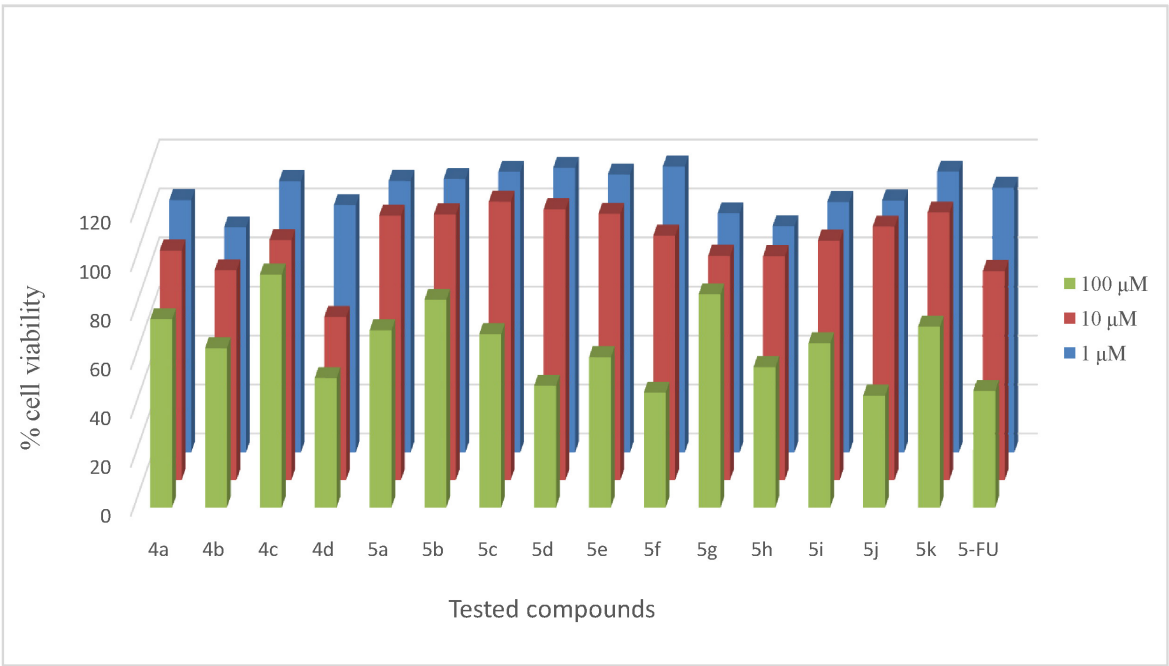

Figure 3. Cytotoxic activities of thiazolo[3,2-c]pyrimidines against MCF-7 Cell lines in 72 h.

Table 2. Cytotoxic effects of thiazolo[3,2-c]pyrimidines against MCF-7 Cell Lines for 24 h.

Treatment	% Cell Viability[a]					
	500 µM	300 µM	200 µM	100 µM	10 µM	1 µM
5d	64.25±3.48	73.42±6.99	87.33±0.84	98.44±0.21	109.55±3.39	92.80±6.44
5f	52.54±3.18	60.52±2.26	82.15±2.35	96.31±7.39	87.38±6.74	122.39±7.77
5j	75.36±2.71	86.60±0.21	96.88±0.07	109.99±4.80	112.17±7.54	111.67±5.65

[a] Mean values (±standard deviation) for triplicate assays.

As a toxicity parameter, IC_{50} values of 5d, 5f, 5j derivatives that show %50 inhibition of cell proliferation and of 5-FU were calculated. They corresponded to 99µM, 94µM and 92µM, respectively (Table 4). Calculated IC_{50} value of 5-FU (85 µM) complies with its other published literature data against human breast cancer cell lines (MCF-7) [27-32]. Twelve other derivatives (4a-c, 5a-c, 5e, 5g-i, 5k) showed moderate to weak cytotoxic activities (53-87% cell viability) (Table 1) and so, their IC_{50} values were obtained higher than 100µM which were not very significant results for this test.

A further cytotoxicity study in different concentrations (1, 10, 100, 200, 300, 500 µM) of the most cytotoxic compounds (5d, 5f, 5j), which were found at 100µM concentration in 72 h viability test, was performed aganist MCF-7 cell lines for 24 and 48 h. The aim of 24 or 48 h cell viability tests were to reveal whether the tested compounds may exhibit much stronger or weaker cytotoxicities at lower concentrations in shorter time periods. As it is expected, all tested compounds exhibited moderate cytotoxic effects against MCF-7 cell lines only at higher concentrations (>300 µM) in 24 h test. Unfortunately, all tested compounds did not provide significant cytotoxic effects at concentrations lower than 100 µM in 24 h (Table 2). Since percentage cell viabilities of the tested compounds were not under %50 at all concentrations, IC_{50} values of the compounds (5d, 5f, 5j) were considered over 500µM in 24 h test (Table 2,4). Besides, the results of 48 h cell viability test were meaningless and inconsistent within each other, so their data were not presented, and

also the IC_{50} values of the compounds were not considered for this test.

Lastly, three most cytotoxic compounds (5j, 5f, 5d) and 5-FU through different concentrations (1, 10, 100, 200, 300, 500 μM) were investigated for their cytotoxicities against HEPG2/C3A cancer cell lines in 24 , 48 and 72 h cell viability tests. In 24 h cell viability test, significant cytotoxic effects were only observed for the compounds 5d (p-Cl-benzyl substituted) and 5f (3-CF_3-benzyl substituted) at higher concentrations (>300 μM) (Table 3, 24 h treatment). However, in 48 h cell viability test, only the compound 5d (p-Cl-benzyl substituted) showed moderately strong cytotoxic effect at 100 μM concentration against HEPG2/C3A cell lines. In addition, the compounds 5d and 5f exhibited much stronger cytotoxic effects at higher concentrations (300, 500 μM) when compared to the effect of compound 5j (phenyl substituted). Nevertheless, cytotoxic effect of compounds at higher concentrations are not considered as significant effects against cancer cell lines. The compound 5j (phenyl substituted) showed moderate to weak cytotoxicities against HEPG2/C3A cell lines at all concentrations. In 72 h test, two compounds 5d (p-Cl-benzyl substituted), 5f (3-CF_3-benzyl substituted) exhibited strong cytotoxic effects against HEPG2/C3A cell lines at 100μM concentration levels, but the cytotoxic effect of compound 5j (phenyl substituted) was moderate (Table 3, 72 h treatment). At 10 and 1 μM concentration levels, cytotoxic effects of compounds 5d (p-Cl-benzyl substituted) and 5f (3-CF_3-benzyl substituted) have changed from moderate to strong against HEPG2/C3A cell lines and the cell viabilities were obtained as 60-61% for 5d (p-Cl-benzyl substituted) and 55-59% for 5f (3-CF_3-benzyl substituted) (Table 3, 72-hour treatment).

Since the percentage cell viabilities of compound 5d (p-Cl-benzyl substituted) decreased to %47 only at 200 μM in 48-hour test and to %49 at 100 μM in 72 h test, the IC_{50} values (128.9 μM and 34.6 μM) of the compound 5d were calculated for these tests (Table 4). However, the percentage cell viabilities of the compounds 5j (phenyl substituted) and 5f (3-CF_3-benzyl substituted) for 24 and 72 h tests and of the compound 5d for 24 h test did not decrease under %50 at concentrations lower than 200 μM (Table 3). Therefore, IC_{50} values of the compounds 5j, 5f and 5d were considered over 500 μM for the specified tests. Similarly, the IC_{50} values of the compounds 5f and 5j were found at higher concentrations (186 μM and 370 μM) for 48 h viability test against HEPG2/C3A cell lines (Table 4).

Table 3. Cytotoxic effects of thiazolo[3,2-c]pyrimidines against HEPG2/C3A Cell Lines for 24-72 h.

Treatments		% Cell Viability[a]					
		500 μM	300 μM	200 μM	100 μM	10 μM	1 μM
24 h	5d	56.25±3.18	57.61±3.32	70.02±0.42	77.40±1.55	89.15±0.63	99.66±0.35
	5f	53.02±1.41	54.59±2.68	60.45±1.23	94.85±0.28	109.84±0.42	104.59±3.60
	5j	66.87±0.82	92.28±1.06	95.53±0.84	100.11±4.31	95.19±2.47	100.34±2.89
48 h	5d	26.16±0.36	32.72±0.56	47.33±0.56	56.32±5.16	88.39±2.54	96.02±4.17
	5f	23.96±3.39	31.41±0.98	57.23±0.76	81.15±0.35	82.83±0.42	104.82±0.63
	5j	36.33±3.47	59.02±4.78	78.67±6.67	80.64±0.98	80.06±0.14	93.64±3.67
72 h	5d	28.32±2.48	38.52±5.32	48.84±3.25	49.36±1.13	61.82±3.86	60.36±1.14
	5f	56.15±2.47	63.71±4.31	52.85±2.76	53.74±5.55	59.42±0.63	55.72±1.13
	5j	68.16±3.29	79.02±5.58	89.85±7.21	65.52±0.05	67.15±0.63	72.83±7.56

[a] Mean values (±standard deviation) for triplicate assays.

Table 4. Calculated IC_{50} value of compounds 5d, 5f, 5j and 5-FU against MCF-7 and HEPG2/C3A cell lines.

		IC_{50}±SEM (μM)		
	Treatments	24 h	48 h	72 h
HEPG2\C3A	5-FU	n.t.	n.t.	85.1 ± 4.4
	5d	> 500	> 500	99.7±4.6
	5f	> 500	> 500	94.2±4.6
	5j	> 500	> 500	92.6±4.5
MCF-7	5d	> 500	128.9±4.9	34.6±3.5
	5f	> 500	186.3±5.2	> 500
	5j	> 500	370.9±5.9	> 500

n.t: no treatment. IC_{50}: Concentration of extract that cause 50% inhibition of cell proliferation.

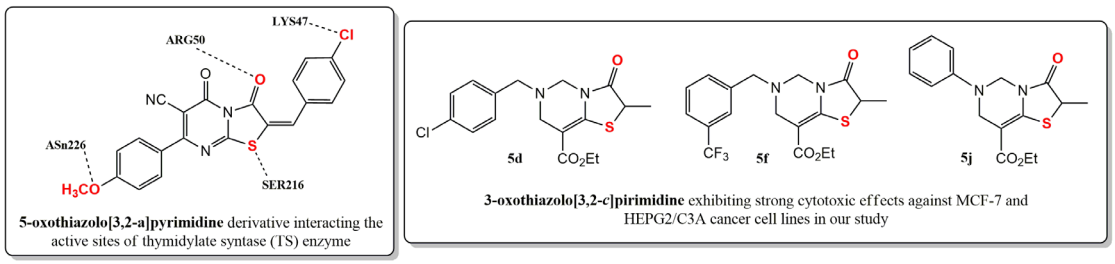

Figure 4. 5-oxothiazolo[3,2-a]pyrimidine interacting with the active sites of TS enzyme over 4 hydrogen bonding and title compounds 5d, 5f, 5j exhibiting strong cytotoxic effect in our work.

According to the cell viability test results of nitrothiazolo[3,2-c]pyrimidines (4) against MCF-7 cancer cell lines, only the compound 4d exhibited significant cytotoxic effect (53% at 100 μM) and this activity may be attributed to the bis(methyleneoxyphenyl) group in the molecule. However, oxothiazolo[3,2-c]pyrimidines (5) showed better cytotoxic effects against both MCF-7 and HEPG2/C3A carcinoma cell lines at lower concentrations. The promising results obtained may be attributed to para-chlorobenzyl- and meta-trifluoromethylbenzyl-substitutions on 6-position of thiazolo[3,2-c]pyrimidine derivatives 5d (50%) and 5f (47%) at 100 μM, respectively. And also, p-methylphenyl- and phenyl-substituted derivatives (5h,57% and 5j,46% at 100 μM) exhibited strong cytotoxic effects. Alkyl substitution or some other aryl substituted benzyl and phenyl groups in compounds 4 and 5 did not result in any significant activity other than moderate or weak, and sometimes, proliferative effects were also observed.

In a very recent cytotoxicity study of 5-oxothiazolo[3,2-a]pyrimidines, stronger cytotoxic effects were obtained against MCF-7 and HEPG2 cancer cell lines as compared to reference anticancer agent, 5-FU. Since 5-FU is in similar structure to thiazolopyrimidines and it stopped DNA synthesis by inhibiting thymidylate synthase (TS) enzyme, the binding affinities of the most cytotoxic 5-oxothiazolo[3,2-a] pyrimidine and 5-FU were investigated to enzyme active sites by molecular docking. Hydrogen bonding interactions of S atom in thiazolidinone ring with aminoacid Ser216 residue and of O atom with aminoacid Arg50 residue were identified with other two interactions [36]. Regarding the interactions of 5-oxothiazolo[3,2-a]pyrimidine found by docking studies and its structural similarity to the compound 5d (para-chlorophenyl substitution) in our study, the reason why strong cytotoxic effects were obtained against MCF-7 and HEPG2 cell lines in our work can be explained (Figure 4).

In other recent studies supporting our findings, p-methoxy- or dimethoxy-phenyl subtituted thiazolopyrimidine analogues showed moderate cytotoxic acitivities against HEPG2 and MCF-7 cell lines [33]. Similarly, p-MeO, p-Cl-phenyl substituted arylthiazolopyrimidines displayed very strong cytotoxic effects against MCF-7 cell lines [16]. In addition, phenylsulfonamido-substituted thiazolo[3,2-a]pyrimidines demonstrated very significant antitumor activities against colon cancer-HT-29, human liver-HEPG2 and MCF-7 cell lines at very low concentrations [34]. Also, some aryl and benzyl substituted 2-thioxothiazolo[4,5-d]pyrimidinones were found to be significantly active against lung-NCI-H-460, breast-MCF-7 and CNS-SF-268 cancer cell lines [35].

CONCLUSIONS

The current cytotoxicity study contains some novel findings. We believe that this work provides the first, most current and up-to-date cytotoxicity data (concentration, IC_{50} etc.) regarding 6-aryl or benzyl substituted thiazolo[3,2-c]pyrimidines, particularly on human breast and hepatocellular carcinoma cell lines, since there was no biological activity, in particular antiproliferative or cytotoxic activity, of thiazolo[3,2-c]pyrimidines reported before the current cytotoxicity study of title compounds (4,5). Besides, this study clearly explains the cytotoxic effects of thiazolo[3,2-c] pyrimidines against MCF-7 and HEPG2/C3A cell lines on time-dependent manner (24-, 48- and 72-hour). Further studies on the preparation of more specific thiazolo[3,2-c]pyrimidines, their molecular docking, in vivo and drug targeting research studies are underway in collaboration with other laboratories.

ACKNOWLEDGEMENTS

The financial supports of Abant Izzet Baysal University, BAP Commission (BAP grant no. 2013.03.03.600 and BAP grant no. 2017.03.03.1218) and TUBITAK (Turkish Scientific and Technological Research Council) (grant no. 113Z012) are gratefully acknowledged.

References

1. D. Peer, J.M. Karp, S. Hong, O.C. Farokhzad, R. Margalit, R. Langer, Nanocarriers as an emerging platform for cancer therapy, Nat. Nanotechnol., 2 (2007) 751-760.
2. F. Arcamone, Doxorubicin: anticancer antibiotics, (2012) Elsevier, New York, NY, USA.
3. A. Nagy, P. Armatis, A.V. Schally, High yield conversion of doxorubicin to 2-pyrrolinodoxorubicin, an analog 500-1000 times more potent: structure-activity relationship of daunosamine-modified derivatives of doxorubicin, Proceedings of the National Academy of Sciences, 93 (1996) 2464-2469.
4. G. Rodriguez-Berna, M.J.D. Cabañas, V. Mangas-Sanjuán, M. Gonzalez-Alvarez, I. Gonzalez-Alvarez, I. Abasolo, S. Schwartz Jr, M. Bermejo, A. Corma, Semisynthesis, Cytotoxic Activity, and Oral Availability of New Lipophilic 9-Substituted Camptothecin Derivatives, ACS Med. Chem. Lett., 4 (2013) 651-655.
5. M.C. Wani, H.L. Taylor, M.E. Wall, P. Coggon, A.T. McPhail, Plant antitumor agents. VI. Isolation and structure of taxol, a novel antileukemic and antitumor agent from Taxus brevifolia, J. Am. Chem. Soc., 93 (1971) 2325-2327.
6. P.B. Schiff, J. Fant, S.B. Horwitz, Promotion of microtubule assembly in vitro by taxol, Nature, 277 (1979) 665-667.
7. D.B. Longley, D.P. Harkin, P.G. Johnston, 5-fluorouracil: mechanisms of action and clinical strategies, Nature reviews. Cancer, 3 (2003) 330-338.
8. B. Shi, B. Yaremko, G. Hajian, G. Terracina, W.R. Bishop, M. Liu, L.L. Nielsen, The farnesyl protein transferase inhibitor SCH66336 synergizes with taxanes in vitro and enhances their antitumor activity in vivo, Cancer Chemoth. Pharm., 46 (2000) 387-393.
9. O. Cuvillier, V. Nava, S. Murthy, L. Edsall, T. Levade, S. Milstien, S. Spiegel, Sphingosine generation, cytochrome C release, and activation of caspase-7 in doxorubicin-induced apoptosis of MCF7 breast adenocarcinoma cells, Cell Death. Differ., 8 (2001) 162-171.
10. F.W. Symmans, Breast cancer response to paclitaxel in vivo, Drug Resist. Update, 4 (2001) 297-302.
11. J. Wichmann, G. Adam, S. Kolczewski, V. Mutel, T. Woltering, Structure-activity relationships of substituted 5H-thiazolo[3,2-a]pyrimidines as group 2 metabotropic glutamate receptor antagonists, Bioorg. Med. Chem. Lett., 9 (1999) 1573-157.
12. F.A. Al-Omary, G.S. Hassan, S.M. El-Messery, H.I. El-Subbagh, Substituted thiazoles V. Synthesis and antitumor activity of novel thiazolo[2,3-b]quinazoline and pyrido[4,3-d] thiazolo[3,2-a] pyrimidine analogues, Eur. J. Med. Chem., 47 (2012) 65-72.
13. S. Fatima, A. Sharma, R. Saxena, R. Tripathi, S.K. Shukla, S.K. Pandey, R. Tripathi, R.P. Tripathi, One pot efficient diversity oriented synthesis of polyfunctional styryl thiazolopyrimidines and their bio-evaluation as antimalarial and anti-HIV agents, Eur. J. Med. Chem., 55 (2012) 195-204.
14. M. Yıldırım, D. Çelikel,Y. Dürüst, D.W. Knight, B.M. Kariuki, A rapid and efficient protocol for the synthesis of novel nitrothiazolo[3,2-c]pyrimidines via microwave-mediated Mannich cyclisation, Tetrahedron, 70 (2014) 2122-2128.

15. E. Flefel, M. Salama, M. El-Shahat, M. El-Hashash, A. El-Farargy, A novel synthesis of some new pyrimidine and thiazolopyrimidine derivatives for anticancer evaluation, Phosphorus Sulfur., 182 (2007) 1739-1756.
16. R. Lin, S.G. Johnson, P.J. Connolly, S.K. Wetter, E. Binnun, T.V. Hughes, W.V. Murray, N.B. Pandey, S.J. Moreno-Mazza, M. Adams, Synthesis and evaluation of 2,7-diamino-thiazolo[4,5-d]pyrimidine analogues as anti-tumor epidermal growth factor receptor (EGFR) tyrosine kinase inhibitors, Bioorg. Med. Chem. Lett., 19 (2009) 2333-2337.
17. B. Singh, S.K. Guru, S. Kour, S.K. Jain, R. Sharma, P.R. Sharma, S.K. Singh, S. Bhushan, S.B. Bharate, R.A. Vishwakarma, Synthesis, antiproliferative and apoptosis-inducing activity of thiazolo[5,4-d] pyrimidines, Eur. J. Med. Chem., 70 (2013) 864-874.
18. T.A.A. Yahya, J.H. Abdullah, M.A.H. Al-Ghorafi, S.H. Yassin, H.M. Almahbshi, Synthesis of some arylidene derivatives of thiazolopyrimidineas anticancer, Der Pharma Chemica, 7 (2015) 106-110.
19. N.A. Abdel-Hafez, S.F. Mohamed, F.A. El-Hag, U.W. Hawas, H.M. Awad, Synthesis and Cytotoxicity Evaluation of Some New Pyrimidinethione and Thiazolopyrimidine Derivatives Linked to N-Propylpiperidone, Der Pharma Chemica, 8 (2016) 57-66.
20. B. Kuppast, H. Fahmy, Thiazolo[4,5-d]pyrimidines as a privileged scaffold in drug discovery, Eur.J. Med. Chem., 113 (2016) 198-213.
21. S. Kolb, O. Mondésert, M.L. Goddard, D. Jullien, B.O. Villoutreix, B. Ducommun, C. Garbay, E. Braud, Development of novel thiazolopyrimidines as CDC25B phosphatase inhibitors, ChemMedChem, 4 (2009) 633-648.
22. A.A. Abu-Hashem, M.M. Youssef, H.A. Hussein, Synthesis, antioxidant, antituomer activities of some new thiazolopyrimidines, pyrrolothiazolopyrimidines and triazolo pyrrolothiazolopyrimidines derivatives, J.Chil. Chem. Soc., 58 (2011) 41-48.
23. M. Yıldırım, D. Çelikel, A rapid access to novel and diverse 3-oxothiazolo[3,2-c]pyrimidine-8-carboxylates using multicomponent Mannich cyclisation reactions, Mol. Divers., 19 (2015) 1-13.
24. M. Stojanović, R. Marković, E. Kleinpeter, M. Baranac-Stojanović, endo-Mode cyclizations of vinylogous N-acyliminium ions as a route to the synthesis of condensed thiazolidines, Tetrahedron, 67 (2011) 9541-9554.
25. D. Çelikel, Synthesis of new thiazolopyrimidine, thiazolo(imidazolo) pyridinone derivatives via multicomponent reactions M.Sc. Master Thesis, (2015) Abant İzzet Baysal University, Bolu,Turkey.
26. F.P. Karakas, A.B. Yildirim, R. Bayram, M.Z. Yavuz, A. Gepdiremen, A.U. Turker, Antiproliferative activity of some medicinal plants on human breast and hepatocellular carcinoma cell lines and their phenolic contents, Trop. J. Pharm. Res., 14 (2015) 1787-1795.
27. M.M. Kamel, H.I. Ali, M.M. Anwar, N.A. Mohamed, A.M. Soliman, Synthesis, antitumor activity and molecular docking study of novel sulfonamide-Schiff's bases, thiazolidinones, benzothiazinones and their C-nucleoside derivatives, Eur. J. Med. Chem., 45 (2010) 572-580.
28. X. Liu, W. Wei, S. Huang, S-S. Lin, X. Zhang, C. Zhang, Y. Du, G. Ma, M. Li, S. Mann, Bio-inspired protein-gold nanoconstruct with core–void–shell structure: beyond a chemo drug carrier, J. Mater. Chem. B., 1 (2013) 3136-3143.
29. G.S. Hassan, Synthesis and antitumor activity of certain new thiazolo[2,3-b]quinazoline and thiazolo[3,2-a] pyrimidine analogs, Med. Chem. Res., 23 (2014) 388-401.
30. L. Shen, J. Hu, H. Wang, A. Wang, Y. Lai, Y. Kang, Synthesis and biological evaluation of novel uracil and 5-fluorouracil-1-yl acetic acid-colchicine conjugate, Chem. Res. Chinese. U., 31(2015) 367-371.
31. P.N. Le, N.H. Nguyen, C.K. Nguyen, N.Q. Tran, Smart dendrimer-based nanogel for enhancing 5-fluorouracil loading efficiency against MCF7 cancer cell growth, B. Mater. Sci., 39 (2016) 1493-1500.
32. J.M. Gichumbi, B. Omondi, G. Lazarus, M. Singh, N. Shaikh, H.Y. Chenia, H.B. Friedrich, Influence of Halogen Substitution in the Ligand Sphere on the Antitumor and Antibacterial Activity of Halfć sandwich Ruthenium (II) Complexes [RuX(ć6ć6arene) (C5H4N2ćCH=Nć Ar)]+, Z. Anorg. Allg. Chem., 643 (2017) 699-711.
33. I.M. Abbas, S.M. Gomha, M.M. Elaasser, B.K. Mabrouk, Synthesis and characterisation of some novel fused thiazolo[3,2-a]pyrimidinones and pyrimido[2,1-b][1,3] thiazinones, J. Chem. Res., 39 (2015) 719-723.
34. S. Awad, O. Fathalla, J. Wietrzyk, M. Milczarek, A. Soliman, M.S. Mohamed, Synthesis of new pyrimidine derivatives and their antiproliferative activity against selected human cancer cell lines, Res. Chem. Intermediat., 41 (2015) 1789-1801.
35. S.M. Rida, S.A. El-Hawash, H.T. Fahmy, A.A. Hazza, M.M. El-Meligy, Synthesis and in vitro evaluation of some novel benzofuran derivatives as potential anti-HIV-1, anticancer, and antimicrobial agents, Arch. Pharm. Res., 29 (2006) 16-25.
36. M.M. Mohamed, A.K. Khalil, E.M. Abbass, A.M. El-Naggar, Design, Synthesis of New Pyrimidine Derivatives as Anticancer and Antimicrobial Agents, Synthetic Commun., 47 (2017) 1441-1457.

Characterization of Local *Trichoderma* spp. as Potential Bio-Control Agents, Screening of in vitro Antagonistic Activities and Fungicide Tolerance

Potansiyel Biyokontrol Ajanları Olarak Yerel *Trichoderma* spp. Türlerinin Karakterizasyonu, in vitro Antagonistik Aktivitelerinin ve Fungisit Toleransların İncelenmesi

Research Article

Sengul Alpay Karaoglu*, Arif Bozdeveci, Necla Pehlivan*
Recep Tayyip Erdogan University, Deparment of Biology, Rize, Turkey.

ABSTRACT

Enlightening effects of biocontrol agents as *Trichoderma* spp. to provide disease control by combating pathogens is an important alternative in agricultural crop production. To that end, 9 species of Hypocrea/ Trichoderma having green ascospores isolated from the soil that tea plants cultivated in are identified by ITS sequences and were found to be close relative of *Trichoderma* sect. Pachybasium (77%). Ethyl acetate extracts of fungal isolates exhibited the antimicrobial activity against to *Vibrio* sp, *Serratia marcescens*, *Mycobacterium smegmatis* and *Bacillus cereus* but no antifungal activity was detected. The highest level of inhibitory activity was observed against to *M. smegmatis* by *Trichoderma* harzianum ID4A, ID4B and ID6B. In dual culture test, all *Trichoderma* strains were found to be showing the highest inhibitory activity against to the plant pathogens *Botrytis cinerea*, *Sclerotonia sclerotiorum* and *Rhizoctonia solani* (AG3), but relatively low activity against to the entomopathogen fungi. Volatile metabolites of *Trichoderma* spp. caused maximum reduction in mycelial growth and sclerotial production. Tested strains showed the highest tolerance to the fungicide Dikozin, whereas the lowest tolerance was against to the Captan regardless of the dosage.

Key Words
Trichoderma, bio-control agent, Antimicrobial activity, Fungicide.

ÖZ

Trichoderma spp. gibi biyokontrol ajanlarının etkilerini incelemek tarımsal üretimde patojenlerle mücadele yoluyla hastalık kontrolünü sağlamada önemli bir alternatiftir. Bu amaçla, çay bitkilerinin topraklarından izole edilmiş yeşil askosporlara sahip 9 Hypocrea/ *Trichoderma* türü, ITS sekansları ile tanımlanmış ve türlerin % 77 oranında *Trichoderma* sect. *Pachybasium* ile yakın akraba olduğu belirlenmiştir. Fungal izolatların etil asetat ekstraktlarının, *Vibrio* sp., *Serratia marcescens*, *Mycobacterium smegmatis* ve *Bacillus cereus*'a karşı antimikrobiyal aktivite sergilediği tespit edilmesine karşın, izolatlarda antifungal aktivite gözlenmemiştir. En yüksek inhibisyon aktivitesinin, *Trichoderma harzianum* ID4A, ID4B ve ID6B tarafından *M. smegmatis*'e karşı oluşturulduğu ortaya çıkarılmıştır. Çift kültür testinde, tüm *Trichoderma* suşlarının *Botrytis cinerea*, *Sclerotonia sclerotiorum* ve *Rhizoctonia solani* (AG3) bitki patojenlerine karşı en yüksek inhibitör aktivite gösterdiği, fakat entomopatojen mantarlara karşı nispeten düşük etkide oldukları bulunmuştur. *Trichoderma* spp. uçucu metabolitleri, misel artışı ve sklerotik üretimde maksimum azalmaya neden olmuştur. Test edilen suşların, dozajdan bağımsız olarak en yüksek toleransı Dikozin fungisitine karşı, en düşük toleransı ise; Captan'a karşı gösterdiği belirlenmiştir.

Anahtar Kelimeler
Trichoderma, biyokontrol ajanı,antimikrobiyal aktivite, fungisit.

Article History: Received: Sep 11, 2017; Oct 18: XX, 2017; Accepted: Jan 11, 2018; Available Online: Mar 26, 2018.

DOI: 10.15671/HJBC.2018.233

Correspondence to: N. Pehlivan, Sengul Alpay Karaoglu, Recep Tayyip Erdogan University, Deparment of Biology, Rize, Turkey.
Tel: +90 464 2236126-1839 Fax: +90 464 2235376 E-Mail: neclapehlivan@hotmail.com

INTRODUCTION

Trichoderma is one of the most common fungal biocontrol agents in agriculture for the management of plant diseases caused by an extensive spectrum of fungal pathogens [1]. Some studies showed that several strain of *Trichoderma* had significant remedial effect on plant diseases caused by pathogens such as B*otrytis cinerea Fusarium oxysporum, F. culmorum, F. moniliforme, Sclerotium rolfsii, Sclerotium sclerotonia, Rhizoctonia solani* and *Aspergillus flavus* [2].

Trichoderma spp. are primarily present in all agricultural soils including decaying wood. In the past studies, nine species were distinguished based on the morphological features according to Rifai [3]. This first classification has been considered preliminary, since some aggregates formed among morphologically indistinguishable species and have made identification harder [4]. Consistent results have been obtained through the sequence analyses of ITS1, ITS2, and of genes such as β-tubulin and hydrophobin or all combined [5]. Major mechanism involved in the biocontrol activity of *Trichoderma* spp. is the ability of competition for space and nutrients in the rhizosphere flora, production of diffusible and/or volatile antibiotics, prevention of abiotic stresses such as salt, heat and drought and finally mycoparasitism [6].

Trichodermin was a secondary metabolite isolated from the fermented broth of *T. harzianum* and showed antifungal activity against mycelial growth of phytopathogenic fungi, such as *Botrytis cinerea*. In contrast to other fungi, T*richoderma* spp. has been reported to have limited applications in biocontrol of pathogenic bacteria [7]. In addition, it has been reported that *Trichoderma* spp. is able to produce antibacterial compounds that act against human-pathogenic bacteria such as *E. coli, S. aerus, K. pneumoniae* [8].

The combined use of biocontrol agents and chemical pesticides has attracted much attention by either farmers or producers in order to obtain synergestic or additive effects in the control of soilborne diseases up to now [9]. *Trichoderma* spp. strains with greater biocontrol efficiency also have better tolerance against to pesticides to be used as major component in Integrated Pest Management (IPM). To date, fungicides and insecticides are extensively used by farmers to control insects, pests and diseases in agro-economically important crops such as cotton, rice, maize and tomato [10], however agriculture needs to be sustained by more cleaner and safer processes to pursue an eco-friendly approach. In this manner, identifying biocontrol agents and understanding the mechanisms underlying the antagonistic effects of *Trichoderma* spp. especially on plant pathogens are important in creating effective and safe bio-control strategies.

In the present study, we aimed to determine the physical properties of strains with molecular characterization and their culture effect and the biocontrol potential. In this regard, *Trichoderma* spp. isolated from the soil which indigenous tea plants cultivated in İkizdere, Rize, Turkey identified with molecular tools and the capabilities of strains such as sporulation properties under different growth temperatures, heat tolerance, antibacterial and antifungal activities and fungicide tolerance were examined.

MATERIAL and METHODS

Culture Medium and Inoculum Development

Trichoderma spp. strains formerly isolated from the indigenous tea cultivation area in Rize province of Turkey were used in this study [11]. Strains were stored in Recep Tayyip Erdogan University, Microbiology and Molecular Biology Laboratory culture collection unit for further use. Control strain *T. harzianum* KUENS 1585 was purchased by the Simbiyotek Company in Istanbul. *Trichoderma* spp. strains were grown on Potato Dextrose Agar (PDA) (Merck, Germany) for 7 days. *Hyphae* and spores gained from pure cultures were transfered into 500 mL flasks containing 100 mL of Malt Extract Broth and were shaken at 150 rpm in a rotary shaker (GFL, Germany) at 28 °C for 10 days. *Mycelia* were harvested by filtration, washed with distilled water and powdered in liquid nitrogen.

DNA Extraction and PCR Amplification of Fungi

Genomic DNA extraction was carried out using DNeasy Plant Mini Kit (Qiagen, Hilden, Germany). Primers ITS4 and ITS5 described by Kanematsu and Naito [12] were used to amplify the 5.8S

rDNA gene with the ITS-1 and ITS-2 regions. PCR amplification of ITS1-5.8S-ITS2 genes of fungal isolates were performed with universal primers of ITS5 (5′ -GGAAGTAAAAGTCGTAACAAGG-3′) as forward primer and ITS4 (5′ -TCCTCCGCTTATTGATATGC-3′) as reverse primer [13]. PCR amplifications were established in a total volume of 50 μL. The components of reaction were 5 μL 10×Taq-DNA polymerase buffer, 200 μM of dNTPs, 0.05 nmol of the primer pairs, 2.5 unit Taq-DNA polymerase (Fermentase), and 0.05 μg genomic DNA. After the primary denaturation at 95 °C for 5 min, 95 °C for 1 min, 55 °C for 55 s, 72 °C for 2 min, with an extension step at 72 °C for 10 min were operated with thirty-five cycles in thermocycler (Eppendorf, Germany). Separated PCR products on 1% agarose gel, visualized with ethidium bromide and photographed under UV light.

Characterisation of physical properties

Studies were performed based on the effects of temperature on the sporulation and mycelial growth. Optimum temperature for growth [14] and effect on volatile metabolite production of *Trichoderma* spp. strains were also investigated according to Keszler et al. [15]. Effect of temperatures (15-32°C) on the linear hyphal growth of *Trichoderma* spp. strains were studied in vitro on PDA medium in 9 cm Petri plates for each temperature. A bit (5 mm) of pure culture of *Trichoderma* spp. strains were placed at the center of Petri plates, replicated thrice with the help of sterile cork borer. The inoculated Petri plates were kept at 15, 20, 24, 28 and 32°C in the incubator and daily observation on mycelial growth of *Trichoderma* spp. strains were recorded at every 24 hrs up to 15 days. Radial development after the first 48 h culture was taken into account. On the 4th, 7th and 15th days of fungi cultures, the number of spores was determined. Spore suspensions were prepared by adding 15 ml of sterile distilled water to mature (7th and 15th days) fungal colonies on PDA plates to dislodge the spores from the mycelium. The spores were counted using a heamocytometer (Neubauer, Germany) as mentioned before [14].

A 1x107 cfu mL^{-1} spore suspension was prepared to determine the tolerance of *Trichoderma* spp. spores to different temperatures. The spor suspension was distributed to ependorfs (1 mL) and each ependorf was exposed to heat in a heater for 15 min at 45, 55, 65 and 75 ° C. Subsequently, 100 μL was added to the surface of the DRBC agar and spreading was carried out by baguette. Incubation was allowed for 3 days at 28 ° C [22].

In vitro Antagonistic Activity Assays

In vitro antagonistic activities were tested against to plant (*Sclerotonia sclerotiorum*, *Rhizoctonia solani* (AG3), *Botrytis cinerea*), human (*Aspergillus flavus*, *Aspergillus niger* RSKK4017) and insect pathogens (*Beauveria bassiana* ARSEF 8664, *Isaria fumosorosea* ARSEF 8333, *Metarhizium anisopliae* ARSEF 8433). All fungi were revived and cultured on PDA at 28±1 °C for seven days. The antagonistic activity of *Trichoderma* spp. strains were tested in vitro using 85 mm petri dishes containing 20 mL of PDA medium with pH 5.5. Mycelial discs (5 mm in diameter) of *S. sclerotium, R. solani, B. cinerea, A. flavus* and *A. niger* were placed on one edge of a petri dish containing PDA, while mycelial discs of *Trichoderma* spp. strains were placed on the opposite edge of the plate. Control petries consisted of the individual cultures of the pathogen. Each dual culture (pathogen–antagonist) had three replicates under 28±1 °C. After 4, 7 and 14 days, the plates were evaluated for antagonistic activity of the strains, considering the ability of the microorganisms to reduce pathogen colony expansion. The equation for the percentage inhibition of radial growth (PIRG) applied as below:

$$\%PIRG = \frac{R_1 - R_2}{R_1} x100 \quad (1)$$

PIRG = Percentage inhibition of radial growth;
R1 = Radial growth of control;
R2 = Radial growth of *Trichoderma* spp. in the presence of the antagonist

The production of volatile compounds from *Trichoderma* spp. were determined as follows; two Petri dishes containing PDA were individually inoculated with a disc of S. sclerotium and *Trichoderma* spp. and bottom parts were adjusted and attached by tape. The control sets did not contain the *Trichoderma* spp. The plates were randomized and incubated at 28±2°C for 7 days.

The diameters of *Sclerotonia sclerotium* colony cultures were measured daily. Three replicate plates were set for each treatment [16].

Antimicrobial Activity Tests

Trichoderma spp. were cultivated and maintained on slants of PDA media for 7 days at 28±1 °C. Conidia were scrapped from mycelia which grown on slants and cultivated on potato dextrose broth (PDB) media. Conidial densities in the suspension were determined by using the hemocytometer under a light microscope. Fungal inoculum (1×10^7 spore/mL) of each strain was prepared by blending PDA-grown cultures of the fungus with sterile distilled water for 14 days. A spore suspension of each strain was 10^7 spores inoculated in 250 mL flasks containing 50 mL of PDB incubated for 21 days at 28±1 °C [17]. Fermentation broth was filtered and extracted by 50 mL 100% ethyl acetate, agitated for 60 min and then centrifuged at 1500 g for 30 min. After separating two phases, organic phase was collected and dried at 40 °C under vacuum using a rotary evaporator. Extracts were dissolved in 1 mL of DMSO which was then used to screen for their antimicrobial activity by agar diffusion assay method.

All test microorganisms except for plant pathogen fungi obtained from Abant Izzet Baysal and Gaziosmanpasa University were obtained from the Hifzisihha Institute of Refik Saydam (Ankara, Turkey). The antimicrobial activities were evaluated against eight selected gram negative bacteria; *Escherichia coli* ATCC25922, *Klebsiella pneumonia* ATCC13883, *Pseudomonas aeruginosa* ATCC43288, *Yersinia pseudotuberculosis* ATCC911, five Gram positive bacteria; *Bacillus cereus* 709 ROMA, *Staphylococcus aureus* ATCC25923, *Enterococcus faecalis* ATCC29212, *Bacillus subtilis* ATCC6633, *Listeria monocytogenes* ATCC43251, an acid-fast bacterium; *Mycobacterium smegmatis* ATCC607, yeast like fungi; *Candida albicans* ATCC60193, *Candida tropicalis* ATCC13803 and *Saccharomyces cerevisiae* RSKK 251, two plant pathogenic fungi; *Botryts cinerea*, *Rhizoctonia solani* AG3 and a saprofit fungus; *Aspergillus niger* RSKK4017. *Salmonella* sp., *Proteus vulgaris*, *Vibrio* sp. and *Serratia marcescens* were clinically isolated strains.

Simple susceptibility screening test via agar-well diffusion method was used. Each bacterium was suspended in Mueller Hinton (MH) (Difco, Detroit, MI) broth, whereas target fungi were suspended in the yeast extract broth. The microorganisms were diluted approximately to 10^6 cfu mL^{-1} with the aid of the McFarland 0.5 standard All fungi species were cultivated on PDA and M. smegmatis was cultivated on Brain Heart Infusion Agar (BHIA) (Difco, Detriot, MI). Those were flood-inoculated onto the surface of MHA, BHIA and PDA and then air-dried. Five-milimeter diameter wells were created from the agar cutting with a sterile cork-borer and 50 μL of the *Trichoderma* spp. extracts were placed into the wells. Plates that consist bacteria incubated for 24-48 h at 35°C, whereas the fungi plates were incubated for 3-5 days at 28 °C. *M. smegmatis* was grown for 3 days on BHIA plates at 35 °C [18]. Antimicrobial activity was evaluated by measuring inhibition zone against to the target microorganism. Streptomycin (10 μg), ampicillin (10 μg) and fluconazole (5 μg) were standard drugs used in the experiment. Ethyl acetate and dimethyl sulfoxide were used as negative control.

Assay of Fungucide Tolerance

Fungicides used by farmers extensively were selected to assess their effect on the growth of the *Trichoderma* spp. isolates. To that end, *Trichoderma* spp. isolates were exposed to three fungicides; Captan, Dikozin and Cuprenax. Three different fungicides Dikozin (75% Mancozeb), Captan (Captan M 50 WP) and Cuprenax (Cupper oxychloride) were added to PDA medium with a final concentration of 2.5, 5.0 and 10.0 mg mL^{-1}. A mycelial block in 5 mm diameter from one week of *Trichoderma* spp. culture was cut and placed into the center of the plates. After 7 days, *Trichoderma* spp. mycelial radial growth zone were measured [19]. Calculations were conducted based on the formula for the percentage inhibition of radial growth (PIRG) in duplicate.

RESULTS and DISCUSSION

The identification were performed based on the macroscopic and microscopic properties of nine *Trichoderma* spp. strains formerly isolated from the soil which tea plants cultivated in 100-1000 meter high. A commercial strain was tested for its properties as control (*T. harzianum* KUEN 1585). Isolates of *Trichoderma* spp. were characterized based on their 700 bp fragment of the ITS1-5.8S-

Table 1. Examined *Hypocrea* and *Trichoderma* spp. isolates and GenBank accession numbers of target sequences.

Strain no	Species	Similarity	
(%)	ITS 1- 5.8- ITS2		
Gen Bank. No			
ID4A	*Hypocrea lixii* BHU 221	100%	JN604833.1
	Trichoderma harzianum A12	99%	KC139308.1
	Hypocrea lixii BHU18	99%	JN604835.1
	Hypocrea lixii BHU110	99%	JN604836.1
	Hypocrea lixii BHU226	99%	JN604834.1
ID4B	*T. harzianum* NBAII-Th13	99%	JX644593.1
	Trichoderma harzianum T12	99%	KC609759.1
	Trichoderma harzianum IBSD-T142	99%	JX518931.1
	Trichoderma harzianum IBSD-T47	99%	JX518904.1
	Trichoderma harzianum IBSD-T11	99%	JX518894.1
ID6B	*Trichoderma harzianum* FUE15	99%	KC200074.1
	Trichoderma harzianum T65-NI	99%	U78881.1
	Hypocrea lixii BHU51	99%	JN618343.1
	Hypocrea lixii BHU159	99%	JN618342.1
	Hypocrea lixii BHU166	99%	JN618339.1
ID7C	*Trichoderma harzianum* NR6929	98%	AF194011.1
	Trichoderma harzianum 2930	98%	AJ224016.1
	Trichoderma harzianum A14	98%	KC139307.1
	Hypocrea lixii ATCC 20847	98%	FJ545255.1
	Hypocrea lixii IB32E1	98%	FN598939.1

ITS2 gene. According to the cluster analysis based on the ITS sequence of the genomic rRNA gene of 10 potential biocontrol agents, most *Trichoderma* spp. isolates were found to be very similar to *Trichoderma* sect. *Pachybasium* (77%), whereas the others were similar to *Trichoderma* sect. *Trichoderma* spp. section (Table 1). Three groups of similar isolates were identified by cluster analysis. Seven isolates were found identical to *T. harzianum*, one isolate to ID17E of *T. hamatum* and one to ID20G *T. atroviride*. According to the sequencing data, seven strains were found similar to *T. harzianum* (99%), one strain is to *T. hamatum* (94%) and a strain is to *T. atroviride* (97%).

Factors in determining the survivals of certain fungi on natural environment are important. One of these factors is the growing ability at different temperatures. Growth properties of *Trichoderma* spp. strains at different temperatures (2,4,10,15, 20, 24, 28, 32, 37 and 42 °C) were investigated and no growth was observed on the strains at 2 to 10 °C. In addition to that, increasing the temperature above 37-42 °C inhibited mycelial growth (Table

Table 1. Examined *Hypocrea* and *Trichoderma* spp. isolates and GenBank accession numbers of target sequences (continue).

ID9A	*Trichoderma aureoviride* T77	100%	HQ596945.1
	Trichoderma aureoviride T59	100%	HQ596942.1
	Hypocrea lixii JBSERB241	100%	EF191311.1
	Hypocrea lixii NMMX3008	99%	JQ040357.1
	Trichoderma harzianum GJS 05-93	99%	FJ442645.1
ID11C	*Hypocrea lixii* DAOM 222136	100%	JN942884.1
	Trichoderma citrinoviride T200	99%	HQ596983.1
	Hypocrea lixii DAOM 229959	99%	AY605733.1
	Trichoderma harzianum TR040	99%	AF443925.1
	Trichoderma harzianum GJS 92-61	99%	HQ608080.1
ID11D	*Hypocrea lixii* GJS 04-227	100%	FJ442266.1
	Hypocrea lixii GJS 91-138	100%	AF443917.1
	Hypocrea lixii DAOM231402	99%	AY605732.1
	Hypocrea lixii JBT1244	99%	AY605741.1
	Trichoderma harzianum P134	99%	JF311950.1
ID17E	*T. hamatum* HBJZ1001	94%	JQ040347.1
	T. hamatum CQJB2001	94%	JQ040344.1
	T. hamatum T090	94%	HQ608116.1
	T. hamatum DAOM237553	94%	EU280136.1
	T. hamatum GHJ-5	94%	GQ331987.1
ID20G	*Trichoderma atroviride* DR19	97%	KC311841.1
	Trichoderma atroviride EGE-K-65	97%	JX119037.1
	Trichoderma atroviride ATCC20476	97%	JQ745258.1
	Trichoderma atroviride T39	97%	FJ975597.1
	Trichoderma atroviride KUC5026	97%	GQ241294.1
T.h1585	*Hypocrea lixii* T 22	99%	GU570562.1
	Hypocrea lixii BHU199	99%	JN618342.1
	Hypocrea lixii BHU162	99%	JN604838.1
	Hypocrea lixii DLY1202	99%	HQ259304.1
	Hypocrea lixii T18-1	99%	EU744189.1

2). However, it was observed that it maintains the viability of the *Trichoderma* spp. spores. Increasing temperature from 15 to 24°C led to an increase on the growth rates of *Trichoderma*, followed by a plateau. Optimum temperature for mycelial growth was observed between 24 and 28 °C. Strains ID11C and ID11D were found to show the highest growth characteristics in all tested temperatures (from 4 to 32 °C). In contrast, it was noted that ID7C strains exhibited the lowest growth level.

Temperature is considered as one of the most important parameters of biocontrol activity of *Trichoderma* spp [10]. In biocontrol organisms, the presences of tolerance against to temperature fluctuations are important parameters for the maintainability of life of the organism in extreme environments. The common incubation temperature for fungi growth such as *Trichoderma* sp., *Fusarium* sp., *Penicillium* sp. and *Graphium* sp. is 30°C [20]. and researchers also reported that none of the *Trichoderma* species grew at or above 40°C. Therefore it could be concluded that time and incubation temperature were two effective criteria on the sporulation [14]. Some isolated *Trichoderma* strains from the higher altitude (2000-3500 m) of Garhwal Himalayan region in India presented similar results with previous reports [21]. In this study, *Trichoderma* spp. strains were revealed to exhibit the ideal growth at 24 °C and 28°C, however, the maximum temperature for *Trichoderma* spp. growth was examined at 32 °C when incubated on Tryptic Soy Agar under 4 °C conditions. The fungus was able to grow normally, characterized with heavily induced sporulation within three weeks of the incubation. Induction of sporulation via exposure to low temperatures appeared to be one of the strategies for survival of these species in extreme cold environments such as at 4 to 5 °C.

Trichoderma spp. spores were found to show heat tolerance at a certain range of temperature values (45-75°C) after 10 min exposure (Table 2). In the heat tolerance test of this study , although all strains of *Trichoderma* spp. were detected to be able to germinate spores at the range of 45 to 65°C, only three strains (ID11D, ID4A and ID4B) were observed to be able to protect the vitality of spores at 75 °C. Kucuk and Kivanc [22] indicated that 6 strains out of 7 isolates germinated at 75°C. This result indicated that *Trichoderma* spp. spores are heat-tolerant for a certain period of time at a range of 45 to 75°C. As *Trichoderma* spp. is well accepted being a potential and ecofriendly biological control agent by the community, it is necessary to grow it at suitable conditions before it could be used against to other soil borne plant pathogens or for commercial purposes. In this regard, heat tolerance of *Trichoderma* spp. spores is very important to maintain the viability during storage and after formulation processes.

Table 2. Radial growth of *Trichoderma* spp. at different temperatures on PDA medium for 48 hours and heat tolerance of fungi spores (cfu/mL).

Strain No	Incubation of temperature (°C) and radial growth (cm)					Heat (°C) tolerance of spore (10 min)			
	15	20	24	28	32	45	55	65	75
ID4A	3.5	4.2	7.5	7.3	2.0	$\geq 10^3$	$\geq 10^3$	$\geq 10^3$	2×10^2
ID4B	2.5	3.7	5.2	6.0	2.0	$\geq 10^3$	$\geq 10^3$	$\geq 10^3$	3×10^2
ID6B	3.7	4.1	6.2	7.0	2.0	$\geq 10^3$	$\geq 10^3$	$\geq 10^3$	-*
ID7C	3.5	4.5	5.5	4.0	1.5	$\geq 10^3$	$\geq 10^3$	$\geq 10^3$	-
ID9A	3.5	4.2	6.8	7.0	2.0	$\geq 10^3$	$\geq 10^3$	$\geq 10^3$	-
ID11C	4.0	5.1	7.0	9.0	3.5	$\geq 10^3$	$\geq 10^3$	$\geq 10^3$	-
ID11D	4.0	5.3	8.5	9.0	3.5	$\geq 10^3$	$\geq 10^3$	$\geq 10^3$	10^2
ID17E	4.0	5.1	5.5	7.0	3.0	$\geq 10^3$	$\geq 10^3$	$\geq 10^3$	-
ID20G	3.9	5.5	8.5	6.0	3.0	$\geq 10^3$	$\geq 10^3$	$\geq 10^3$	-
KUEN 1585	3.5	3.0	8.0	6.0	3.0	$\geq 10^3$	$\geq 10^3$	$\geq 10^3$	-

Since optimization of the bio-control agents has vital importance, the best growth temperature and sporulation time were determined for the isolated strains in present work. The strain ID17E was found to have some growth parameters like commercial strain KUEN 1585 and no generated spore was detected under test conditions (Table 3). The highest number of spore was obtained from the strains ID9A, ID11C and ID11D at 28°C on day15, sporulation capacity of the strains were marked similar at 15, 20 and 24°C however, 28°C was significantly different in terms of strain's sporulation ability. The best incubation time and temperature was determined on day 15 at 28°C for *Trichoderma* spp. strains.

It is notorious notion that *Trichoderma* spp. species are effective against various gram positive and negative bacterial species [17]. In the present study, we analyzed that whether our isolated strains have anti-microbial activity or not. Ethyl acetate extract of *Trichoderma* spp. isolates were found to display antibacterial activity but not antifungal activity (Table 4). All extracts were detected to show antibacterial activity against *Vibrio* sp., S. *marcescens*, L. *monocytogenes*, *B. cereus* and *B. subtilis* except for ID17E and ID20G. The ID17E extract was observed to effective against to human pathogen *S. aureus* and the other strains' (ID4A, ID4B and ID6B) extracts were effective for *M. smegmatis* a causative agent of tuberculosis. These results indicate that the exercised strains are effective against bacterial plant pathogens. It was shown that *T. harzianum* and *T. atroviride* have produced some kind of antibiotics by other studies

Table 3. Spore production of *Trichoderma* spp. at different time intervals and in different temperatures (cfu/mL).

Strain No	Days	Incubation Temperatures and viable spores/mL			
		15°C	20°C	24°C	28°C
ID4A	7	-*	8.60×10^{7}	1.79×10^{8}	3.01×10^{8}
	15	1.81×10^{7}	2.73×10^{8}	2.78×10^{8}	5.73×10^{8}
ID4B	7	-	1.00×10^{8}	1.22×10^{8}	1.95×10^{8}
	15	2.53×10^{7}	2.63×10^{8}	1.63×10^{8}	3.59×10^{8}
ID6B	7	-	3.91×10^{7}	1.70×10^{8}	7.53×10^{7}
	15	2.31×10^{7}	2.06×10^{8}	3.65×10^{8}	6.78×10^{8}
ID7C	7	-	6.00×10^{7}	4.30×10^{6}	8.50×10^{8}
	15	2.75×10^{7}	6.10×10^{8}	1.20×10^{8}	3.20×10^{8}
ID9A	7	-	1.30×10^{8}	2.49×10^{8}	3.28×10^{8}
	15	2.13×10^{7}	1.81×10^{8}	5.77×10^{8}	3.36×10^{9}
ID11C	7	-	2.32×10^{8}	5.60×10^{6}	1.10×10^{8}
	15	1.63×10^{7}	6.10×10^{8}	6.50×10^{8}	7.70×10^{8}
ID11D	7	-	3.41×10^{8}	2.01×10^{8}	3.59×10^{8}
	15	1.63×10^{8}	4.06×10^{8}	4.53×10^{8}	5.37×10^{8}
ID17E	7	-	-	-	-
	15	-	-	-	-
ID20G	7	-	2.68×10^{8}	1.76×10^{8}	2.95×10^{8}
	15	1.41×10^{7}	2.82×10^{8}	1.41×10^{8}	2.94×10^{7}
KUEN 1585	7	-	-	1.78×10^{7}	1.26×10^{7}
	15	4.06×10^{6}	4.94×10^{6}	5.03×10^{7}	2.43×10^{8}

*- No growth

Table 4. Inhibition zone (mm) of *Trichoderma* spp. fermentation broth extracts against some microorganisms.

	ID4A	ID4B	ID6B	ID7C	ID9A	ID11C	ID11D	ID17E	ID20G	KUEN 1585	ET.AS.	DMSO	Ant.
Ec	-	-	-	-	-	-	-	-	-	-	-	-	10
Pv	-	-	-	-	-	-	-	-	-	-	-	-	18
Ss	-	-	-	-	-	-	-	-	-	-	-	-	18
Vs	12	12	10	10	10	11	10	6	7	8	8	-	10
Sm	12	12	11	10	10	11	10	-	6	7	7	-	10
Kp	-	-	-	-	-	-	-	-	-	-	-	-	18
Yp	-	-	-	-	-	-	-	-	-	-	-	-	18
Pa	-	-	-	-	-	-	-	-	-	-	-	-	18
Sa	-	-	6	-	-	-	6	15	-	-	-	-	35
Ef	-	-	-	-	-	-	-	-	-	-	-	-	10
Lm	8	7	6,5	-	6	6	6	-	6	6	-	-	10
Bc	10	9	6	-	6	7	6	7	-	-	-	-	15
Bs	8	7	-	-	6	6	-	9	-	-	-	-	20
Ca	-	-	-	-	-	-	-	-	-	-	-	-	25*
Ct	-	-	-	-	-	-	-	-	-	-	-	-	25*
Sc	-	-	-	-	-	-	-	-	-	-	-	-	>25*
Ms	17	14	10	-	-	-	-	-	-	-	8	6	35**
An	-	-	-	-	-	-	-	-	-	-	-	-	ND
Bcin	-	-	-	-	-	-	-	-	-	-	-	-	ND
Rs	-	-	-	-	-	-	-	-	-	-	-	-	ND

Ec: E. coli ATCC25922, *Pv: P. vulgaris*, *Ss: Salmonella sp.*, *Vs: Vibrio sp.*, *Sm: S. marcescens*, *Kp: K. pneumonia* ATCC13883, *Yp: Y. pseudotuberculosis* ATCC 911, *Pa: P. aeruginosa* ATCC43288, *Sa: S. aureus* ATCC25923, *Ef: E. faecalis* ATCC29212, *Lm: L. monocytogenes* ATCC43251, *Bc: B. cereus* 709 ROMA, *Bs: B. subtilis* ATCC6633, *Ca: C. albicans* ATCC60193, *Ct: C. tropicalis* ATCC13803, *Sc: S. cerevisiae* RSKK251, *Ms: M. smegmatis* ATCC607, *An: A. niger* RSKK4017, *Bcin: B. cinerea*, *Rs: R. solani* AG3, (-); no effect, , KUEN 1585*; T. harzianum* KUEN 1585, ET.AS: Ethyl acetate, DMSO: Dimethyl sulfoxide, Ant.: Antibiotics, ND: Not determined, *: fluconazole **: Streptomycin.

[15]. When *T. harzianum* strains analyzed for their antagonistic activity, the isolates were found to be effective at various concentrations against to many bacterial species (*S. aureus*, *E. coli*, *Proteus* and *Klebsiella*) [23]. On the other hand, antimicrobial activities of 317 Basidiomycetes isolates were screened against nine human pathogens and the most susceptible micro-organism were reported as *B. subtilis* [24], which is very identical to our results. Tarus et al. [25] demonstrated that *T. harzianum* secondary metabolites (i.e. trisol, 6-phenyl prion and sorbicilin) were effective against to pathogen fungi of tea plants (*Armillaria mella, Mucor* and *Nematospora corylii*). That compounds (especially 6-phenyl prion) were found to be effective against an array of microorganisms (*Paecilomyces vericoti*, *Penicilium notatum*, *Nematospora coryli*, *Bacillus brevis*, *B. subtilis*, *Sercinia lutea* and *Enterobacter dissolvens*) with either their antibacterial and or antifungal activities. Liouane et al. [26] were reported that the analysed extract exhibited an intriguing antibacterial activity against to all tested bacteria except for the gram-negative *E. coli* and *P. aeruginosa*, but no antifungal activity was detected for the extracts. In our study, *T. harzianum* was found to show very high antagonistic activity against *A. terreus and A. fumigatus*. Clinical bacterial isolates of *S. aureus* and *E. coli* were found to be sensitive to *T. harzianum* extract.

Table 5. Effect of *Trichoderma* spp. at day 4, 7 and 15 on in-vitro growth inhibition of some fungi through Dual Plate Culture Technique.

Strains No	Growth range inhibition some of fungi (%)								
	Days	Rs	Bcin	Ssc	An	Af	Bb	If	Ma
ID4A	4	30	49	67	23	8	29	2	9
	7	70	61	70	73	17	62	25	26
	15	64	59	69	73	50	83	51	59
ID4B	4	1	48	58	8	0	3	0	3
	7	33	58	58	72	14	33	20	33
	15	63	56	58	77	52	63	46	63
ID6B	4	16	57	64	8	4	3	1	3
	7	56	61	68	71	20	35	23	35
	15	64	62	69	74	52	63	50	63
ID7C	4	23	56	68	0	8	6	2	6
	7	54	61	71	68	27	41	25	41
	15	64	78	72	71	58	68	50	68
ID9A	4	15	56	61	15	13	12	1	12
	7	40	62	67	77	33	44	32	44
	15	67	78	68	77	60	68	55	68
ID11C	4	59	66	66	8	17	17	14	17
	7	70	68	75	73	43	45	36	45
	15	75	78	75	72	66	70	64	70
ID11D	4	55	73	71	23	17	13	8	13
	7	68	81	75	74	37	47	36	47
	15	69	83	78	74	66	70	64	70
ID17E	4	45	68	72	26	13	17	2	17
	7	68	71	74	71	37	56	34	56
	15	77	70	76	72	62	77	64	77
ID20G	4	39	69	68	15	17	12	11	12
	7	67	74	76	76	47	55	39	55
	15	75	78	79	78	68	76	66	76
KUEN 1585	4	25	58	66	8	8	11	2	11
	7	58	63	69	70	24	46	30	46
	15	71	57	69	71	58	70	50	70

Rs: R. solani (AG3), Bcin: B. cinerea, Sc: S. sclerotiorum, As: A. flavus, An: A. niger, Bb: B. bassiana ARSEF8664, Is: I. fumosorosea ARSEF8333, Ma: M. anisopliae ARSEF8433.

In dual culture test, isolates of *Trichoderma* spp. showed variable effects against to other tested fungi. All *Trichoderma* spp. strains have high inhibition activities against plant pathogen strain *B. cinerea, S. sclerotiorum* and *R. solani* (AG3) (Table 5). *Trichoderma* spp. showed inhibition on tested fungi with a significant difference. There was not significant difference between day 7th and 15th (mean rank 26.39 and 29.34) but there was a significant difference between day 4 and other days (mean rank 44.77). In dual culture of *Trichoderma-R. solani* (plant pathogen) the inhibition was detected between 63% and 77% (Table 5). The best inhibition values were calculated as 77%, 75% and 69% for strain ID17E, ID20G and ID11D, respectively. In dual culture of *Trichoderma - B. cinerea* (plant pathogen), inhibition was determined between 56% and 83%. The best inhibition values were calculated as 83% for ID11D and 78% for ID20G, ID11C, ID7C and ID9A. In dual culture of *Trichoderma - S. sclerotium* (plant pathogen), inhibition was determined between 58% and 79%. The best inhibitory strains were observed as ID20G, ID11D, ID17E and ID11C (79-75%). In *Trichoderma - A. niger* and *A. flavus* (opportunist human pathogen) dual cultures inhibition percentages were calculated as 68%-78% and 50%-68%, respectively. The best effective strains against to A. niger, were determined as ID9A (77%) and ID20G (78%). The majority of Trichoderma isolates were found not to have significant effects on entomopathogenic fungi of *I. fumosorosea, B. bassiana* and *M. anisopliae*. *Trichoderma* spp. isolates were found to inhibit the growth of plant and human pathogens strongly, but there was no observed inhibition on insect pathogens. Therefore it is suggested that *Trichoderma harzianum* strains can be used either against to plant pathogens or in combination with insect pathogens in the environment safely as a biocontrol agent. Based on this knowledge, the analyzed isolates of *Trichoderma* spp. can be classified into 2 distinct groups based on their biocontrol capacity. The first group consists ID11C, ID11D, ID17E and ID20G, were true effective as potential bio-control agents. The second group consists ID4A, ID4B, ID6A, ID7C, ID9A, were effected the activities of tested pathogenic fungi but can not be categorized as good biocontrol agents in this study.

Antal et al. [27] reported that, 14 of *Trichoderma* spp. strains were identified as T. *atroviride, T. harzianum* and *T. viride* out of 360. It was stated that these strains had good growth parameters at 5°C, and inhibitory effects against *R. solani* and *F. oxysporum* in dual culture at 10 °C. Soil amendment with formulated *Trichoderma* spp. proved to be effective in controlling *Sclerotium rolfsii*, the causative agent for seedling disease of many crops and many researchers reported antagonistic activity of *Trichoderma* spp. isolates against plant pathogens especially against fungal ones such as *Rhizoctonia solani* and *Sclerotium rolfsii* [28]. Lone et al. [29] reported that *T. harzianum* isolated from the rhizosphere of *Juglans regia* L., caused inhibition the growth of A. niger by 75%, *C. spherospermum* by 72.2% and *F. oxysporum* by 25%. Isolated *Trichoderma spp.* from chickpea rhizosphere and root endophytic region, 7 isolates were found to show the highest (83.3%) inhibition percentage out of ten isolates tested against *Rhizoctonia bataticola* [30]. It was determined that *Trichoderma* spp. had a significant effect against entomopathogenic biocontrol strains of *B. bassiana, I. fumosorosea* and *M. anisopliae* (Table 5). Due to the rapid growth of *Trichoderma* spp. strains, it was observed that the strains limited growth area of entomopathogens, showed vertical growth instead of radial growth and blocked the contact between *Trichoderma* spp. and entomopathogenic strain. In a report of Lopez and Orduz [31] entomopathogenic fungus, *M. anisopliae* (strain M-137), or the antagonist fungus, *T. viride* (strain T-26) or a combination of both entomopathogenic and antagonist fungi were applied to control *A. cephalotes* nests. The mortality of nests was found as 100% with *M. anisopliae* and the combined fungal treatment, and 80% mortality in the treatment with *T. viride*. Combined application of entomopathogens (*B. bassiana, M. anisopliae* and *Paecilomyces fumosoroseus*) with mycoparasites (*Clonostachys spp., T. harzianum* and *Lecanicillium lecanii)* did not influence their biological control efficacy in vivo, although the re-isolation success of entomopathogens could be significantly reduced, especially from smaller insect species according to Krauss et al. [32]. Our results also supported these data and it was concluded that there is no effect of co-application of *Trichoderma*

spp. strains with entomopathogens. *Trichoderma* spp. strain ID4B, ID11D and ID20G were found not to generate spores when tested to produce volatile metabolites (Table 6). All *Trichoderma* spp. strains were detected to produce volatile metabolite having effect in reducing sclerotia and radial growth of *S. sclerotiorum*.

In a report, volatile and non-volatile compounds produced from *Trichoderma* spp., *T. saturnisporum, T. harzianum, T. viride, T. reesei* were studied against *Colletotrichum capsici*. The volatile compounds produced from all the selected Trichoderma species were found to show 30 to 67% inhibition of *C. capsici* [33]. Approximately 250 volatile organic compounds have been identified from fungi up to know and *Trichoderma* spp. species are known to produce numerous volatile organic compounds [34]. Mohiddin et al. [35] reported that 6 isolated *T. viride* inhibited sclerotia production of *S. rolfsii* (48%) and *S. sclerotium* (78%) and developed *mycelia* by 40%. Fungal volatile organic compounds are important in the functioning of both atmospheric and soil ecosystems [36]. When twelve isolates were tested for the production of volatile and non-volatile metabolites, it was found that some of these compounds (Isobutyric acid, 1.8-Cineole and 6-Pentyl-a-pyrone) showed antifungal and antibacterial activity and in addition to the biocontrol strategies [37]. In our study, *Trichoderma* spp. produced some volatile metabolites, inhibited production of *sclerotia* and growth of pathogens at the same time. The best effective strains were determined as ID6B, ID11C, ID11D and ID20G in terms of volatile compound production.

Captan is a broad-spectrum fungicide that belongs to the phthalimide chemical family. There are number of fungicides that contain copper hydroxide and Cuprenax is one of them. Mancozeb (Dikozin) contains zinc and manganese ethylene bis-dithiocarbamate [38]. All of these fungicides are used for greenhouse and/or nursery of plants depends on the formulation. *Trichoderma* spp. strains were tested against to various concentrations of different groups of fungicide (Captan (Phthalimide), Dikozin (dithiocarbamate) and Cuprenax (inorganic)) and the highest tolerance was detected against to Dikozin and the lowest to the Captan (Table 7). It was not determined that there is a significant difference among Cuprenax concentrations (2.5, 5, 10 mg mL^{-1}) on the growth rate of *Trichoderma* spp.

Table 6. Evaluation of volatile metabolites produced by *Trichoderma* spp. isolates against mycelial growth and spore production in *Sclerotonia sclerotium*.

Trichoderma Strain No	*Trichoderma* spp.		*Sclerotonia sclerotium*	
	Growth	Spore production	Growth	Sclerotia production
ID4A	+++	++	++	*-
ID4B	++	-	++	-
ID6B	+++	+	+	-
ID7C	+++	++	++	-
ID9A	+++	++	++	-
ID11C	+++	++	+	-

(+); low, (++); good, (+++); very good, (-); negative, *; no sporulation

ID11D	+++	-	+	-
ID17E	++	-	++	-
ID20G	+++	-	+	-
KUEN 1585	++	-	+	-
Negative control	+++	+++		
Sclerotonia control			+++	+++

Table 7. The growth zone of Trichoderma spp. on PDA medium containing fungisit (on day 7, mm).

Strain No	Captan (mg mL^{-1})			Dikozin (mg mL^{-1})			Cuprenax (mg mL^{-1})		
	2.5	5	10	2.5	5	10	2.5	5	10
ID4A	40	20	14	85	85	39	35	35	40
ID4B	40	20	14	85	85	40	35	34	38
ID6B	38	21	19	85	85	35	36	30	29
ID7C	38	20	18	85	85	20	30	30	29
ID9A	28	22	18	85	85	30	34	30	30
ID11C	48	20	19	85	85	80	50	45	40
ID11D	35	35	19	85	85	85	42	40	40
ID17E	28	15	5	85	60	50	39	34	30
ID20G	20	12	9	85	70	40	20	17	15
KUEN 1585	75	35	25	85	85	20	35	35	30

*The zone diameter of the control groups were 85 mm at day 7.

strains. However, there was a significant difference among 2.5 mg mL^{-1} and other doses of Captan and among 10 mg mL^{-1} and other doses of Dikozin. It was observed that 10 mg mL^{-1} of Captan inhibited the growth of *Trichoderma* spp. strains by 80%. Dikozin and Cuprenax inhibited the growth at the same concentration by 50% and 62%, respectively. *Trichoderma* spp. was found to be the most sensitive to Captan, Propiconazole and Tebuconazole in our study. Among tested fungicides the most resistant strains were determined as ID11C and ID11D, the most susceptible strain was determined as ID20G. Thiram, Mancozeb, Tebuconzole were found to be the best effective fungicides and the least effective ones were reported as Pyrocymidone and Captan on *T. harzianum* C52 spore germination in a previous study [39]. Khan and Shahzad [19] reported that *T. harzianum* were able to proliferate under the low doses of various fungicides (Benomly, Topsin-M, Carbendazim and Cuprocaffro). A similar report on *T. harzianum*'s potential integration as a biological agent was reported by Saxena et al. [40]. The compatibility was assessed at different concentrations and the concentration of Carbendazim, Metalaxyl, Captan, Mancozeb, Thiram and Nemacur were under the safe tolerance limit for *T. harzianum* whereas the corresponding values for *T. virens* were found as 40, 1000, 125, 177, 9, and 700 μg/mL, respectively according to Mohiddin and Khan.[35] The in-vitro effect of 6 commonly used fungicides on the mycelial growth of *Trichoderma harzianum* PBT 23 were evaluated in another study and Captan, Thiram, Chlorothalonil and Copper hydroxide were reported compatible with the test antagonist up to 100 μg/mL, while Mancozeb was compatible with up to 250 μg/mL. It is reported that these affect the growth of test antagonist adversely [40]. Parab et al. [41] studied the sensitivity of *T. harzianum* against to different fungicides and the results indicated that all systemic fungicides were found to inhibit the growth of *T. harzianum* completely whereas Zineb, Copper hydroxide, Mancozeb and copper oxychloride were found safe for the growth of *T. harzianum*.

Based on our results, although there was a reduction in growth rate, used and over dose concentrations of the strain of interest were detected to sustain growth. The strains ID11C, ID11D and ID20G were characterized as potential bio-control agents that did not affect the vitality.

CONCLUSION

With this study an attempt has been made to grow different species of *Trichoderma* spp. at various temperatures, with their antifungal and antibacterial activity in order to reveal all

the relevant and favorable parameters. The *Trichoderma* spp. species inhibits the growth of pathogens by releasing antibiotics and other volatile compounds that are harmful to the pathogens. We showed that *mycelia* growth inhibition affects *Trichoderma*'s volatile organic compounds without direct physical contact between the pathogen and fungus. The temperature is an important parameter for the growth of pathogen and biocontrol agent because it affects spore germination, mycelial growth and competitive saprophytic ability. It is important using *Trichoderma* spp. as a potential bio-control agent in different geographic regions, because strains maintain their spore vitality at a temperature range of 4-75°C and can grow at 15-37°C. This characteristic provides the adaptation of bio-control agents to temperatures at application fields and sustainability of the adapted strains. Considering the reproductive properties, spore production, fungisit tolerance and pathogen inhibition it can be concluded that ID11D and ID11C might be better bio-control agents. Identifying biocontrol agents and understanding the mechanisms underlying the antagonistic effect of *Trichoderma* spp. on plant pathogens are important in creating effective and safe bio-control strategies. Possible mechanisms of antagonism employed by *Trichoderma* spp. includes nutrient and niche competitions, antibiosis by producing volatile components and non-volatile antibiotics that are inhibitory against a range of soil-borne fungi, as well as parasitism. Different soil isolates of *Trichoderma* spp. can variable in their ability to fight against to different fungal pathogens. Therefore, enlightening the effects of new biocontrol agents to provide disease control is important.

ACKNOWLEDGEMENTS

The study was supported by a grant of Recep Tayyip Erdogan University scientific research projects unit (Project No: 2012.102.03.3). We thank Assos. Prof. Dr. Sevim A., (for providing entomopathogenic fungi), Kırşehir Ahi Evran University, Prof. Dr. Özer G. (for R. solani AG3) Abant İzzet Baysal University, Prof. Dr. Yanar Y. (for S. sclerotiorum) Gazi Osman Paşa University, Prof. Dr. Karakaya, A., (for B. cinerea) Ankara University for their valuable help. Commercial strain T. harzianum KUEN 1585 were obtained from Simbiyotek Biyolojik Ürünler San. ve Tic. A.Ş.

References

1. Y. Elad, Biological control of foliar pathogens by means of *Trichoderma harzianum* and potential modes of action, Crop Prot., 19 (2000) 709-714.
2. E. Demirci, E. Dane, C. Eken, In vitro antagonistic activity of fungi isolated from sclerotia on potato tubers against Rhizoctonia solani, Turk. J. Biol., 35 (2011) 457-462.
3. M.A. Rifai, Revision of the genus *Trichoderma*, Myc. Papers., 116 (19691) 56.
4. N. Sadfi-Zouaoui, S. Châabani, M. Rouaissi, A. Hedi, M. Hajlaoui, A. Boudabous, Analysis of the diversity of *Trichoderma* spp. in soil horizons using digested ITS regions, Ann. Microbiol., 59 (2009) 459-463.
5. D.M. Geiser, J.C. Frisvad, J.W. Taylor, Evolutionary relationships in *Aspergillus* section Fumigati inferred from partial β-tubulin and hydrophobin DNA sequences. Mycologia, (1998) 831-845.
6. W.J. Janisiewicz, L. Korsten, Biological control of postharvest diseases of fruits, Annu. Rev. Phytopathol., 40 (2002) 411-441.
7. M. Verma, KB. Satinder, R.D. Tyagi, Bench-scale fermentation of *Trichoderma viride* on wastewater sludge: rheology, lytic enzymes and biocontrol activity, Enzyme Microb. Tech., 41 (2007) 764-771.
8. R.M. Saleh, Screening and production of antibacterial compound from *Trichoderma* spp. against human-pathogenic bacteria, Afr. J. Microbiol. Res., 5 (2011) 1619-1628.
9. J. Locke, J. Marois, G. Papavizas, Biological control of Fusarium wilt of greenhouse-grown chrysanthemums. Plant Dis. 69 (1985) 167-169.
10. L. Kredics, Z. Antal, L. Manczinger, Influence of environmental parameters on *Trichoderma* strains with biocontrol potential, Food. Technol. Biotechnol., 41 (2003) 37-42.
11. S.A. Karaoglu, S. Ulker, Isolation, identification and seasonal distribution of soilborne fungi in tea growing areas of Iyidere-Ikizdere vicinity (Rize-Turkey), J. Basic. Microbiol., 46 (2006) 208-218.
12. S. Kanematsu, S. Naito, Genetic characterization of rhizoctonia solani ag-2-3 by analyzing restriction fragment length polymorphisms of nuclear ribosomal DNA internal transcribed spacers, Jap. J. Phytopathol., 61 (1995) 18-21.
13. K.J. Martin, P.T. Rygiewicz, Fungal-specific PCR primers developed for analysis of the ITS region of environmental DNA extracts, BMC Microbiol., 5 (2005) 28-28.
14. A. Singh, Influence of temperature, pH and media for growth and sporulation of *Trichoderma atroviride* and its shelf life study in different carrier based formulation, J. Plant. Dis. Sci., 6 (2011) 32-34.
15. Á. Keszler, E. Forgács, L. Kótai, Separation and identification of volatile components in the fermentation broth of *Trichoderma atroviride* by solid-phase extraction and gas chromatography-mass spectrometry, J. Chromatogr. Sci. 38 (2000) 421-424.
16. S. Siddiquee, U.K. Yusuf, K. Hossain, S. Jahan, In vitro studies on the potential *Trichoderma harzianum* for antagonistic properties against Ganoderma boninense, J. Food Agric. Environ., 7 (2009) 970-976.

17. J.A. Vizcaino, S. Luis, B. Angela, F. Vicente, S. Gutierrez, M.R. Hermosa, E. Monte, Screening of antimicrobial activities in *Trichoderma* isolates representing three *Trichoderma* sections, Mycol. Res., 109 (2005) 1397-1406.
18. G.L. Woods, A.B.E. Barbara, S.C. Patricia, Susceptibility testing of Mycobacteria, nocardiae, and other aerobic actinomycetes; Approved Standard 2nd ed. Wayne (2003) Pennsylvania.
19. M.O. Khan, S. Shahzad, Screening of *Trichoderma* species for tolerance to fungicides, Pak. J. Bot., 39 (2007) 945-951.
20. V. Santos, V.R. Linardi, Biodegradation of phenol by a filamentous fungi isolated from industrial effluents-identification and degradation potential, Process. Biochem., 39 (2004) 1001-1006.
21. B.B. Joshi, M.P. Vishwakarma, D. Bahukhandi, R.P. Bhatt, Studies on strains of *Trichoderma* spp. from high altitude of Garhwal Himalayan region, J. Environ. Biol., 33 (2012) 843-847.
22. C. Kucuk, M. Kivanc, Isolation of *Trichoderma* spp. and determination of their antifungal, biochemical and physiological features, Turk J. Biol., 27 (2003) 247-253.
23. F.B.H. Khethr, S. Ammar, D. Saidana, M. Daami, J. Chriaa, K. Liouane, M.A. Mahjoub, A.N. Helal, Z. Mighri, Chemical composition, antibacterial and antifungal activities of *Trichoderma* spp. growing in Tunisia, Ann. Microbiol., 58 (2008) 303-308.
24. I. Suay, F. Arenal, F.J. Asensio, A. Basilio, M.A. Cabello, M.T. Diez, J.B. Garcia, A.G. Del Val, J. Gorrochategui, Screening of basidiomycetes for antimicrobial activities, Antonie van Leeuwenhoek, 78 (2000) 129-139.
25. P. Tarus, C.C. Lang'at-Thoruwa, A.W. Wanyonyi, Bioactive metabolites from *Trichoderma harzianum* and *Trichoderma longibrachiatum*, Bull. Chem. Soc. Ethiop., 17 (2003) 185-190.
26. K. Liouane, D. Saidana, S. Ammar, Chemical composition and antimicrobial activity of methanolic extract of *Trichoderma* sp. growing wild in Tunisia. J. Essent. Oil Bear. Pl., 12 (2009) 531-540.
27. Z. Antal, L. Manczinger, G. Szakacs, R. Tengerdy, L. Ferenczy, Colony growth, in vitro antagonism and secretion of extracellular enzymes in cold-tolerant strains of *Trichoderma* species, Mycol. Res., 104 (2000) 545-549.
28. B. Ngo, D. Vu, D. Tran, Analyze antagonist effects of *Trichoderma* spp. for controlling southern stem rot caused by Sclerotium rolfsii on peanut, Plant Prot., 1 (2006) 12-14.
29. M.A. Lone, M.R. Wani, S.A. Sheikh, Antagonistic potentiality of *Trichoderma harzianum* against *Cladosporium spherospermum*, *Aspergillus niger* and *Fusarium oxysporum*, J. Biol. Agric. Healthc., 2 (2012) 72-76.
30. G.A. Veena, R. Eswara, R. Bhasakara, Pathogenicity tests and evaluation of efficacy of fungicides against *Rhizoctonia bataticola*, the causal agent of dry root rot of chickpea, Int. J. Appl. Biol. Pharm., 5 (2014) 283-287.
31. E. Lopez, S. Orduz, *Metarhizium anisopliae* and *Trichoderma viride* for control of nests of the fungus-growing ant, Atta cephalotes, Biol. Control, 27 (2003) 194-200.
32. U. Krauss, E. Hidalgo, C. Arroyo, Interaction between the entomopathogens *Beauveria bassiana*, *Metarhizium anisopliae* and *Paecilomyces fumosoroseus* and the *mycoparasites Clonostachys* spp., *Trichoderma harzianum* and *Lecanicillium lecanii*, Biocontrol. Sci. Techn., 14 (2004) 331-346.
33. P. Ajith, N. Lakshmidevi, Effect of volatile and non-volatile compounds from *Trichoderma* spp. against *Colletotrichum capsici* incitant of anthracnose on bell peppers, Nat. Sci., 8 (2010) 265-269.
34. N. Stoppacher, B. Kluger, S. Zeilinger, R. Krska, R. Schuhmacher, Identification and profiling of volatile metabolites of the biocontrol fungus *Trichoderma atroviride* by HS-SPME-GC-MS, J. Microbiol. Methods., 1 (2010) 187-193.
35. F. Mohiddin, M. Khan, Tolerance of fungal and bacterial biocontrol agents to six pesticides commonly used in the control of soil borne plant pathogens, Afr. J. Agric. Res., 8 (2013) 5331-5334.
36. M. Shaik, Non-volatile and volatile metabolites of antagonistic *Trichoderma* against collar rot pathogen of mentha arvensis, Int. J. Pharm., 2 (2011) 56-58.
37. S.U. Morath, R. Hung, JW. Bennett, Fungal volatile organic compounds: a review with emphasis on their biotechnological potential, Fungal Biol. Rev., 26 (2012) 73-83.
38. H.H. Oruc, Fungicides. InTech: Chapter 17, Fungicides and their effects on animals, (2010) 349-362.
39. K. McLean, J. Hunt, A. Stewart, S. Zydenbos, Compatibility of the biocontrol agent *Trichoderma harzianum* C52 with selected fungicides, In: Proceedings of The New Zealand Plant Protection Conference, (2001) New Zealand Plant Protection Society.
40. D. Saxena, A. Tewari, D. Rai, The in vitro effect of some commonly used fungicides, insecticides and herbicides for their compatibility with *Trichoderma harzianum* PBT23, World Appl. Sci. J., 31 (2014) 444-448.
41. P. Parab, M. Diwakar, U. Sawant, J. Kadam, Exploration of *Trichoderma harzianum* as antagonist against *Fusarium* spp. causing damping off and root rot disease and its sensitivity to different fungicides, J. Plant Dis. Sci., 4 (2009) 52-56.

The Effect of *Trichoderma* Seed Priming to Drought Resistance in Tomato (*Solanum lycopersicum* L.) Plants

Domates Bitkisinde (*Solanum lycopersicum* L.) Tohumların *Trichoderma* ile Ön Muamelesinin Kuraklık Direncine Etkisi

Research Article

Necla Pehlivan[1]*, Neslihan Saruhan Güler[2], Şengül Alpay Karaoğlu[1]

[1]Department of Biology, Faculty of Arts and Sciences, Recep Tayyip Erdogan University, Rize, Turkey.

[2]Department of Nutrition and Dietetics, Faculty of Health Sciences, Karadeniz Technical University,Trabzon, Turkey.

ABSTRACT

Tomato is one of the most important food crops immensely affected by water scarcity. Therefore, it is vital to find biocontrol agents for improving the yield of tomato crop in arid areas. The fungal genus, *Trichoderma* is widely used as an eco-friendly, biocontrol agent in commercial formulas because of the various beneficial effects it has on plants including the resistance to biotic and abiotic stresses. In the present study, the effects of an isolate of *Trichoderma atroviride* ID20G (Ta) on tomato (*Solanum lycopersicum* L.) seedlings were investigated under drought stress. The isolated fungus was identified using ITS (internal transcribed spacer) sequences. Root colonization by Ta induced changes in growth performance indexes such as root growth, root branching, and leaf number as compared to the untreated seedlings. Chlorophyll and carotenoid contents of the untreated tomato seedlings decreased after drought stress along with extensive membrane deterioration, whereas seed colonization by Ta prevented lipid oxidation and ameliorated the harmful effects of drought on pigment contents. Antioxidant enzyme activity was elevated and hydrogen peroxide (H_2O_2) concentration was found to decrease under drought stress in the Ta treated seedlings. These observations suggest that colonization of tomato seedlings by Ta is effective in counteracting the injurious effects of drought, and therefore, may have a prominent role in increasing the drought tolerance of tomato plant by decreasing H_2O_2 concentration and activating the antioxidant enzymes. Furthermore, fungus-based biocontrol agent formulation of Ta might serve as a potential tool in tomato agriculture owing to its low cost, effectiveness, and characteristics required for balancing the natural ecology.

Key Words

Seed priming, drought, tomato, *Trichoderma atroviride* ID20G.

ÖZ

Domates, su kıtlığından etkilenen en önemli besin ürünlerinden biridir. Bu nedenle kurak bölgelerde yetişen domates verimini arttırmak için biyokontrol ajanları bulmak hayati önem taşır. *Trichoderma* mantar cinsi, biyotik ve abiyotik streslere direnç de dahil olmak üzere bitkiler üzerinde sahip olduğu çeşitli yararlı etkiler sayesinde ticari formüllerde çevre dostu bir biyolojik kontrol ajanı olarak yaygın şekilde kullanılmaktadır. Bu çalışmada, *Trichoderma atroviride* ID20G (Ta) izolatının kuraklık stresi altında domates bitkilerindeki (*Solanum lycopersicum* L.) etkileri araştırılmıştır. İzole edilen mantar, ITS (internal transcribed spacer) dizileri kullanılarak tanımlanmıştır.Ta kök kolonizasyonu, uygulama yapılmamış bitkilere nazaran kök büyümesi, kök dallanması ve yaprak sayısı gibi büyüme performansı endekslerinde değişiklikler meydana gelmesini sağlamıştır. Mantar ile muamele edilmemiş domates bitkilerinin klorofil ve karotenoid içerikleri ağır membran hasarı ile birlikte kuraklık stresi sonrasında azalırken, tohumların Ta ile muamele edilmesi lipit oksidasyonunu önlemiş ve kuraklığın pigment içeriğindeki zararlı etkilerini azaltmıştır. Antioksidan enzim aktivitesi yükselmiş ve Ta ile muamele edilen kuraklık stresi altındaki bitkilerde hidrojen peroksit (H_2O_2) konsantrasyonunun azaldığı görülmüştür. Bu gözlemler, domates tohumlarının Ta ile muamelesinin, kuraklığın zararlı etkilerine karşı etkili olduğunu ve antioksidan enzimleri aktive ederek ve H_2O_2 konsantrasyonunu azaltarak domates bitkisinin kuraklık toleransını arttırmada önemli bir role sahip olabileceğini önermektedir. Dahası, Ta mantarı tabanlı bir biyo-kontrol ajan formülasyonu, düşük maliyetli olması, etkinliği ve ekolojiyi dengeleyebilecek özelliklerden dolayı domates tarımı için potansiyel bir araç görevi görebilir.

Anahtar Kelimeler

Tohuma ön muamele, kuraklık, domates, *Trichoderma atroviride* ID20G.

Article History: Received: Jan 31, 2018; Revised: Feb 19, 2018; Accepted: Mar 2, 2018; Available Online: Mar 26, 2018.

DOI: 10.15671/HJBC.2018.234

Correspondence to: N. Pehlivan, Dept of Biology, Faculty of Arts and Sci., Recep Tayyip Erdogan Uni., Rize, Turkey.

Tel: :+90 464 223 6126 Fax: +90 464 223 40 19 E-Mail: neclapehlivan@hotmail.com

INTRODUCTION

Drought is the main cause of loss of crop biomass and yield across the world. Based on the statistics, the drought-affected land has more than doubled in the recent years [1]. It is visualized as one of the most important threats to agriculture in the near future. Basic agricultural practices are remarkably affected by drought stress due to the fluctuations in global climate, reduction in rainfall, and a decrease in soil fertility. This decrease may be attributed to the use of chemical and/or synthetic fertilizers across the globe [1]. To avoid the catastrophic effects of drought stress, it is fundamental to look for alternative ways to obtain better soil fertility and stimulate the growth of plants. Thus, mankind is in need of some nature-friendly biocontrol agents that might help to overcome injurious effects of drought. One of the best eco-friendly biocontrol agents for plants is the genus, *Trichoderma*. *Trichoderma* is a cosmopolitan fungus belonging to the family, *Hypocreaceae*, and is commonly found in the rhizosphere as well as in agricultural areas, forests, or in different zones and ecosystems. They may also be present as parasites together with other fungi. *Trichoderma* spp. is broadly utilized as biofertilizers and/or biopesticides in commercial formulas because of their multiple beneficial effects on plant growth [2]. Furthermore, *Trichoderma* genus releases some metabolites analogous to phytohormones, which in turn induce growth under stress.

Plant cells can generate reactive oxygen species (ROS) even under normal conditions; however, these get eliminated by defense mechanisms of the cell. Under stressful conditions, such as drought, oxidative stress is induced by the generation of ROS [3]. Nevertheless, plants have defense mechanisms, both enzymatic and non-enzymatic (antioxidants) against ROS. The enzymatic components include superoxide dismutase (SOD), ascorbate peroxidase (APX), catalase (CAT), and glutathione reductase (GR), whereas the non-enzymatic ones are ascorbic acid (ASA) and glutathione (GSH). Mitigation of ROS employed by *Trichoderma* genus has been demonstrated as one of the important mechanisms in plants under drought stress. In recent years, several studies have suggested that colonization of plants with *Trichoderma* enhances the water-stress tolerance of plants through the regulation of expression of genes coding for antioxidant enzymes or transcription factors [4]. In a previous work of our lab, the presented data proved that *Trichoderma atroviride* ID20G-inoculated seedlings demonstrated increased antioxidant activity than the uninoculated ones under drought stress conditions [5]. In addition, several studies have shown that root colonization by *Trichoderma* result in increased levels of plant enzymes consisting of different peroxidase types, chitinases, glucanases, lipoxygenases, and phytoalexins-like compounds that provide reliable protection against oxidative stress [6,7].

Tomato (*Solanum lycopersicum* L.) is one of the most consumed crops worldwide. According to a 2015 report by Food and Agriculture Organization (FAO) [8], fresh fruit production of tomato increased to 160 million tons in 2013. Because of its excellent nutritional value, the tomato is either consumed as a fresh or processed fruit. Additionally, it is a great source of vitamins, folate, and some phytochemicals [9]. Tomato plants need a well-irrigated system, and unfortunately, most of the cultivars are drought sensitive at all steps of plant development. However, seed germination and early seedling growth are the most sensitive stages. Since tomato growth and yield are severely threatened by various abiotic factors, the use of nature-friendly *Trichoderma* strains may be a suitable strategy for improving the yield of tomatoes in arid areas.

Although many studies report different scenarios to mitigate drought stress-mediated damage with the help of *Trichoderma* genus, no direct evidence is present as to whether this newly identified *T. atroviride* ID20G (our local fungal strain) induces stress tolerance in tomato plants. At the same time, it may be important to examine the locally and newly defined biocontrol agents under drought conditions, since new isolates might have different protection mechanisms due to their ecotypic variations and genetic backgrounds. Therefore, the objective of the present investigation was to evaluate whether Ta can serve as a candidate strain for controlling abiotic stress in tomato, thereby increasing the

drought tolerance of the plant, and to explain the underlying fundamental physiological and biochemical changes associated with its practice as a seed inoculant before germination stage.

MATERIAL and METHODS

Isolation and Identification of Ta

The various strains of *Trichoderma* were formerly isolated with the method demonstrated by [10] from a tea cultivation area of Rize province of Turkey. Molecular identification was performed as described by [5]. The target strain of *Trichoderma* named as ID20G was used as a seed biopriming agent for the present study.

Plant Material and Preparation of Ta Formulation

Hyphae and spores of Ta were produced as described by [5] from 14-day-old strains. Measurements of the fungal inoculation (Ta, 1 ✣ 10^7 conidia/mL) and the conidial densities in the suspension were determined based on the methods mentioned by [5]. Seed inoculation was conducted on the tomato seeds (*Solanum lycopersicum* L.) in the adjusted amount of microbial suspension. Seeds were sterilized using 1% bleach. After 20 min, seeds were washed in sterile distilled water several times and submerged in 50 mL of a spore suspension (Ta, 1 ✣ 10^7 conidia/mL) and incubated for 1 h. The control group of seeds was placed in the same volume of distilled water for 1 h.

Pot Experiment

Plant soil was autoclaved twice for 1 h before its transfer to polyethylene bags. Six seeds were placed in each pot and put into a growth chamber with 16 h of light/8 h of dark period at 25 °C. The effects of Ta on the growth of tomato seedlings were assayed after four weeks of daily watering. Drought stress was mimicked by withholding water after four weeks of germination for 12 days. Control plants were irrigated with tap water as the same stress period of drought plants. Afterward, the seedlings were arranged as listed: treated with plain water (untreated control, C), pre-treated with Ta and not drought stressed (Ta), drought-stressed only (DS), and pre-treated with Ta and drought-stressed (Ta + DS).

Macroscopic Phenotyping Analysis of the Target Fungus

At the end of experimental period, the roots were separated from the soil under sterile conditions and washed directly with sterile water. They were then examined directly on a stereo microscope (Leica S6 D Product; Leica Microsystems, Wetzlar, Germany) to check if the Ta was actually present in the environment and absent from the control group. Cotton blue staining was performed to distinguish the fungus hyphae from the plant roots, and the samples were inspected under the microscope. Thin long filamentous hyphal structure with septum was accepted as Ta. After the roots were separated from the soil, they were washed with ethanol (70%) and small pieces (three pieces for each group) were cut for further use by scalpel and placed onto the dichloran rose-bengal chloramphenicol (DRBC) agar under sterile conditions. Pictures were taken before and after four days of incubation at 28 °C.

Analyses of Chemical Compounds

The second fully developed apical leaves were used to measure photosynthetic pigment contents, namely total chlorophyll (chl) and total carotenoid (car) by acetone (80%) extraction method. Absorbance measurements were obtained at 663, 645, and 450 nm by an ultraviolet-visible (UV-VIS) absorption spectrophotometer (Biochrom Libra S70, UK) [11,12].

The rate of oxidation of lipids (fatty acids) was measured via the concentration of malondialdehyde (MDA, e = 155 mM^{-1} cm^{-1}) with the help of the basic method of Heath and Packer [13].

The accumulation of endogenous hydrogen peroxide (H_2O_2) was assayed with the help of the method described by Velikova et al. [14].

Antioxidant Enzyme Assays

Extractions for the activity assays were performed in 50 mM of potassium phosphate (K_2HPO_4) buffer (pH 7.0) set up with 1% polyvinylpolypyrrolidone and 1 mM EDTA mix. Bovine serum albumin as a standard was used for soluble protein content calculations [15].

Superoxide dismutase (SOD; EC, 1.15.1.1) activity was detected based on the method of Beauchamp et al. [16]. The activity of guaiacol peroxidase (GPX; EC, 1.11.1.7) was detected as the increase in 470 nm absorbance (25°C, e = 26.6 mM^{-1} cm^{-1}) [17]. Catalase (CAT; EC, 1.11.1.6) activity was assayed by an H2O2 decrease (25°C, e = 39.4 mM^{-1} cm^{-1}) at 240 nm [18]. Ascorbate peroxidase (APX; EC, 1.11.1.11) activity was measured via oxidation of the ascorbate at 290 nm (25°C, e = 2.8 mM^{-1} cm^{-1}) [19].

Statistical Analysis

Data were evaluated by SPSS Version 15.0 (SPSS Inc., USA). Duncan's multiple range test was applied for the analysis of mean values. The statistical significance of differences was set to a level of 5% ($p < 0.05$).

RESULTS

Macroscopic Phenotyping Analysis of the Target Fungus

We initially checked if Ta was actually present in the environment and absent in the control group. We tested this notion in the roots and did not find any other fungus phenotype (Figure 1). The data demonstrated that Ta treatment has an important effect on tomato growth. We found that it particularly improved the root development even under normal conditions without drought (Figure 2). The number of roots and leaves for Ta-treated

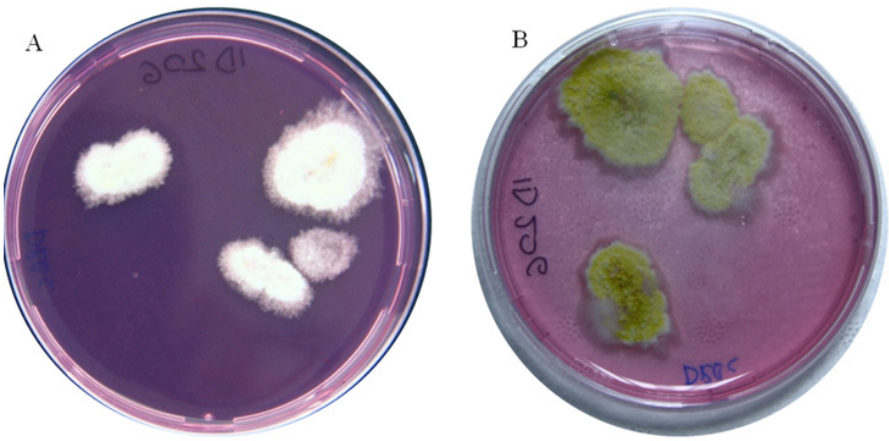

Figure 1. Contamination test of tomato root samples on DRBC agar (Dichloran Rose Bengal Chloramphenicol Agar) before (A) and after (B) the sporulation phase.

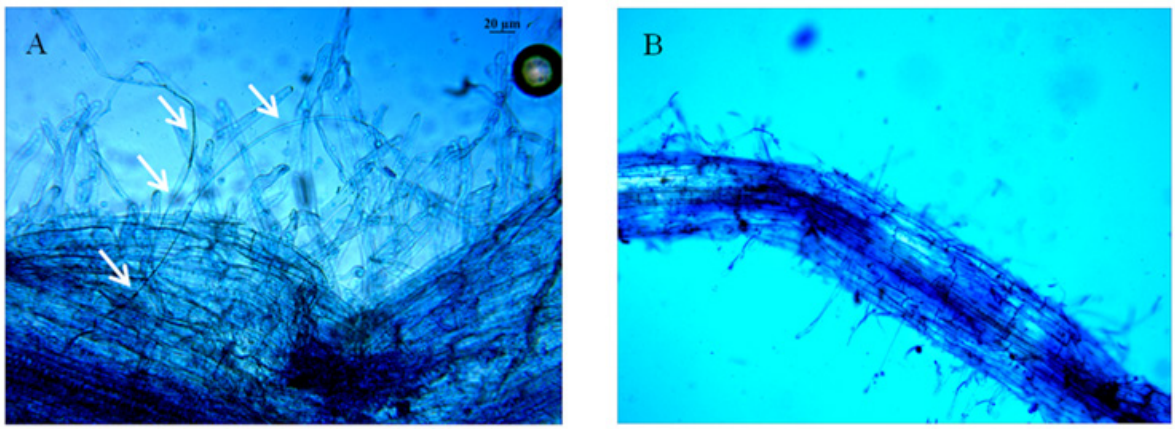

Figure 2. Root staining analysis with (A) or without (B) ID20G inoculation. The presence of ID20G hyphae was detected by staining the tomato roots with cotton blue (chitin staining dye). White arrows indicate ID20G hyphae.

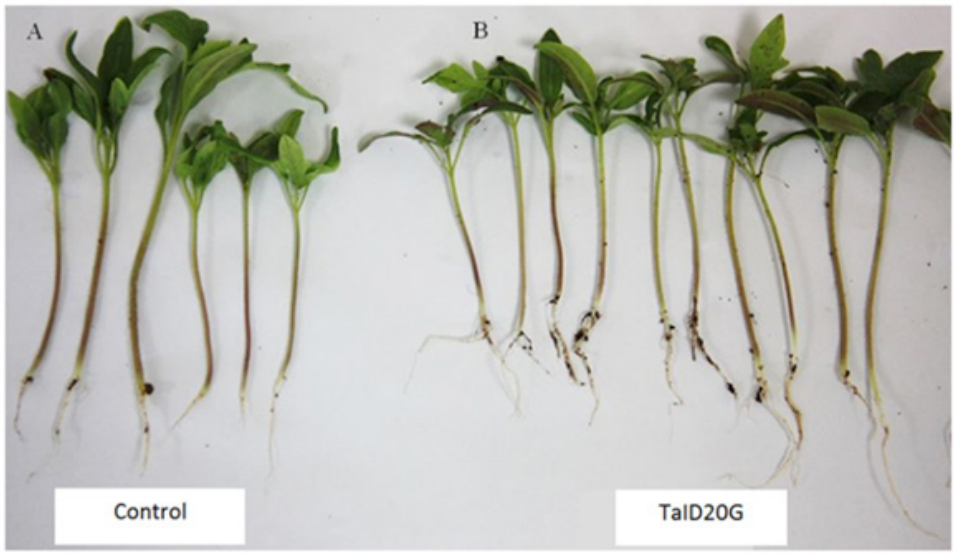

Figure 3. Stimulation of tomato root growth by *Trichoderma* strain ID20G under normal (no drought) Control (A) and ID20G inoculated (B) conditions.

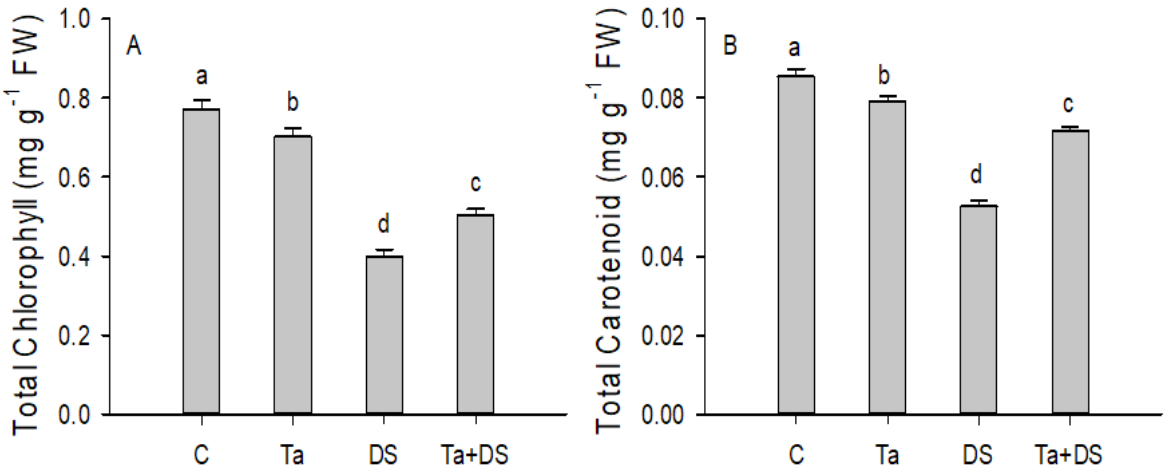

Figure 4. The potency of seed biopriming of *T. atroviride* strain ID20G on total chlorophyll (A) and total carotenoid (B) contents of tomato plants under drought stress. The plants were subjected to four treatments: with distilled water (untreated control, C), with *T. atroviride* strain ID20G and not drought stressed (Ta), drought-stressed only (DS), and pre-treated with *T. atroviride* strain ID20G and drought stressed (Ta+DS). FW: Fresh weight. Vertical bars indicate standard deviation and different letters indicate significant difference ($P<0.05$) among the treatments.

tomato seedlings was significantly higher than the untreated ones (Figure 3).

Ta Inoculation Under Drought Improves Photosynthetic Pigments

Drought stress significantly increased the percent reduction of pigment contents in tomato seedlings. The percent decrease rate was calculated to be 48.5% and 38.4% in total chlorophyll and carotenoids, respectively, in drought-treated only seedlings (DS) compared to the untreated ones.

Moreover, drought stress reduced the pigment contents more than in the seedlings inoculated with Ta only. Pigment contents in Ta + DS were found to be greater than in the drought-stressed only (DS) seedlings (Figure 4).

Ta Inoculation Under Drought Reduces Membrane Damage and H_2O_2 Accumulation

An increase in MDA content was observed following drought stress. MDA content increased significantly by 32% in drought only treated seedlings (DS) in comparison to untreated seedlings (C). However, Ta colonization mitigated the lipid peroxidation under stress. The percentage increase in MDA content under stress was recorded to be 15.4 % in Ta-colonized

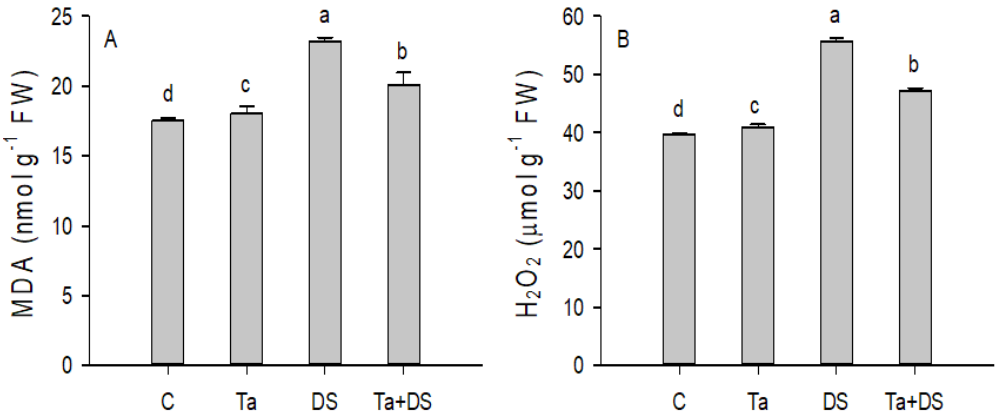

Figure 5. The potency of seed biopriming of *T. atroviride* strain ID20G on malondialdehyde (MDA) (A) and hydrogen peroxide (H_2O_2) (B) contents of tomato plants under drought stress. The plants were subjected to four treatments: with distilled water (untreated control, C), with *T. atroviride* strain ID20G and not drought stressed (Ta), drought-stressed only (DS), and pre-treated with *T. atroviride* strain ID20G and drought stressed (Ta+DS). FW: Fresh weight. Vertical bars indicate standard deviation and different letters indicate significant difference ($P<0.05$) among the treatments.

seedlings when compared to drought only treated seedlings (Figure 5A).

Drought also caused a severe H_2O_2 accumulation in the seedlings. The concentration of H_2O_2 increased significantly by 40.3 % in drought only treated seedlings in comparison to the control. However, this change was less obvious in seedlings treated with Ta. Ta inoculation resulted in a substantial decline of endogenous H_2O_2 concentration under drought stress. The percentage increase in H_2O_2 concentration after Ta inoculation was recorded to 18% in comparison to drought only treated seedlings (Figure 5B).

Ta Inoculation Under Drought Induces Antioxidant Eenzyme Activities

Drought stress significantly induced and increased the antioxidant enzyme activities in tomato seedlings (Figure 6). The SOD, CAT, GPX, and APX activities increased to 40, 78, 118, and 89% in drought stressed only seedlings compared to the untreated control group, respectively. It is obvious that the Ta inoculation alone (in the absence of drought stress) led to a significant increase in GPX and APX activities compared to the control (Figure 6C, D). However, no significant change in SOD and CAT activities between the control and Ta-inoculated seedlings was obtained (Figure 6A, B). In addition, the activities of antioxidant enzymes were significantly increased after root colonization with Ta under drought stress in comparison to drought only treated seedlings. The percentage increase recorded were 11%, 19%, 57%, and 23% for SOD, CAT, GPX, and APX, respectively (Figure 6A, B, C, D).

DISCUSSION

Drought stress is one of the major stress factors in the environment that causes biochemical alterations in plants, including limiting plant growth and decreasing plant productivity. Plants develop different strategies to avoid drought stress. One of these strategies is the use of biocontrol agents such as *Trichoderma* due to its, effectiveness, and compatible nature with the ecology. Rhizosphere-competent fungus of the genus, *Trichoderma* plays an essential role in many metabolic processes of host plants tolerant to drought stress. This genus increases water holding capacity of plants, induces osmolyte synthesis to protect the plants from osmotic stress, helps in the uptake of crucial minerals, and enhances photosynthetic efficiency [20]. Although the abiotic stress tolerance-promoting capability of *Trichoderma spp.* in plants colonized with the fungi has been previously reported [4,21] there is no information concerning drought tolerance responses in tomato induced by our local isolate, Ta. According to the best of our knowledge, the present study is the first one to discover the role of the local isolate, Ta candidate strain as a control agent in enhancing the tolerance of

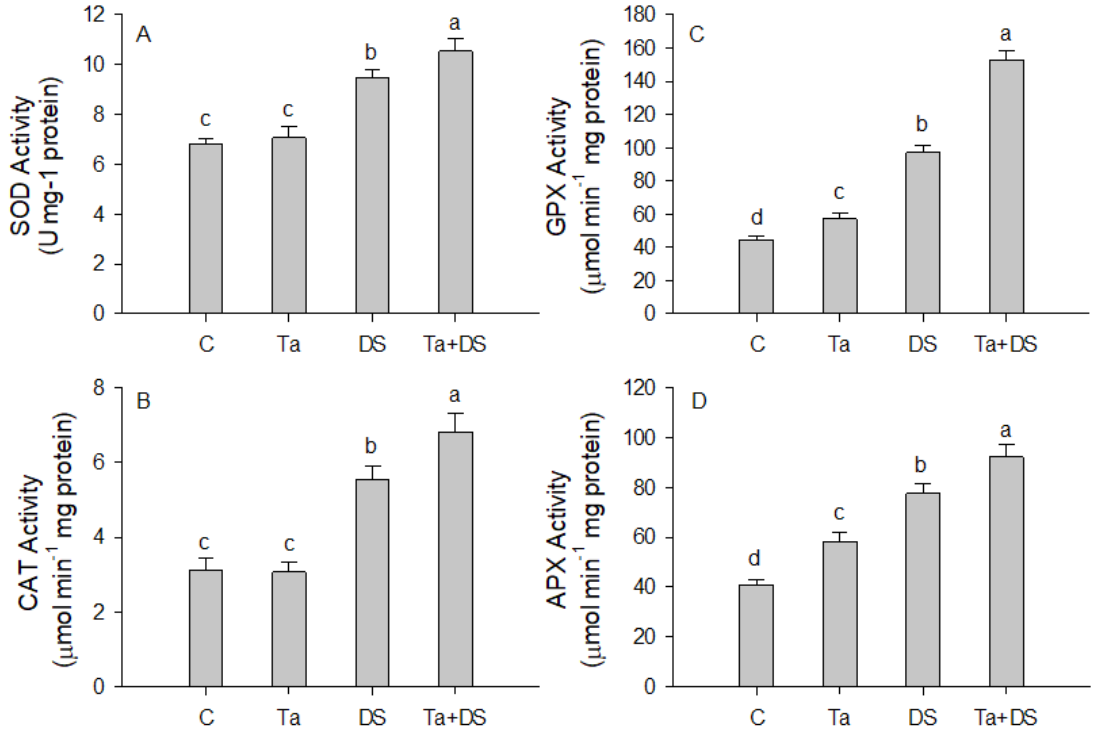

Figure 6. The potency of seed biopriming of *T. atroviride* strain ID20G on superoxide dismutase (SOD) (A), catalase (CAT) (B), guaiacol peroxidase (GPX) (C) and ascorbate peroxidase (APX) (D) enzyme activities of tomato plants under drought stress. The plants were subjected to four treatments: with distilled water (untreated control, C), with *T. atroviride* strain ID20G and not drought stressed (Ta), drought-stressed only (DS), and pre-treated with *T. atroviride* strain ID20G and drought stressed (Ta+DS). Vertical bars indicate standard deviation and different letters indicate significant difference ($P<0.05$) among the treatments.

tomato seedlings to drought stress. *Trichoderma* genus can improve plant growth through various mechanisms, which include enhanced nutrient uptake and mineral solubilization, sequestration of inorganic nutrients, and promotion of root hair growth [6]. In this study, we checked the ability of our local isolate, ID20G to enhance tomato growth. The root growth and leaf-root numbers were significantly higher in Ta-treated tomato seedlings as compared to the controls (Figure 3). The capability of Ta to produce phytohormones may serve as a fundamental factor in the elevation of components required for tomato growth. Better nutrient uptake by increasing the root number in seedlings treated with Ta enhances the physiological processes in tomato seedlings, thereby leading to good growth performance.

It is well illustrated that drought stress inhibits the photosynthetic pigments in plant species. A decrease in the chlorophyll concentration under drought stress has been considered to be one of the main symptoms of oxidative injury; it might be a result of photo-oxidation and degradation of the pigment. Similarly, the loss of chlorophylls under water stress is the primary cause of photosynthesis inactivation [7]. Carotenoids, on the other hand, exert an antioxidant capacity and provide photoprotection to chlorophylls with ROS scavenging potential [22]. Therefore, a reduction in carotenoid content following drought stress results in the ROS overproduction. Indeed, it is clear that total chlorophyll and carotenoid contents were negatively affected by drought stress in the present work. However, less reduction in pigment contents was found in Ta-colonized tomato seedlings. This data is consistent with the experiments of [23] who demonstrated increased chlorophyll content in the drought tolerant, *T. hamatum DIS* 219b-colonized plants. Additionally, Harman et al. [24] proved that *T. harzianum (T22)* improved leaf greenness in

maize, which in turn makes more energy and carbon source to available for plant growth. Similar to the report of Harman et al. [24], our data indicated that the local isolate, Ta may lead to improved nutrient bioavailability by increasing the capacity of solubilization and/or chelation of essential minerals. Thus, pigment synthesis might be enhanced in tomato seeds inoculated with Ta. On the other hand, it is considered that *Trichoderma* genus plays a key role in releasing some metabolites analogous to phytohormones that balance growth under drought stress [25]. Based on the above information, we may conclude that increased pigment content after Ta colonization of tomato seedlings might be due to the production of some hormone or hormone-like metabolites, such as cytokinine-like molecules, e.g., zeatin, and gibberellins-related compounds that contribute to the protection of chlorophyll degradation.

Our data demonstrated that the MDA content significantly increased in the drought-stressed tomato seedlings as compared to control. However, a decrease in MDA concentration was detected in Ta-treated tomato seedlings. Based on the presented results, we may conclude that Ta inoculation abrogated the effects of lipid peroxidation and protected the tomato seedlings from oxidative injury. Moreover, root colonization by Ta increased the antioxidant enzyme activities that mitigate the ROS attacks on membranes, thereby decreasing the rate of lipid oxidation. It has also been proved that *Trichoderma* upregulates the expression of stress-related proteins, such as glutathione S-transferase (GST), glutathione-dependent enzymes (formaldehyde dehydrogenases), which may lead to the decrements in the MDA content [20]. Our data are compatible with the data obtained from chickpea, exhibiting greater MDA concentration for non-inoculated plants than *Trichoderma*-inoculated ones [26].

Drought stress triggers the generation of ROS such as hydrogen peroxide in the cells. In tomato seedlings, drought stress triggered the accumulation of H_2O_2. However, Ta-treated seedlings exhibited low levels of H_2O_2 in the present study, which might provide protection against H_2O_2 accumulation by increasing its scavenging or avoiding its production under drought stress. The decrease found in H_2O_2 levels following Ta colonization corroborates with the conclusion of Shukla et al. [21] in rice plants. Furthermore, when ROS is generated, detoxifying enzymes act as defense molecules and reverse the impact of oxidative damage with the help of *Trichoderma* [21]. Similarly, Hajiboland et al. [27] demonstrated that tomato seedlings with arbuscular mycorrhizal fungi (AMF) performed better in terms of H_2O_2 accumulation, and in turn, mitigated the oxidative damage as compared to non-mycorrhizal plants.

The avoidance of oxidative damage has been reported as one of the vital processes of stress tolerance, and this type of protection mechanism is attributed to an improved antioxidant capacity within the cell. The findings from the present study demonstrated that drought stress induced higher levels of SOD, GPX, CAT, and APX activities in tomato seedlings than in the controls. Furthermore, root colonization by Ta resulted in a higher increase in the antioxidant enzyme activities of tomato seedlings, which is in accordance with the data of Mastouri et al. [4] who demonstrated the role of T. harzianum T22 in tomato plants in mitigating water stress by an anti-oxidative defense system. The detoxification enzymes might be H_2O_2 scavengers, thereby preserve the membrane integrity [21]. Our results suggested that the coordination of CAT, GPX, and APX activities along with SOD activity played a central protective role in the H_2O_2 scavenging process in tomatoes treated with Ta. The higher antioxidant enzyme activities by Ta coincided with a decrease in the concentration of H_2O_2, suggesting that root colonization by Ta improved the potential capability of tomatoes to scavenge H_2O_2 via the upregulation of antioxidant enzymes under drought stress. However, the difference in the levels of antioxidant activity in colonized and uncolonized tomato seedlings explains the ability of colonized plants to maintain a redox potential higher than the unstressed seedlings [4].

CONCLUSIONS

Soil environment is really complex and the interaction between plant and beneficial organisms living in the soil is of great importance

in adapting plants to adverse abiotic stress conditions. From our data, it is clear that drought stress has been found to induce deleterious effects on tomato seedlings. However, Ta, as a seed inoculant, was found to mitigate the hazardous effects of drought. Root colonization by Ta restored the pigment contents and decreased the level of both MDA and H_2O_2 accumulation. Antioxidant enzyme activity, including SOD, GPX, CAT, and APX, was triggered by drought stress, as expected. However, root colonization by Ta further enhanced the activities of these enzymes, thereby protecting the tomato seedlings from further damage. Within this context, the data presented here provides evidence that our local *Trichoderma* fungal strain (Ta) as an organic-based abiotic stress biocontrol agent may be effective against damages induced by drought stress in the cells.

References

1. H.D.V. Saba, M. Manisha, K.S. Prashant, H. Farham, A. Tauseff, *Trichoderma* a promising plant growth stimulator and biocontrol agent, Mycosphere, 3 (2012) 524-531.
2. M. Tucci, M. Ruocco, L.D. Masi, M.D. Palma, M. Lorito, The beneficial effect of *Trichoderma spp.* on tomato is modulated by the plant genotype, Mol. Plant Pathol., 12 (2011) 341-354.
3. M. Farooq, A. Wahid, N. Kobayashi, D. Fujita, S.M.A. Basra, Plant drought stress: effects, mechanisms and management, Agro. Sust. Dev., 29 (2009) 185-212.
4. F. Mastouri, T. Bjorkman, G.E. Harman, *Trichoderma harzianum* enhances antioxidant defense of tomato seedlings and resistance to water deficit, Mol. Plant-Microbe Interact. J., 25 (2012) 1264-1271.
5. N.S. Guler, N. Pehlivan, S.A. Karaoglu, S. Guzel, A. Bozdeveci, *Trichoderma atroviride* ID20G inoculation ameliorates drought stress-induced damages by improving antioxidant defence in maize seedlings, Acta Physiol. Plant., 38 (2016) 132.
6. G.E. Harman, Overview of mechanisms and uses of *Trichoderma* spp. Phytopathol., 96 (2006) 190-194.
7. N. Shukla, R.P. Awasthi, L. Rawat, Seed biopriming with drought tolerant isolates of *Trichoderma harzianum* promote growth and drought tolerance in *Triticum aestivum*, Annals Appl. Biol., 66 (2015) 171-182.
8. F.A.O. (2015). http://www.fao.org/faostat/en/#data/QC/visualize. [accessed December 2015]
9. H.T. Aldrich, K. Salandanan, P. Kendall, M. Bunning, F. Stonaker, O. Kulen, C. Stushnoff,. Cultivar choice provides options for local production of organic and conventionally produced tomatoes with higher quality and antioxidant content, J. Sci. Food. Agric., 90 (2010) 2548-2555.
10. S.A. Karaoglu, S. Ulker, Isolation, identification and seasonal distribution of soilborne fungi in tea growing areas of Iyidere-Ikizdere vicinity (Rize-Turkey), J. Basic Microbiol., 46 (2006) 208-218.
11. D.I. Arnon, Copper Enzymes in Chloroplasts, Polyphenoloxidase in *Beta vulgaris*, Plant Physiol., 24 (1949) 1-15.
12. E.M.J. Jaspars, Pigmentation of tobacco crown-gall tissues cultured in vitro in dependence of the composition of the medium, Physiol. Plant., 18 (1965) 933-940.
13. R.L. Heath, L. Packer, Photoperoxidation in isolated chloroplast, I. Kinetics and stochiometry of fatty acid peroxidation, Arc. Biochem Biophys., 125 (1968) 189-198.
14. V. Velikova, I. Yordanov, A. Edreva, Oxidative stress and some antioxidant systems in acid rain-treated bean plants, protective role of exogenous polyamines, Plant Sci., 151 (2000) 59-66.
15. M.M. Bradford, A rapid and sensitive method for the quantitation of microgram quantities protein utilizing the principle of protein-dye binding, Anal. Biochem., 72 (1976) 248-254.
16. C. Beauchamp, I. Fridovich, Superoxide dismutase: improved assays and an assay applicable to acrylamide gels, Anal. Biochem., 44 (1971) 276-287.
17. H. Urbanek, E. Kuzniak-Gebarowska, K. Herka, Elicitation of defense responses in bean leaves by *Botrytis cinerea* polygalacturanase, Acta. Physiol. Plant., 13 (1991) 43-50.
18. H.E. Aebi, Catalase, (Ed: Bergmeyer HU), Methods of Enzymatic Analysis. 3rd edn. Verlag Chemie, Weinheim, Florida, (1983) 273-286.
19. Y. Nakano, K. Asada, Hydrogen peroxide is scavenged by ascorbate-specific peroxidase in spinach chloroplasts, Plant Cell Physiol., 22 (1981) 867-880.
20. A. Hashem, E.F. Abd Allah, A.A. Alqarawi, A. Asma, A.A. Al-Huqail, D. Egamberdieva, Alleviation of abiotic stress in *Ochradenus baccatus (Del.) by Trichoderma hamatum* (Bonord.) Bainier, J. Plant Interact., 9 (2014) 857-868.
21. N. Shukla, R.P. Awasthi, L. Rawat, J. Kumar,. Biochemical and physiological responses of rice (*Oryza sativa* L.) as influenced by *Trichoderma harzianum* under drought stress, Plant Physiol. Biochem., 54 (2012) 78-88.
22. R.K. Behera, PC. Mishra, N.K. Choudhary, High irradiance and water stress induced alterations in pigment composition and chloroplast activities of primary wheat leaves, J. Plant Physiol., 159 (2002) 967-973.
23. H. Bae, R.C. Sicher, M.S. Kim, S.H. Kim, M.D. Strem, RL. Melnick, BA. Bailey, The beneficial endophyte *Trichoderma hamatum* isolate DIS 219b promotes growth and delays the onset of the drought response in *Theobroma cacao*, J. Exp. Bot., 60 (2009) 3279-295.
24. G.E. Harman, C.R. Howell, A. Viterbo, I. Chet, *Trichoderma* spp.: opportunistic avirulent plant symbionts, Nature Rev., 2 (2004) 43-56.
25. A. Martı´nez-Medina, M.D.M. Alguacil, J.A. Pascual,

S.C.M. van Wees, Phytohormone profiles induced by *Trichoderma* isolates correspond with their biocontrol and plant growth-promoting activity on melon plants, J. Chem. Ecol., 40 (2014) 804-815.

26. L. Rawat, Y. Singh, N. Shukla, J. Kumar, Salinity tolerant *Trichoderma harzianum* reinforces NaCl tolerance and reduces population dynamics of *Fusarium oxysporum f.sp. ciceri* in chickpea (*Cicer arietinum* L.) under salt stress conditions, Arch. Phytopath. and Plant Protect., 146 (2013) 1442-1467.
27. R. Hajiboland, N. Aliasgharzadeh, S.F. Laiegh, C. Poschenrieder, Colonization with arbuscular mycorrhizal fungi improves salinity tolerance of tomato (*Solanum lycopersicon* L.) plants, Plant Soil., 331 (2012) 313-327.

Development of MIP-based QCM Sensors for Determination of Hyaluronic Acid (HA)

Hiyalüronik Asit (HA) Tayini İçin MIP Temelli QCM Sensörler Geliştirilmesi

Research Article

Sibel Emir Diltemiz
Anadolu University, Faculty of Science, Chemistry Department, Eskişehir, Turkey.

ABSTRACT

In this study, quartz crystal microbalance (QCM) based recognition systems have been developed for the determination of hyaluronic acid (HA). For this purpose, firstly; N-methacryloyl-l-tyrosine (MAT), MAT-D-Glucuronic acid (MAT-D-GA) and MAT-Cu(II)-D-Glucuronic acid (MAT-Cu(II)-D-GA) pre-organized monomers have been synthesized, and characterized. Then, D-glucuronic acid active sites of HA biomacromolecule have been imprinted on QCM sensor surface to create HA selective binding sites. In the last step, the binding interactions, usabilities in recognition and determination of prepared sensors have been investigated.

Key Words
Hyaluronic acid, MIP-QCM, mıp, quartz crystal microbalance, molecularly ımprinted polymers.

ÖZ

Bu çalışmada, hyalüronik asit (HA) tayini için kuvarz kristal mikrobalans (QCM) temelli tanıma sistemleri geliştirilmiştir. Bu amaçla, öncelikle N-metakriloil-1-tirosin (MAT), MAT-D-Glukoronik asit (MAT-D-GA) ve MAT-Cu(II)-D-Glukorkonik asit (MAT-Cu(II)-D-GA) ön-organize monomerleri sentezlenmiş ve karakterize edilmiştir. Ardından, HA biyomakromolekülünün D-glucoronic asit aktif bölgeleri, HA molekülüne seçici bağlanma bölgeleri oluşturmak için QCM sensor yüzeyinde baskılanmıştır. Son adımda, elde edilen sensörlerin bağlanma etkileşimleri, tanımlama ve tayinde tekrar kullanılabilirlikleri incelenmiştir.

Anahtar Kelimeler
Hyalüronik asit, kuvars kristal mikroterazi, QCM-MIP, MIP, moleküler baskılı polimerler.

Article History: Received: Nov 30, 2017; Revised: Jan 23, 2018; Accepted: Feb 22, 2018; Available Online: Mar 26, 2018.

DOI: 10.15671/HJBC.2018.235

Correspondence to: S. Emir Diltemiz, Anadolu University, Faculty of Science, Chemistry Department, Eskişehir, Turkey.
Tel: +90 222 335 05 80 Fax: +90 222 220 49 10 E-Mail: semir@anadolu.edu.tr

INTRODUCTION

Hyaluronic acid (HA) is a high-molecular-mass polysaccharide polymer that form by β-(1,4) and β-(1,3) glycosidic linking of D-glucoronic acid and N-Acetyl glycosamine groups. Chemically, called glycosminoglycans, its connective tissue is the only and simplest member of protein groups which not contain sulfate [1,2]. The general formula of HA is $C_{14}H_{20}NNaO_{11}$, it can be found in different type of sodium salts that vary by source, isolation procedure and defining methods [3]. HA is one of the most important components of epithelia and nervous tissue and can be found in various region of human body such as synovial liquid, extracellular matrix of connective tissue, eye liquid, hyaline cartilage, joint liquids, dermis, epidermis and umbilical cord. It plays a critical role in fulfilling of rheological, physiochemical and biological functions. HA also plays an important role in tissue's hydration and moisturizing, cell's moving, differentiation and division, joint lubricity, transport of matter from tissues and is used in wound treatment. Due to these beneficial functions, HA is used in orthopedics, rheumatology, ophthalmology, dermatology and cosmetology [4–7].

When comparing with other natural and synthetic polymers, HA has much more water absorption capacity, nearly thousand times more from own weight [8]the hyaluronan synthase (HAS. This water absorption capacity helps important biological functions (eg. supplying of food, removing of residues) of cells that have not direct blood supply such as cartilage cells [9–11]. Due to its' shape and structure protection capability where injected without deformation for a long time, HA serves as the most preferable filling material. Carboxylic acid and hydroxyl groups that found in the structure of HA are the target locations for chemical modifications [5,12]. HA derivative biomaterials can be produced by these target locations. High bio compatibility and its' abundance in tissues' extracellular matrix made HA very popular for biomaterial frame material in tissue engineering studies [7,13]. Besides, HA is used as tumor markers in prostate and breast cancer diagnosis and treatment [14,15]. HA is also used in cosmetic industry for reducing age dependent wrinkles by using as filling material and skin care products due to its' moisturizing effect [16,17]. Generally, the high-performance liquid chromatography (HPLC) (direct UV and mass spectrometry detection, and indirect fluorescence detection after derivatization) based studies had been used for determination of HA in the literature [18-20]. Also capillary electrophoresis (CE), and multi-angle laser light scattering combined with size-exclusion chromatography (SEC-MALLS) methods were applied to determine of HA [21-22].

Molecular imprinting technology is a unique polymerization system to create recognition sites to target molecule [23–25]. In this method, target molecule is polymerized using monomers, which have specific binding sites to target molecule, cross-linker, which is suitable for monomer-target molecule interaction kind, and initiator. After removal of target molecule from the polymer structure, remaining cavity has specific shape and binding sites and this cavity can be interact with target molecule even in high interference media [26]. Therefore, Molecularly Imprinted Polymers (MIPs) called "artificial antibodies", have ability to bind target compound by their 3-D shape [27,28]. Also, MIPs are very useful to create recognition layer on the Quartz Crystal Microbalance (QCM) sensor systems [29,30]. The change in the mass due to binding of the target molecule to the binding sites on the QCM makes it possible to determine the analyte at the nano-gram level by correlating with the frequency. MIP based QCM studies exhibit wide potential use because of stability in extreme environmental conditions and cheap and easy synthesis [31].

In this study, a novel sensor system was developed for determination of HA level which is very important for living organisms. Nowadays; biotechnology, sensor systems based on nanotechnology platform technology, isolation and production of new biomaterials are also being studied extensively and accepted as priority areas for the country's economy. By accounting these factors, this study aims preparation of QCM crystals that have glucuronic acid memories for new generation biosensor systems which have mimic sites for recognition of HA bio molecule, determination of binding efficiency and finally HA determination from aqueous samples. The molecular imprinting of larger molecules like bio-

molecules has shown limited success because of their large molecular size, conformational complexity and flexibility. So in this study, these disadvantages were overcome by using a short glucuronic acid that represents an exposed fragment of the target HA as a template. This imprinting method could open a new way to prepare imprinted polymers for the recognition of various kinds of unknown or unidentified bio-molecules, if small parts of bio-molecules could be known.

MATERIALS and METHODS

The N,N'-Methylenebisacrylamide (N,N´-MBAA) and initiator ($Na_2S_2O_5/K_2S_2O_8$) were purchased from Fluka AG (Buchs, Switzerland). HA, D-Glucuronic acid and 2-Propene-1-thiol were obtained from Aldrich (Milwaukee, WI, USA). All other chemicals and bio-chemicals were of analytical grade purity and obtained from Merck AG (Darmstadt, Germany). All glassware was extensively washed with dilute nitric acid before use. All water used in the experiments was purified using a Barnstead (Dubuque, IA) ROpure LP® reverse osmosis unit with a high flow cellulose acetate membrane (Barnstead D2731) followed by a Barnstead D3804 NANO pure® organic/colloid removal and ion exchange packed-bed system. The conductivity of pure water obtained was 18 megaohmcm^{-1}.

For the characterization of the prepared monomers, "JASCO FTIR 300E" spectrometer was used for FTIR analysis. pH measurements were made by WTW Series InoLab pH730 model pHmeter and AFM images were acquired by Q-Scope 250, Quesant Instruments, CA, USA. Binding events were followed using a Research Quartz Crystal Microbalance (RQCM) with phaselock oscillator, Kynar crystal holder, 100 μL cell volume flow cell, and 1-in., Ti/Au, AT-cut, 5-MHz quartz crystals (all purchased from Maxtek, Inc). The RQCM phase-lock oscillator was provided loading resistance measurements and allowed for the examination of crystal damping resistance during frequency measurements. All measurements were recorded at room temperature. Sensitivity was 56.6 Hz cm^2 μg^{-1} for a 5-MHz crystal. The AFM images of the QCM electrodes, standard silicon cantilevers (Quesant) with a force constant ~ 40 N / m, resonant frequency ~137 kHz, and radius of curvature <10 nm were used. Topography and phase images were simultaneously collected at a scan rate of 2 Hz under ambient laboratory conditions.

Synthesis of N-Methacryloyl-L-Tyrosine Methyl Ester Monomer

For the synthesis [32] of N-methacryloyl-l-tyrosine methyl ester monomer, firstly, methacryloyl benzotriazole (MA-Bt) compound was synthesized. Then, L-Tyrosine (2 g, 11 mmol) was dissolved in 1 M NaOH aqueous solution and the MA-Bt solution in 1,4-dioxane was added slowly into this solution at room temperature. The reaction mixture was stirred at room temperature for 10 min. (the reaction was controlled under UV light in a 1/2 EtOAc/Hexane mixture by thin layer chromatography), extracted with EtOAc (3×50 mL) and the collected water phase was acidified with a 10% HCl solution to pH=6-7. The water phase was evaporated in a rotary evaporator to give 3-(4-hydroxyphenyl)-2-[(2-methacryloyl) amino] propanoic acid (MAT) as a white solid (2.46 g, 90% yield).

Synthesis of Methacryloyltyrosine-D-Glucuronic Acid (MAT-D-GA) Pre-organized Momomer

Methacrylamidotyrosine-D-glucuronic acid monomer [MAT-D-GA] was synthesized by the interaction of methacrylamidotyrosine (MAT), 0.1 mmol monomer and D-glucuronic acid (D-GA), 0.1 mmol compounds (Figure 1) dissolving in dimethylsulfoxide. And then, MAT-D-GA monomer was purified by crystallization with ethanol/ethyl acetate.

Pre-organization of Methacryloyltyrosine-Cu(II)-D-Glucuronic Acid [MAT-Cu-D-GA] Metal-Chelate Momomer

For the synthesis of Methacryloyltyrosine-Cu(II)-D-Glucuronic Acid [MAT-Cu(II)-D-GA] metal-chelate monomer (Figure 2), firstly, MAT-Cu(II) monomer system was prepared. For this purpose, MAT (0.1 mmol) and copper nitrate [$Cu(NO_3)_2.9H_2O$] (0.1 mmol) were dissolved in dimethylsulfoxide, D-GA (0.1 mmol) was added into this solution and stirred for 24 h. And then, [MAT-Cu(II)-D-GA] monomer was purified by crystallization with ethanol/ethyl acetate.

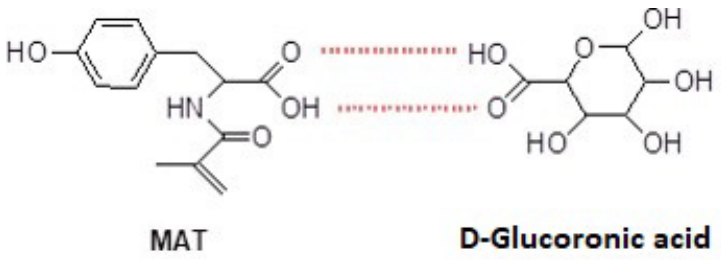

Figure 1. Interaction of MAT and D-GA.

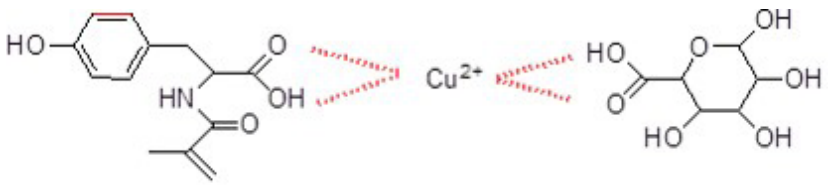

Figure 2. Structure of MAT-Cu(II)-D-GA metal-chelate monomer.

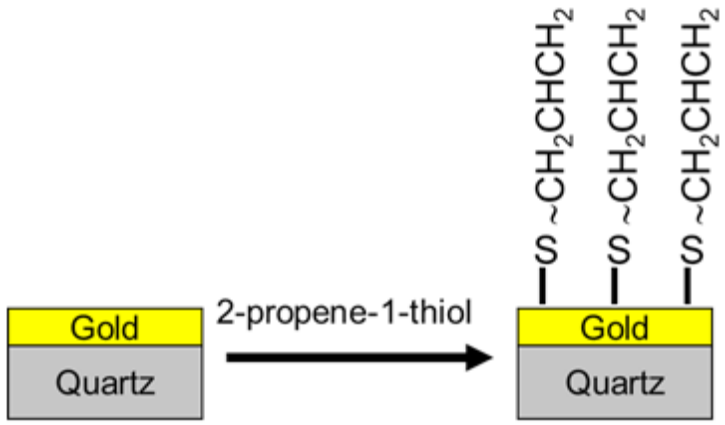

Figure 3. Activation of QCM electrodes with 2-propene-1-thiol.

Activation of QCM Electrodes

The QCM electrode surfaces were cleaned with freshly prepared piranha solution (1:3 30% H_2O_2/concentrated H_2SO_4) for 2 min, then extensively rinsed with Milli-Q water and dried with compressed air just before using. Then, the cleaned QCM electrodes were immersed into 2-propene-1-thiol (0.30 mM in ethanol) for 24 h, in order to introduce thiol groups onto gold surface of QCM electrode. Subsequently, the electrode surfaces were washed with ethanol and then deionized water, to remove excess thiol groups from the surface. Thus, a stable and homogeneous layer was formed on the gold surface (Figure 3).

Preparation of the [MAT-D-GA] and [MAT-Cu(II)-D-GA] Imprinted QCM Electrodes

The reaction mixture containing monomer [MAT-D-GA] (0.25 mmoL), crosslinking monomer (03.75 mmoL, N,N´-MBAA) and initiator ($Na_2S_2O_5$/$K_2S_2O_8$) was prepared, degassed and squeezed on allyl-activated QCM sensors. Polymerization was carried out at room temperature applying UV light irradiation for 4 h under nitrogen atmosphere. The control QCM electrodes that do not have D-GA memories was also prepared for comparison. QCM electrodes were washed with 0.1 M glycine-HCl and phosphate buffer to form D-GA memory. D-GA-imprinted polymer formation and Atomic Force Microscopy (AFM) images of this polymer were shown in Figures 4(a) and (b), respectively.

Preparation of MAT-Cu(II)-D-GA-imprinted QCM electrodes was carried out using the metal-chelate monomer, [MA-Cu(II)-D-GA], as described in previous section. QCM electrodes were washed with 0.1 M glycine-HCl and phosphate buffer to form D-GA memory. Schematic representation

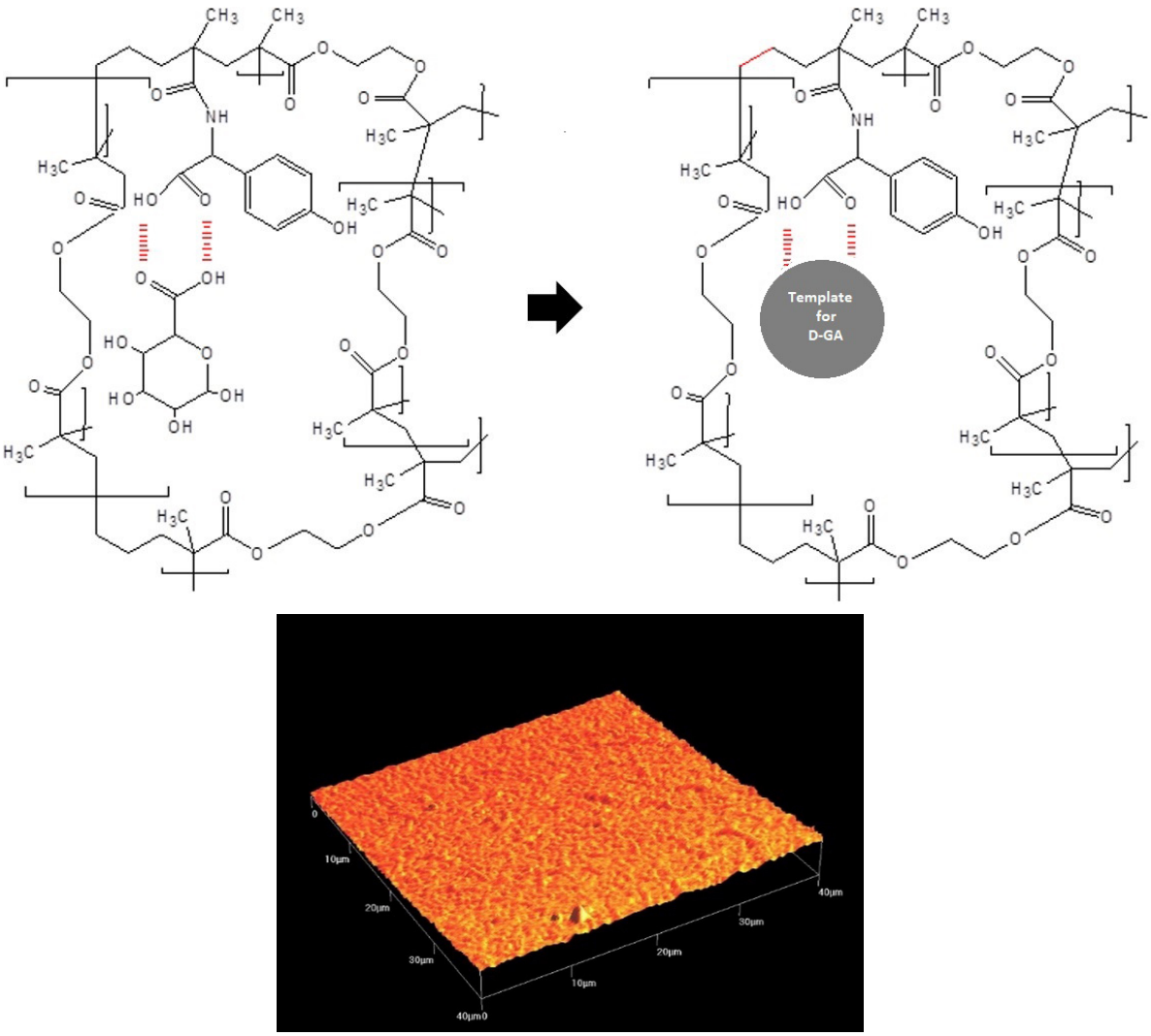

Figure 4. (a) Schematic representation of D-GA template formation on QCM sensors (b) AFM images of the [MA-D-GA] coated QCM electrode surface.

of D-GA-imprinted polymer formation and AFM images of this polymer were shown in Figures 5 (a) and (b), respectively.

Evaluation of QCM-MIP Sensor Response

The D-GA imprinted [MAT-D-GA] and [MAT-Cu(II)-D-GA] coated crystals were mounted in the holder/flow cell, rinsed with pH 7.4 HBS buffer (10 mM HEPES, 150 mM NaCl, 3.4 mM EDTA), and brought to resonance frequency. HA was dissolved in HBS buffer (pH 7.4) to have a concentration in the range of 0-250 mgmL^{-1} and pumped through the flow cell at 0.1 mLmin^{-1}. The frequency of the sensor was monitored until it became stable. The frequency shift for each concentration of HA was determined and the evaluation was performed in triplicate. After each assay, HA was removed from the coating by washing with 0.1 M Glycine-HCl (0.5 mlmin^{-1}, 60 min) and then, three times with HBS buffer. The frequency of the sensor approximately recovered to the value of beginning resonant frequency.

RESULTS and DISCUSSION

Characterizations of Pre-Organized [MAT-D-GA] and [MAT-Cu(II)-D-GA] Monomers

[MAT-D-GA] and [MAT-Cu(II)-D-GA] molecularly imprinted polymers were characterized with FT-IR and Raman spectrometer before and after washing with 0.1 M glycine-HCl buffer. The FT-IR bands that were observed at 809-951 cm^{-1} aliphatic -CH stretching, 1305 cm^{-1} aliphatic -OH

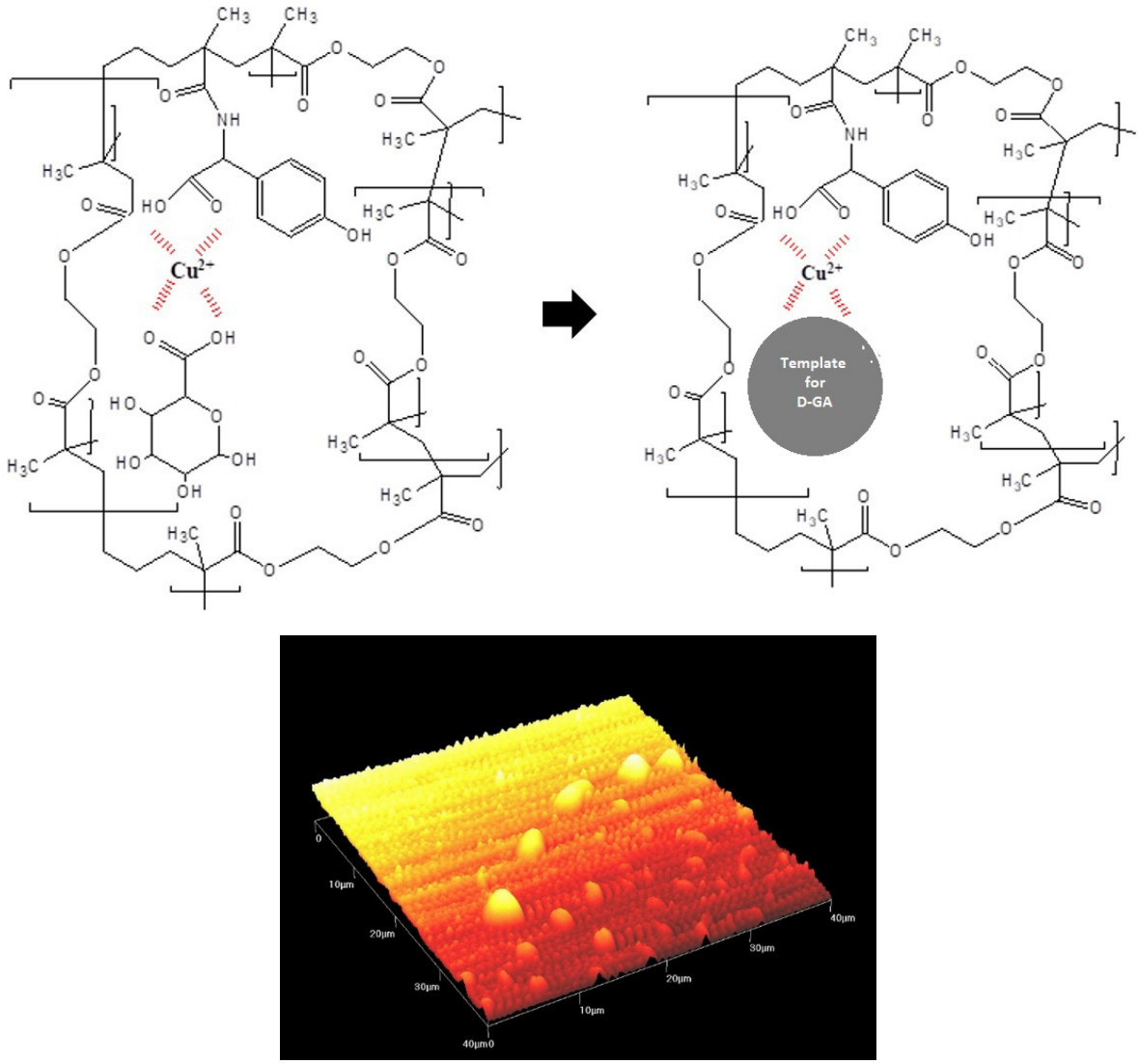

Figure 5. (a) Schematic representation of D-GA template formation on QCM sensors (b) AFM images of the [MA-Cu(II)-D-GA] coated QCM electrode surface.

bending. The –OH stretching band at 1409 cm^{-1} disappeared and –CH vibration band intensity at 3000 cm^{-1} decreased after removing of D-GA from the polymer structure (Figures 6 a and b).

As seen from Figure 7a and Figure 7b, 809-951 cm^{-1} aliphatic -CH stretching, 1305 cm^{-1} aliphatic -OH bending, 1409 cm^{-1} –OH stretching bands disappeared and 3000 cm^{-1} –CH vibration of D-GA intensity has decreased after removing of D-GA from the [MAT-Cu(II)-D-GA] structure.

Sensor Assembly of [MAT-D-GA] and [MAT-Cu(II)-D-GA] Coated QCM Sensors

We have developed a new method to form allyl based self-assembled monolayer and prepare imprinting polymer on QCM sensors. The binding of HA to the methacryloyl-based polymer on gold quartz crystals caused a mass change, Δm, and reflection in the crystal frequency. The relationship between Δm and the frequency shift can be expressed by the Sauerbrey's equation [33].

The D-GA imprinted [MAT-D-GA] and [MAT-Cu(II)-D-GA] polymers are expected to bind the HA sensing. As seen in Figure 8, the frequency of the [MAT-D-GA] (Figure 8a) and [MAT-Cu(II)-D-GA] (Fig 8b) coated sensor decreased after pumping the HA solution. In the 0–250 ppm HA concentration range, the MIP coated QCM sensors showed a high frequency change for HA. These

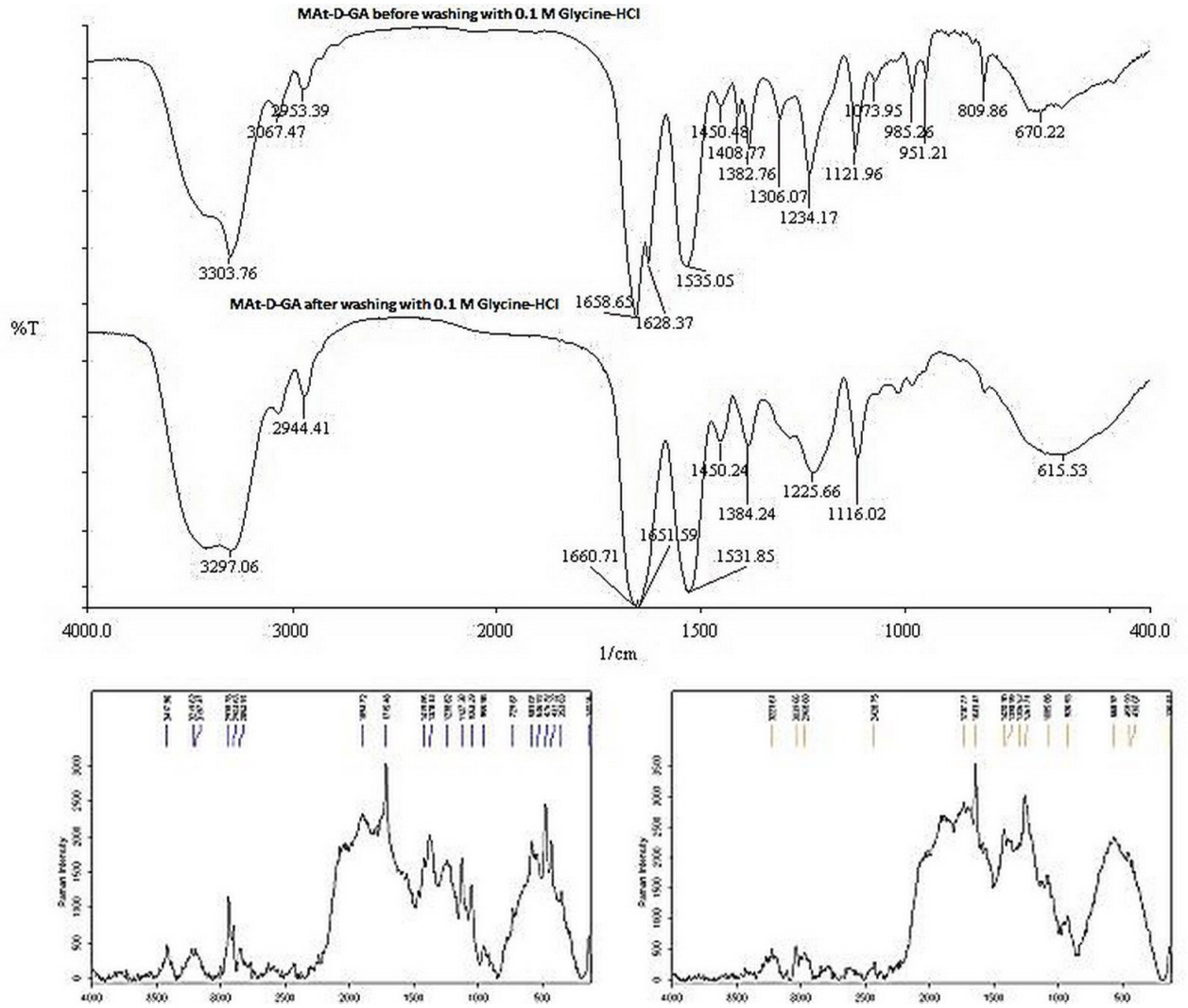

Figure 6. (a) FT-IR and (b) Raman spectra of [MAT-D-GA] polymer.

frequency changes strongly indicated that the HA molecules bound to the imprinted polymeric film on the quartz crystal via D-GA sites. Therefore, the MIP coated QCM sensors have sensitive response to HA due to the imprinting effect. The experiments were performed in replicates of three and the samples were analyzed in replicates of three as well.

Analytical Features of QCM Based HA Imprinted Sensors

Scatchard equilibrium isotherm model was examined to describe the interaction model between D-GA imprinted [MAT-D-GA] and [MAT-Cu(II)-D-GA] coated QCM sensors. Scatchard equation:

$$\frac{Q}{C} = \frac{Q_{maks}}{K_D} - \frac{Q}{K_D}$$

In this equation;

Q : HA concentration of binding polymers

C : Free HA concentration

Q_{maks} : Maximum binding site

K_D : Dissociation rate constant

Figure 9 and Figure 10 showed that mass-frequency relationship and Scatchard graph of [MAT-D-GA] and [MAT-Cu(II)-D-GA] coated QCM sensors. By the results, K_A values were found to be 9.8 and 13.5 μM^{-1} for [MAT-D-GA] and [MAT-Cu(II)-D-GA], respectively. As seen from K_A values, the affinity of the binding sites is strong. This study showed that via imprinting of D-GA which is a small part of HA molecule, was carried out for the determination of HA.

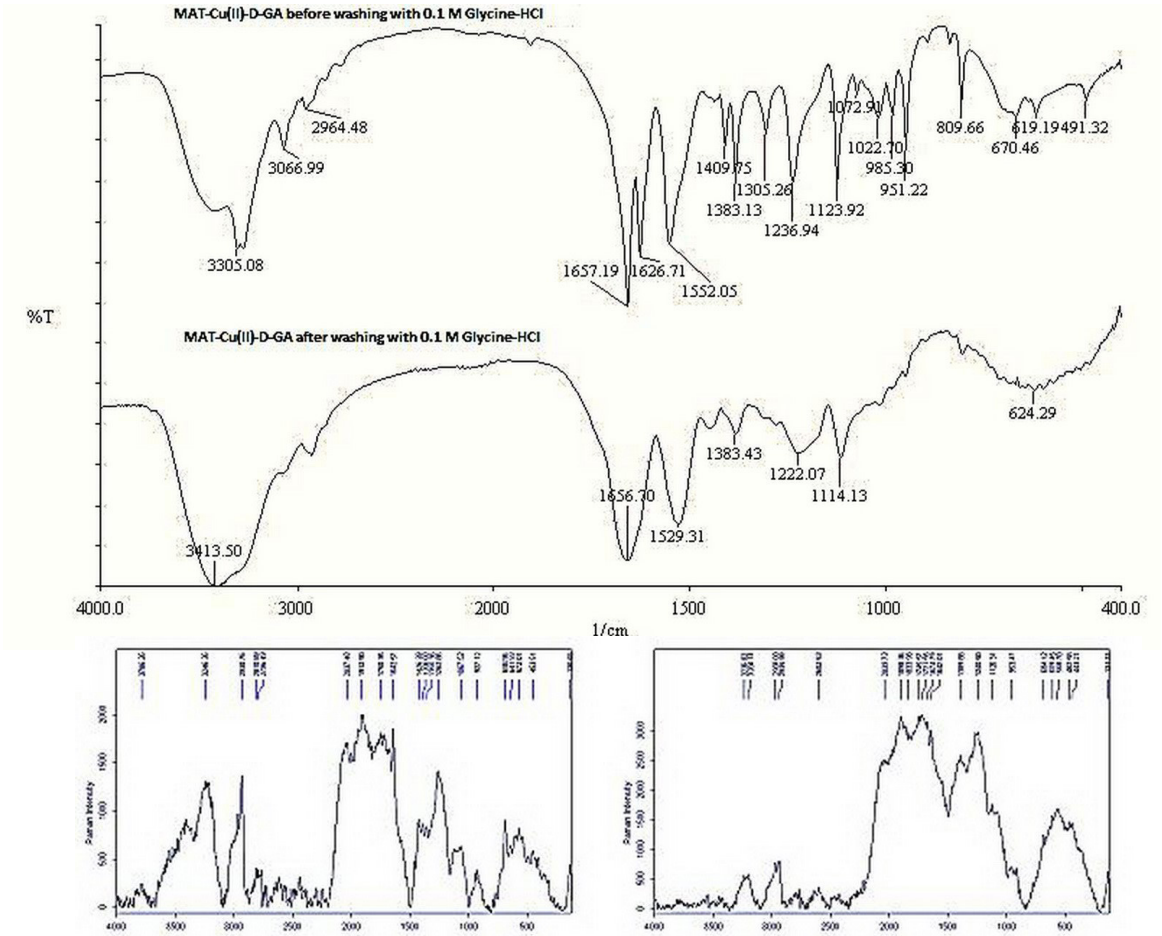

Figure 7. (a) FT-IR and (b) Raman spectra of [MAT-Cu(II)-D-GA] polymer.

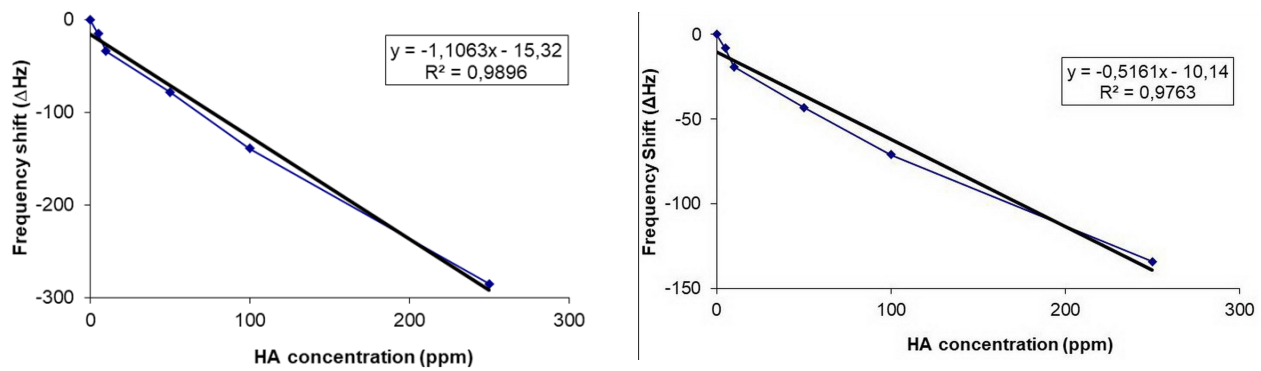

Figure 8. QCM response of (a) [MAT-D-GA] coated sensor (b) [MAT-Cu(II)-D-GA] coated sensor.

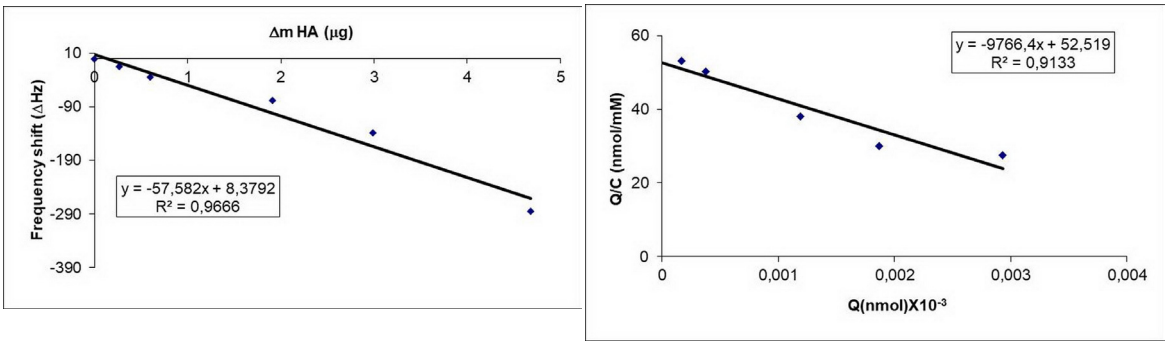

Figure 9. (a) Mass-frequency relationship of [MAT-D-GA] coated QCM sensor (b) Scatchard graph of [MAT-D-GA] coated QCM sensor.

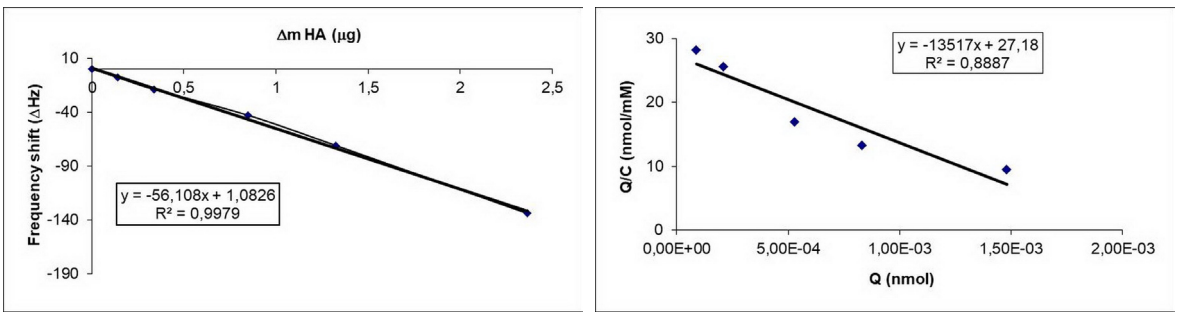

Figure 10. (a) Mass-frequency relationship of [MAT-Cu(II)-D-GA] coated QCM sensor (b) Scatchard graph of [MAT-Cu(II)-D-GA] coated QCM sensor.

Also, two different pre-organized monomer systems were used to determine HA and it can be said that the system which was prepared by using Cu(II) ions monomer provided increase in selectivity due to the strong interaction between Cu(II) ions and amino acid.

CONCLUSIONS

In the work carried out, QCM-based systems which were covered with MIPs for the identification of biologically important biochemical HA were developed. Amino acids are very specific and effective ligands for metal ions and especially numerous studies on complexation of Cu(II) ions by aromatic and aliphatic amino acids indicated an increased complex stability [34–37]leading to a formation of multiple weak interactions around Cu(II. Therefore, in this study two different monomer systems, [MAT-D-GA] and [MAT-Cu(II)-D-GA], were selected and compered for the determination of HA molecule. For this purpose, firstly, MAT monomer and pre-organized monomers were synthesized and characterized by FT-IR and Raman methods. Then, the steps of polymerizing [MAT-D-GA] precursor monomer system and [MAT-Cu(II)-D-GA] metal chelate monomer system on 2-propene-1-thiol activated sensor surfaces under UV light were performed. The binding constants of polymer systems for HA solutions at different concentrations were determined by the measuring frequency shift for polymeric film coated sensors. As a result, K_A values were determined as 9.8 and 13.5 μM^{-1} for [MAT-D-GA] and [MAT-Cu(II)-D-GA], respectively. These values suggested that affinity of the binding sites was very durable as well as biological receptors (0.1–10 μM^{-1}). Also, the system which was prepared using Cu(II) ions monomer provided increase in selectivity because of the strong Cu(II) ions-amino acid interactions. It can be concluded that based on our findings HA was adsorbed onto MIP-QCM sensor system by D-GA unit. Finally, the results showed that MIP-QCM designed for HA purification have high selectivity, low cost and are compatible with biological systems.

References

1. L. Lapcík, L. Lapcík, S. De Smedt, J. Demeester, P. Chabrecek, Hyaluronan: preparation, structure, properties, and applications, Chem. Rev., 98 (1998) 2663-2684.
2. J.R.E. Fraser, T.C. Laurent, U.B.G. Laurent, Hyaluronan: its nature, distribution, functions and turnover, J. Intern. Med., 242 (1997) 27-33.
3. M. Karl, The polysaccharide of the vitreous humor, J. Biol. Chem., 107 (1934) 629-634.
4. T. Luan, Y. Fang, S. Al-Assaf, G.O. Phillips, H. Zhang, Compared molecular characterization of hyaluronan using multiple-detection techniques, Polymer, 52 (2011) 5648-5658.
5. H. Yu, G. Stephanopoulos, Metabolic engineering of Escherichia coli for biosynthesis of hyaluronic acid, Metab. Eng., 10 (2008) 24-32.
6. L. Liu, Y. Liu, J. Li, G. Du, J. Chen, Microbial production of hyaluronic acid: current state, challenges, and perspectives, Microb. Cell Fact., 10 (2011) 1-9.
7. M.N. Collins, C. Birkinshaw, Hyaluronic acid based scaffolds for tissue engineering—a review, Carbohydr. Polym., 92 (2013) 1262-1279.
8. K. Kumari, P.H. Weigel, Molecular cloning, expression, and characterization of the authentic hyaluronan synthase from group C *Streptococcus equisimilis*., J. Biol. Chem., 272 (1997) 32539-32546.
9. Z. Cai, H. Zhang, Y. Wei, F. Cong, Hyaluronan-inorganic nanohybrid materials for biomedical applications, Biomacromolecules, 18 (2017) 1677-1696.
10. T. Luan, L. Wu, H. Zhang, Y. Wang, A study on the nature of intermolecular links in the cryotropic weak gels of hyaluronan, Carbohydr. Polym., 87 (2012) 2076-2085.
11. T. Luan, Y. Fang, S. Al-Assaf, G.O. Phillips, H. Zhang, Compared molecular characterization of hyaluronan using multiple-detection techniques, Polymer (Guildf), 52 (2011) 5648-5658.
12. C. Iavazzo, S. Athanasiou, E. Pitsouni, M.E. Falagas, Hyaluronic acid: an effective alternative treatment of interstitial cystitis, recurrent urinary tract infections, and hemorrhagic cystitis?, Eur. Urol., 51 (2007) 1534-1541.
13. L. Wang, H. Zhang, A. Qin, Q. Jin, B.Z. Tang, J. Ji, Theranostic hyaluronic acid prodrug micelles with aggregation-induced emission characteristics for targeted drug delivery, Sci. China Chem., 59 (2016) 1609-1615.
14. J. Hernandez, I.M. Thompson, Diagnosis and treatment of prostate cancer., Med. Clin. North Am., 88 (2004) 267-79.
15. F. Yu, F. Zhang, T. Luan, Z. Zhang, H. Zhang, Rheological studies of hyaluronan solutions based on the scaling law and constitutive models, Polymer (Guildf), 55 (2014) 295-301.
16. H. Kim, H. Jeong, S. Han, S. Beack, B.W. Hwang, M. Shin, S.S. Oh, S.K. Hahn, Hyaluronate and its derivatives for customized biomedical applications, Biomaterials, 123 (2017) 155-171.
17. L. Sherman, J. Sleeman, P. Herrlich, H. Ponta, Hyaluronate receptors: key players in growth, differentiation, migration and tumor progression, Curr. Opin. Cell Biol., 6 (1994) 726-733.
18. T. Imanari, T. Toida, I. Koshiishi, H. Toyoda, High-performance liquid chromatographic analysis of glycosaminoglycan-derived oligosaccharides, J. Chromatogr. A, 720 (1996) 275-293.
19. A. L. Fluharty, J. A. Glick, N. M. Matusewicz, H. Kihara, High performance liquid chromatography determination of unsaturated disaccharides produced from chondroitin sulfates by chondroitinases, Biochem. Med., 27 (1982) 352-360.
20. M. E. Zebrower, F. J. Kieras, W. T. Brown, Analysis by high-performance liquid chromatography of hyaluronic acid and chondroitin sulfates, Anal. Biochem., 157 (1986) 93-99.
21. M. Kinoshita, H. Shiraishi, C. Muranushi, N. Mitsumori, T. Ando, Y. Oda, K. Kakehi, Determination of molecular mass of acidic polysaccharides by capillary electrophoresis, Biomed. Chromatogr., 16 (2002) 141-145.
22. S. Hokputsa, K. Jumel, C. Alexander, S.E. Harding, A comparison of molecular mass determination of hyaluronic acid using SEC/MALLS and sedimentation equilibrium, Eur. Biophys. J. Biophys. Lett., 32 (2003), 450-456.
23. B.B. Prasad, A. Kumar, R. Singh, Molecularly imprinted polymer-based electrochemical sensor using functionalized fullerene as a nanomediator for ultratrace analysis of primaquine, Carbon, 109 (2016) 196-207.
24. E.B. Özkütük, S.E. Diltemiz, E. Özalp, R. Say, A. Ersöz, Ligand exchange based paraoxon imprınted QCM sensor, Mater. Sci. Eng. C, 33 (2013) 938-942.
25. S.E. Diltemiz, D. Hür, R. Keçili, A. Ersöz, R. Say, New synthesis method for 4-MAPBA monomer and using for the recognition of IgM and mannose with MIP-based QCM sensors, Analyst, 138 (2013) 1558-1563.
26. E. Yilmaz, D. Majidi, E. Ozgur, A. Denizli, Whole cell imprinting based *Escherichia coli* sensors: A study for SPR and QCM, Sens. Actuat. B Chem., 209 (2015) 714-721.
27. M. Karabörk; E. Birlik Özkütük; A. Ersöz; R. Say, Selective Preconcentration of Fe^{3+} Using Ion-Imprinted Thermosensitive Particles Hacettepe J. Biol. Chem., 38 (2010) 27-39.
28. Ç. Çiçek, F. Yılmaz, E. Özgür, H. Yavuz, A. Denizli, Molecularly Imprinted Quartz Crystal Microbalance Sensor (QCM) for Bilirubin Detection, Chemosensors, 4 (2016) 1-13.
29. D. Croux, A. Weustenraed, P. Pobedinskas, F. Horemans, H. Diliën, K. Haenen, T. Cleij, P. Wagner, R. Thoelen, W. De Ceuninck, Development of multichannel quartz crystal microbalances for MIP-based biosensing, Phys. Status Solidi., 209 (2012) 892-899.
30. G. Sener, E. Ozgur, E. Yılmaz, L. Uzun, R. Say, A. Denizli, Quartz crystal microbalance based nanosensor for lysozyme detection with lysozyme imprinted nanoparticles, Biosens. Bioelectron., 26 (2010) 815-821.

31. S. Emir Diltemiz, R. Keçili, A. Ersöz, R. Say, Molecular imprinting technology in quartz crystal microbalance (QCM) sensors, Sensors (Basel), 17 (2017) 454-473.
32. D. Hur, S. Ekti, R. Say, N-acylbenzotriazole mediated synthesis of some methacrylamido amino acids, Lett. Org. Chem., 4 (2007) 585–587.
33. U. Latif, S. Can, O. Hayden, P. Grillberger, F.L. Dickert, Sauerbrey and anti-Sauerbrey behavioral studies in QCM sensors—detection of bioanalytes, Sens. Actuators B Chem., 176 (2013) 825–830.
34. W. Bal, M. Dyba, H. Kozłowski, The impact of the amino-acid sequence on the specificity of copper(II) interactions with peptides having nonco-ordinating side-chains., Acta Biochim. Pol., 44 (1997) 467–476.
35. L. Uzun, R. Uzek, S. Şenel, R. Say, A. Denizli, Chiral recognition of proteins having L-histidine residues on the surface with lanthanide ion complex incorporated-molecularly imprinted fluorescent nanoparticles, Mater. Sci. Eng. C, 33 (2013) 3432-3439.
36. C.L. Gatlin, F. Tureček, T. Vaisar, Gas-phase complexes of amino acids with Cu(II) and diimine ligands. Part I. Aliphatic and aromatic amino acids, J. Mass Spectrom., 30 (1995) 1605–1616.
37. H.A. Akdamar, N.Y. Sarıözlü, A.A. Özcan, A. Ersöz, A. Denizli, R. Say, Separation and purification of hyaluronic acid by glucuronic acid imprinted microbeads, Mater. Sci. Eng. C, 29 (2009) 1404–1408.

Cholesterol Adsorption from Artificial Human Plasma with Molecular Imprinted Polymeric Nanostructures

Moleküler Baskılanmış Polimerik Nanoyapıları ile Yapay İnsan Plazmasından Kolesterol Adsorpsiyonu

Research Article

Tülden Inanan[1,2*] and Nalan Tüzmen[3]

[1]Dokuz Eylul University, The Graduate School of Natural and Applied Sciences, Izmir, Turkey.
[2]Aksaray University, Tech. Voc. Sch. of Higher Education, Dept. of Chem. and Chemical Processing Technology, Aksaray, Turkey.
[3]Dokuz Eylul University, Faculty of Science, Chemistry Division, Izmir, Turkey.

ABSTRACT

This study reports cholesterol adsorption from artificial human plasma using MIP nanostructures prepared with different template:monomer ratios. The adsorption capacity of CP is 19.9% and 16.1% higher than those of C3P and CP3, respectively and adsorption capacity of CP is significantly higher than NIP nanostructures. All selectivity coefficients and relative selectivity values were higher than 1 for artificial human plasma. Under optimum conditions, considerably high cholesterol was adsorbed from hypercholesterolemic plasma (95.33 %).

Key Words
Cholesterol; molecular imprinting; plasma; nanostructures.

ÖZ

Bu çalışma, farklı kalıp-monomer oranları kullanılarak hazırlanmış MIP nanoyapıları ile yapay insan plazmasından kolesterol adsorpsiyonunu sunmaktadır. CP'nin adsorpsiyon kapasitesi C3P ve CP3'e göre sırayla %19,9 ve %16,1 daha yüksektir ve CP'nin adsorpsiyon kapasitesi NIP nanoyapılarına göre önemli derecede yüksektir. Tüm seçicilik katsayıları ve bağıl seçicilik değerleri yapay insan plazması için 1'den büyüktür. Optimum koşullarda, hiperkolesterolemik plazmadan oldukça yüksek kolesterol (%95.33) adsorplanmıştır.

Anahtar Kelimeler
Kolesterol; moleküler baskılama; plazma; nanoyapılar.

Article History: Received: Oct 07, 2017; Revised: Oct 26, 2017; Accepted: Feb 23, 2018; Available Online: Mar 26, 2018.

DOI: 10.15671/HJBC.2018.236

Correspondence to: T. Inanan, Dokuz Eylul University, The Graduate School of Natural and Applied Sciences, Izmir, Turkey.
Tel: +90 382 288 20 21 Fax: +90 382 288 20 99 E-Mail: tkalburcu@gmail.com

INTRODUCTION

Molecular imprinted polymers (MIPs) are multi-purpose synthetic materials which are contemplated with pre-specified selectivity for a target molecule [1-4]. MIPs gain certain interest due to their selectivity to target molecules [5]. In comparison with biological counterparts such as antibodies, enzymes or biological receptors, MIPs have superior advantages: easy to prepare, good physical and chemical stability, economic, and applicability in harsh chemical media without loss of binding features [6-8].

In the preparations of MIPs, firstly functional monomers are arranged around the template and polymerized in the presence of cross-linking agent [7,9]. Covalent [10] or noncovalent interactions [11-13] can be exploited to organize the functional monomers around the template [14]. Recognition and binding properties are influenced by the functional monomers, cross-linker used in polymerization. In addition, cross-linking degree and monomer:template ratio are critical parameters for MIP performance [15-16].

This rapidly developing technique that ensured excellent molecular recognition [17] has potential use in chromatographic separations, [18], sensors [19-21] and several extraction methods [22-23]. Extraction or determination of several molecules by MIPs were applied to environmental samples such as tap, river, well, lake, surface, waste and pond water samples; to biological samples such as urine, plasma, serum, blood and to food matrices such as milk, tomato, egg [24].

Cholesterol is one of the important biological molecule that is precursor of bile acids and steroid hormones. However, high cholesterol levels in blood induce coronary heart disease, arteriosclerosis, myocardial infarction, brain thrombosis, lipid metabolism dysfunction, hypertension, etc [25]. Thus, studies by several methods including physical, chemical, and biomedical approaches [26] had been done for cholesterol removal [27]. Physical methods are based on adsorption by hybrid material [28] supercritical fluid extraction [29], hydrophobic adsorbent [30] and molecular imprinted technique [28, 31-33].

In this study, MIP nanostructures were prepared by surfactant free emulsion co-polymerization using different monomer:template ratios (1:1 [35]; 1:3 and 3:1) and applied for cholesterol adsorption from artificial human plasma. N-Methacryloylamido-(L)-phenylalanine methyl ester (MAPA) and 2-hydroxyethyl methacrylate (HEMA) were used as monomers and ethylene glycol dimethacrylate (EGDMA) and cholesterol were used as the cross-linker and the template, respectively. Pre-polymerization complexes were characterized by FTIR, UV and NMR spectroscopies. After polymerization process, 86% of imprinted cholesterol was removed and removed template was identified by high performance liquid chromatography (HPLC) and FTIR. Cholesterol adsorption onto nanostructures was studied from commercial human plasma by investigating the effects of solvent and dilution ratio. Finally, cholesterol adsorption was applied from hypercholesterolemic plasma.

MATERIALS and METHODS

Materials

HEMA (99%) was supplied from Fluka. Methacyloyl chloride, EGDMA, cholesterol and human plasma were supplied from Sigma. Poly(vinyl alcohol) (PVA, high molecular weight, more than 99%) and potassium persulphate (KPS) were purchased from Merck. All organic solvents were chromatographic- and all other chemicals were analytical-grade. Deionised water was obtained from a Millipore S.A.S 67120 Molsheim-France facility.

Preparation and Characterization of Pre-Polymerization Complexes

The synthesis of MAPA co-monomer was performed in accordance with the method of Say et al. [34]. Pre-polymerization complexes of cholesterol with MAPA were prepared with the template:monomer ratio as 1:1 [35], 1:3 and 3:1; and termed as CP, CP3 and C3P. Cholesterol solution was prepared in THF and mixed with MAPA at room temperature for 3 h in the dark. Preparation procedures of pre-polymerization complexes were summarized in Table 1.

Table 1. Preparation procedures of pre-polymerization complexes.

	CP (1:1)	CP3 (1:3)	C3P (3:1)
CHO	$4.950x10^{-5}$ mol	$4.950x10^{-5}$ mol	$1.485x10^{-4}$ mol
(M_W: 386.7 g/mol-30mg/mL)	638 μL	638 μL	1914 μL
MAPA	4.950×10^{-5} mol	$1.485x10^{-4}$ mol	$4.950x10^{-5}$ mol
(M_W: 234 g/mol-0.34 g/mL)	34 μL	102.2 μL	34 μL

Characterization of pre-polymerization complexes was carried out with UV, NMR, and FTIR spectroscopies. Cholesterol, MAPA and pre-polymerization complexes were scanned to determine maximum wavelengths with UV-spectrophotometer (Schimadzu 1601, Japan). H-NMR spectra of MAPA and pre-polymerization complexes were taken by liquid MERCURYplus-AS 400 with 400 mHz operation frequency. FTIR spectra of cholesterol, MAPA and pre-polymerization complexes were recorded with FTIR spectrophotometer (Perkin Elmer spectrum 100 FT-IR spectrometer) with a universal ATR sampling accessory.

Preparation and Characterization of Cholesterol Imprinted and Non-Imprinted Polymeric Nanopheres

Synthesis of MIP and NIP nanostructures could be summarized as: pre-polymerization complexes were added to stabilizer solution, 0.2775 g PVA in 25 mL water, and suspended for 5 min. HEMA (600 μL) and EGDMA (300 μL) were added as functional monomer and cross-linker, respectively. Finally, KPS (0.0198 g in 45 mL distillated water) was added as the initiator and polymerization mixture was sonicated and mixed to homogenate. After N_2 flow for 5 min, polymerization was initiated at 70°C and shacked at 65 rpm for 24 h in a temperature controlled water bath shaker (GFL 1092). Non-imprinted polymeric (NIP) nanostructures were synthesized by the same method without adding cholesterol into polymerization mixture. Characterization studies such as FTIR analysis, particle size measurement, and scanning electron microscopy (SEM) analysis were performed synthesis and characterization data for MIP with the template:monomer ratio as 1:1 were given in our previous study [35].

Thermal gravimetric (TG) and derivated thermal gravimetric (DTG) curves at the thermal degradation of cholesterol imprinted and non-imprinted polymeric nanostructures were evaluated by an EXSTAR S11 7300 at a heating rate of 10°C/min.

Template Removal Studies

Various template removal solutions were studied for the determination of the most efficient one. Surfactants such as cetyl trimethylammonium bromide (CTAB), sodium dodecyl sulfate (SDS) and triton X-100 (0.00001%), $(NH_4)_2SO_4$ solution (0.1 M) and THF were tested for template removal and performed two times at room temperature by shaking at 225 rpm for 2 h. Cholesterol concentrations of template removal solutions were analyzed with HPLC. Also, template removal supernatants were concentrated under N_2 stream and were analyzed by FTIR spectrophotometer with a universal ATR sampling accessory (Perkin Elmer spectrum 100 FTIR spectrometer).

Cholesterol Adsorption Studies from Artificial Human Plasma

Firstly, adsorption capacities of MIP and NIP nanostructures were identified in methanol. 100 ppm cholesterol solution prepared in methanol was adsorbed onto 1 mg MIP and NIP nanostructures for 30 min (saturation period for adsorption) at room temperature. Polymeric nanostructures were separated by centrifugation at 12000 rpm. Initial and final cholesterol concentrations were determined by HPLC.

Artificial human plasma was used for cholesterol adsorption and different dilution ratios were tested for the determination of matrix effect and dilutions were performed with

50 mM pH 7.4 phosphate buffer and methanol to specify the most appropriate solvent. All diluted plasma solutions were used in cholesterol adsorption studies. Final solutions removed from nanostructures were filtered (0.2 μm Sartorius filter) and analyzed by HPLC. For cholesterol adsorption from hypercholesterolemic plasma, artificial human plasma was diluted with methanol at 1:5 dilution ratio. Then, it was spiked with 1000 ppm CHO solution (prepared in methanol) at 5:9 volume ratio. Initial cholesterol concentration of spiked artificial plasma for hypercholesterolemic plasma experiments was determined as 265 mg/dL. All cholesterol adsorption experiments were performed in three replicates. For each set of data, standard statistical methods were used to determine the mean values and standard deviations. Confidence intervals of 95% were calculated for each set of samples in order to determine the margin of error.

Selectivity Experiments

Selectivity experiments were performed by competitive adsorption of progesterone, testosterone, estrone and estradiol that are the analogues of CHO. Artificial human plasma was spiked with estrone, estradiol, progesterone and testosterone as all components would be at some concentration with CHO.

Cholesterol analogues were quantified by the method of group Navakova with some modification with HPLC. HPLC analyses of estron (E1), estradiol (E2), testosterone (T) and progesterone (P) were perfomed with Thermo Hypersil Gold 150x4.6mm, 5μ column and acetonitrile:methanol:1% acetic acid (40:30:30, v/v/v) as mobile phase at 1.2 mL/min at 30°C [36]. Retention times for E1, E2, T and P at 225 nm were 2.5, 2.7, 3.0 and 4.8 min, respectively. For determination of selectivity, selectivity coefficient and relative selectivity were calculated by using equations below:

$$K_d = (C_i - C_f) / C_f x V/m = Q/C_f \quad (1)$$

where K_d represents the distribution coefficient (mL/g); C_i and C_f are initial and final concentrations of cholesterol (mg/L), respectively. V is the sample volume (L) and m is the nanostructure weight (g).

$$k = K_d(\text{cholesterol})/K_d(X) \quad (2)$$

$$k' = k(MIP)/k(NIP) \quad (3)$$

where k represents selectivity coefficient; X is the cholesterol analogue and k' is relative selectivity.

RESULTS and DISCUSSION

Characterization of Pre-Polymerization Complexes

Complexation between monomers and template molecules has been observed by changes in spectroscopic properties of the complexes. Maximum absorption wavelengths for cholesterol and MAPA were detected as 205 nm and 318 nm, respectively. All pre-polymerization complexes have UV absorption peaks at 310 nm. Shifts observed at the maximum wavelengths of pre-polymerization complexes demonstrated the complexation of cholesterol with MAPA.

FTIR spectra of pre-polymerization complexes were recorded for comparison of incorporation into pre-polymerization complexes and given in Figure 1. Stretching vibrations of O-H and C-O of cholesterol were observed at 3530 cm^{-1} and 1053 cm^{-1}, respectively. An intensive band at 1740 cm^{-1} and a band at 1020 cm^{-1} correspond to C=O and C-O stretching of MAPA, respectively. The peak observed at 750 cm^{-1} was due to aromatic character in MAPA. O-H and C-H stretching (3400 and 2900 cm^{-1}) and C-H bending (1100 cm^{-1}) vibrations of cholesterol were seen in pre-polymerization complexes. Asymmetric C=O stretching vibration (1750 cm^{-1}) of MAPA was also seen in pre-polymerization complexes. On the other hand, the intensities of N-H stretching vibrations of MAPA (3400-3500 cm^{-1}) and O-H stretching vibrations of cholesterol (3400 cm^{-1}) decreased in pre-polymerization complexes. These findings demonstrate the complexation of cholesterol with MAPA. O-H and C-H stretching and C-H bending vibrations were sharper in C3P than the others because of the higher incorporation of cholesterol into pre-polymerization complex structure. Aromatic C=C stretching vibration, seen in both cholesterol and MAPA (sharper), were detected in

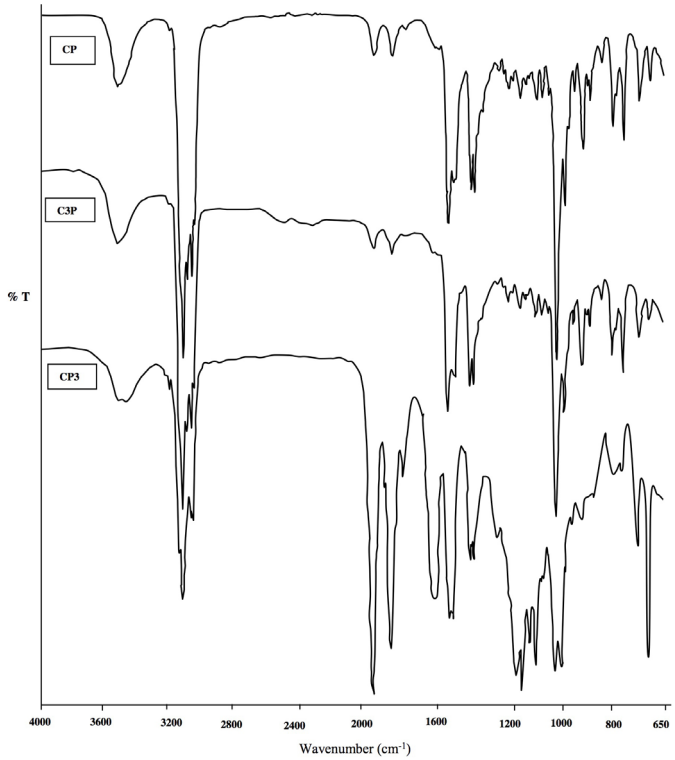

Figure 1. FTIR spectra of pre-polymerization complexes (CP, C3P, CP3).

all pre-polymerization complexes but sharper in CP3. Also, asymmetric C=O stretching vibrations are sharper in CP3 than the others. These findings can be resulted from higher incorporation of MAPA into CP3 pre-polymerization structure.

^{1}H-NMR chemical shift ranges for MAPA in $CDCl_3$ were specified as (ppm) = 1.78 (s, 3H, CH3); 5.32 (s, H, $=CH_2$), 5.57 (s, H, $=CH_2$), 5,62 (s, 1H, CH); 7.17 (d, 1H, ArH); 7.23 (d, 2H, 2xArH); 7.25 (t, 2H, 2xArH), 8.29 (s, 1H, NH)

^{1}H-NMR chemical shift ranges for CP pre-polymerization complex in $CDCl_3$ were specified as (ppm) = 0.86 (d, 6H, $2xCH_3$); 0.91 (d, 3H, CH_3); 1.00 (s, 3H, CH_3); 1.07-1.22 (m, 8H, $4xCH_2$), 1.25 (s, 3H, CH_3); 1.32-1.60 (m, 17H), 1.65 (d, 1H, CH), 1.92 (s, 3H, CH_3); 1.95-2.08 (m, 2H, CH_2); 2.23-2.30 (m, 2H, CH_2); 3.49-3.55 (m, 1H, CH); 3.71 (t, 1H, CH); 3.73 (d, 2H, CH_2); 5.34 (m, 1H, =CH); 7.08-7.12 (m, 2H, 2xArH); 7.23-7.31 (m, 3H, 3xArH).

Shifts (around 7 ppm) belong to aromatic CH protons of MAPA. Proton belonging to C=C of cholesterol is seen at 5.34 ppm. Shifts at 3.71 and 3.73 ppm belong to MAPA. CH proton of polar head of cholesterol is seen around 3.5 ppm. Shifts between 0-2.3 ppm belong to CH, CH_2 and CH_3 protons of cholesterol and CH_3 protons of MAPA. OH proton of cholesterol and -NH proton of MAPA are not seen in H-NMR spectrum of pre-polymerization complex. The absence of these chemical shifts makes us think that interactions between cholesterol and MAPA in pre-polymerization complex occur at these regions. Similar shifts were determined for C3P and CP3 correlatively to the ones of CP. The very few interactions for cholesterol binding are either H-bonding or hydrophobic interactions [37]. Polar chemical groups, such as -OH group inmethanoldo not cause the hydrophobic effect. H-bonding interactions occur in methanol. Thus, it may be concluded that interactions at cholesterol binding to imprinted nanostructures will be H-bonding. It was supposed that binding of several steroids to MIPs were mainly occurred through H-bonding interactions [38]. Consequently, possible interactions between template and functional monomer may be H-bonding.

Characterization of Cholesterol Imprinted Polymeric Nanostructures

TG and DTG curves at the thermal degradation of cholesterol imprinted and non-imprinted polymeric nanostructures were given in Figure 2. As seen in Figure 2, the temperature point for the maximum weight loss based on the curve of DTG was 367, 408, 403 and 364°C for CP (green), CP3 (black), C3P (blue) and NIP (red) nanostructures, respectively. Degradation rates of polymeric nanostructures followed the order NIP > CP3 > C3P > CP. DTG curves of all polymeric nanostructures demonstrated high thermal resistance. At about 200°C, the polymers exhibited an obvious weight loss because of the loss of water or solvent molecules captured in the polymeric nanostructures. Therefore, this temperature was the initial decomposition temperature. In the range of 300-460°C, polymeric nanosheres had two processes of weight loss, which was due to the production of co-polymers between HEMA and MAPA. The results showed that the prepared polymeric nanostructures have good thermal stability [33].

Template Removal Studies

Polymeric nanostructures were washed with methanol and water. Some of cholesterol was removed by ultrasonication effect in methanol washing. Several solutions were tested to remove the residual template from nanostructures.

Total cholesterol removal percentage was increased to 85.8% with THF [35], 70.3% with $(NH_4)_2SO_4$, 76.7% with Triton X-100, 74.7% with SDS, 75.7% with CTAB, and. Most efficient template removal was achieved by ultrasonic effect in MeOH and subsequent THF washings. Cholesterol was removed from all imprinted polymeric nanostructures and then, these nanopheres were washed with water several times to avoid from solvent remnant.

FTIR spectra of removal solution concentrated under N_2 stream (a) and cholesterol standard (b) were matched and all the bands found in standard cholesterol spectrum were determined in the spectrum of removal solution. Shifts seen at some bands and also changes at the intensities of some bands might be due to chemical changes at cholesterol structure in the synthesis of pre-polymerization complexes.

Cholesterol Adsorption Studies from Human Plasma

Adsorption capacities of all imprinted polymeric nanostructures were identified with 100 ppm standard cholesterol in methanol to

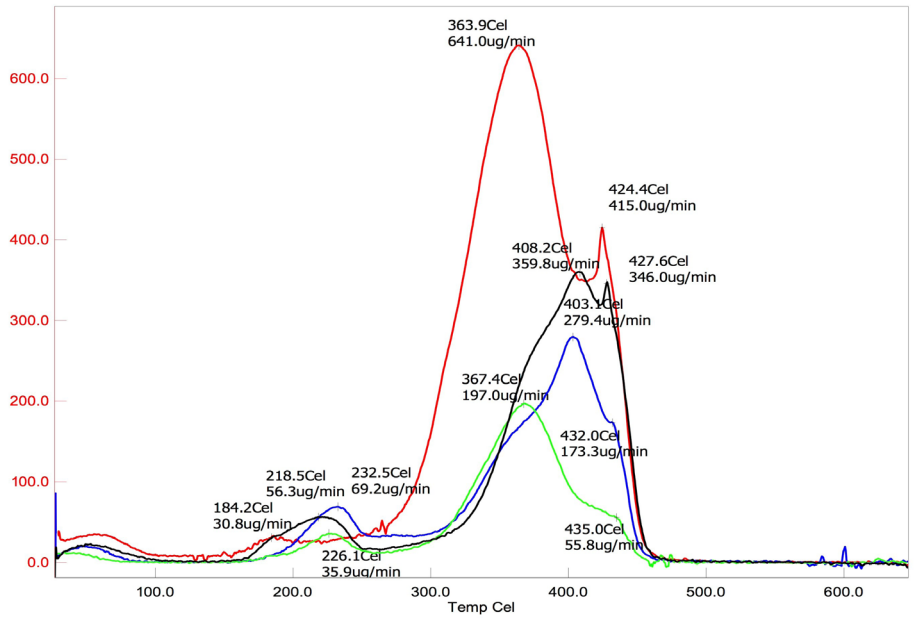

Figure 2. DTG curves of CP (green), CP3 (black), C3P (blue) and NIP (red) nanostructures.

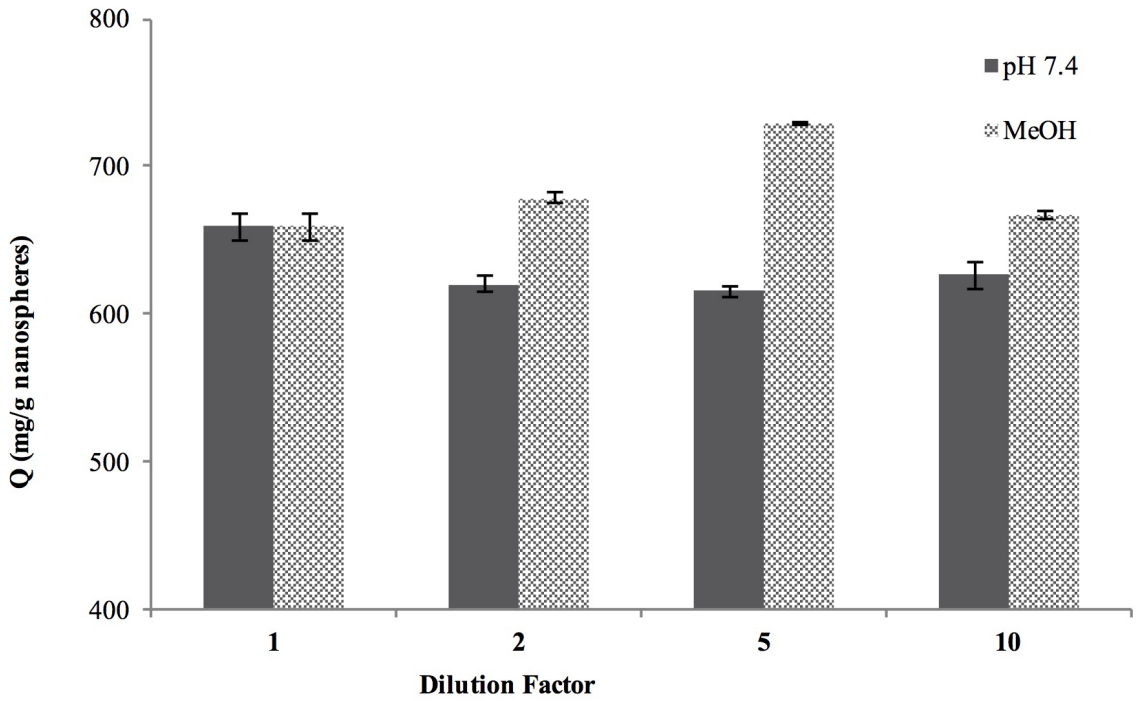

Figure 3. Adsorption capacity of CP nanostructures from artificial human plasma in different dilution solution and ratio (25°C, 225 rpm, 1 mg nanostructures).

determine the effect of monomer:template ratio. Cholesterol adsorption capacities of CP, C3P and CP3 nanostructures were determined as 25.9 [35], 21.6 and 22.3 mg/g nanostructures. The adsorption capacity of CP is 19.9% and 16.1% higher than those of C3P and CP3, respectively. Then, cholesterol adsorption studies were performed with CP nanostructures from artificial human plasma with several dilutions with the 50 mM phosphate buffer (pH 7.4) and methanol to determine the effects of dilution ratios and dilution solutions. Cholesterol adsorption capacity of CP nanostructures from artificial human plasma in different dilution solution and ratio were given in Figure 3.

As seen in Figure 3, adsorption capacity of CP nanostructures was higher with methanol dilution than the one with pH 7.4 phosphate buffer. 1:5 dilution with methanol was the most favorable one and applied in further cholesterol adsorption studies from human plasma. In this optimum conditions, cholesterol adsorption capacities of CP, C3P and CP3 nanostructures were determined and given in Figure 4.

As seen in Figure 4, cholesterol adsorption capacities were detected as 729.4, 693.9 and 715.4 mg/g for CP, C3P and CP3 nanostructures and 647.8 mg/g nanostructures for NIP, respectively. It can be concluded that CP nanostructures are more effective in cholesterol removal from human plasma. This result, compatible with the result from adsorption capacity in methanol, can be concluded that monomer:template ratio 1:1 is more convenient for cholesterol imprinting. The high adsorption capacity of NIP from artificial human plasma was a result of non-specific hydrophobic interactions.

Cholesterol removal percentage of CP nanostructures from hypercholesterolemic plasma was calculated as high as 95.33%. This result clearly shows that these CP nanostructures can be used effectively for cholesterol removal from human plasma.

Selectivity Experiments

Selectivity experiments were performed by competitive adsorption of progesterone, testosterone, estrone and estradiol that are the

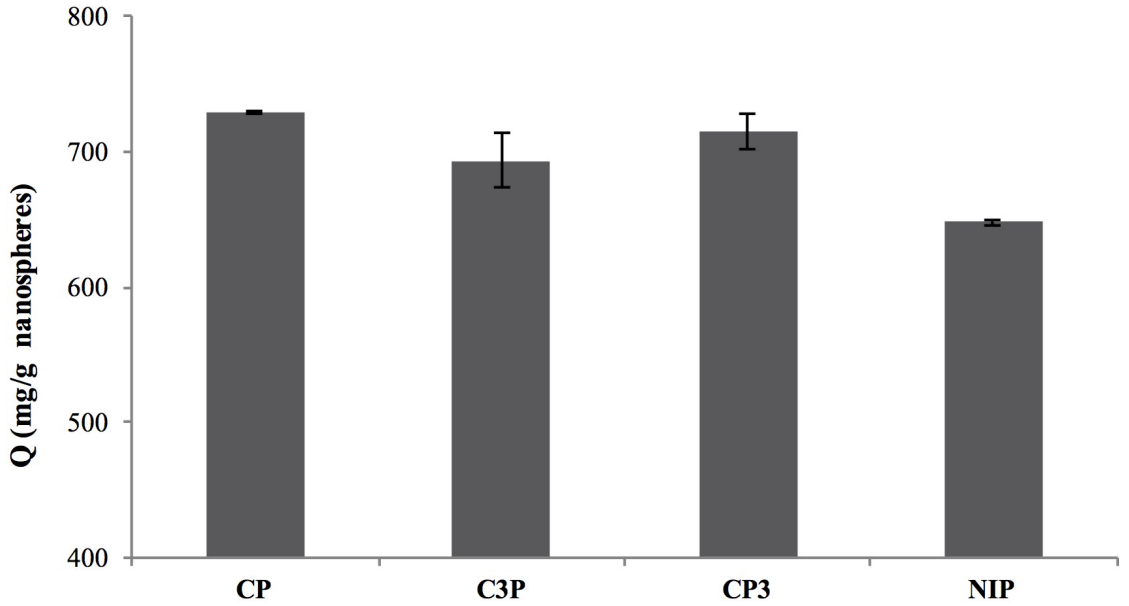

Figure 4. Cholesterol adsorption capacities of CP, C3P and CP3 nanostructures from artificial human plasma (25°C, 225 rpm, 1 mg nanostructures).

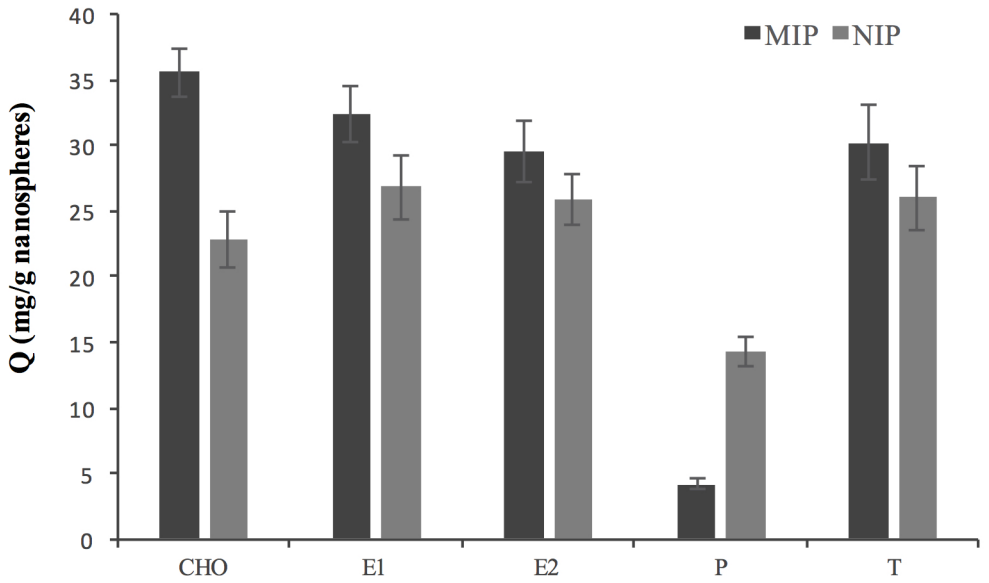

Figure 5. Amount of cholesterol and its analogues adsorbed onto MIP and NIP nanostructures in artificial human plasma (25°C, 225 rpm, 1 mg nanostructures).

Table 2. Selectivity coefficients and relative selectivities for artificial human plasma.

	$k= K_d(CHO)/K_d(x)$	$k'= k (MIP)/k(NIP)$
CHO-E1	1.130	1.377
CHO-E2	1.267	1.480
CHO-T	1.233	1.453
CHO-P	10.781	6.259

Table 3. Comparison of the CHO imprinted nanostructures with the reported adsorbents for cholesterol. removal.

Adsorbents	Removal % or Q (mg/g)	Medium	Ref.
Tetraethyl orthosilicate adsorption coloumn with artificial neural networks (ANN) models	67.8%	Milk	[40]
β-cyclodextrin	95.9%	Milk	[41]
CHO-imprinted poly(GMA-N-methacryloyl-(L)-tyrosine microspheres embedded p(HEMA) cryogels	80% and 42.2 mg/g	Milk and IMS	[42]
Cholesterol imprinted poly(HEMA-N-methacryloyl-(L)-tyrosine methylester)	7.7 mg/g	IMS	[43]
CHO imprinted poly(HEMA-methacryloyloamidotryphan) particles embedded composite membrane	9.24 mg/g	IMS	[44]
Cholesterol imprinted poly(HEMA-N-methacryloyl-(L)- phenylalanine methylester)	11.72 mg/g	IMS	[35]
Co-precipitation, kneading, physical mixture complexation methods with β-cyclodextrin	91.54; 27.85 and 16.81 %	Butter	[45]
β-cyclodextrin immobilized chitosan beads cross-linked with 1,6-hexamethylene diisocyanate	92%	Egg yolk (30-fold diluted)	[46]
Thymus vulgaris L. Powder before and after milling	47 and 38%	Human serum	[47]
CHO imprinted granular polymers by co-polymerization on the surface of selenium nanoparticles	40.2%	Blood plasma	[48]
Random and oriented anti-LDL antibody immobilized p(HEMA) cryogel	111 and 129 mg LDL/g	Hypercholesterolemic plasma	[49]
Cholesterol imprinted solid-phase extraction sorbents with methacrylic acid	92.7 and 91.1% recovery	CHO std. serum and human serum	[50]
Cholesterol imprinted solid-phase extraction sorbents with methacrylic acid	80.4 and 86.6% recovery	Yolk and milk	[50]
Cholesterol imprinted solid-phase extraction sorbents with methacrylic acid	81.4 and 80.1% recovery	Pork and beef	[50]
Cholesterol imprinted poly(HEMA-N-methacryloyl-(L)- phenylalanine methylester)	729.4 mg/g	Artificial human plasma	This work
Cholesterol imprinted poly(HEMA-N-methacryloyl-(L)- phenylalanine methylester)	95.3%	Hypercholesterolemic plasma	This work

analogues of CHO. Artificial human plasma was spiked with estrone, estradiol, progesterone and testosterone as all components would be at some concentration with CHO.

Adsorption of cholesterol and its analogues was performed from plasma to determine the selectivity of MIP nanostructures. Amount of cholesterol and its analogues adsorbed onto MIP and NIP nanostructures were given in Figure 5.

As seen in Figure 5, amount of cholesterol adsorbed onto MIP nanostructures was higher than that of its analogues. For NIP nanostructures, amount of adsorbed estrone (E1), estradiol (E2) and testosterone (T) was higher than that of cholesterol. Using these results, selectivity coefficients and relative selectivity values have been calculated and given in Table 2.

All selectivity coefficients and relative selectivity values for artificial human plasma were higher than 1. These results demonstrate that adsorption of cholesterol onto MIP nanostructures was more selective than NIP nanostructures. Moreover, MIP nanostructures adsorbed cholesterol more selectively than its analogues in artificial human plasma. The relative selectivity value for CHO-P was calculated higher than those values for other analogues.

CONCLUSION

Monomer-template ratio is one of the parameters that are very effective on MIPs' performance [16,28,39]. In this study, cholesterol imprinted polymeric nanostructures were prepared by free surfactant emulsion polymerization with different monomer:template ratios. Characterization studies of pre-polymerization complexes by NMR and FTIR suggested that cholesterol may be complexed with MAPA by H-bonding interactions. Template removal was successfully performed by 85% with methanol and THF. Thermal characterizations proved that imprinted polymeric nanostructures were resistant to high temperatures such as 400°C. Dilution of plasma with methanol 5-times decreases the shielding effect of the plasma medium and increases the removal efficacy greatly. Moreover, notably high cholesterol removal efficacy was achieved by MIP nanostructures from hypercholesterolemic plasma. Cholesterol removal efficiency of MIP nanospheres were compared with reported adsorbents and given in Table 3. Selectivity coefficients indicate that adsorption of cholesterol onto MIP nanostructures was more selective than NIP nanostructures. Relative selectivity values show that MIP nanostructures adsorbed cholesterol more selectively than its analogues in artificial human plasma.

ACKNOWLEDGEMENTS

This study was financially supported by the Scientific Research Projects Coordination of Dokuz Eylül University, Turkey (Project number: 2012-KBFEN-107).

References

1. S.N. Hashim, R.I. Boysen, L.J. Schwarz, B. Danylec, M.T. Hearn, A comparison of covalent and non-covalent imprinting strategies for the synthesis of stigmasterol imprinted polymers, J. Chromatogr. A, 1359 (2014) 35-43.
2. E. Verheyen, J.P. Schillemans, M. Wijk, M.A. Demeniex, W.E. Hennink, C.F. Nostrum, Challenges for the effective molecular imprinting of proteins, Biomaterials, 32 (2011) 3008-3020.
3. M. Behbahani, S. Bagheri, M.M. Amini, H.S. Abandansari, H.R. Moazami, A. Bagheri, Application of a magnetic molecularly imprinted polymer for the selective extraction and trace detection of lamotrigine in urine and plasma samples, J. Sep. Sci., 37 (2014) 1610-1616.
4. C. Lu, H. Li, M. Xu, S. Wang, G. Li, W. Zhong, S.Qin, Preparation of nicotine-imprinted monolith by insitu surface imprinting onto internal hole surface of macroporous silica for selective enrichment and separation of nicotine in environmental water sample, Sep. Sci. Technol., 50 (2015) 2124-2133.
5. J. Ding, F. Zhang, X. Zhang, L. Wang, C. Wang, Q. Zhao, Y. Xu, L. Ding, N. Ren, Determination of roxithromycin from human plasma samples based on magnetic surface molecularly imprinted polymers followed by liquid chromatography-tandem mass spectrometer, J. Chromatogr. B, 1021 (2016) 221-228.
6. X. Xu, S. Liang, X. Meng, M. Zhang, Y. Chen, D. Zhao, Y. Li, A molecularly imprinted polymer for the selective solid-phase extraction of dimethomorph from ginseng samples, J. Chromatogr. B, 988 (2015) 182-186.
7. X. Kong, R. Gao, X. He, L. Chen, Y. Zhang, Synthesis and characterization of the core–shell magnetic molecularly imprinted polymers (Fe_3O_4@MIPs) adsorbents for effective extraction and determination of sulfonamides in the poultry feed, J. Chromatogr. A, 1245 (2012) 8-16.
8. M. Andaç, I.Y. Galaev, A. Denizli, Affinity based and molecularly imprinted cryogels: Applications in biomacromolecule purification, J. Chromatogr. B, 1021 (2016) 69-80.

9. J. Yang, Z. Wang, T. Zhou, X. Song, Q. Liu, Y. Zhang, L. He, Determination of cyproheptadine in feeds using molecularly imprinted solid-phase extraction coupled with HPLC, J. Chromatogr. B, 990 (2015) 39-44.
10. C. Hwang, W.C. Lee, Chromatographic characteristics of cholesterol imprinted polymers prepared by covalent and non-covalent imprinting methods, J. Chromatogr. A, 962 (2002) 69-78.
11. E. Caro, N. Masque, R.M. Marce, F. Borrull, P.A.G. Cormack, D.C. Sherington, Non-covalent and semi-covalent molecularly imprinted polymers for selective on-line solid-phase extraction of 4-nitrophenol from water samples, J. Chromatog. A, 963 (2002) 169-178.
12. F. Lanza, A.J. Hall, B. Sellergen, A. Bereczki, G. Horvai, S. Bayoudh, P.A.G. Cormack, D.C. Sherington, Development of semiautomated procedure for the synthesis and evaluation of molecularly imprinted polymers applied to the search for functional polymers for phenytoin and nifedipine, Anal. Chim. Acta, 435 (2001) 91-106.
13. A. Ersöz, A. Denizli, İ. Şener, A. Atılır, S. Diltemiz, R. Say, Removal of phenolic compounds with nitrophenol-imprinted polymer based on p-p and hydrogen-bonding interactions, Sep. Purif. Technol., 38 (2004) 173-179.
14. R. Say, A. Ersöz, İ. Şener, A. Atılır, S. Diltemiz, A. Denizli, Comparison of adsorption and selectivity characteristics for 4βnitrophenol imprinted polymers prepared via bulk and suspension polymerization, Sep. Sci. Technol., 39 (2004) 3471-3484.
15. E. Yılmaz, K. Mosbach, K. Haupt, Influence of functional and cross-linking monomers and the amount of template on the performance of molecularly imprinted polymers in binding assays, Anal. Commun., 36 (1999) 167-170.
16. C.H. Hu, T.C. Chou, Albumin molecularly imprinted polymer with high template affinity-prepared by systematic optimization in mixed organic/aqueous media, Microchem. J., 91 (2009) 53-58.
17. X. Sun, J. Wang, Y. Li, J. Yang, J. Jin, S.M. Shah, J. Chen, Novel dummy molecularly imprinted polymers for matrix solid-phase dispersion extraction of eight fluoroquinolones from fish samples, J. Chromatog. A, 1359 (2014) 1-7.
18. S. Aşir, D. Sari, A. Derazshamshir, F. Yılmaz, K. Şarkaya, A. Denizli, Dopamine imprinted monolithic column for capillary electrochromatography, Electrophoresis, 0 (2017) 1-10.
19. A.G. Sarıkaya, B. Osman, T. Çam, A. Denizli, Molecularly imprinted surface plasmon resonance (SPR) sensor for uric acid determination, Sens. Actuators B Chem., 251 (2017) 763-772.
20. G. Sener, E. Ozgur, E. Yılmaz, L. Uzun, R. Say, A. Denizli, Quartz crystal microbalance based nanosensor for lysozyme detection with lysozyme imprinted nanoparticles. Biosens. Bioelectron., 26 (2010) 815-821.
21. Y. Saylan, S. Akgönüllü, D. Çimen, A. Derazshamshir, N. Bereli, F. Yılmaz, A. Denizli, Development of surface plasmon resonance sensors based on molecularly imprinted nanofilms for sensitive and selective detection of pesticides, Sens. Actuators B Chem., 241 (2017) 446-454.
22. L.I. Andersson, Molecular imprinting for drug bioanalysis A review on the application of imprinted polymers to solid-phase extraction and binding assay, J. Chromatogr. B, 739 (2000)163-173.
23. E. Turiel, A. Martin-Esteban, Molecularly imprinted polymers for sample preparation: a review, Anal. Chim. Acta, 66 (2010) 887-899.
24. L. Chen, S. Xu, X. Li, Recent advances in molecular imprinting technology: current status, challenges and highlighted applications, Chem. Soc. Rev., 40 (2011) 2922-2942.
25. A. Aghaei, M.R.M. Hosseini, M. Najafi, A novel capacitive biosensor for cholesterol assay that uses an electropolymerized molecularly imprinted polymer, Electrochimica Acta, 55 (2010) 1503-1508.
26. A. Sinha, S. Basiruddin, A. Chakraborty, N.R. Jana, Cyclodextrin functionalized magnetic mesoporous silica colloid for cholesterol separation, ACS Appl. Mater. Interfac., 7 (2015) 1340-1347.
27. Y. Su, Y. Tian, R. Yan, C. Wang, F. Niu, Y. Yang, Study on a novel process for the separation of phospholipids, triacylglycerol and cholesterol from egg yolk, J. Food Sci. Technol., 52 (2015) 4586-4592.
28. D.N. Clausen, I.M.R. Pires, C.R.T. Tarley, Improved selective cholesterol adsorption by molecularly imprinted poly(methacrylic acid)/silica (PMAA–SiO_2) hybrid material synthesized with different molar ratios, Mat. Sci. Eng. C, 44 (2014) 99-108.
29. M.M. Jimenez-Carmona, M.D.L. de Castro, Reverse micelle formation for acceleration of the supercritical fluid extraction of cholesterol from food samples, Anal. Chem., 70 (1998) 2100-2103.
30. E.E.G. Rojas, J.S.D. Coimbra, L.A. Minim, Adsorption of egg yolk plasma cholesterol using a hydrophobic adsorbent, Eur. Food Res. Technol., 223 (2006) 705-709.
31. A. Zengin, E. Yildirim, U. Tamer, T. Caykara, Molecularly imprinted superparamagnetic iron oxide nanoparticles for rapid enrichment and separation of cholesterol, Analyst, 138 (2013) 7238-7245.
32. Y. Tong, H. Guan, S. Wang, J. Xu, J. He, Syntheses of chitin-based imprinting polymers and their binding properties for cholesterol, Carbohyd. Res., 346 (2011) 495-500.
33. R. Gupta, A. Kumar, Synthesis and characterization of sol–gel-derived molecular imprinted polymeric materials for cholesterol recognition, J. Sol-Gel Sci. Technol., 58 (2011) 182-194.
34. R. Say, S. Emir, B. Garipcan, S. Patir, A. Denizli, Novel methacryloylamidophenylalanine functionalized porous chelating beads for adsorption of heavy metal ions, Adv. Polym. Tech., 22 (2003) 355-364.
35. T. Inanan, N. Tuzmen, S. Akgöl, A. Denizli, Selective cholesterol adsorption by molecular imprinted polymeric nanospheres and application to GIMS, Int. J. Biol. Macromolec., 92 (2016) 451-460.
36. L. Navakova, P. Solich, L. Matysova, J. Sıcha, HPLC determination of estradiol, its degradation product, and preservatives in new topical formulation estrogel HBF, Anal. Bioanal. Chem., 379 (2004) 781-787.
37. M.A. Gore, R.N. Karmalkar, M.G. Kulkarni, Enhanced capacities and selectivities for cholesterol in aqueous media by molecular imprinting: role of novel cross-linkers, J. Chromatog. A, 804 (2004) 211-221.
38. X. Li, M. Li, J. Li, F. Lei, X. Su, X. Liu, P. Li, X. Tan, Synthesis and characterization of molecularly imprinted polymers with modified rosin as a cross linker and selective SPE-HPLC detection of basic orange II in foods, Anal. Met., 6 (2014) 6397-6406.

39. H.S. Andersson, J.G. Karlsson, S.A. Piletsky, A.C. Koch-Schmidt, K. Mosbach, I.A. Nicholls, Study of the nature of recognition in molecularly imprinted polymers, influence of monomer–template ratio and sample load on retention and selectivity, J. Chromatogr. A, 848 (1999) 39-49.
40. G.R. Oliveira, A.V. Santos, A.S. Lima, C.M.F. Soares, M.S. Leite, Neural modelling in adsorption column of cholesterol-removal efficiency from milk, LWT- Food Science and Technol., 64 (2015) 632-638.
41. D.K. Lee, J. Ahn, H.S. Kwak, Cholesterol removal from homogenized milk with β-cyclodextrin, J Dairy Sci., 82 (1999) 2327-2330.
42. K. Çaktü, G. Baydemir, B. Ergün, H. Yavuz, Cholesterol removal from various samples by cholesterol-imprinted monosize microsphere-embedded cryogels, Artif. Cells Nanomed. Biotechnol., 42 (2014) 365-375.
43. H. Yavuz, V. Karakoç, D. Türkmen, R. Say, A. Denizli, Synthesis of cholesterol imprinted polymeric particles, Int. J. Biol. Macromol., 41 (2007) 8-15.
44. M. Odabaşı, L. Uzun, G. Baydemir, N.H. Aksoy, Ö. Acet, D. Erdönmez, Cholesterol imprinted composite membranes for selective cholesterolrecognition from intestinal mimicking solution, Colloids Surf. B Biointer., 163 (2018) 266–274.
45. H.M.A.M. Dias, F. Berbicz, F. Pedrochi, M.L. Baesso, G. Matioli, Butter cholesterol removal using different complexation methods with beta-cyclodextrin, and the contribution of photoacoustic spectroscopy to the evaluation of the complex, Food Res. Int., 43 (2010) 1104–1110.
46. S.H. Chiu, T.W. Chung, R. Giridhar, W.T. Wu, Immobilization of b-cyclodextrin in chitosan beads for separation of cholesterol from egg yolk, Food Res. Int., 37 (2004) 217-223.
47. E. Salehi, S. Afshar, M.Z. Mehrizi, A. Chehrei, M. Asadi, Direct reduction of blood serum cholesterol using *Thymus vulgaris* L.: Preliminary biosorption study, Process Bichem., accepted manuscript
48. I. Polyakova, L. Borovikova, A. Osipenko, E. Vlasova, B. Volchek, O. Pisarev, Surface molecularly imprinted organic-inorganic polymers having affinity sites for cholesterol, React. Funct. Polym., 109 (2016) 88-98.
49. N. Bereli, G. Şener, H. Yavuz, A. Denizli. Oriented immobilized anti-LDL antibody carrying poly(hydroxyethyl methacrylate) cryogel for cholesterol removal from human plasma, Mater. Sci. Eng. C, 31 (2011) 1078–1083.
50. Yun S., J.H. Zhang, D.Shi, M. Jiang, Y.X. Zhu, S.R. Mei, Y.K. Zhou, K. Dai, B. Lu, Selective solid-phase extraction of cholesterol using molecularly imprinted polymers and its application in different biological samples, J. Pharm. Biomed. Anal., 42 (2006) 549–555.

The Effects of Juvenile Hormone Analogue, Fenoxycarb on the Last Instar Testes of *Bombyx mori*

Son İnstar *Bombyx mori* Testislerine Juvenil Hormon Analoğu Fenoxycarb'ın Etkileri

Research Article

Gamze Turgay İzzetoğlu[1]*, Asiye Pak[1], Tuğba Zülfikaroğlu[1], Taylan K. Öztürk[2]
[1]Ege University, Faculty of Science, Department of Biology, Section of Zoology, İzmir, Turkey.
[2]Ege University, Faculty of Science, Department of Biochemistry, İzmir, Turkey.

ABSTRACT

The development and metamorphosis of insects is regulated by juvenile hormone (JH) and ecdysone hormone, which are worked antagonist. Fenoxycarb is an effective juvenile hormone analogue on many insects. In this study, the effect of fenoxycarb on the last larval stage *Bombyx mori* testes was investigated. Male larvae on the 6th day of the last instar are divided into 2 groups. 1 ng of fenoxycarb dissolved in acetone was topically applied to larvae in the treatment group and the remaining 18 larvae were used as the control group. Control and treated groups were followed to until pupation from day when they showed cocoon spinning behavior. After dissection, several of testes were entreated routine histological processes and photographed. In treatment group, it was seen that fenoxycarb reduced spermatogonium formation by suppressing ecdysone release and caused a decrease in mature sperm. Remaining testes are used to the analysis of total carbohydrate and glycogen content. In conclusion, fenoxycarb has the reducing effect on spermatogenesis and it can cause to decrease of total carbohydrate content because of stress in insects. These histological and biochemical results may be in support of the use of fenoxycarb as an insect growth regulator (IGR) for harmful insects.

Key Words
Fenoxycarb, histology, spectrophotometry, testis of *Bombyx*.

ÖZ

Böceklerin gelişimi ve başkalaşımı başlıca birbiriyle zıt çalışan juvenil ve ekdizon hormonları tarafından düzenlenir. Fenoxycarb, birçok böcek üzerinde etkili bir juvenil hormon analoğudur. Bu çalışmada, fenoxycarbın son larval evredeki *Bombyx mori* testisleri üzerindeki etkisi araştırılmıştır. Son instar 6. güne ait erkek larvalar 2 gruba ayrılmıştır. Bir gruba 1ng fenoxycarb uygulanmış, geriye kalan larvalar kontrol grubu olarak kullanılmıştır. Kontrol ve uygulama grubu larvalar, koza örme davranışı gösterdikleri günden itibaren pupalaşıncaya kadar takip edilmiştir. Diseksiyon sonrası testislerin bir kısmı rutin histolojik işlemlerden geçirilmiş ve fotoğrafları çekilmiştir. Uygulama grubunda fenoxycarbın ekdizon salınımını baskılayarak spermatogonium oluşumunu azalttığı ve olgun spermlerin azalmasına neden olduğu görülmüştür. Diğer kısmı ise toplam karbohidrat ve glikojen içeriğinin analizi için kullanılmıştır. Sonuç olarak, fenoxycarb spermatogenezi azaltıcı bir etkiye sahiptir ve böcekler üzerinde stres oluşturarak toplam karbohidrat içeriğinin de azalmasını etkileyebilir. Bu histolojik ve biyokimyasal sonuçlar fenoxycarbın zararlı böcekler için böcek büyüme regülatörü (IGR) olarak kullanımını destekleyici nitelikte olabilir.

Anahtar Kelimeler
Fenoxycarb, histoloji, spektrofotometri, *Bombyx* testisi

Article History: Received: Oct 20, 2017; Revised: Feb 19, 2018; Accepted: Mar 03, 2018; Available Online: Mar 26, 2018.

DOI: 10.15671/HJBC.2018.237

Correspondence to: G. Turgay İzzetoğlu, Section of Zoology , Department of Biology, Faculty of Science, Ege University, İzmir, Turkey.
Tel: +90 232 311 1791 Fax: +90 232 388 1036 E-Mail: gamze.turgay@ege.edu.tr

INTRODUCTION

Silkworm *Bombyx mori* (Lepidoptera, Bombycidae), which is a holometabolous insect; pass through a complete metamorphosis including egg, larval, pupal and adult stages [1]. The male reproductive system of silkworms consists of many structures. These are; a pair of testis, a pair of vas deferens and seminal vesicles, a median ejaculatory duct and various accessory glands [2]. The testis is connected to the seminal vesicle and median ejaculatory duct. It is called the vas deferens channel, which connects the testis to the seminal vesicle. Accessory glands, which are usually present in many species, also open to the vas deferens and ejaculatory duct [3].

In Lepidoptera, testis consists of follicles and many testicular tubules. It is a single median organ that is covered with a common peritoneal membrane [2,4]. In each testis follicle a series of stages of development occur. These development stages take place in the growth zone, the maturation zone and the differentiation zone, respectively. When each spermatogonium formed in the germarium is transported to the growth zone, it is introduced into the somatic cell layer forming the cyst. Primary germ cells in the cyst bring about a number of spermatocytes (usually 64 to 256) in mitotic divisions. In the maturation zone, spermatocytes undergo two meiotic divisions, and four haploid spermatids occur from each spermatocyte. In the proximal part of the follicle, the differentiation zone, the spermatids turn into flagellate sperm [2].

Because of the main differences in meiotic division in Lepidoptera, two types of sperm occur. Eupyrene (nucleus) sperms are responsible to fertilize the egg. It has been thought that the apyrene (non-nucleus) sperms have various functions such as helping the seminal vesicles to move the eupyrene sperm from testes, feeding the eupyrene sperm and destroying the sperm from the previous matings [5]. In lepidopterans, apyrene sperm differentiation from eupyrene sperm occurs with exposure to a hemolymph-sourced apyrene spermatogenesis-inducing factor [3]. The sperm are transported to the seminal vesicles for storage by peristaltic movements of the vas deferens from the testis [2].

The development and metamorphosis of insects are under the control of several major hormones. Especially prothoracicotropic hormone (PTTH), ecdysone and Juvenile hormone (JH) play an important role in metamorphosis. Neurosecretory cells that found in the invertebrates brain ganglia secrete PTTH. It is also called the brain hormone. Ecdysone regulates normal molting with JH that is secreted from corpora allata [6]. JH is a multifunctional hormone that plays a role in various physiological events such as molting, metamorphosis, sexual maturation and diapause [7].

The rate of formation of spermatocytes from spermatogonia increases with the level of 20-hydroxyecdysone being high, but high JH values abolish this increase. The spermatocytes then begin dividing meiosis, which is preserved until the end of the larval period. The peak of the 20-hydroxyecdysone inhibits the meiosis and allows to progress metaphase of the cells. In some insects, JH accelerates spermatogenesis [3].

Among the JH analogues that prolong larval life in insects, the most active molecule is fenoxycarb which is O-ethyl N-[2-(4-fenoxy fenoxy) ethyl] carbamate structure [7]. Fenoxycarb that is a synthetically produced insect growth regulator and it has JH activity interferes with development in many insects by disrupting the metamorphosis process. When applied at high doses, the larvae may prolong its larval duration, inhibit molting, or cause it to become dauer (permanent) larvae. Fenoxycarb is one of the most commonly used JH analogues. It is not neurotoxic since it has no anti-cholinesterase activity due to its carbamate structure. It binds to the JH receptor but cannot be destroyed by the JH esterase [8].

The prothoracic gland is inactivated between days 0 and 2 of the 5th larval stage. For this reason, it may secrete ecdysone in response to PTTH from day 3. On the 3rd and 4th days, the ecdysone levels are reduced. The secretory activity starts to increase on the 5th day, and on the 6th day, the first peak occurs of the hormone secretion. Intensive ecdysone release continues on days 7. and 8. on the 9th day, this secretion

makes the second peak. This secretory activity begins to decrease from day 10 [9]. In this study, it was aimed to investigate effects of fenoxycarb on testis and sperm formation in addition total carbohydrate and glycogen content on which day ecdysone activity reach a peak.

MATERIALS and METHODS

Insect Rearing

Bombyx mori hybrid eggs used as study material were obtained from Bursa Kozabirlik. After 10-12 days, larvae that hatched eggs were fed long day period (16 hours light and 8 hours dark). The larvae reared in laboratory conditions at 25±1°C and 75-80% humidity and they were fed on fresh leaves of mulberry trees that present in Ege University Campus three times a day [10,11].

Application of Fenoxycarb

On the 6th day of the last instar, larvae were separated from 50 male larvae which selected by looking at the Herold's gland. 1ng of fenoxycarb dissolved in acetone was applied on 15 larvae topically [12]. The remaining 15 larvae were used as the control group. Control and treated groups were followed up to 1, 2, 3, 4 spin, and 0 pupae until pupation from day when they showed cocoon spinning behavior. Three larvae dissected from every group that was followed. 30 larvae were dissected for preparation. Insect physiological water was used during the dissection in order to kept pH in balance. 20 larvae were dissected for biochemical analyses. Removed testes were kept in -80°C freezer.

Histology

Testes removed from silkworm larvae were fixed in Bouin's solution for 24 hours. Samples were embedded in paraffin. Tissues were sectioned at a thickness of 5-6µ by using the microtome. Mayer's Hematoxylin-Eosin (H&E) was used to stain for tissue section [13,14]. The preparates were photographed using ZEN image analysis software with a Zeiss Axio Scope A1 microscope.

Homogenization

In total 20 larvae were dissected for determination of total carbohydrate content and glycogen. The tissue was weighed and placed in the centrifuge tube with 0.2 ml of sodium sulphate solution (2% aq). 0.8 ml of chloroform and 0.8 ml methanol was stirred in tube and centrifuged at 3000 rpm for 1 min. The supernatant was taken to clean tube. The pellet was used for determination of total glycogen. 0.6 ml of deionized water was added into the supernatant and mixed. Again centrifuged at 3000 rpm for 1 min. The upper fraction was used for determination of total carbohydrate content [15].

Determination of Total Carbohydrate Content

Van Handel (1985) method was used for that process. 750 mg anthrone was dissolved in 150 ml deionized water and 380 ml H_2SO_4. Before determination, standard solutions were prepared 7.5, 15, 25, 50, 100, 200 and 300µl glucose solution (1 mg/ml) in tubes and anthrone reagent was added until the final volume was 5ml. The upper fraction samples were similarly prepared. All of them heated for 17 min at 90-110°C. Let cooled and read at 625 nm.

Determination of Total Glycogen

As determination of total carbohydrate content, standard solutions and pellet samples were also prepared for determination of total glycogen. All of them heated for 17 min at 90-110°C. Let cooled and read at 625 nm [15].

RESULTS

The control group silkworms showed spinning behavior as expected on the 7th and 8th day of the 5th larval stage. Fenoxycarb-treated groups also began to spin cocoons with the control group at the same time. No difference was observed in the pupation process. When control and fenoxycarb-treated groups were compared macroscopically, a difference was undetermined.

Histological Results

When the control group is examined on the 2nd day of the spin (Figure 1A), the testicular follicles were generally in the appearance of tangerine slices. On the same day, the fenoxycarb-treated group (Figure 1B) showed small deformations in the follicles.

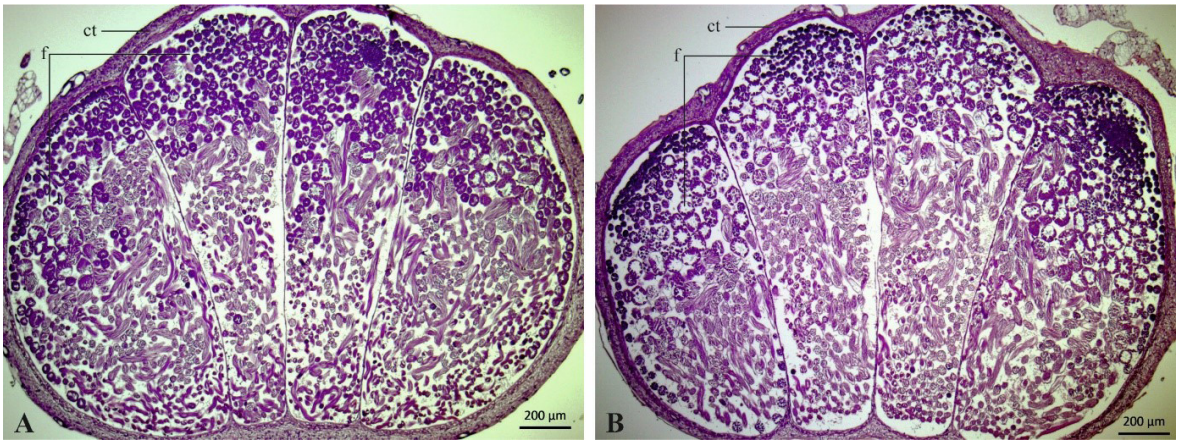

Figure 1. General structure of testis on the 2nd of spin A. Control group, B. Fenoxycarb-treated group. ct: connective tissue, f: follicle.

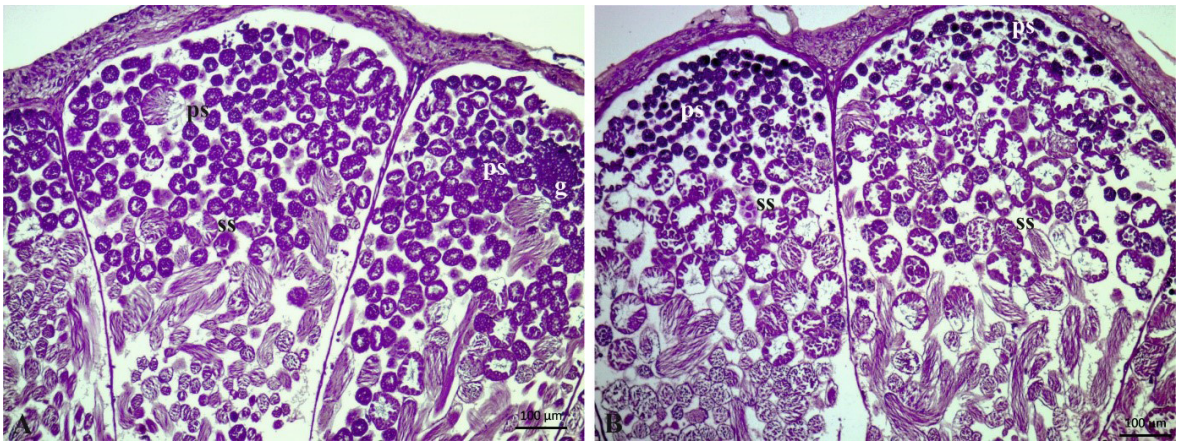

Figure 2. In the growth and maturation region of testis on the 2nd of spin A. Control group, B. Fenoxycarb-treated group. g: germarium, ps: primary spermatocyte, ss: secondary spermatocyte.

While spermatogonium was found intensively in the growth region of the control group (Figure 2A), it was observed that the amount of spermatogonium decreased in the fenoxycarb group compared to the control group (Figure 2B) on the 2nd day of the spin.

On the 2nd day of the spin, the spermatids in the maturation region of the control group were observed to be transformed into sperms bunchy in the differentiation zone (Figure 3A). When the fenoxycarb-treated group was examined, it was found that the spermatids were denser but the differentiated sperm were less (Figure 3B). Therefore, it was seen that the eupyrene sperm bundle in the treatment group was less than the control group.

When the control group was examined on the 4th day of spin (Figure 4A), it was observed that there was dense spermatogonium in the growth zone and spermatogonium was less in the fenoxycarb-treated group (Figure 4B).

On the 4th day of spin, the spermatids in the maturation region of the control group (Figure 5A) were observed to be transformed into sperms tightly in the differentiation zone. However, when compared to the application group (Figure 5B), it was found that the conversion of spermatids to sperm was very low and that the sperm was not transformed in tight bundles but in a less rare. It was also found that, on the 4th day, the eupyrene sperm were less in the treatment group than in the control group, as in the second day of spin.

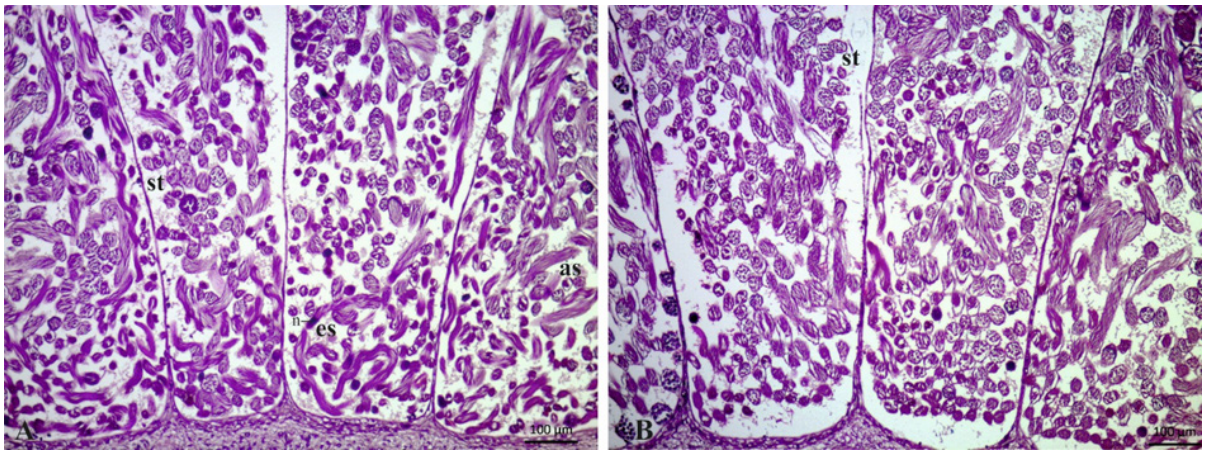

Figure 3. In the maturation and differentiation region of testis on the 2nd of spin A. Control group, B. Fenoxycarb-treated group. as: apyrene sperm bundle, es: eupyrene sperm bundle, n: nucleus, st: spermatid.

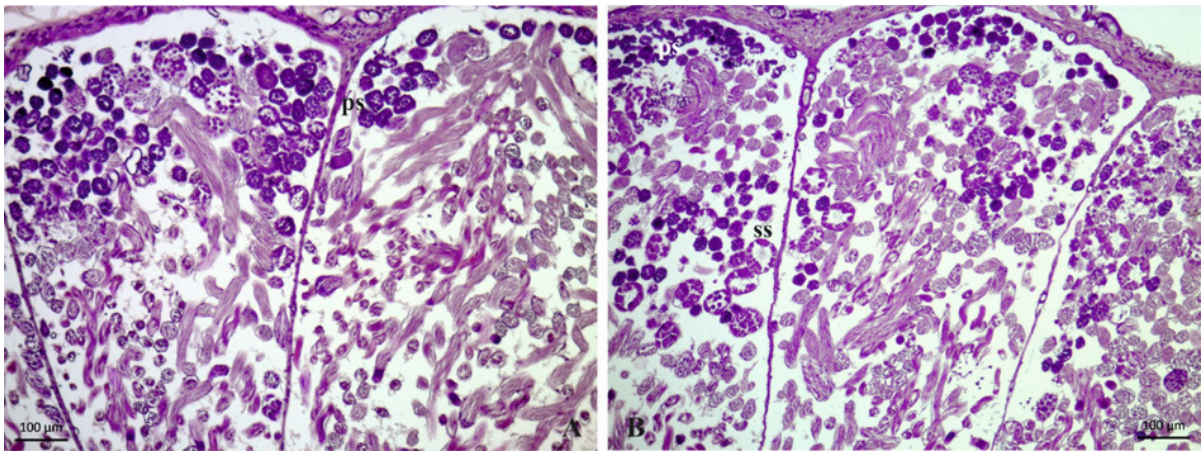

Figure 4. In the growth and maturation region of testis on 4th of spin A. Control group, B. Fenoxycarb-treated group. ps: primary spermatocyte, ss: secondary spermatocyte.

On day 0 (Figures 6A and 7A), a decrease in the concentration of spermatogonium was observed in the growth zone of the pupa control group, while an increase in the mature sperm concentration in the differentiation zone was observed. In the group treated with fenoxycarb (Figures 6B and 7B), spermatogonia were found more frequently and mature sperm are less common. Furthermore, there was no significant difference in the eupyrene sperm bundle concentration in the differentiation area were compared in the control and treatment groups.

Total Carbohydrate Content Results

The total carbohydrate amounts in the two groups were same in the first 24 hours (Table 1). However, 24 hours later fenoxycarb treated group significantly showed remarkable decrease from 0.8 mg to 0.5 mg, and control group showed increased carbohydrate from 0.8mg to 1.3 mg. After 48 hours, there was no significant change in carbohydrate content in the treated group, while control group demonstrated slight decrease in carbohydrate content.

Total Glycogen Results

Glycogen content reached a minimum amount at 96th hour of application for treated and untreated samples as seen Table 2. After this point, slight increase of glycogen content was observed for both group but significant increase was for hormone treated samples. When the rate of formation of glycogen measured after 96 hours was compared, the rate of synthesis in the group of hormones was 0.26 mg/24 h, whereas the rate of production in the control group was 0.08

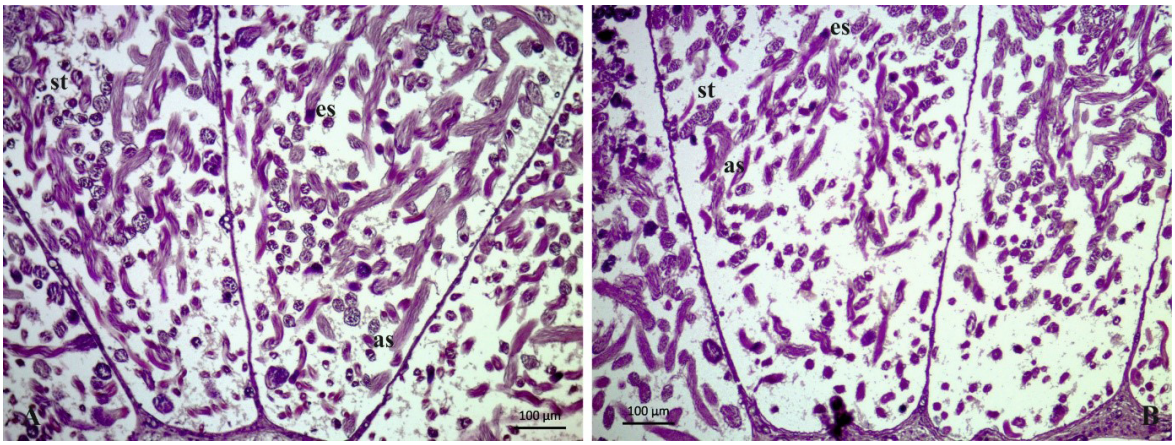

Figure 5. In the maturation and differentiation region of testis on the 4th of spin A. Control group, B. Fenoxycarb-treated group. as: apyrene sperm bundle, es: eupyrene sperm bundle, st: spermatid.

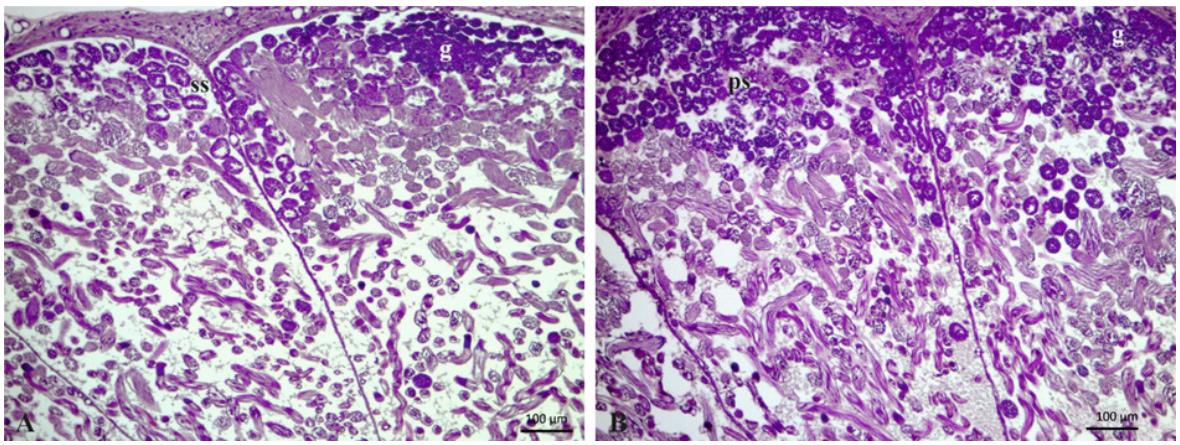

Figure 6. In the growth and maturation region of testis on the 0th of pupa A. Control group, B. Fenoxycarb-treated group. g: germarium, ps: primary spermatocyte, ss: secondary spermatocyte.

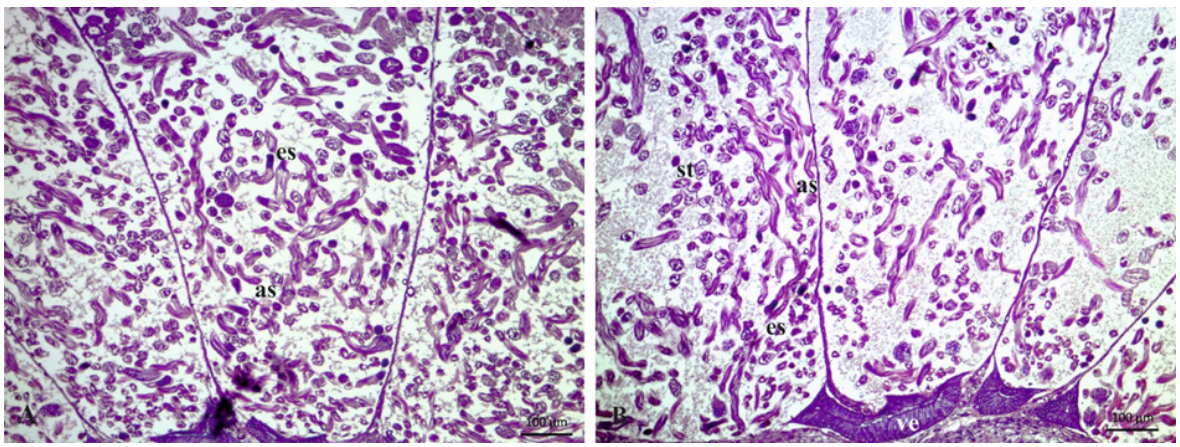

Figure 7. In the maturation and differentiation region of testis on the 0th of pupa A. Control group, B. Fenoxycarb-treated group. as: apyrene sperm bundle, es: eupyrene sperm bundle, st: spermatid, ve: vas efferent.

Table 1. Total carbohydrate content in *Bombyx mori* testis between 1st of spin (S) and 0th of pupa (P).

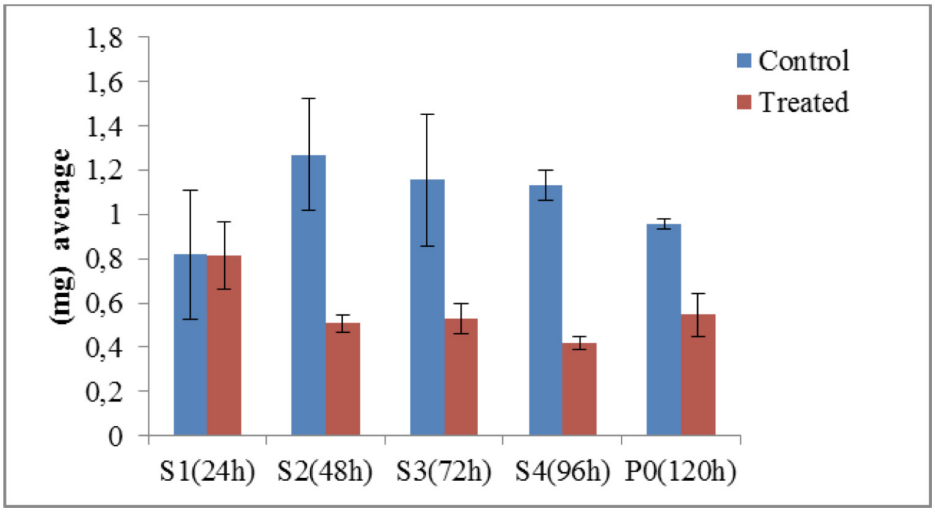

Table 2. Total glycogen content in *Bombyx mori* testis between 1st of spin (S) and 0th of pupa (P).

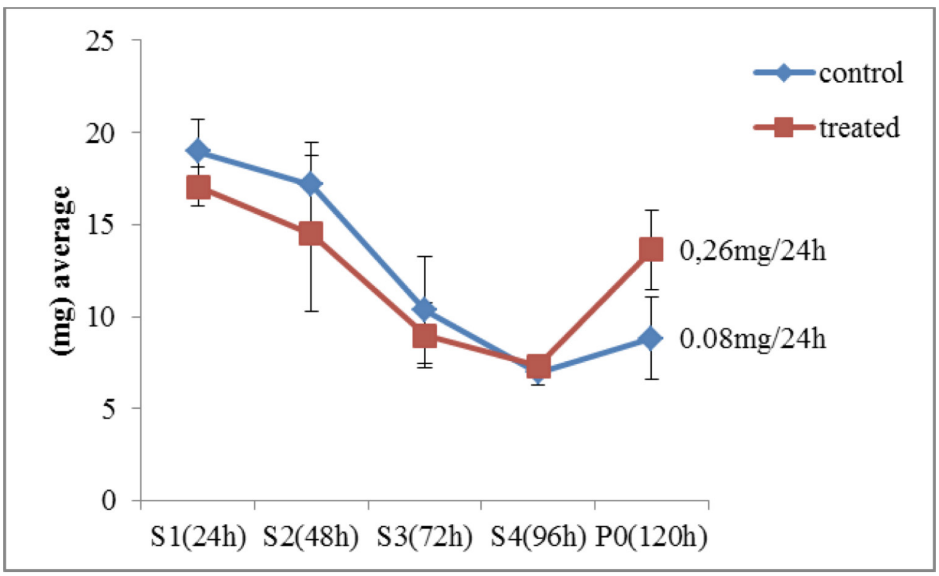

mg/24 h. In fenoxycarb treated group, because the rate of synthesis tripled, demonstrated 50% increase in glycogen content.

DISCUSSION

The effect of hormones on the development of insects is quite high. The most important are Juvenile hormone (JH) secreted from corpora allata and ecdysone hormones secreted from the prothoracic gland. JH plays an important role in the development and reproduction of insects. It determines the characteristic of ecdysis in molting and metamorphic processes. Increases in ecdysteroids in the presence of JH trigger larval-larval ecdyses, but their absence also leads to larval-pupae and then pupal-adult transformations. During larval development, JH or JH analogous used in many insect, have been reported to damage endocrine balance, resulting cause to be abnormal development [12]. Many experiments were done with fenoxycarb that is an efficient JH analog and was observed different effects.

Kamimura and Kiuchi's study [12] has examined the effect of fenoxycarb in the formation of cocoon and pupae during the 5th larval period. The study was divided into 3 groups in the 5th instar according to the reactions against fenoxycarb. The first group, 0-2. on days, fenoxycarb prolonged the eating period and prevented pupation due to dose, but no extra ecdyses was seen. The second group, 3-5. on days, fenoxycarb prolonged the eating period and caused an extra ecdyses in the pupal characteristic 6th stage. In both cases, pupation was precisely inhibited. In the third group involving days 6 and 7th, fenoxycarb has only a small effect on subsequent growth.

1ng of fenoxycarb application on day 0th stops the release of ecdysteroids and keeps it below the threshold level required to initiate metamorphic tissue change, thereby extending the eating period It also suppress ecdysteroid release in a complex way. First, fenoxycarb ceases the secretory activity of prothoracic gland to stops the ability of the gland to respond to PTTH. Thus, it prevents PTTH release. After application of fenoxycarb on day 4, the ecdysteroid titer began to increase and peaked when extra ecdyses started. Contrary to day 0th, treatment on day 4th causes ecdysteroid release because the secretory activity of the prothoracic gland is accelerated [12].

Kamimura [16], Fugo and Dedos [17], Leonardi et al. [18] found that fenoxycarb was effective on larval-pupa ecdyses in silkworms in their studies. Fenoxycarb can also be used for controlling fire ants, fleas, mosquitoes, cockroaches, moths, coccids, and insects attacking vines, olives, cottonseed and fruits [7].

Parlak et al. [19] showed that was delayed the pupal alteration of the larvae, like all other tissues, in the JH application results on day 0 or day 1 of the 5th instar larvae. JH is known to be applied as an inhibitory factor for the synthesis of ecdysone secreted by the prothoracic gland in the early 5th instar. Therefore, it is thought that the ecdysteroid levels induce ovarian development and pupal differentiation in the larval stage and JH inhibit the development of eggs in the larval stage either directly or by suppressing the production of ecdysteroids.

Insects have a balance between synthesis, storage and degradation of nutrients during metamorphosis. According to the study of Pant and Kumar [20], total carbohydrates accumulated during larval stages are used to synthesize of lipid, supply energy need and synthesis of chitin. The rise of total carbohydrate in the larval stages may reflect the use as a potential reserve for pupa-adult development [21]. Another component that accumulates during the larval stage, which has high juvenile hormone value, is glycogen. It is found in entire insect body and used during metamorphosis [22].

Larval forms of holometabolous insects are susceptible to insecticidal stress. Also some pesticides can affect their metabolism of carbohydrates, proteins and lipids [23]. Most researchers determine a reduction of carbohydrate in hemolymph following poisoning with insecticides [24]. The decrease of total carbohydrate content may be indicated production of extra energy to combat insecticidal stress [23].

In this study suggest that as clearly shown in Table 2; the glycogen content of the treatment group is 50% higher than the control group. In addition, in Table 1, it is seen that the amount of total carbohydrate in control group is increased in order to use in various metabolic activities. However, in the treatment group, fenoxycarb caused a decrease in total carbohydrate content. Therefore, the animal synthesizes more glycogen to preserve homeostasis. As a result, fenoxycarb can cause stress in insects, which causes component content to decrease.

The results in this study suggest that as from the 2nd day of cocoon, fenoxycarb reduced spermatogonium formation by suppressing ecdysone release and caused a decrease in mature sperm. Furthermore, our results show that fenoxycarb also affected sperm productivity by reducing functional eupyrene sperm. In conclusion, fenoxycarb has the effect of reducing the formation of spermatogenesis. These biochemical and histological results may be in support of the use of fenoxycarb as an insect growth regulator (IGR) for harmful insects.

ACKNOWLEDGEMENT
We are sincerely grateful to Dr. Ramazan Uranlı for his help with the spectrophotometric analysis.

References

1. O. Parlak, İpekböceği Biyolojisi, Ege Üniversitesi Basımevi, İzmir, No: 171 (2001) 127s ISBN 975-483-485-7.
2. C. Gillott, Entomology, 3rd edit., University of Saskatchewan Saskatoon, Saskatchewan, Canada (2005) 831 p.
3. M.J. Klowden, In physiological systems in insects, Chapter 4 – Reproductive Systems, 2. edit, University of Idaho, Moscow Idaho (2008) 181-238.
4. N. Kılınçer, Ş. Bayram, Böceklerde üreme sistemleri, Ankara Üniversitesi, Ziraat Fakültesi, Bitki Koruma Bölümü (1999) 59s.
5. J.L. Nation, Insect physiology and biochemistry, 2nd edit., Department of Entomology and Nematology University of Florida, U.S.A (2008) 500 p, ISBN 978-1-4200-6177-2.
6. B. Yılmaz, Omurgasızlarda hormonlar, Ankara Üniv. Vet. Fak. Derg., 35 (1988) 218-226.
7. J. Devillers, Juvenile hormones and juvenoids, 3rd edit., CTIS-centre de traitement de l'information scientifique rillieux la pape, France (2013) 410 p, ISBN 978-1-4665-1322.
8. E. Göncü, O. Parlak, The influence of juvenile hormone analogue, fenoxycarb on the midgut remodeling in *Bombyx mori* (L., 1758) (Lepidoptera: Bombycidae) during larval-pupal metamorphosis, Turkish J. Ent., 35 (2011) 179-194.
9. E. Batır, E. Göncü, and O. Parlak, Ecdysone receptor B1 in *Bombyx mori* L. (Lepidoptera:Bombycidae) prothoracic gland under various organ culture conditions, IUFS J. Bio., 71 (2012) 31-42.
10. G. Turgay İzzetoğlu, A. Öber, Histological investigation of the rectal sac in *Bombyx mori* L., Turk J Zool., 35 (2011) 213-221.
11. G. Turgay İzzetoğlu, A. Öber, Total proteolytic activity on the pupal rectal sac of *Bombyx mori* L. (Lepidoptera: Bombycidae), Hacettepe J. Bio. Chem., 41 (2013) 67-72.
12. M. Kamimura, M. Kiuchi, Effects of a juvenile hormone analog, fenoxycarb, on 5th stadium larvae of the silkworm, *Bomyx mori* (Lepidoptera:Bombycidae), Appl. Ent Zool., 33 (1998) 333-338.
13. J.K. Presnell, M.P. Schreibman, Humason's animal tissue techniques, 5th edition, The Johns Hopkins University Press (1997) 572p, ISBN 0-8018-5401-6.
14. A. Öber, Zoolojide Laboratuvar Teknikleri, 3. Baskı, Ege Üniversitesi Basımevi Bornova İzmir, No: 183 (2009) 209s. ISBN 978-975-483-824-4.
15. E. Van Handel, Rapid determination of glycogen and sugars in mosquitoes, J. Am. Mosq. Control Assoc., 1 (1985) 199-301.
16. M. Kamimura, Effects of a juvenile hormone analogue, fenoxycarb, on larval growth of the silkworm, *Bombyx mori* (Lepidoptera: Bombycidae), JSAEZ, 30 (1995) 487-489.
17. S.G. Dedos, H. Fugo, Induction of dauer larvae by application of fenoxycarb early in the 5th instar of the silkworm, *Bombyx mori*, J. Insect Physiol., 45 (1999) 769-775.
18. M.G. Leonardi, S. Cappellozza, L. Cappellozza, P. Lanne, P. Parentis, B. Giordana, Effects of the topical application of an insect growth regulator (fenoxycarb) on some physiological parameters in the fifth instar larvae of the silkworm *Bombyx mori*, Comp. Biochem. Physiol., 113 (1996) 361-365.
19. O. Parlak, S. Sakurai, M. Kaya, T. Ohtaki, Content and possible role of ecdysterids in the larval ovary of the silkworm, *Bombyx mori*, Invertebrate Reprod. Develop., 21 (1992) 1-6.
20. R. Pant, S. Kumar, Metabolic fate of carbohydrates and lipids during moulting of *Philosamia ricini* (Lepidoptera: Saturnidae), Insect Biochem., 9 (1979) 577-582.
21. D. Mandal, D.K. Chaudhuri, Studies on carbohydrate, protein and lipid levels in normal and stress conditions in fat body and integument as compared to whole body during development of rice moth, *Corcyra cephalonica* (ST), Insect Sci. Applic., 13 (1992) 121–128.
22. M.L.M. Garcia, R.P. Mello, B.C.M. Mello, Effect of Precocene II, Ecdysone and juvenile hormone on the glycogen concentration in pupae of *Stomoxys calcitrans* (Dipter Muscidae), Mem. Inst. Oswalda Cruz, 83 (1988) 451–454.
23. K. Fotouhi, M.M. Fazel, A. Kavousi, Effects of pyriproxyfen on bioenergetic resources of *Leptinotarsa decemlineata* (Say) (Coleoptera: Chrysomelidae), Türk. Entomol. Derg., 39 (2015) 11–22.
24. G.J.P. Singh, Hemolymph carbohydrate and lipid mobilization in *Locusta migratoria* in relation to the progress of poisoning following bioresmethrin treatment, Pest. Biochem. Phys., 25 (1986) 264–269.

A Bacterial Machinery for Surface Displayed Enzymes

Yüzeyde Gösterilen Enzimler İçin Bakteriyel Bir Mekanizma

Research Article

Urartu Özgür Şafak Şeker
Bilkent University, UNAM- Institute of Materals Science and Engineering, National Nanotech. Res. Center, Ankara, Turkey.

ABSTRACT

Biomaterial based protein delivery systems have been utilized for many applications in biomedicine. Despite their great success, there is a need to develop innovative living, decision making systems for protein delivery. In this context, here, a cellular system is proposed for protein release and delivery. Such systems can be used not for biomedical purposes but also for other biochemical applications. In this regard a *Escherichia coli* autotransporter protein, Ag43 was engineered to display on its cell membrane. Using this system alkaline phosphatase protein is displayed on the cell surface as a fusion of Ag43-ALP which is also carrying a specific TEV protease excision site. It was shown that the active from of the enzyme was released upon its interaction with TEV protease from the cell surface. In this study a cellular machinery is proposed to be used as a controlled enzyme delivery system.

Key Words
Whole cell biocatalysis, autotransporter, synthetic biology.

ÖZ

Biyomateryal temelli protein taşıma sistemleri birçok biyotıp uygulamasında kullanılmak üzere iyileştirildi. Büyük başarılarına rağmen yenilikçi ve karar verme mekanizmasına sahip sistemlere protein taşınmasında hala ihtiyaç duyulmaktadır. Bu çalışmada protein salınımı ve taşınması için hücresel bir sistem tasarlanmıştır. Bu sistemler sadece biyotıp uygulamalarında değil, aynı zamanda diğer biyokimyasal sistemler için de uyarlanabilir. Bu bağlamda bir *Escherichia coli* oto-taşıyıcı protein, Ag43 hücre zarında gösterilmek üzere tasarlanmıştır. Alkali fosfataz proteinli bu sistem kullanılarak Ag43 ve özellikli TEV proteaz kesme bölgesi taşıyan ALP'nin birleşmesi gösterilmiştir. Enzimin aktif formunun hücre yüzeyinden salgılanan TEV proteaz ile iletişimi sonucunda salındığı açıklanmıştır ve bu makalede kontrollü enzim taşıma sistemini sağlayan bir hücresel mekanizma önerilmiştir.

Anahtar Kelimeler
Tüm hücre biyokatalizi, oto-taşıyıcı, sentetik biyoloji.

Article History: Received: Feb 25, 2018; Revised: Mar 03, 2018; Accepted: Mar 05, 2018; Available Online: Mar 26, 2018.

DOI: 10.15671/HJBC.2018.238

Correspondence to: U.Ö.Ş. Şeker, Bilkent Uni., UNAM-Ins. of Mat. Sci. and Eng., National Nanotech. Res. Center, Ankara, Turkey.
Tel: +90 312 290 3573 Fax: +90 290 266 4365 E-Mail: urartu@bilkent.edu.tr

INTRODUCTION

Enzymes are critical molecules for many biomedical and biotechnological applications, their engineering and structural control is critical for their functions [1]. Generally purified forms of the enzymes are being used, however, their immobilized versions are also popular in many industrial settings [2]. Additionally, instead of using pure enzymes, bacterial machines for whole cell biocatalysts can be designed and used [3]. In such applications cells can be programmed as a whole cell biocatalyst using specific genetic circuits. In most of the whole cell biocatalyst applications enzymes are expressed intracellularly [4,5]. However there is a need to display such enzymes on the cell surfaces to accommodate them for extracellular activities. In the case of the bacteria there is a limited number of opportunities to display enzymes in an active, and intact form on the cell surface. Despite many available surface displayed systems, autotransporter systems are very promising to display enzymes and proteins on the cell surfaces [6-8].

Autrotransporters are specific membrane proteins. These proteins are displaying functional polypeptides on the cell membrane. These systems are promising as engineered cell surface display systems. Among those Ag43 protein in *Escherichia coli* is under great interest due to its phase variable behaviours and controlled protein secretion capability [9]. Ag43 is coded by flu gene in *E. coli* genome. Ag43 is synthesized as a chain of 1039 amino acids. Dam methylase and OxyR global regulator control the expression of the Ag43 protein [10-12]. In it was found that the Ag43 protein has 50000 copies when it is expressed [13,14]. Ag43 protein does not need any specific chaperone proteins for folding as it can carry out also a chaperone function as well. Initially Ag43 protein is synthesized as a form of a single chain, however these whole chain is processed into alpha and beta subunits. Alpha subunit of the protein assembles in to the cell membrane and upon its integration into the cell membrane it forma beta barrel structure, which leads a pore formation. The remaining part of the protein, namely the beta subunit forms is transferred to the outer space of the cell and remained attached to the cell membrane through its interaction with alpha-subunit embedded to the cell membrane. [15, 16] The interaction between the subunits is not very tight and mediated by the non-covalent interactions. The interaction between alpha and beta subunits of the Ag43 can be broken by increasing the temperature to 60°C [17]. The expression of the Ag43 protein also triggered the settlement of the cell population through the interaction between the beta subunits of the Ag43 proteins.

Dues do its versatility as a possible cell surface display tool initial attempts made to use Ag43 protein as an surface display of non-native proteins for *E. coli* however these attempts are limited. Another reason for the Ag43 as an optimal candidate for surface display of the protein is its copy number in *E. coli* is very high to serve as a surface displaying systems for enzymes compared to the other surface displayed proteins. These makes Ag43 protein as an ideal model cell surface display systems for protein display. Up to date some of the immunological factors and proteins have been displayed on the cell of the *E. coli* using Ag43 protein [18,19].

In this study, a model whole cell biocatalyst system was proposed. Whole cell biosensor has been designed to carry out a certain biocatalysis function by expressing enzyme of interest upon induction of the genetic design to produce and secrete the enzyme. Compared to the conventional catalysis system whole cell catalysis systems are convenient in terms of providing flexibility to display enzymes for a lower cost. In such systems enzymes are attached to the membrane of the cells which enables the users to remove the enzymes easily from the solution by centrifugation. Additionally, cells can be programmed to express the cells at a given time and they can start to secreted the enzymes when they are wanted to act on the substrate. Whole cell catalysis can used to program the cells to secrete multi-enzymes, which means that a heterologous catalysis can be achieved through cellular programming of the cells, while the enzymes are displayed on the cell membrane. In this context cell displayed enzyme systems provide new insights in developing next generation of biocatalysis apparoach with a systems based thinking towards

creating system biocatalysis. In current work we have engineered Ag43 protein of *E. coli* to display a well-known, widely used enzyme alkaline phosphatase (named as ALP). Employing the genetic engineering approaches we achieved to display the engineered ALP on the cell membrane of *E. coli*, the activity of the enzymes was noted both when it is displayed on cell membrane and the displayed protein was released from the cell membrane.

MATERIALS and METHODS

Cloning of ALP 6H PelB Ag43 160N Pet22b Vector

The ALP gene with N-terminal 6x His tag and C-terminal flexible linker was amplified from *E. coli* DH5α genome using P1 and P2 primers. TEV recognition site was added to ALP gene via PCR using P1 and P3 primers. P4 and P5 primers was used to amplify the N-terminal truncated Ag43 gene from *E. coli* DH5α genome. Truncated Ag43 gene and modified ALP gene was assembled into NcoI-XhoI digested Pet22b vector using Gibson Assembly [20].

P1: 5′ GCCGGCGATGGCCATGGGCCACCACCAC-CACCACCACGGTGGCGGTGGATCCCGGACAC-CAGAAATGCCTGT 3′

P2: 5′ GCCCTGAAAGTACAGGTTTTCGCTACCAC-CGCCACCTTTCAGCCCCAGAGCGGCTTTC 3′

P3: 5′ TTTATTGATGGTTGTGCGCTTAAGGCTAC-CACCGCCACCGCCCTGAAAGTACAGGTTTTC 3′

P4: 5′ TCAGTGGTGGTGGTGGTGGTGCTCGAGT-CATCAGAAGGTCACATTCAGTG 3′

P5: 5′ TTTCAGGGCGGTGGCGGTGGTAGCCTTA-AGCGCACAACCATCAATAAAAACG 3′

Following the cloning of the Ag43 fusion partner, the clones were sent for sequencing the check the alkalinephopsphatase protein sequence identitiy. The alignment results is presented in Figure 2.

Trypsin digestion assay for surface displayed ALP

Sequence verified construct was transformed into *E. coli* BL21 (DE3) strain. A single colony was picked from agar plate and inoculated into 5ml of LB medium with appropriate antibiotics. The overnight grown cells were subcultured 1:100 into 10ml of fresh LB supplemented with %1 (w/v) glucose and antibiotics. At mid log phase (OD_{600}: 0.4-0.6), the gene was induced with 1mM IPTG at 18˚C for overnight.

Detection of the Alkaline phosphatase enzymatic activity

Fresh ALP expressed cells were collected and centrifuged at 8000xg for 5 minutes. Cells were resuspended with 1x PBS, and stored at 4˚C for

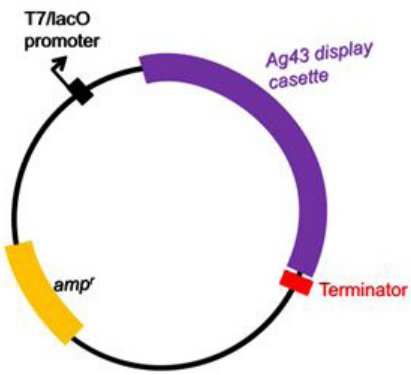

Figure 1. Plasmid map used for the expression of the fusion protein Ag43-ALP.

Figure 2. Sequence alignment of the cloned ALP protein.

further experiments. For trypsin treatment, $5x10^8$ cells were taken and suspended with 200 µl 1x PBS. 10 µg trypsin protease (Sigma- Aldrich) was added, and incubated 37˚C for 2 hours. After incubation, cells were centrifuged, and washed twice with 1x PBS. The washed cells were resuspended with 200 µl of p-nitrophenylphosphate (pNPP) substrate solution (Sigma-Aldrich). The resuspended cells were incubated at 37˚C for 3 hours. Total ALP activity was measured as p-nitrophenol (pNP) absorption at 405 nm.

TEV Protease Accessibility Assay

$5x10^8$ fresh ALP expressed cells were centrifuged and washed with TEV protease buffer (50mM Tris-HCl pH=8, 0.5mM EDTA) without DTT. Cells were resuspended in 200 µl of TEV protease buffer, and 5 unit of AcTEV protease (Invitrogen) was added. The cleavage reaction was incubated at 4˚C for overnight. Cells were centrifuged at full speed for 5 minutes. Supernatants were collected. 100 µl of supernatant after cleavage reaction was mixed with 100 µl of PnPP substrate solution. The mixture were incubated at 37 C for 3 hours. Supernatant ALP activity was measured as pNP at 405nm.

RESULTS

Enzymes are valuable biocatalysts and they have been heavily used in many areas including biomedicine, fine chemical synthesis. However, generally enzymes are used in their pure form and the cost for the enzymes may cause problems in their co-effectiveness. In this regard, there have been studies to immobilize enzymes and protein on solid supports to provide a longer lifetime and better durability for them [21]. In a whole cell system these optimizations can be achieved through engineering of the cellular genetic regulation systems [22]. In our study we have formed a system where the timely control of the enzyme secretion was achieved through an inducible system. To create such a system Ag43 autotransporter system is engineered. The genetic parts of the Ag43 protein can be found in Figure 3.

The signalling peptide allow the polypeptide chain to be recognised by the cellular machine for transportation. In our design we have included a specific signalling part that is called the tobacco etching virus protease (TEV protease) recognition site. TEV recognition site is added

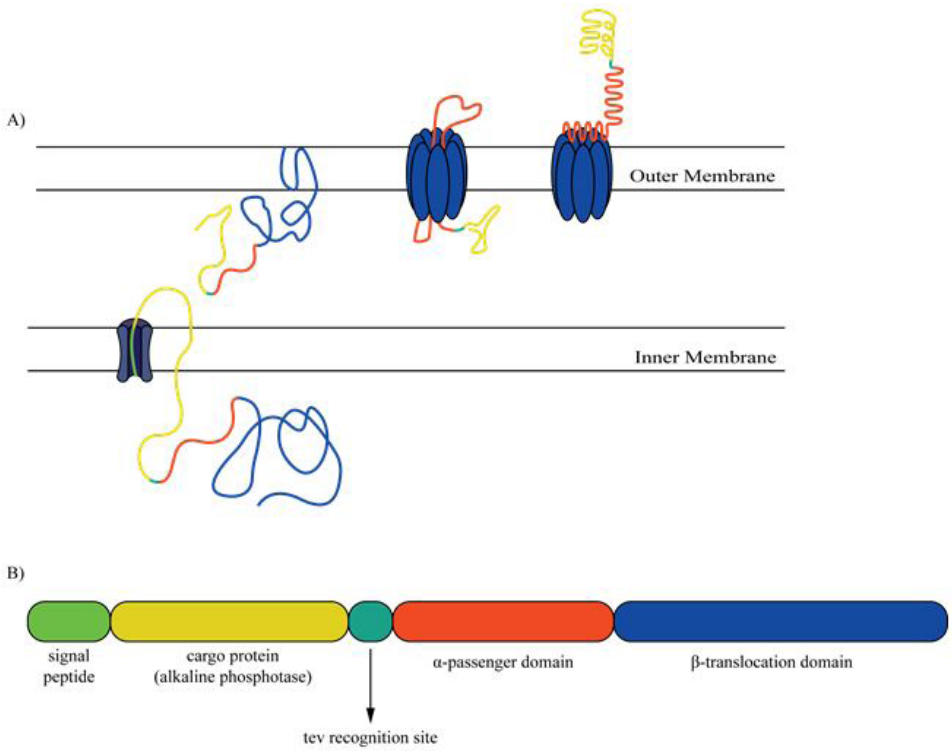

Figure 3. A. The secretion of the Ag43 autotransporter system, the polypeptide chain is translated and transported through the dedicated secretion machinery. The polypeptide chain cleaved and two distinct polypeptide chains are formed, blue polypeptide chain forms a pore on the cell membrane that helps the cargo protein to be transported through the cell membrane. B. The parts of the expressed autotransporter within the cytoplasm.

to remove the cargo protein after is displayed on the surface of the bacteria. This will allow on to control the release of the protein from the surface of the bacteria at a timely manner. TEV protease has a specific digestion site formed by the following amino acid sequence : (Glu-Asn-Leu-Tyr-Phe-Gln↓Gly). We have selected the alkaline phosphatase enzyme as the model enzyme to display opn the cell surface and to show its release from the cell membrane upon addition of the TEV protein from the surface of the bacteria.

The gene encoding for the engineered autotransporter system was cloned under the control of a P_{LacO} promoter. This promoter is inducible and transformed into *E. coli* BL21 cell. This cell is suitable for the production of the proteins under the control of the LacI repression along with pLac promoter system. [22] As descried in materials and methods section the cell were grown and induced to initiate the engineered autotransporter protein expression. Following the expression and folding of the protein the cell membrane of the protein was expected to be displayed on the cell surface. In this study, ALP enzyme was expected to be displayed on the cell surface, and should show enzymatic activity. In order to probe the existence of the ALP and its activity the ALP displaying cell were used to probe enzymatic activity of ALP. ALP enzymatic activity was followed by the breakdown of pNPP substrate as given in materials and methods section. Following the collection of the ALP displaying cells the activity of the cell was measured and data was normalized by cell number, the result of this measurement is given in Figure 4. In order to confirm that the protein are displayed on the cell surface, we have used trypsin digestion. Trypsin is a non-specific protease that attacks amino acid sequences without a sequence preference. [24] So, trypsin is a good tool to detect the presence of the displayed protein on the cell surface. During this removal we do expect to see a decrease in the enzymatic activity. As seen on Figure 4 upon trypsin exposure the ALP activity has decrease dramatically.

As stated earlier the removal of ALP from the cell surface is initially tested with trypsin and this protease is attacking the displayed enzymes instead of releasing it from the cell membrabe. After the verification of the ALP display on the cell surface, using trypsin assay we took a step further and decide to do a programmed ALP release from the cell surface using a dedicated protease. The number of specific proteases are limited and one of the best studied one among them is TEV protease. TEV protease can target a specific recognition site and carry out the cleavage of the protein of interest from it fusion partner. We have employed the TEV protease.

In order to propose a programmed release of the ALP from the cell surface, TEV protease was added to the cell suspension. As described in the materials section protease was incubated with the cell suspension and at the end of the incubation the released ALP activity was measured from solution after removing the cells with centrifugation. As seen on Figure 5, the result of the experiments points the release of the intact and functional ALP enzyme. Compared to the initial enzyme activity there is

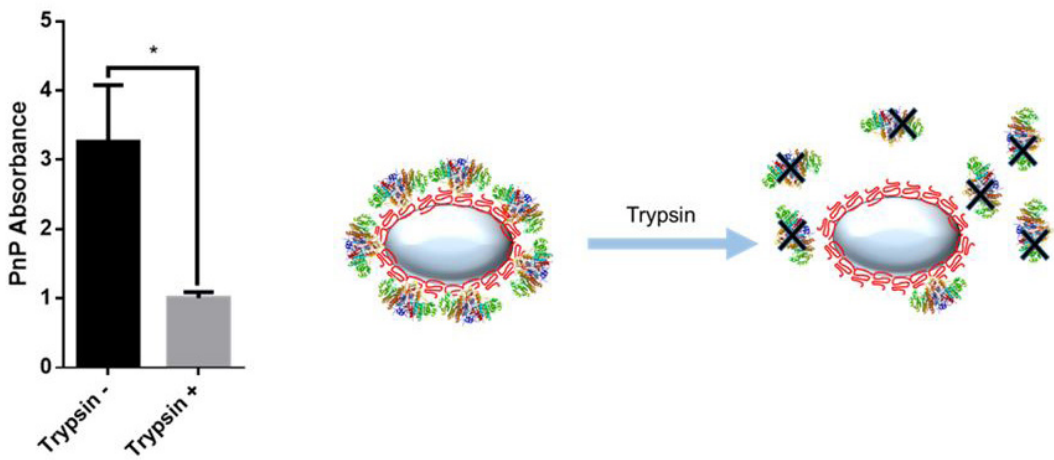

Figure 4. Trypsin based release of the ALP protein, and activity of the ALP protein before and after trypsin enzyme treatments. The decrease in the enzyme activity is statistically significant (t-test, $p < 0.05$).

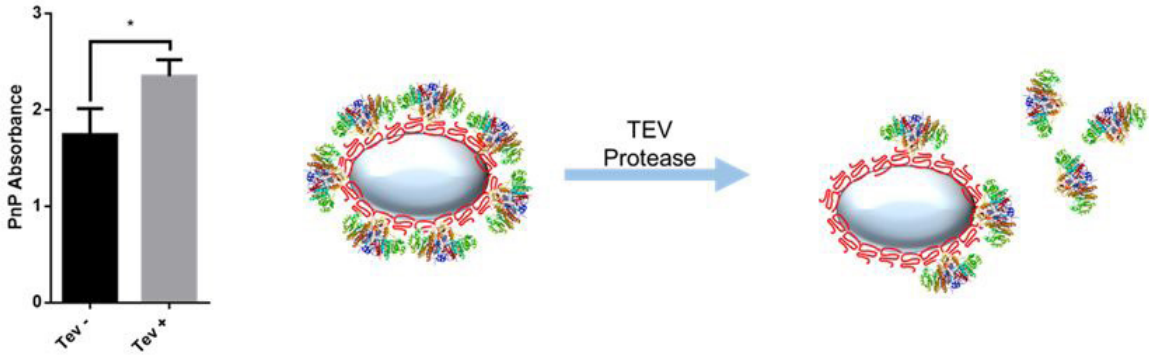

Figure 5. ALP release from the surface of the cells displaying the enzyme upon addition of the TEV protease. The increase in the enzyme activity is statistically significant (t-test, $p < 0.05$).

an increase in the enzyme activity, this because of the unintentionally released of the ALP protein from the *E. coli* periplasmic space. However upon exposure to the TEV protease an obvious increase in the activity of the free enzyme was noted after removing the cells from the solution. Another point that needs to be discussed is the decrease in the enzyme activity in the case of the trypsin addition. Upon addition of the trypsin activity one may expect to see also an increase in the ALP activity in the solution however this was not the case. The main reason for this case is the non-specific nature of the trypsin enzyme. Trypsin enzyme cuts the available protein in a random way which lead the degradation of the enzyme, and finally loss of enzyme activity.

DISCUSSIONS

Cellular programming for the secretion of enzymes and small molecules is a promising approach to create biological machines to control bioprocesses. In this regard synthetic biology gains more importance and provides new functionalities for cellular programming. In cellular programming innovative genetic switches are needed and these can be utilized as a part of the whole cell biocatalyst systems. In this work the utilization of an autotransporter protein is presented as a tool to display functional enzymes. The design of the genetic construct is critically important to control the release of the displayed enzymes from the cell surface. Using a timely control can provide an opportunity to control a given process conditions at a given time. However, due to the molecular barriers it may not be feasible to use natural display system in the designs for controlled protein release. One of the critical barrier in such work is the docking of the protease of interest to release the displayed protein from the cell surface. In order to prevent such hindrances a specific tag can be used that may allow the protein of interest to be displayed from a distance from the cell surface. In the presented work the system can be enhanced by co-expressing the TEV protease and the enzyme of the interest at the same time from the cell surface. This will give the flexibility not to add the external TEV protease. There is also a need to underline that the choice of the protease is critical to release the protein of interest in an active form. That is why proteases targeting very specific recognition sites should be chosen. To sum up, whole cell biocatalyst systems can be designed and implemented for many diverse applications, including to deliver protein based drug molecules in gut by using probiotics. Such innovative applications will open new avenues for our understanding to develop smart, living drug delivery systems.

ACKNOWLEDGEMENTS

We thank Recep Erdem Ahan for technical help during the experiments. Dr. Seker acknowledges financial support from TUBA-GEBIP.

References

1. D.D. Boehr, R.N. D'Amico, N. Rebecca, K.F. O'Rourke, F. Kathleen, Engineered control of enzyme structural dynamics and function, Prot. Sci., 27 (2018) 825-838.
2. C. Silva, M. Martins, S. Jing, J.J. Fu, J. Fu, A. Cavaco-Paulo, Practical insights on enzyme stabilization, Crit. Rev. Biotechnol., 38 (2018) 335-350.
3. J.H. Schrittwieser, S. Velikogne, M. Hall, Artificial biocatalytic linear cascades for preparation of organic molecules, Chem. Rev., 118 (2018) 270-348.

4. F. Kazenwadel; M. Franzreb, B.E. Rapp, Synthetic enzyme supercomplexes: co-immobilization of enzyme cascades, Anal. Methods, 7 (2015) 4030-4037.
5. M. Jeschek, S. Panke, T.R., Artificial metalloenzymes on the verge of new-to-nature metabolism, Trends Biotech. 36 (2018) 60-72.
6. T. Nicolay, J. Vanderleyden, S. Spaepen, Autotransporter-based cell surface display in gram-negative bacteria, Critical Reviews in Microbiology, 41 (2015) 109-123.
7. H. Nakatani, K. Hori, Cell surface protein engineering for high-performance whole-cell catalysts, Frontiers of Chemical Science and Engineering, 1 (2017) 46-57.
8. Decorating microbes: surface display of proteins on *Escherichia coli*, E. van Bloois, R.T. Winter, H. Kolmar, M.W. Fraaije, Trends in Biotechnology, 29 (2011) 79-86.
9. N. Dautin, H. D. Bernstein, Protein secretion in gram-negative bacteria via the autotransporter pathway. Annu. Rev. Microbiol., 61 (2007) 89–112.
10. W. Haagmans, M. van der Woude M., Phase variation of Ag43 in *Escherichia coli*: Dam-dependent methylation abrogates OxyR binding and OxyR-mediated repression of transcription, Mol. Microbiol., 35 (2000) 877–887.
11. D.E. Waldron, P. Owen, C.J. Dorman, Competitive interaction of the OxyR DNA-binding protein and the Dam methylase at the antigen 43 gene regulatory region in *Escherichia coli*, Mol. Microbiol., 44 (2002) 509–520.
12. A. Wallecha, V. Munster, J. Correnti, T. Chan, M. van der Woude, Dam- and OxyR-dependent phase variation of agn43: essential elements and evidence for a new role of DNA methylation, J. Bacteriol., 184 (2002) 3338–3347.
13. G.C. Ulett, J. Valle, C. Beloin, O. Sherlock, J.M. Ghigo, M. A. Schembri1, Functional analysis of antigen 43 in uropathogenic *Escherichia coli* reveals a role in long-term persistence in the urinary tract, Infect. Immun., 75 (2007) 3233-3244.
14. H. Hasman, T. Chakraborty, P. J. Klemm, Antigen-43-mediated autoaggregation of *Escherichia coli* is blocked by fimbriation, J. Bacteriol., 181(1999) 4834-4841.
15. K. Kjaergaard, M.A. Schembri, H. Hasman, P.J. Klemm, Antigen 43 from *Escherichia coli* induces inter- and intraspecies cell aggregation and changes in colony morphology of *Pseudomonas fluorescens*, J. Bacteriol., 182 (2000) 4789-4796.
16. O. Sherlock, U. Dobrindt, J.B. Jensen, R.V. Munk, P. Klemm, Glycosylation of the self-recognizing *Escherichia coli* Ag43 autotransporter protein, J. Bacteriol., 188 (2006) 1789-1807.
17. K. Kjaergaard, H. Hasman, M.A. Schembri, P. Klemm, Antigen 43-mediated autotransporter display, a versatile bacterial cell surface presentation system, J. Bacteriol., 184 (2002) 4197-4204.
18. F.Y. Huang, C.C. Wang; Y.H. Huang, H.G. Zhao, J.L. Guo, S.L. Zhou, H. Wang, Y.Y. Lin, G.H. Tan, Antigen 43/Fc epsilon 3 chimeric protein expressed by a novel bacterial surface expression system as an effective asthma vaccine, Immunology, 143 (2014) 230-240.
19. I.Munoz-Gutierrez, C.Moss-Acosta, B.Trujillo-Martinez, G. Gosset, A. Martinez, Ag43-mediated display of a thermostable beta-glucosidase in *Escherichia coli* and its use for simultaneous saccharification and fermentation at high temperatures, Microb. Cell Fact., 13 (2014) 106- .
20. D.G. Gibson, L. Young, R.Y. Chuang, J.C. Venter, C.A. Hutchison, H.O. Smith, Enzymatic assembly of DNA molecules up to several hundred kilobases, Nat. Methods, 6 (2009) 343-345.
21. C.W. Lee, S.H. Jang, H. Chung, Improving the stability of cold-adapted enzymes by immobilization, Catalysts, 7 (2017) 112.
22. Y. Liu, D.S. Kim, M. Jewett, C. Michael, Repurposing ribosomes for synthetic biology, Curr. Opin. Chem. Biol., 40 (2017) 87-94.
23. R. Lutz, H. Bujard, Independent and tight regulation of transcriptional units in *Escherichia coli* via the LacR/O, the TetR/O and AraC/I-1-I-2 regulatory elements, Nucleic Acids Res., 25 (1997) 1203-1210.
24. C. Magni, F. Sessa, J. Capraro, M. Duranti, E. Maffioli, A. Scarafoni, Structural and functional insights into the basic globulin 7S of soybean seeds by using trypsin as a molecular probe, Biochem. Biophys. Res. Commun., 496 (2018) 89-94.